The Dynamics and Dynamic Discharge of the Ice Masses and Tidewater Glaciers of the Canadian High Arctic

Wesley Van Wychen

Thesis submitted to the
Faculty of Graduate and Postdoctoral Studies
in partial fulfillment of the requirements for the degree of
Doctorate of Philosophy in Geography

Department of Geography
Faculty of Arts
University of Ottawa

ABSTRACT

Speckle tracking of synthetic aperture RADAR imagery (Radarsat-1/2, ALOS PALSAR) and feature tracking of optical (Landsat-7 ETM+) imagery is used to determine the entire surface velocity structure of the major ice masses of the Canadian High Arctic in 2000, 2010-2015 and for select tidewater terminating glaciers from 1999-2010. At the termini of tidewater glaciers, surface ice velocities are combined with measured/modelled ice thicknesses to derive an estimate of mass loss via dynamic (iceberg) discharge. The total dynamic discharge for the ice masses of the southern Canadian Arctic Archipelago (SCAA: Baffin and Bylot Islands) is between ~17 and 180 Mt a^{-1} (0.017 to 0.180 Gt a^{-1}) for the period 2007-2011, compared to a dynamic discharge of ~2.47 ± 0.88 Gt a^{-1} for the northern Canadian Arctic Archipelago (NCAA: Devon, Ellesmere, Axel Heiberg Islands) for the period 2011-2015. A comparison of these values with rates of mass loss via climatic mass balance (surface melt and runoff) indicates that dynamic discharge accounted for ~3.1% of total ablation for the NCAA in 2012 and ~0.11% of total ablation in the SCAA between 2007 and 2010. This reveals that total ablation in the Canadian Arctic is currently dominated by surface melt and runoff.

The glacier velocity dataset provides the most comprehensive record of ice motion and dynamic discharge in the Canadian Arctic to date and reveals a large degree of variability in glacier motion within the region over the last ~15 years. Most of the major glaciers in the NCAA have decelerated and their resultant dynamic discharge has decreased over the observation period, which is largely attributed to cyclical phases attributed to surging and pulsing. On pulse-type glaciers, variation in ice motion is largely confined to regions where the bed is located below sea level. A notable departure from the overall trend of regional velocity slowdown is the widespread acceleration of the Trinity and Wykeham Glaciers of the Prince of Wales Icefield (the largest glacier complex in the Canadian Arctic), which cannot be explained by surge or pulse mechanisms. The increased discharge from these two glaciers nearly compensates (within error) for the decrease in iceberg discharge from other glaciers across the study region and indicates that total dynamic discharge from the Canadian Arctic can be sensitive to the variations of ice flow of just a few glaciers.

TABLE OF CONTENTS

ABSTRACT ..... **II**
LIST OF ACRONYMS ..... **IX**
ACKNOWLEDGEMENTS ..... **X**
CHAPTER ONE: INTRODUCTION **1**
1.1 INTRODUCTION 1
1.2 BACKGROUND 2
1.3 PURPOSE 4
1.4 RESEARCH OBJECTIVES AND THESIS ORGANIZATION 4
1.5 AUTHORSHIP AND CO-AUTHOR CONTRIBUTIONS 7
1.6 REFERENCES: 8
CHAPTER TWO: GLACIER VELOCITIES AND DYNAMIC ICE DISCHARGE FROM THE QUEEN ELIZABETH ISLANDS, NUNAVUT, CANADA **11**
ABSTRACT: 11
2.1 INTRODUCTION AND STUDY AREA 12
2.2 METHODS 12
2.2.1 Determination of Surface Motion *12*
2.2.2 Calculation of Dynamic Ice Discharge *14*
2.3 RESULTS AND DISCUSSION 16
2.4 CONCLUSIONS 19
2.5 REFERENCES: 21
CHAPTER THREE: GLACIER VELOCITIES AND DYNAMIC DISCHARGE FROM THE ICE MASSES OF BAFFIN AND BYLOT ISLANDS, NUNAVUT, CANADA **28**
ABSTRACT: 28
3.1 INTRODUCTION 29
3.2 STUDY SITE 30
3.3 METHODS 31
3.3.1 Determination of Surface Motion *31*
3.3.2 Error Analysis *33*
3.3.3 Determination of Dynamic Discharge *34*
3.4 RESULTS AND DISCUSSION 37
3.4.1 Glacier Velocity Structure of Baffin and Bylot Islands *37*
3.4.2 Dynamic Discharge *39*
3.5 CONCLUSIONS 40
3.6 REFERENCES 43
CHAPTER FOUR: CHARACTERIZING INTER-ANNUAL VARIABILITY OF GLACIER DYNAMICS AND DYNAMIC DISCHARGE (1999-2015) FOR THE ICE MASSES OF ELLESMERE AND AXEL HEIBERG ISLANDS, NUNAVUT, CANADA **54**
4.1 BACKGROUND AND STUDY SITE 55
4.2 METHODS AND DATA 57
4.2.1 Satellite Imagery *57*
4.2.2 DETERMINATION OF ICE MOTION 58
4.2.1 Speckle Tracking of RADARSAT Data *58*
4.2.2 Feature Tracking of Landsat-7 ETM+ Datasets *59*
4.2.3 Velocity Error Analysis *60*
4.2.3.1 Speckle Tracking Error Analysis *60*
4.2.3.2 Feature Tracking Error Analysis *61*
4.3.4 Identification of Surge Features and Terminus Positions *61*
4.3.5 Determination of Dynamic Discharge *61*
4.3.5.1 Longitudinal Bed Elevation Profiles *63*
4.4 RESULTS 64
4.4.1 General Ice Dynamics of Ellesmere and Axel Heiberg Islands *64*

4.4.2 Comparison of "Winter" (Speckle Tracking) and "Annual" (Feature Tracking) Velocities *64*
4.4.3 Areas of Velocity Change *65*
4.4.3.1 Glaciers with Velocity Decrease *65*
4.4.3.2 Glaciers with Variable Velocity Change *66*
4.4.3.3 Glaciers with Velocity Increase *66*
4.4.4 Bed Elevations and Velocity Variability *67*
4.4.5 Patterns of Dynamic Change *67*
4.4.6 Velocity Fluctuations and Terminus Positions *68*
4.5 DISCUSSION 70
4.5.1 Surge-Type Flow Variability *70*
4.5.2 Pulse-Type Flow Variability *71*
4.5.3 Consistent Acceleration *73*
4.5.4 Dynamic Discharge *75*
4.6 CONCLUSIONS 75
4.7 REFERENCES 78
CHAPTER FIVE: VARIABILITY IN ICE MOTION AND DYNAMIC DISCHARGE FROM DEVON ICE CAP, NUNAVUT, CANADA 98
ABSTRACT 98
5.1 INTRODUCTION 99
5.2 STUDY SITE 100
5.3 METHODS 101
5.3.1 Feature Tracking of Landsat-7 Imagery *101*
5.3.2 Speckle Tracking of RADARSAT-2 Imagery *102*
5.3.3 Removal of Erroneous Displacements and Creation of Velocity Rasters *102*
5.3.4 Ice Displacement Error Analysis *103*
5.3.5 Glacier Bed Profiles *103*
5.3.6 Flow Regime Mapping *104*
5.3.7 Calculation of Dynamic Discharge *105*
5.4 RESULTS 106
5.4.1 Ice Dynamics *106*
5.4.2 Areas of Dynamic Change *106*
5.4.2.1 Variability in Annual Motion 1999-2010 ..... *107*
5.4.2.2 Variability in Winter Motion 2009-2015 ..... *108*
5.4.3 Bed Morphology and Areas of Dynamic Variability *109*
5.4.4 Updated Flow Regime Mapping *110*
5.5 DISCUSSION 111
5.5.1 Spatial and Temporal Evolution of the Flow of Devon Ice Cap *111*
5.5.1.1 Velocity Variability Attributed to Surging *111*
5.5.1.2 Velocity Variability Attributed to Pulsing *113*
5.5.1.3 Other Forms of Velocity Variability *113*
5.5.3 Dynamic Discharge *115*
5.6 CONCLUSIONS 116
5.7 REFERENCES: 118
CHAPTER SIX: CONCLUSIONS 131
6.1 SUMMARY AND CONCLUSIONS 131
6.2 KEY CONTRIBUTIONS 133
6.3 FUTURE RESEARCH DIRECTIONS 134
6.4 THESIS REFERENCES 136

LIST OF TABLES

TABLE 2-1: 2012 DYNAMIC ICE LOSS FROM ALL TIDEWATER CALVING GLACIERS IN THE QUEEN ELIZABETH ISLANDS. 24
TABLE 2-2: ERROR ANALYSIS DETERMINED FROM APPARENT MOTION OVER STATIONARY REGIONS (BEDROCK OUTCROPS AND ICE DIVIDES). 25
TABLE 2-3: PAN-ARCTIC COMPARISON OF ICE DISCHARGE ESTIMATES. 26
TABLE 3-1: SUMMARY OF ALOS PALSAR IMAGERY USED IN THIS STUDY. ALL IMAGERY WAS 9 M RESOLUTION, AND ALL BEAM MODES WERE FINE BEAM SINGLE POLARIZATION, EXCEPT FOR A SINGLE PAIR (22-10-2011 TO 07-12-2011), WHICH WAS FINE BEAM DOUBLE POLARIZATION. 46
TABLE 3-2: COMPARISON OF DISPLACEMENTS DERIVED FROM IN SITU (DGPS) AND SPECKLE-TRACKING ON A TRANSECT ACROSS PENNY ICE CAP (LOCATION OF DGPS STATIONS ARE DENOTED ON FIGURE 3-4A). 47
DIFFERENCE (%) 47
TABLE 3-3: ESTIMATED FRONTAL ABLATION FROM THE TIDEWATER TERMINATING GLACIERS OF BAFFIN AND BYLOT ISLANDS. "*" DENOTE GLACIERS WHERE THE "OUTLET" GLACIER SCENARIO WAS USED TO ESTIMATE ICE THICKNESS. 48
TABLE 4-1: SUMMARY OF REMOTE SENSING IMAGERY USED IN THIS STUDY. SAR IMAGE PAIRS FROM 2000-2008 WERE RADARSAT-1 FINE BEAM (9M RESOLUTION); FROM 2009-2011 RADARSAT-2 FINE BEAM (9 M RESOLUTION); FROM 2011-2014 RADARSAT-2 WIDE FINE BEAM (9 M RESOLUTION). 82
TABLE 4-2: ERROR ANALYSIS DETERMINED FROM APPARENT MOTION OVER STATIONARY REGIONS (BEDROCK (BR) AND ICE DIVIDES (ID)). ESTIMATES OF ICE DIVIDES ARE NOT POSSIBLE IN 2006-2010 DUE TO SURFACE VELOCITY MOSAICS THAT ARE RESTRICTED TO THE LOWER REGIONS OF ICE MASSES. SUPERSCRIPTS INDICATE THE STANDARD DEVIATION OF THE DATASET. UNITS IN M A^{-1}. 84
TABLE 4-3: DYNAMIC CHANGE, TERMINUS RESPONSE AND IDENTIFICATION OF SURFACE FEATURES INDICATIVE OF SURGING FOR THE 16 GLACIERS THAT UNDERWENT SIGNIFICANT VELOCITY VARIATION OVER THE 1999-2015 PERIOD. "*" INDICATES GLACIERS THAT HAVE PREVIOUSLY BEEN IDENTIFIED AS SURGE-TYPE BY COPLAND ET AL. [2003A]. 85
TABLE 4-4: CHARACTERISTICS DISTINGUISHING GLACIERS IDENTIFIED AS "PULSE-TYPE" FROM THOSE IDENTIFIED AS "SURGE-TYPE" IN THE CANADIAN HIGH ARCTIC 86
TABLE 4-5: TEMPORAL VARIABILITY IN DYNAMIC DISCHARGE FOR INDIVIDUAL GLACIERS AND ICE MASSES OF THE CANADIAN HIGH ARCTIC. ICE THICKNESS DATA SOURCES: [1] = 2014 NASA OPERATION ICEBRIDGE, [2] = 2012 NASA OPERATION ICEBRIDGE, [3] = 2006 NASA OPERATION ICEBRIDGE. FLUXGATE METHOD: CS = CROSS SECTION, CS_{INT} = CROSS SECTION WITH INTERPOLATED ICE THICKNESS VALUES TO FILL IN PARTIAL MISSING DATA, CL = CENTRELINE METHOD. SUPERSCRIPT NOTATION PRESENTS (±) UNCERTAINTY FOR EACH ESTIMATE. 87
TABLE 4-6: TEMPORAL VARIABILITY IN DYNAMIC DISCHARGE FOR INDIVIDUAL GLACIERS AND ICE MASSES OF THE CANADIAN HIGH ARCTIC. ICE THICKNESS DATA SOURCES: 1 = 2014 NASA OPERATION ICEBRIDGE, 2 = 2012 NASA OPERATION ICEBRIDGE, 3 = 2006 NASA OPERATION ICEBRIDGE. FLUXGATE METHOD: CS = CROSS SECTION, CL = CENTRELINE METHOD. SUPERSCRIPT NOTATION PRESENTS (±) UNCERTAINTY FOR EACH ESTIMATE. 88
TABLE 5-1: SUMMARY OF LANDSAT-7 IMAGE PAIRS USED TO DERIVE VELOCITY MAPS VIA THE FEATURE TRACKING METHOD. BL = BELCHER GLACIER, SV = SVERDRUP GLACIER, ES = EASTERN GLACIER, FZ = FITZROY GLACIER, NC = NORTH CROKER BAY GLACIER, SC = SOUTH CROKER BAY GLACIER, SE1 = SOUTHEAST 1 GLACIER, SE2 = SOUTHEAST 2 GLACIER; GLACIER LOCATIONS ARE DENOTED ON FIGURE 5-1. 121
TABLE 5-2: SUMMARY OF RADARSAT-2 IMAGE PAIRS USED TO DERIVE VELOCITY MAPS OF DEVON ICE CAP VIA THE SPECKLE TRACKING METHOD. BL = BELCHER GLACIER, SV = SVERDRUP GLACIER, ES = EASTERN GLACIER, FZ = FITZROY GLACIER, NC = NORTH CROKER BAY GLACIER, SC = SOUTH CROKER BAY GLACIER, SE1 = SOUTHEAST 1 GLACIER, SE2 = SOUTHEAST 2 GLACIER, SE3 = SOUTHEAST 3 GLACIER, E5 = EAST 5 GLACIER, E6 = EAST 6 GLACIER, E7 = EAST 7 GLACIER; GLACIER LOCATIONS ARE DENOTED ON FIGURE 5-1. 122
TABLE 5-3: DYNAMIC DISCHARGE FOR MAJOR GLACIERS OF DEVON ICE CAP CALCULATED FROM SURFACE VELOCITIES DERIVED FROM LANDSAT 7 ETM+ IMAGERY (1999-2010). FLUX GATE LOCATIONS ARE DENOTED ON FIGURE 5-1. NOTE: FLUX COULD ONLY BE CALCULATED FROM THE SOUTHERN ARMS (SA) OF BELCHER AND FITZROY GLACIERS. UNCERTAINTY (±) VALUE FOR EACH ESTIMATE IS PRESENTED AS SUPERSCRIPT. OVERALL MEAN DISCHARGE FOR DEVON ICE CAP IS NOT PRESENTED DUE TO MISSING DATA FROM PROMINENT GLACIERS OVER THIS TIME PERIOD. 123
TABLE 5-4: DYNAMIC DISCHARGE FOR DEVON ICE CAP CALCULATED FROM RADARSAT-2 DERIVED SURFACE ICE VELOCITIES. LOCATION OF FLUX GATES ARE DENOTED ON FIGURE 5-1. FLUX FROM BELCHER AND FITZROY GLACIERS ARE CALCULATED SEPARATELY FOR THE NORTHERN ARM (NA) AND SOUTHERN ARM (SA) OF EACH GLACIER. UNCERTAINTY (±) VALUE FOR EACH ESTIMATE IS PRESENTED AS SUPERSCRIPT. 124

LIST OF FIGURES

FIGURE 1-1: OVERVIEW OF THE MAJOR ICE MASSES OF THE CANADIAN HIGH ARCTIC (DENOTED BY GREEN SHADING) DISCUSSED BY THIS STUDY (1 = NORTHERN ELLESMERE ICEFIELD; 2 = AGASSIZ ICE CAP; 3 = PRINCE OF WALES ICEFIELD; 4 = MANSON ICEFIELD; 5 = SYDKAP ICE CAP; 6 = MÜELLER ICE CAP, 7 = STEACIE ICE CAP; 8 = DEVON ICE CAP; 9 = BYLOT ISLAND ICE CAP, 10 = BARNES ICE CAP; 11 = PENNY ICE CAP; 12 = COASTAL GLACIERS AND ICE CAPS OF BAFFIN ISLAND). 10

FIGURE 2-1: SURFACE VELOCITIES FOR: A) NORTHERN ELLESMERE ICEFIELD; B) AGASSIZ ICE CAP; C) PRINCE OF WALES ICEFIELD; D) MANSON ICEFIELD; E) SYDKAP ICE CAP; F) MÜLLER AND STEACIE ICE CAPS; G) DEVON ICE CAP. MAJOR ICE DIVIDES USED TO DETERMINE ERRORS DENOTED IN WHITE. NOTE DIFFERENCE IN VELOCITY SCALE BETWEEN IMAGES, ALTHOUGH ICE DISCHARGE SCALE REMAINS CONSTANT (BASE IMAGE: MODIS JULY 4TH, 2011). INSET MAP: STUDY SITE. 27

FIGURE 3-1: LOCATION OF THE MAJOR ICE MASSES OF BAFFIN AND BYLOT ISLANDS (SHOWN IN GREEN). BASE IMAGE: MODIS TERRA, JULY 2, 2011. DASHED BOXES INDICATE THE EXTENTS OF FIGURES 3-2 TO 3-4 49

FIGURE 3-2: SURFACE VELOCITY STRUCTURE OF A) BYLOT ISLAND ICE CAP AND B) AND THE COASTAL GLACIERS OF NORTHERN BAFFIN ISLAND. STANDALONE NUMBERS DENOTE GLACIER IDS PRESENTED IN TABLE 3-3. WHITE DASHED LINES AND STANDALONE LETTERS INDICATE THE LOCATION OF EXTRACTED CENTERLINE VELOCITIES PRESENTED IN FIGURE 3-5. BASE IMAGE: MODIS TERRA, JULY 2, 2011. 50

FIGURE 3-3: SURFACE VELOCITY STRUCTURE OF A) THE CENTRAL COASTAL GLACIERS OF BAFFIN ISLAND AND B) BARNES ICE CAP. STANDALONE NUMBERS DENOTE GLACIER IDS PRESENTED IN TABLE 3-3. WHITE DASHED LINES AND STANDALONE LETTERS INDICATE THE LOCATION OF EXTRACTED CENTERLINE VELOCITIES PRESENTED IN FIGURE 3-5. BASE IMAGE: MODIS TERRA, JULY 2, 2011. 51

FIGURE 3-4: SURFACE VELOCITY STRUCTURE OF (A) PENNY ICE CAP, (B) CENTRAL COASTAL GLACIERS AND (C) SOUTHEASTERN COASTAL GLACIERS ("**+**" INDICATES LOCATIONS OF IN SITU DGPS OBSERVATIONS AND CG/P NOTATIONS PROVIDE REFERENCE IDS REFERRED TO IN TABLE 3-2). STANDALONE NUMBERS DENOTE GLACIER IDS PRESENTED IN TABLE 3-3. WHITE DASHED LINES AND STANDALONE LETTERS INDICATE THE LOCATION OF EXTRACTED CENTERLINE VELOCITIES PRESENTED IN FIGURE 3-5. BASE IMAGE: MODIS TERRA, JULY 2, 2011. 52

FIGURE 3-5: SOLID LINES DENOTE CENTRELINE GLACIER VELOCITIES FOR SELECT GLACIERS ON BYLOT ISLAND ICE CAP (A-D), BARNES ICE CAP (E-F) AND PENNY ICE CAP (G-J). EXACT LOCATIONS OF EACH CENTRELINE ARE PRESENTED IN FIGURES 3-2 TO 3-4. DASHED LINES INDICATE THE SURFACE ELEVATION PROFILE OF EACH GLACIER AS EXTRACTED FROM THE 1:250 000 CANADIAN DIGITAL ELEVATION DATASET (CDED). 53

FIGURE 4-1: DISTRIBUTION OF DYNAMIC CHANGES AND VELOCITY CLASSIFICATION FOR MAJOR GLACIERS MEASURED IN THIS STUDY. "*" INDICATES GLACIERS WITH PREVIOUS VELOCITY MAPS DERIVED BY SHORT AND GRAY [2005], "^" DERIVED BY WILLIAMSON ET AL. [2008] AND "#" DERIVED BY COPLAND ET AL [2003A]. 89

FIGURE 4-2: COMPARISON OF NEAR TERMINUS GLACIER VELOCITIES DERIVED FROM FEATURE TRACKING OF SUMMER LANDSAT-7 IMAGERY ("ANNUAL" VELOCITIES: RED LINE) AND GLACIER VELOCITIES DERIVED FROM SPECKLE TRACKING OF WINTER RADARSAT IMAGERY ("WINTER" VELOCITIES": BLUE LINE), BLACK DASHED LINES INDICATE THE AVERAGE DIFFERENCE ACROSS THE FLUX GATE FOR A) ANTOINETTE GLACIER, B) TUBORG GLACIER, C) CANON GLACIER, D) CADOGAN GLACIER, E) OTTO GLACIER, F) WYKEHAM GLACIER, G) EKBLAW GLACIER. 90

FIGURE 4-3: TEMPORAL EVOLUTION (SLOW DOWN) OF CENTERLINE GLACIER SURFACE VELOCITIES FOR A) ANTOINETTE GLACIER, B) TUBORG GLACIER, C) EUGENIE GLACIER, D) ICEBERG GLACIER, E) MITTIE GLACIER, F) EKBLAW GLACIER, G) GOOD FRIDAY BAY GLACIER, H) MIDDLE GLACIER. WHERE AVAILABLE, SOLID BLACK LINE INDICATES GLACIER BED ELEVATION, DASHED BLACK LINE INDICATES SEA LEVEL (BOTH PLOTTED ON SECONDARY AXIS). NOTE: VELOCITY PROFILES THAT SPAN MORE THAN ONE YEAR REPRESENT DISPLACEMENTS DERIVED FROM FEATURE TRACKING (I.E., "ANNUAL VELOCITIES") AND PROFILES PLOTTED FOR A SINGLE YEAR REPRESENT DISPLACEMENTS DERIVED FROM SPECKLE TRACKING (I.E., "WINTER VELOCITIES"). 91

FIGURE 4-4: TEMPORAL EVOLUTION OF CENTERLINE GLACIER SURFACE VELOCITIES FOR A) DOBBIN GLACIER, B) CAÑON GLACIER, C) PARRISH GLACIER, D) SYDKAP GLACIER, E) CHAPMAN GLACIER, F) OTTO GLACIER. WHERE AVAILABLE, SOLID BLACK LINE INDICATES GLACIER BED ELEVATION, DASHED BLACK LINE INDICATES SEA LEVEL (BOTH PLOTTED ON SECONDARY AXIS). NOTE: VELOCITY PROFILES THAT SPAN MORE THAN ONE YEAR REPRESENT DISPLACEMENTS DERIVED FROM FEATURE TRACKING (I.E., "ANNUAL VELOCITIES") AND PROFILES PLOTTED FOR A SINGLE YEAR REPRESENT DISPLACEMENTS DERIVED FROM SPECKLE TRACKING (I.E., "WINTER VELOCITIES"). 92

FIGURE 4-5: TEMPORAL EVOLUTION (SPEED-UP) OF CENTERLINE GLACIER SURFACE VELOCITIES FOR A) WYKEHAM GLACIER, B) TRINITY GLACIER, BOTH OF PRINCE OF WALES ICEFIELD. SOLID BLACK LINE INDICATES GLACIER BED ELEVATION, DASHED BLACK LINE INDICATES SEA LEVEL (BOTH PLOTTED ON SECONDARY AXIS). NOTE: VELOCITY PROFILES THAT SPAN MORE THAN ONE YEAR REPRESENT DISPLACEMENTS DERIVED FROM FEATURE TRACKING (I.E., "ANNUAL VELOCITIES") AND

profiles plotted for a single year represent displacements derived from speckle tracking (i.e., "winter velocities").....93
Figure 4-6: a) Patterns of annual surface ice velocity extracted every 500 m along the centreline of Dobbin Glacier, b) patterns of surface ice velocity difference along the centreline of Dobbin Glacier c) surface elevation and bed profile of Dobbin Glacier (black dashed line indicates sea level), d) change in centreline ice thickness profiles between 2000 (derived by Dowdeswell et al. [2004]) and 2014 (derived by NASA Operation Icebridge MCoRDS sensor) for Dobbin Glacier, background image: ASTER scene acquired June 11, 2012 (for Figures 4-6a,b,d: solid red lines indicate the location where the bed descends below sea level, dashed red line indicates sill location).....94
Figure 4-7: a) Patterns of annual surface ice velocity extracted every 500 m along the centreline of Parrish Glacier, b) patterns of surface ice velocity difference along the centreline of Parrish Glacier c) surface elevation and bed profile of Parrish Glacier (black dashed line indicates sea level), d)) change in centreline ice thickness profiles between 2000 (derived by Dowdeswell et al. [2004]) and 2014 (derived by NASA Operation Icebridge MCoRDS sensor) for Parrish Glacier, background image: ASTER scene acquired August 4, 2013 (for Figures 4-7a,b,d: solid red lines indicate the location where the bed descends below sea level, dashed red line indicates sill location).....95
Figure 4-8: a) Patterns of annual surface ice velocity extracted every 500 m along the centreline of Trinity Glacier, b) patterns of surface ice velocity difference along the centreline of Trinity Glacier c) surface elevation and bed profile of Trinity Glacier (black dashed line indicates sea level), d) surface elevation change from 2008 (SPOT DEM) and 2014 NASA Operation Icebridge ATM data for Trinity Glacier, background image: Landsat-8 scene acquired Sept 7, 2014 (for Figures 4-8a, b, d: solid red lines indicate the location where the bed descends below sea level).....96
Figure 4-9: Distribution of glaciers identified as "surge", "pulse" and "consistent acceleration" across the QEI. 97
Figure 5-1: Devon Ice Cap velocity structure derived from speckle tracking of Radarsat-2 Wide Fine imagery acquired in winter 2015. Red on white lines indicate locations of flux gates used to determine dynamic discharge estimates in Figure 5-2; black dashed lines indicate locations of centerline velocities shown in Figures 5-3, 5-4 and 5-5; Dark grey areas on inset map indicate glaciated terrain in the Canadian High Arctic.....125
Figure 5-2: Comparison of near terminus velocities at flux gates (see Figure 5-1 for location) derived from feature tracking (red line) and speckle tracking (blue line) for: a) Belcher Glacier, b) North Croker Bay Glacier, c) South Croker Bay Glacier, d) Sverdrup Glacier, e) Fitzroy Glacier, f) Eastern Glacier. Dashed lines indicate mean percent difference between feature tracking and speckle tracking velocities across each terminus flux gate.....126
Figure 5-3: For the centrelines of Belcher (location denoted as BL-BL' on Figure 5-1), Fitzroy (location denoted as FZ-FZ' on Figure 5-1), Southeast-1 (location denoted as SE1-SE1' on Figure 5-1) and Southeast-2 (location denoted as SE2-SE2' on Figure 5-1) glaciers, respectively: (a-d) Surface velocities from 1999-2010 derived from feature tracking; (e-h) Surface velocities from 2009-2015 derived from speckle tracking; (i-l) Surface velocities from 1999-2015 derived from both feature tracking and speckle tracking; (m-p) Bed and surface elevation profiles. Solid black lines denote the location where the glacier bed descends below sea level, red dashed lines indicate basal topographic features that influence ice motion for glaciers described in text.....127
Figure 5-4: For the centrelines of Sverdrup (location denoted as SV-SV' on Figure 5-1), Eastern (location denoted as ES-ES' on Figure 5-1), North Croker Bay (location denoted as NCB-NCB' on Figure 5-1) and South Croker Bay (location denoted as SCB-SCB' on Figure 5-1) glaciers, respectively: (a-d) Surface velocities from 1999-2010 derived from feature tracking; (e-h) Surface velocities from 2009-2015 derived from speckle tracking; (i-l) Surface velocities from 1999-2015 derived from both feature tracking and speckle tracking; (m-p) Bed and surface elevation profiles. Solid black lines indication where the glacier bed descends below sea level.....128
Figure 5-5: For the centrelines of East-5 (location denoted as E5-E5' on Figure 5-1), East-6 (location denoted as E6-E6' on Figure 5-1) and East-7 (location denoted as E7-E7' on Figure 5-1) glaciers, respectively: (a-c) Surface velocities from 2009-2015 derived from speckle tracking; (d-f) Surface velocities from 1999-2015 derived from both feature tracking and speckle tracking; (g-i) Bed and surface elevation profiles. Solid black lines indicate the location where the glacier bed descends below

SEA LEVEL, RED DASHED LINES INDICATE BASAL TOPOGRAPHIC FEATURES THAT INFLUENCE ICE MOTION FOR GLACIERS DESCRIBED IN TEXT.....129
FIGURE 5-6: FLOW REGIME MAP OF DEVON ICE CAP, "*" INDICATES AREAS CLASSIFIED AS FLOW REGIMES DIFFERENT FROM THOSE DERIVED BY BURGESS ET AL. [2005].....130

LIST OF ACRONYMS

ALOS	Advanced Land Observation Satellite
ASF	Alaska Satellite Facility
ASL	Above Sea Level
ASTER	Advanced Spaceborne Thermal Emission and Reflection Radiometer
ATM	Airborne Topographic Mapping
CAA	Canadian Arctic Archipelago
CDED	Canadian Digital Elevation Dataset
CEOS	Committee on Earth Observations Satellites
DIC	Devon Ice Cap
dGPS	differential Global Positioning System
ELA	Equilibrium Line Altitude
ERS	European Remote Sensing Satellite
ESS	Earth Science Sector
ETM	Enhanced Thematic Mapper
FR	Flow Regime
GIC	Glaciers and Ice Caps
GIS	Geographic Information System
GLIMS	Global Land Ice Measurements from Space
IDW	Inverse Distance Weighting
MCoRDS	Multichannel Coherent RADAR Depth Sounder
MODIS	Moderate-Resolution Imaging Spectroradiometer
NASA	National Aeronautics and Space Administration
NCAA	Northern Canadian Arctic Archipelago
NERC	Natural Environment Research Council
NRCan	Natural Resources Canada
NSERC	National Science and Engineering Research Council
NSIDC	National Snow and Ice Data Center
OIB	Operation IceBridge
OLI	Operational Land Imager
PALSAR	Phased Array type L-band Synthetic Aperture RADAR
POW	Prince of Wales
QEI	Queen Elizabeth Islands
RACMO	Regional Atmospheric Climate Model
RADAR	Radio Detection and Ranging
RGI	Randolph Glacier Inventory
SAR	Synthetic Aperture RADAR
SCAA	Southern Canadian Arctic Archipelago
SLC	Single Look Complex
SPRI	Scott Polar Research Institute
USGS	United States Geological Survey
UTM	University Transverse Mercator

ACKNOWLEDGEMENTS

This thesis would not have been possible without the help and guidance of many people and organizations. I thank my supervisors, Dr. Luke Copland of the Laboratory of Cryospheric Research (LCR) and Dr. David Burgess of the National Glaciology Program (NRCan), for their guidance, patience, and meticulous reviews of my work throughout this endeavour. This work would not have been possible without the tremendous support I have received from my supervisors. I also thank my committee members, Dr. M. Sawada, Dr. A. Viau and Dr. L. Gray for their advice and guidance throughout my Ph.D. program. I would especially like to thank Dr. Gray for allowing me the opportunity to use his speckle-tracking code throughout my post-graduate work. I gratefully acknowledge Dr. Martin Sharp for his insights throughout this project and thank him for his willingness to share data with me that helped improve this thesis. Additionally, I thank C. Mortimer, B. Danielson and J. Davis of the Arctic and Alpine Research Group, University of Alberta for sharing data or insights during this project. I also thank Naomi Short of the Canada Centre for Remote Sensing who helped guide me through the complexities of GAMMA interferometry and for helpful reviews of my work. I gratefully acknowledge T. Benham and J. Dowdeswell of the Scott Polar Research Institute and NASA's Operation IceBridge (especially J. Sonntag) for collecting and sharing the ice thickness measurements across the Canadian Arctic necessary to complete this work. Additionally, I thank A. Gardner of the Jet Propulsion Laboratory and J. Lenaerts (Utrecht University) for providing modelled mass balance data across the Canadian Arctic. I would also like to extend a special thank you to Dr. B. Alt for her excellent support during my comprehensive examinations. I would also like to thank all the members (both past and present) of the Laboratory for Cryospheric Research for their friendship throughout this process (a special thank you to Johannes Tyler de Jong for aiding during fieldwork and for helping me keep my sanity). Finally, this work would not have been possible without the love and support of my family and, especially, my wife. Amanda, thank you for your love and support throughout this journey.

I gratefully acknowledge and appreciate financial funding in support of this project from the following organizations: Natural Sciences and Engineering Research Council of Canada - Alexander Graham Bell Canada Graduate Scholarship and Discovery Grants; the Ontario Graduate Scholarship; Transport Canada – Network of Expertise for Transportation in Arctic

Waters; the Canada Foundation for Innovation; Natural Resources Canada – the Polar Continental Shelf Program; Canadian Polar Commission – Northern Scientific Training Program; the National Research Council of Canada; the International Arctic Science Committee – Network on Arctic Glaciology; ArcticNet; Cryo-Ex and Glacio-Ex Exchange Programs (University of Ottawa & University of Oslo); the Field Workshop on Studies of Tidewater Glaciers – Polish Academy of Science; the Technical University of Denmark; International Workshop on Calving; International Association of Cryospheric Sciences – Cryosphere Working Group; Stability and Variations of Arctic Land Ice (SVALI) - Nordic Centre of Excellence; Ambassade de France au Canada – the France-Alberta Science and Technology Initiative; the University of Alberta; the University Centre in Svalbard; the Transatlantic Science Week – Royal Norwegian Embassy to Canada; the Faculty of Graduate and Post-Doctoral Studies (University of Ottawa); and the University of Ottawa.

CHAPTER ONE: Introduction

1.1 Introduction

The Canadian Arctic contains ~146 000 km^2 of terrestrial ice (Figure 1-1), making it the largest glaciated region outside of the ice sheets, and potentially a large contributor to global sea level rise [Sharp et al. 2014]. Mass balance measurements in the Canadian Arctic began in the late-1950s to early-1960s at four monitoring sites (White Glacier, Axel Heiberg Island; Meighen Ice Cap, Meighen Island; Melville Ice Cap, Melville Island; Sverdrup Glacier, Devon Ice Cap), providing an approximately 50 year record of in situ observations [Koerner 2005; Sharp et al. 2011]. This record shows that prior to the late 1980s, the ice masses of the Canadian High Arctic were largely in balance. However, glacier mass balances became negative in the mid-1990s, and have been acutely negative for most years since 2005 (e.g., mass loss from 2005-2009 was nearly five times more negative than the 1963-2004 average) [Koerner 2005; Mair et al. 2009; Sharp et al. 2011]. Mass loss determined from satellite gravimetry over the Canadian Arctic Archipelago from 2007-2009 indicated that the region was the largest contributor to sea level rise outside of the ice sheets over that period [Gardner et al. 2011].

The combination of long-term in situ observations, remote sensing methods and modeling techniques [Gardner et al. 2011; Sharp et al. 2011; Koerner 2005] has meant that the glacier mass balance components due to snow accumulation and surface melt within the Canadian High Arctic have been relatively well constrained. However, much less well known has been the component of glacier mass loss due to dynamic (iceberg) discharge. The major hindrances to quantifying dynamic discharge for the Canadian Arctic has been the lack of remote sensing data required for mapping regional surface velocities, and the paucity of ice thickness measurements at the fronts of tidewater glaciers. Indeed, the lack of remote sensing data has meant that fundamental knowledge of glacier dynamics for large portions of the Canadian Arctic have largely been unknown, and as a consequence, our ability to accurately resolve and partition total mass losses from the glaciers and ice caps of the Canadian High Arctic has been restricted. Knowledge of glacier dynamics is also crucial for understanding and predicting the response of glaciers to climate change, as changes in glacier motion have been identified as a possible mechanism of rapid mass loss from ice caps and ice sheets which could lead to rapid increases in global sea level over short periods of time [Alley et al. 2005].

1.2 Background

Research on glacier dynamics within the Canadian Arctic began in the 1960s, with studies at this time being the first to determine that ice motion within the region varied on both inter- and intra-annual time scales. For example, Cress and Wyness [1961] used repeated surveys of a series of stakes on the surface of Sverdrup Glacier, Devon Ice Cap, to determine that ice motion increased after the onset of surface melt, establishing the first connection between supraglacial hydrology and seasonal changes in ice motion within the region. Similarly, Müller and Iken [1973] investigated the links between ice motion, surface ablation and the subglacial drainage network of White Glacier, Axel Heiberg Island and found that surface velocities increased by ~70% over winter velocities during marked increases in surface melt in the summer. This research further established the link between supraglacial hydrology and seasonality of glacier motion in the Canadian Arctic and speculated on the importance of the evolution of the subglacial drainage network (e.g. an inefficient distributed system transitioning to a highly efficient channelized system as the melt season progresses) on variable responses of ice motion to water inputs throughout the summer season. Hattersley-Smith [1969] and Müller [1969] identified the Otto and Good Friday Bay Glaciers as "surge-type" in the late 1960s, providing the first evidence that glacier dynamics within the Canadian Arctic also varied on multi-annual time scales. Similarly, Løken [1969] and Holdsworth [1973; 1977] used evidence of changes in surface geometry to identify three regions on Barnes Ice Cap where past surge activity likely occurred. Together, these studies demonstrate that multi-annual variations in ice dynamics occur on ice masses located across the entire Canadian Arctic.

These early studies of ice dynamics within the Canadian Arctic were often limited in both their spatial and temporal scope, with most studies only presenting data from a single field season or inferring glacier dynamics based on geomorphological evidence (e.g., changes in terminus positions, looped moraines). In the early 2000s, longer term studies were undertaken that focused on the external processes that drive variations in glacier dynamics within the Canadian Arctic. For example, Bingham et al. [2003], Boon and Sharp [2003], Copland et al. [2003a], Danielson and Sharp [2013], and Wyatt and Sharp [2015] all further established the link between enhanced glacier motion and the onset and drainage of surface melt. At the same time, as remote sensing imagery became more widely available, the first regional studies of glacier motion within the Canadian Arctic were undertaken. For example, Copland et al. [2003b] compared surface

features in Landsat-7 imagery from 1999/2000 with aerial photography from 1959/1960 to create the first inventory of surge-type glaciers within the Canadian Arctic. They also used utilized automated tracking algorithms on pairs of Landsat-7 images to determine surface motion of up to ~1000 m a^{-1} on Mittie Glacier (Manson Icefield) between summer 1999 and 2000. Similarly, Williamson et al. [2008] applied a feature tracking algorithm on Landsat-7 imagery acquired over eight glaciers on Agassiz and Northern Ellesmere Ice Caps in the early 2000s to determine their baseline glacier velocities and iceberg discharge rates.

Short and Gray [2004] was the first study to show the utility of synthetic aperture radar (SAR) imagery to determine glacier dynamics within the Canadian Arctic. This study used a "speckle-tracking" algorithm to determine accurate displacements between subsequent pairs of RADARSAT-1 imagery acquired on the same orbital path. Short and Gray [2005] expanded on this work to produce glacier velocities and estimates of dynamic discharge for 11 glaciers located on Axel Heiberg and Ellesmere Islands. Burgess et al. [2005] used interferometry on ERS-1/2 data (acquired in the mid-1990s) and speckle tracking of RADARSAT-1 imagery (acquired in 2000) over Devon Ice Cap to produce the first velocity map and estimate of iceberg discharge at the scale of an entire ice mass within the Canadian Arctic. Van Wychen et al. [2012] updated the work of Burgess et al. [2005] by utilizing speckle-tracking of RADARSAT-2 imagery acquired in March 2009 to expand the surface velocity map of Devon Ice Cap and update the iceberg discharge rate for the ice mass.

Despite the widespread increase in the availability of remote sensing datasets within the Canadian Arctic over the past decade, glacier dynamics over large portions of the Canadian Arctic have remained unresolved, particularly away from large outlet glaciers. This thesis addresses this fundamental knowledge gap by providing the first regional velocity mapping and estimate of dynamic discharge for all of the ice masses of the Canadian Arctic. This includes the creation of a ~10-15 year record of glacier velocities, the longest to date for this region, to resolve how glacier motion varies both spatially and temporally, and the use of auxiliary datasets (e.g., ice thickness, bed profiles, surface altimetry) to investigate the controls on this variability. Additionally, this thesis compares mass loss via dynamics to mass loss via surface mass balance to determine the relative importance of iceberg calving as a mass loss term within the Canadian Arctic. Taken together, this study provides the most comprehensive record of glacier dynamics

within the Canadian Arctic to date, and provides important insights into how and why glacier motion within this region evolves over time.

1.3 Purpose

The purpose of this thesis is to address the current lack of knowledge regarding regional scale glacier dynamics in the Canadian Arctic and how they vary over time. The major objectives are to:

i. Produce the first measurement of glacier surface motion for the entire glaciated region of the Canadian Arctic.
ii. Develop a long term (~10-15 year) record of surface velocities to determine whether, and how, glacier motion evolves spatially and temporally across the region.
iii. Quantify rates and variability of glacier dynamic discharge (iceberg calving) for the entire Canadian Arctic.

Most measurements are derived from satellite remote sensing, with verification provided by ground-based differential Global Positioning System (dGPS) instruments where available. The results of this research are of direct interest to government agencies (e.g., to allow for the total mass balance of Canadian Arctic glaciers to be constrained by Natural Resources Canada), industry (e.g., to provide bulk estimates and point sources of iceberg hazards for shipping) and academia (e.g., to provide insights into the drivers and controls of glacier dynamics). In addition, the methodology of glacier motion monitoring utilized here provides a framework for the implementation for a large-scale, continuous glacier velocity-monitoring program for the Canadian Arctic.

1.4 Research Objectives and Thesis Organization

This thesis is written in article format. All chapters are related to the common theme of increasing the spatial and temporal knowledge of the glacier dynamics and estimates of mass loss via iceberg discharge in the Canadian Arctic, but each chapter addresses distinct objectives as described below (abstracts and acknowledgements are included for each individual chapter).

Objective 1. Determine regional baseline measurements of glacier velocities and estimates of mass loss via dynamic discharge for the ice masses of the Queen Elizabeth Islands.

Chapter 2 provides the first maps of surface ice motion and estimates of mass loss via dynamic discharge for all the ice masses of the Queen Elizabeth Islands (Devon, Ellesmere and Axel Heiberg Islands). The major objectives of the paper are to determine the spatial velocity structure of the study region, determine maximum surface ice motion rates within the Canadian Arctic and establish which glaciers are the major contributors to dynamic discharge. Another major focus of this chapter is to quantify the relative importance of mass loss via dynamic discharge as a regional mass loss component (e.g., compared with surface melt and runoff). Chapter 2 concludes by comparing the mass loss via dynamic discharge for the Canadian Arctic with other Arctic regions. This chapter has been published in *Geophysical Research Letters* as (and is reproduced here with permission):

Van Wychen, W., D. O. Burgess, L. Gray, L. Copland, M. Sharp, J. A. Dowdeswell, and T. J. Benham, (2014), Glacier velocities and dynamic ice discharge from the Queen Elizabeth Islands, Nunavut, Canada, *Geophysical Research Letters*, 41, doi: 10.1002/2013GL058558.

Objective 2. Determine regional baseline measurements of glacier velocities and estimates of mass loss via dynamic discharge for the ice masses of Baffin and Bylot Islands

Chapter 3 provides the first regional map of glacier dynamics and estimates of mass loss via dynamic discharge for the ice masses of Baffin and Bylot Islands. Major findings from this research include the downward revision of previous regional mass loss estimates via iceberg discharge for the southern Canadian Arctic and further confirmation that mass loss in the Canadian Arctic is currently dominated by surface melt and runoff. The velocity mapping completed for this study can be utilized as inputs to glacier flow models and provides a baseline against which future changes in glacier dynamics in this region can be detected. This chapter has been published in the *Canadian Journal of Earth Sciences* as (and is reproduced here with permission):

Van Wychen, W., L. Copland, D.O. Burgess, L. Gray and N. Schaffer, (2015). Glacier velocities and dynamic discharge from the ice masses of Baffin and Bylot Islands, Nunavut, Canada. *Canadian Journal of Earth Sciences*, doi: 0.1139/cjes-2015-0087.

Objective 3. Determine and characterize variations in glacier dynamics for the ice masses of Ellesmere and Axel Heiberg Islands.

Chapter 4 uses a ~10-15 year record of glacier velocities for the major tidewater glaciers of Axel Heiberg and Ellesmere Islands to determine the spatial and temporal variability in ice motion there. A major finding is the distinction between “surge-type” and “pulse-type” glacier dynamic

behavior, where “surge-type” glaciers experience velocity variability along large sections of their length, while velocity variability on “pulse-type” glaciers is largely restricted to their lower regions where the bed is grounded below sea level. Another major contribution is the identification that Trinity and Wykeham Glaciers have accelerated dramatically since the early 2000s and that the speed-up of these two glaciers cannot be explained in terms of “surging” or “pulsing” mechanisms, meaning that external forcing must be driving the observed change. As a consequence these two glaciers are now the largest source of iceberg discharge for the Canadian Arctic and account for ~62% of total mass loss via dynamic discharge for the ice masses of Axel Heiberg and Ellesmere Islands. This manuscript has been submitted to the *Journal of Geophysical Research: Earth Surface* as:

Van Wychen, W., J. Davis, D.O. Burgess, L. Copland, L. Gray, M. Sharp, C. Mortimer, (*submitted Aug 26, 2015*) Characterizing inter-annual variability of glacier dynamics (1999-2015) and dynamic discharg*e* (2000, 2011-2015) for the ice masses of Ellesmere and Axel Heiberg Islands, Nunavut, Canada, submitted to Journal of Geophysical Research - Earth Surface, (manuscript number: 2015JF003708).

Objective 4. Investigate the spatial and temporal variability of ice motion for Devon Ice Cap and examine the controls on this variability.

Chapter 5 determines the spatial and temporal variability in dynamics of the major outlet glaciers on Devon Ice Cap. This is accomplished by combining a ~10 year record of surface velocities derived from feature tracking of Landsat-7 ETM+ imagery with a ~6 year record of surface velocities derived from speckle tracking of RADARSAT-2 imagery. Measurements of basal topography are compared with areas of velocity variability to determine dominant basal features that influence glacier dynamics. Major contributions from this work include the determination that glacier dynamic variability on Devon Ice Cap is much more extensive than previously reported, a 5-year record of mass loss via dynamic discharge, and updated and expanded flow regime mapping. This manuscript has been prepared for submission to the *Journal of Glaciology* as:

Van Wychen, W., J. Davis, D.O. Burgess, L. Copland, L. Gray, M. Sharp, , J. Dowdeswell, and T. Benham (*in prep*) *Variability in ice motion and dynamic discharge from Devon Ice Cap*, Nunavut, Canada.

1.5 Authorship and Co-author Contributions

I am the primary author of the four chapters presented in this thesis and am responsible for the design of the research methodology, the collection, archiving and processing of all RADAR imagery and the writing of the manuscripts. All of the analysis presented here was created with original ideas from me with guidance provided by my supervisors. Laurence Gray is a co-author on all chapters in recognition for providing the original speckle-tracking algorithm from which my results were generated. Jamie Davis is a co-author on Chapter 4 and Chapter 5 for deriving the original Landsat-7 feature tracking datasets utilized in those manuscripts, and Martin Sharp and Colleen Mortimer are co-authors on those chapters in recognition of their help in facilitating data exchange. Julian Dowdeswell and Toby Benham are credited as co-authors on Chapters 2 in recognition for their sharing of ice thickness datasets over the Canadian Arctic, which was used to augment the work presented in those chapters. Finally, the published chapters (Chapter 2 and Chapter 3) also incorporate suggestions from anonymous reviewers and journal editors. All ideas and analysis presented within this thesis are my own with input, edits and collaboration from my supervisors, co-authors and anonymous reviewers.

1.6 References:

Alley, R.B., P.U. Clark, P. Huybrechts, I. Joughin, (2005), Ice-sheet and sea-level changes, *Science*, 310(5747): 456-460. doi: 10.1126/sciences.1114613.

Bingham, R., P. Nienow, and M. Sharp, (2003), Intra-annual and intra-seasonal flow dynamics of a High Arctic polythermal valley glacier, *Annals of Glaciology, 37, 181-188.*

Boon, S., and M. Sharp, (2003), The role of hydrologically-driven ice fracture in drainage system evolution on an Arctic glacier, *Geophysical Research Letters*, 30, doi:10.1029/2003GL018034.

Burgess, D. O., M. Sharp, D.W.F. Mair, J.A. Dowdeswell, and T.J. Benham, (2005), Flow dynamics and iceberg calving rates of Devon Ice Cap, Nunavut, Canada, *Journal of Glaciology*, 51, 173, 219 - 230.

Copland, L., M. Sharp, and P. Nienow, (2003a), Links between short-term velocity variations and the subglacial hydrology of a polythermal glacier, *Journal of Glaciology*, 49, 407-414.

Copland, L., M. Sharp, and J.A. Dowdeswell, (2003b), The distribution and flow characteristics of surge-type glaciers in the Canadian High Arctic, *Annals of Glaciology*, 36, 73-81.

Cress, P. and R., Wyness, (1961), The Devon Island expedition, observations of glacial movements, *Arctic*, 14(4), 257–259.

Danielson, B., and M. Sharp, (2013), Development and application of a time-lapse photograph analysis method to investigate the link between tidewater glacier flow variations and supraglacial drainage events, *Journal of Glaciology*, 59, 287-302.

Gardner, A. S., M. Moholdt, B. Wouters, G.J. Wolken, D.O. Burgess, M. Sharp, J.G. Cogley, C. Braun and C. Labine, (2011), Sharply increased mass loss from glaciers and ice caps in the Canadian Arctic Archipelago, *Nature*, 473(7347), 357–360, doi: 10.1038/nature10089.

Hattersley-Smith, G., (1969), Recent Observations on the surging of Otto Glacier, Ellesmere Island, *Canadian Journal of Earth Sciences*, 6(4),883–889.

Holdsworth, G., (1973), Evidence of a surge on Barnes Ice Cap, Baffin Island, *Canadian Journal of Earth Sciences*, 10, 1565-1574.

Holdsworth, G., (1977), Surging activity on the Barnes Ice Cap, Nature, 269, 588-590.

Koerner, R.M., (2005), Mass balance of glaciers in the Queen Elizabeth Islands, Nunavut, Canada, *Annals of Glaciology*, 42, 417–423. doi: 10.3189/172756405781813122

Løken, O. H., (1969), Evidence of surges on the Barnes Ice Cap, Baffin Island, *Canadian*

Journal of Earth Sciences, 6, 899-901.

Mair, D., D.O. Burgess, M. Sharp, J.A. Dowdeswell, T. J. Benham, S. Marshall and F. Cawkwell, (2009), Mass balance of the Prince of Wales Icefield, Ellesmere Island, Nunavut, Canada. *Journal of Geophysical Research*, 114, F02011. doi: 10.1029/2008JF001082

Müller, F., (1969), Was the Good Friday Glacier on Axel Heiberg Island surging?, *Canadian Journal of Earth Sciences*, 6(4), 891–894, doi:10.1139/e69-091.

Müller, F., and A. Iken, (1973), Velocity fluctuations and water regime of Arctic valley glaciers, *International Association of Scientific Hydrology Publication*, (95): 165–182.

Sharp, M., Burgess, D.O., Cawkwell, F., Copland, L., Davis, J.A., Dowdeswell, E.K., Dowdeswell, J.A., Gardner, A.S., Mair, D., Wang, L., Williamson, S.N., Wolken, G. J. and Wyatt, F., (2014), Remote sensing of recent glacier changes in the Canadian Arctic. In: Kargel, J.S., Leonard, G.J., Bishop, M.P., Kääb, A. and Raup, B.H. (eds). *Global Land Ice Measurements from Space*, Ch. 9, pp. 205-228. Praxis-Springer. doi: 10.1007/978-3-540-79818-7_9.

Short, N. H. and A. L. Gray, (2004), Potential for RADARSAT-2 interferometry: glacier monitoring using speckle tracking, *Canadian Journal of Remote Sensing*, 30(3), 504-509.

Short, N. H. and A.L. Gray, (2005), Glacier dynamics in the Canadian High Arctic from RADARSAT-1 speckle tracking, *Canadian Journal of Remote Sensing*, 31(3), 225–239.

Van Wychen, W., L. Copland, L. Gray, D. O. Burgess, B. Danielson, M. Sharp, (2012), Spatial and temporal variation of ice motion and ice flux from Devon Ice Cap, Nunavut, Canada. *Journal of Glaciology*, 58(210), 657–664. doi: 10.3189/2012JoG11J164.

Williamson, S., M. Sharp, J. Dowdeswell, and T. Benham, (2008), Iceberg calving rates from northern Ellesmere Island ice caps, Canadian Arctic, 1999-2003, *Journal of Glaciology*, 54(186), 391-400.doi: 10.3189/002214308785837048.

Wyatt, F. and M. Sharp, (2015), Linking surface hydrology to flow regimes and patterns of velocity variability of the Devon Ice Cap, Nunavut, *Journal of Glaciology*, 61: 387-399.

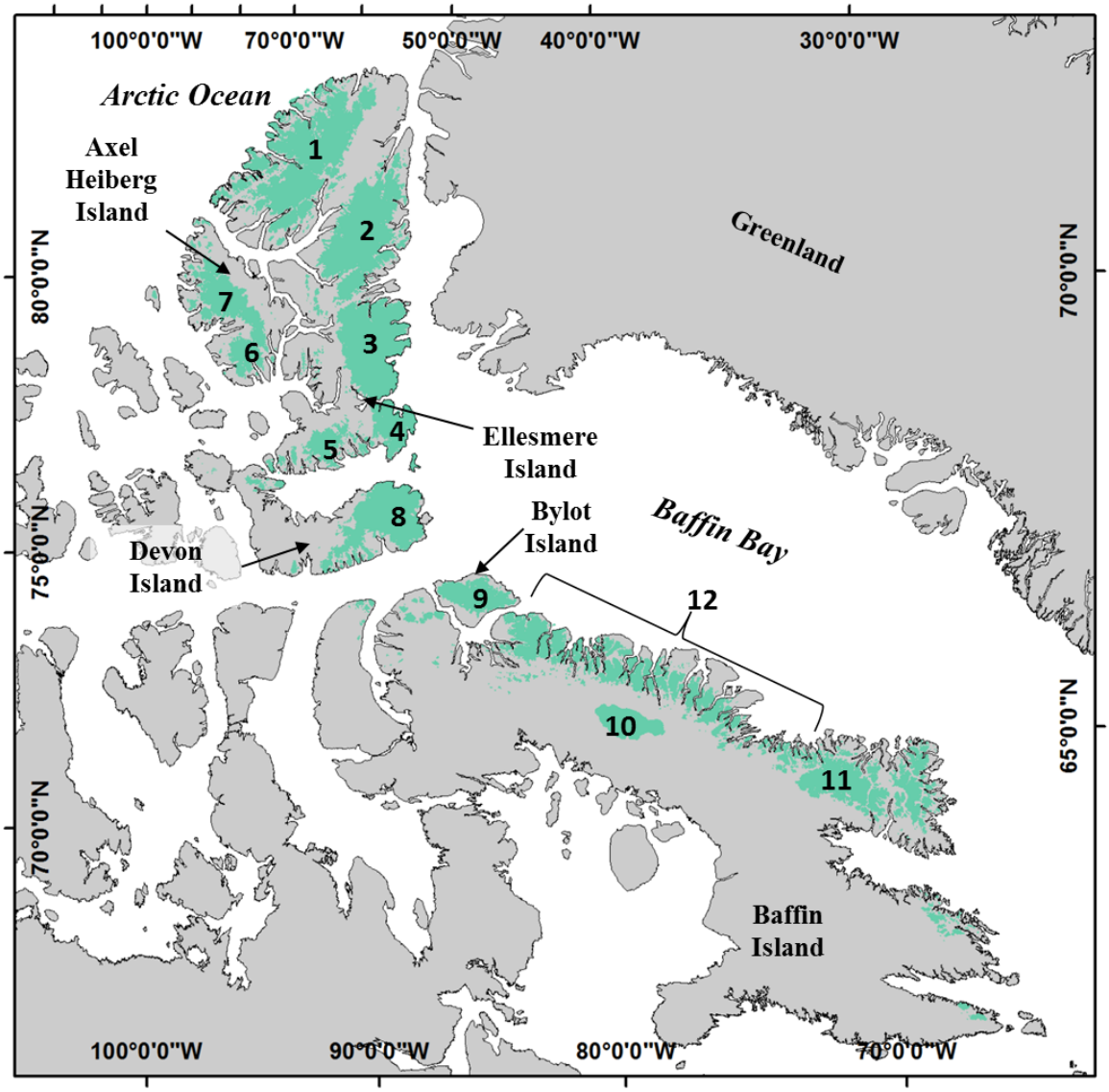

Figure 1-1: Overview of the major ice masses of the Canadian High Arctic (denoted by green shading) discussed in this study (1 = Northern Ellesmere Icefield; 2 = Agassiz Ice Cap; 3 = Prince of Wales Icefield; 4 = Manson Icefield; 5 = Sydkap Ice Cap; 6 = Müller Ice Cap, 7 = Steacie Ice Cap; 8 = Devon Ice Cap; 9 = Bylot Island Ice Cap, 10 = Barnes Ice Cap; 11 = Penny Ice Cap; 12 = Coastal Glaciers and Ice Caps of Baffin Island).

CHAPTER TWO: Glacier velocities and dynamic ice discharge from the Queen Elizabeth Islands, Nunavut, Canada

Abstract:

Recent studies indicate an increase in glacier mass loss from the Canadian Arctic Archipelago as a result of warmer summer air temperatures [Gardner et al. 2011]. However, no complete assessment of dynamic ice discharge from this region exists. We present the first comprehensive surface velocity mapping of all ice masses within the Queen Elizabeth Islands, and show that these ice masses discharged ~2.6 ± 0.8 Gt a^{-1} of ice to the oceans in winter 2012 with ~50% of total dynamic discharge channelled through Trinity and Wykeham Glaciers alone (no known surges in 2012). Dynamic discharge of Mittie Glacier varied between 0.90 ± 0.09 Gt a^{-1} during its 2003 surge and 0.02 ± 0.02 Gt a^{-1} during its 2012 quiescence, highlighting the importance of surge-type glaciers for inter-annual variability in regional mass loss. Queen Elizabeth Islands glaciers currently account for ~7% of reported dynamic discharge from Arctic ice masses outside Greenland.

2.1 Introduction and Study Area

The Queen Elizabeth Islands (QEI; Devon, Ellesmere and Axel Heiberg Islands; Fig 2-1 inset) contain ~104,000 km^2 of glacier ice, which represents 25% of Arctic glacier ice outside the Greenland Ice Sheet [Arendt et al. 2012]. Long-term surface mass balance records from this region indicate that prior to the late 1980s the ice masses were largely in balance [Koerner, 2005; Mair et al. 2009; Sharp et al. 2011]. Since the late 1980s however, and especially since 2005, changing summer atmospheric circulation patterns have increased advection of warm air from the northwest Atlantic to the Canadian High Arctic, leading to increased surface melt, longer melt seasons and increased anti-cyclonic air circulation over the QEI in summer [Gardner et al. 2011; Sharp et al. 2011; Lenaerts et al. 2013]. As a consequence, ice loss via surface mass balance has increased sharply in recent years (averaging -7 ± 18 Gt a^{-1} between 2004-2006, and -61 ± 18 Gt a^{-1} between 2007-2009 for the QEI) [Gardner et al. 2011]. However, little is known about the importance of dynamic discharge as a mechanism of mass loss from the QEI. This study provides the first complete mapping of surface motion for all ice masses of the QEI and combines this with estimates of ice thickness of tidewater terminating glaciers to estimate dynamic ice discharge to the ocean. Here we define dynamic ice discharge as the mass of ice passing through a terminus flux gate (also called iceberg flux in some studies); we do not account for the effects on dynamic ice discharge of terminus advance or retreat.

2.2 Methods

2.2.1 Determination of Surface Motion

Ice surface motion was determined using a custom written MATLAB™ speckle-tracking algorithm on RADARSAT-2 fine beam (resolution; ~8 x 8 m) and ultrafine beam (resolution; ~3 x 3 m) imagery acquired in 24-day pairs between January and May 2012 (Table 2-1). This algorithm tracks the relative displacement of small image chips using a two-dimensional cross-correlation algorithm on accurately co-registered (co-registration completed using an area cross-correlation technique; Gray et al. [2001]) RADARSAT-2 image pairs, and has proven effective for measuring surface ice displacements at the ice cap scale within the Canadian High Arctic [Short and Gray, 2004, 2005; Van Wychen et al. 2012]. Image acquisitions were restricted to mid- to late-winter due to the requirement for good coherence (e.g., little surface melt or snowfall) between scenes. Displacements were determined in both azimuth and range directions

using chip sizes of ~450 m in azimuth and ~350 m in range for fine beam imagery and ~150 m in azimuth and ~125 m in range for ultrafine imagery. The 1:250 000 version of the Canadian Digital Elevation Dataset (CDED), Level 1, was used to remove the topographic component of the slant-range displacement. To remove systematic biases due to inaccuracies in the baseline or squint effects between image acquisitions, displacements were calibrated using manually selected areas of known zero motion, such as bedrock outcrops, to determine the local bias, which is then removed from the rest of the dataset [Gray et al. 2001]. Final velocities were converted to annual values [Short and Gray, 2005]. Displacement editing and filtering of the displacements followed the criteria of Van Wychen et al. [2012]: (1) surface ice velocities should be faster along glacier centrelines than at their margins; (2) flow direction should follow topography and surface flow features; and (3) flow vectors should not deviate dramatically from adjacent vectors in direction or magnitude over short distances. Filtering was performed manually using ArcGIS^{TM} 9.2 and incorrect matches were removed from the dataset. The point velocity results were interpolated to 100 m grid spacing for the entire glaciated region of the QEI using an inverse distance-weighting method with a fixed 500 m search radius.

Output raster grids were mosaicked to produce a single velocity map for each major ice cap. In areas where rasters overlapped, the minimum overlapping value was used to provide a conservative estimate of ice velocity. To assess the consistency between results determined from different image pairs, we compared the absolute difference between overlapping raster pixels at ~6 million locations and determined a mean difference of 5.95 m a^{-1} and standard deviation of 15.5 m a^{-1}. The final raster was clipped using glacier outlines provided in version 3.0 of the Randolph Glacier Inventory (RGI) [Arendt et al. 2012] for the Canadian High Arctic. Due to our use of winter imagery, which does not capture possible summer speed-up events, we assume that velocity maps and calculated discharge represent minimum annual estimates. Comparison of continuous summer and winter dGPS records from the terminus region of Belcher Glacier (tidewater terminating), Devon Ice Cap, indicates that the use of winter only velocities may underestimate the annual velocities by ~10-15% [B. Danielson, Personal Communication, Oct. 2013].

To establish motion errors, we assumed that the mean velocity calculated over marginal bedrock

outcrops provides information about the error limits of the method. Based on a total of ~11 million points, mean displacement over bedrock provided a mean error of 5.9 m a^{-1} and standard deviation of 6.3 m a^{-1} (error for individual ice masses is presented Table 2-2). To determine error throughout the interior regions of ice caps, where bedrock control was not available, displacements were extracted along ice divides where surface motion should be nearly zero [Raymond, 1984]. Major ice divides were derived from version 3.0 of the RGI and are denoted as white lines in Figure 2-1. Mean velocities along ice divides provided an overall mean error of 6.8 m a^{-1} and standard deviation of 3.9 m a^{-1} (Table 2-2).

2.2.2 Calculation of Dynamic Ice Discharge

This study utilizes airborne-radar measurements of ice thickness collected by NASA's Operation IceBridge campaigns over the Canadian High Arctic in May 2012 (56% of glaciers) and 2006 (5% of glaciers) [Gogineni, 2012], the Scott Polar Research Institute in 2000 (32% of glaciers) [Dowdeswell et al. 2004], and by the University of British Columbia in 1981 (5% of glaciers) [Narod et al. 1988]. The terminus centreline ice thickness value for the Good Friday Bay Glacier on Axel Heiberg Island was derived using an area-depth scaling scheme estimate (2% of glaciers) located ~20km upglacier of the calving front [Ommanney, 1969]. This dataset is ascribed a 40% uncertainty based on comparison of ice thickness estimates provided by Ommanney [1969] on 4 outlet glaciers of Axel Heiberg Island with nearby (within 1.5 km) measurements on ice thickness determined by NASA's Operation IceBridge in 2006.

To calculate dynamic ice discharge, both cross-section (20 of 41 glaciers, primarily located on Devon Ice Cap) and centreline methods (21 of 41 glaciers) were used depending on the availability of ice thickness datasets. For glaciers with depth estimates acquired perpendicular to ice flow the cross-section method was used, in which the terminus width was divided into a number of evenly spaced columns depending on the spacing between ice thickness data points unique to each acquisition and post-processing method (typically 20 – 30 m). For each column, upper and lower estimates of ice flux were calculated by assuming different fractional contributions of internal ice deformation to the measured surface velocity. For the lower ice flux estimate (Q_{min}) we assume a depth-averaged velocity of 80% of the measured surface velocity (i.e., 20% of the overall motion is accounted for by internal deformation) [Paterson, 1994]. For

the upper estimate (Q_{max}) we assume that the depth averaged velocity is equal to the surface velocity, and that ice movement is by basal sliding alone. Discharge was then calculated for each column width (W) using:

$$Q_{min} = (0.8 *(V - V_{error})) * (H – H_{error} + (T*E)) * (W) \quad (1)$$

$$Q_{max} = (V + V_{error}) * (H + H_{error} + (T*E)) * (W) \quad (2)$$

where V is surface ice velocity, V_{error} is a constant error derived separately for each ice mass from the velocity errors computed along ice divides (i.e., highest measured error as indicated in Table 2-2), H is measured ice thickness, H_{error} is error associated with each individual ice thickness dataset (Table 2-1), T is the average annual terminus elevation change as determined from ICESat data in the QEI between 2003 and 2009 [Gardner et al. 2011] and E is the number of elapsed years between the acquisition of the ice thickness data and 2012. The ICESat dataset is the most complete elevation change dataset available for this region, and enables a correction to be made for the change in ice thickness between the time an ice thickness measurement was made and 2012. Total Q_{min} and Q_{max} for a cross section were then calculated from the sum of the individual column widths and provide error limits on our estimates.

For glaciers for which only centreline measurements of ice thickness were available, the cross sectional flux gate was assumed to have a “U” shape, based on the morphology of tidewater glaciers in the QEI for which cross-sections are known (e.g. Gogineni, [2012]) and modelling of valley form after long periods of erosion [Harbor, 1992]. This “U” shape was modelled based on:

$$H_{interpolated} = ((10 \text{ m} – C) / (D1^2)) * (D2^2) + C \quad (3)$$

where $H_{interpolated}$ is assumed ice thickness using a parabolic interpolation from the measured ice thickness at the centreline to a marginal ice thickness of 10 m, C is the measured centreline ice thickness, D1 is the distance from the centreline to the glacier margin and D2 is the distance from the centreline to the centre of the interpolated ice column. Ice column thickness was interpolated at 20 m intervals from the centreline to the margins. To assess the quality of the

modelled cross-sectional glacier geometries, we determined the difference between true glacier cross-sectional geometry with the cross-sectional geometry modelled from only a single point at the glacier centreline for all glaciers within the QEI that had depth estimates collected perpendicular to ice flow. This analysis indicated that the centreline method of cross-sectional modelling underestimated the true cross-sectional geometry by ~12%. We therefore multiply the modeled cross-sectional geometry by 1.12 to reflect this bias correction. Minimum and maximum discharges for each column were then calculated from:

$$Q_{min} = (0.8 *(V - V_{error})) * ((H_{interpolated} * 1.12) – H_{error} – (T*E)) * (W) \quad (4)$$

$$Q_{max} = (V + V_{error}) * ((H_{interpolated} * 1.12) + H_{error} + (T*E) * (W) \quad (5)$$

Total Q_{min} and Q_{max} for a cross section were calculated from the sum of the individual column widths and provide error limits on our estimates. Reported dynamic ice discharge values are the average of the Q_{min} and Q_{max}, with the Q_{min} and Q_{max} providing the lower and upper uncertainty bounds respectively.

2.3 Results and Discussion

Glacier velocities in the Queen Elizabeth Islands are generally relatively low (Figure 2-1). In the interior regions of ice caps and icefields, surface velocities are typically < 10 m a^{-1}, indicative of ice frozen to its bed and moving by ice deformation alone. Most tidewater glaciers flow at rates of ~30 – 75 m a^{-1} at the equilibrium line and rise to < 200 m a^{-1} at the terminus, while land-terminating glaciers typically flow at < 10 - 20 m a^{-1} near the equilibrium line and rise to < 75 m a^{-1} near the glacier terminus. This pattern for land-terminating glaciers is different to the peak in velocity that is typically expected near the ELA, and could be due to the fact these glaciers tend to have large accumulation areas that drain into relatively narrow valleys, and/or because they change from cold-bedded to warm-bedded between their accumulation and ablation areas [Copland et al. 2003a]. The only tidewater glaciers with observed velocities > 300 m a^{-1} are the Belcher and Fitzroy Glaciers located in the northeast sector of Devon Ice Cap (DIC) and Trinity and Wykeham Glaciers located in the south-eastern region of Prince of Wales (POW) Icefield, Ellesmere Island. Short and Gray [2005] determined flow speeds of ~800 m a^{-1} at the

terminus of Trinity Glacier and ~400 m a^{-1} at the terminus of Wykeham Glacier in 2004 compared to our flow speeds of ~1200 m a^{-1} and ~500 m a^{-1}, respectively, in 2012. This suggests a recent acceleration, although the moderate velocity increase and lack of other evidence (e.g., looped moraines, new crevassing) suggests that this is unlikely due to surging. Higher velocities of these glaciers may reflect relatively high accumulation rates due to their locations near moisture sources such as the North Open Water Polynya and Baffin Bay [Mair et al. 2009, Koerner, 1979].

Comparison with previously published ice velocities in the QEI indicates that the largest temporal changes occur on surge-type glaciers, which provides a way of identifying them. For example, Copland et al. [2003b] determined flow speeds of 1000 m a^{-1} along the whole 25 km length of Mittie Glacier in 1999 and Short and Gray [2005] determined flow speeds of up to ~1000 m a^{-1} at the terminus of Mittie Glacier in winter 2003 and ~700 m a^{-1} in 2004, whereas our results reveal 2012 flow speeds that are near zero (<10 m a^{-1}). This indicates that between 2004 and 2012 Mittie Glacier entered the quiescent phase of the surge cycle, and that the Mittie Glacier surge cycle is likely at least 5 years in length. Similarly, the main trunk of Iceberg Glacier, Axel Heiberg Island, was flowing at speeds of ~100 m a^{-1} in winter 2004 [Short and Gray, 2005] but was stagnant in 2012. Conversely, the surface flow speeds determined at the front of Good Friday Bay Glacier on southern Axel Heiberg Island are similar to those determined in the 1950s when the glacier was actively surging [Müller, 1969; Copland et al. 2003b] suggesting that this glacier is currently in an active surge phase (although the surge has only a small impact (0.09 Gt a^{-1}) on total regional dynamic ice discharge even when surging). Only two land-terminating glaciers in the QEI have surface velocities exceeding 75 m a^{-1} (Chapman, Unnamed6), both of which have previously been identified as surge-type [Copland et al. 2003b; Hattersley-Smith, 1969].

Overall, fast flowing glaciers in the QEI (including surge-type glaciers) typically occupy deep subglacial troughs that channel flow from the upper reaches of the accumulation area towards the margins [Burgess et al. 2005]. These factors tend to produce a flow asymmetry in the landscape, with faster flowing glaciers located in areas of higher accumulation [Koerner, 1979] and deeply incised terrain, such as found on eastern DIC, eastern POW and western Axel Heiberg Island. In

contrast, slower flowing ice occurs in areas of lower accumulation and where glaciers overlie plateau-like surfaces, such as western DIC, western POW and eastern Axel Heiberg Island.

Total ice discharge from QEI glaciers is currently 2.6 ± 0.8 Gt a^{-1} (Table 2-1). Ice discharge values calculated here are similar to previous estimates from studies of selected glaciers within this region [Van Wychen et al. 2012; Short and Gray, 2005; Mair et al. 2009; Williamson et al. 2008; Burgess et al. 2005]. A limited number of glaciers account for most of the ice discharge from the QEI and ~50% of total ice flux is channelled through just the Trinity and Wykeham Glaciers that drain POW Icefield (although this value likely varies temporally due to the frequent occurrence of tidewater glacier surging in the QEI; Copland et al. [2003b]). Similarly, a small number of glaciers typically dominate the discharge to the ocean from individual ice masses: Belcher and Fitzroy Glaciers (~55% of DIC), Cañon Glacier (~55% from Agassiz Ice Cap), Otto and Yelverton Bay Glaciers (~80% from Northern Ellesmere Icefields) and Good Friday Bay Glacier (~95% from Steacie and Müller Ice Caps). As a consequence, overall ice discharge to the ocean from the QEI may be highly sensitive to changes in the dynamics of only a few glaciers. To assess this, we combine the 2003 surge speeds of Mittie Glacier [Short and Gray, 2005] with our ice depth measurements to compute that in 2003 the Mittie Glacier would have contributed 0.90 ± 0.09 Gt a^{-1} of ice to the ocean (compared to 0.02 ± 0.02 Gt a^{-1} in 2012). This rapid change in ice flux from a single glacier signifies the importance of surge-type glaciers within the region, which may oscillate between being large and negligible contributors to dynamic ice discharge over relatively short periods (<10 years).

Comparison of our estimate of dynamic discharge with recent estimates of surface mass balance in the QEI provides insight into their relative importance to net mass loss (assuming that the dynamic discharge in 2012 is representative of long term values). The 2012 discharge rates presented are equivalent to ~3.7% (2.6 vs. 61.46 Gt a^{-1}) of net mass loss from the region from 2007-2009, the most recent period for which data are available [Gardner et al. 2011]. For the 2004-2006 period, the dynamic discharge would have been equivalent to ~25% of the net mass loss (2.6 vs. 9.46 Gt a^{-1}). Prior to the late 1980s, when the ice masses of the northern Canadian Arctic Archipelago displayed only slightly negative surface mass balances [Koerner 2005], it is likely that the dynamic discharge was equivalent to an even larger proportion of the net mass

loss. This suggests that current net mass loss in the region is dominated by surface melt and run-off and that dynamic discharge within the region has become a proportionally smaller component of net mass loss in recent years. Determining how glacier dynamics and ice discharge rates within the region may respond to this increase in surface melt and runoff requires further study.

To put the ice discharge rates calculated here within a broader context, we compare our estimates with those for other Arctic glaciers and ice caps (GIC) outside of Greenland (Table 2-3). The QEI currently contribute ~6.6% of total reported pan-Arctic GIC dynamic ice discharge, although the exclusion of Greenland GICs (due to lack of data concerning their fluxes) means that this is likely an over-estimate. Nevertheless, Alaska and Svalbard account for the majority of mass loss via dynamic discharge currently reported for the circumpolar Arctic. The large differences in discharge are probably driven by regional variations in accumulation and climate, with more maritime regions experiencing higher rates of mass turnover and thus higher discharge rates (e.g., Alaska, precipitation ~1-5 m w.e. a^{-1}) [Braithwaite, 2005]), while more continental climates experience lower rates of mass turnover and relatively lower discharge (e.g., Canadian High Arctic, precipitation <0.5 m w.e. a^{-1} [Braithwaite, 2005])).

2.4 Conclusions

The first complete surface velocity maps of the glaciated region of the QEI reveal a marked asymmetry in flow structure (Fig. 1), with higher rates of motion in areas of higher accumulation and deeper subglacial troughs, and lower rates in regions underlain by flatter topography and lower accumulation [Koerner, 1979]. Ice velocities on land-terminating glaciers are largely restricted to < 50 - 75 m a^{-1}, with the exception of surge-type glaciers, whereas velocities on tidewater-terminating glaciers are mainly < 150 - 200 m a^{-1}. Total dynamic mass losses are currently 2.6 ± 0.8 Gt a^{-1}, about half of which is drained through the Trinity and Wykeham Glaciers of POW Icefield. Despite accounting for ~25% of Arctic glacier ice outside the Greenland Ice Sheet, the QEI is found to contribute only ~6.6% of the total reported dynamic ice discharge from GIC in the circumpolar Arctic (excluding Greenland). This is largely a function of the QEI's continental climate and lower rate of mass turnover compared to other Arctic regions, together with the fact that large regions of many QEI ice masses terminate on land.

Our results suggest that mass loss by surface melt and runoff currently dominates the loss term in the mass balance of the QEI, and that ice discharge has become a proportionally smaller component of that term in recent years. However, changes in tidewater glacier dynamics due to the termination or initiation of surges may rapidly change the rates at which ice is transported to the oceans in the QEI. For example, the 2003 surge of the Mittie Glacier likely increased total regional ice fluxes by ~35%. This oscillation between faster and slower flow necessitates continued annual mapping of ice motion in order to identify all surge-type glaciers in the QEI and quantify the impact of surge cycles on glacier mass balance. Further studies are also required to understand seasonal and long-term variations in motion on non surge-type glaciers in the QEI.

Acknowledgements

We thank NSERC, Canada Foundation for Innovation, Ontario Research Fund, ArcticNet, Ontario Graduate Scholarship, and the NSERC Canada Graduate Scholarship for funding. RADARSAT-2 data were provided by MacDonald, Dettwiler and Associates under the RADARSAT-2 Government Data Allocation administrated by the Canadian Space Agency. Support to DB is provided through the Climate Change Geosciences Program, Earth Sciences Sector, Natural Resources Canada (ESS Contribution #20130293). We also acknowledge support from U.K. NERC for grants GR3/12469 and NE/K004999 to JAD.

2.5 References:

Arendt, A., T. Bolch, J.G. Cogley, A. Gardner, J.O. Hagen, R. Hock, G. Kaser, W.T. Pfeffer, G. Moholdt, F. Paul, V. Radić, L. Andreassen, S. Bajracharya, N. Barrand, M. Beedle, E. Berthier, R. Bhambri, A. Bliss, I. Brown, E.Burgess, D. Burgess, F. Cawkwell, T. Chinn, L. Copland, B. Davies, H. De Angelis, E. Dolgova, K. Filbert, R. Forester, A. Fountain, H. Frey, B. Giffen, N. Glasser, S. Gurney, W. Hagg, D. Hall, U.K. Haritashya, G. Hartmann, C. Helm, S. Herreid, I. Howat, G. Kapustin, T. Khromova, C. Kienholz, M. Koenig, J. Kohler, D. Kriegel, S. Kutuzov, I. Lavrenti ev, R. LeBris, J. Lund, W. Manley, C. Mayer, E. Miles, X. Li, B. Menounos, A. Mercer, N. Moelg,P. Mool, G. Nosenko, A. Negrete, C. Nuth, R. Pettersson, A. Racoviteanu, R. Ranzi, P. Rastner, F. Rau, B. Raup, J. Rich, H. Rott, C. Schneider, Y. Seliverstov, M. Sharp, O. Sigurðsson, C. Stokes, R. Wheate, S. Winsvold, G. Wolken, F. Wyatt, N. Zheltyhina, (2012), Randolph Glacier Inventory [v3.0]: A Dataset of Global Glacier Outlines. *Global Land Ice Measurements from Space*, Boulder Colorado, USA. Digital Media.

Blaszczyk, M., J.A. Jania, and J.O. Hagen, (2009), Tidewater glaciers of Svalbard: Recent changes and estimates of calving fluxes, *Polish Polar Research*, 30(2), 85-142.

Braithwaite, R.J., (2005), Mass balance characteristics of arctic glaciers, *Annals of Glaciology*, 42(1), 225-229.

Burgess, D. O., M. Sharp, D.W.F. Mair, J.A. Dowdeswell, and T.J. Benham, (2005), Flow dynamics and iceberg calving rates of Devon Ice Cap, Nunavut, Canada. *Journal of Glaciology*. 51(173), 219-230.

Burgess, E.W., R. R. Foster, and C. F. Larsen, (2013), Flow velocities of Alaskan glaciers, *Nature Communications*, 4(2146), 1-8, doi: 10.1038/ncomms3146.

Copland, L., M. Sharp, P. Nienow and R. Bingham, (2003a), The distribution of basal motion beneath a High Arctic polythermal glacier, *Journal of Glaciology*, 49(166), 407-414.

Copland, L., M. Sharp, and J.A. Dowdeswell, (2003b), The distribution and flow characteristics of surge-type glaciers in the Canadian High Arctic, *Annals of Glaciology*, 36, 73-81.

Dowdeswell, J.A., T.J. Benham, M.R. Gorman, D.O. Burgess, and M. Sharp, (2004), Form and flow of the Devon Island ice cap, Canadian Arctic, *Journal of Geophysical Research*, 109, F02002, doi:10.1029/2003JF000095.

Dowdeswell, J.A., T.J. Benham, T. Strozzi, and J.O. Hagen, (2008), Iceberg calving flux and mass balance of the Austfonna ice cap on Nordaustlandet, Svalbard, J. Geophys. Res., 113, F03022, doi:10.1029/2007JF000905.

Gardner, A. S., M. Moholdt, B. Wouters, G.J. Wolken, D.O. Burgess, M. Sharp, J.G. Cogley, C. Braun and C. Labine, (2011), Sharply increased mass loss from glaciers and ice caps in the Canadian Arctic Archipelago, *Nature*, 473(7347), 357–360, doi: 10.1038/nature10089.

Glazovsky, A. and Y. Macheret, (2006), Eurasian Arctic.in, Glaciation in north and central Eurasian in present time [in Russian with English Translation], edited by V.M., Kotlyakov, 97-114 and 438-445, Nauka, Moscow.

Gogineni, P., (2012), Radar Depth Sounder Data Products, Lawrence, Kansas, USA. Digital media. http://data.cresis.ku.edu/

Gray, A.L., N., Short, K.E. Mattar, and K.C. Jezek, (2001), Velocities and flux of the Filchner Ice Shelf and its tributaries determined from speckle tracking interferometry, *Canadian Journal of Remote Sensing*, 27(3), 193–206.

Harbor, J.M., (1992), Numerical modelling of the development of U-shaped valleys by glacier erosion, *Geological Society of America Bulletin*, 104(10), 1364-1375, doi:10.1130/0016-7606(1992)104<1364:NMOTDO>2.3.CO;2.

Hattersley-Smith, G., (1969), Recent observations on the surging Otto Glacier, Ellesmere Island, Can. J. Earth Sci., 6(4), 883–889, 10.1139/e69-090

Herdes, E., L. Copland, B. Danielson, and M. Sharp, (2012), Relationships between iceberg plumes and sea-ice conditions on northeast Devon Ice Cap, Nunavut, Canada, *Annals of Glaciology*, 53(60), 1-9, doi: 10.3189/2012AoG60A163.

Koerner, R. M., (1979), Accumulation, ablation, and oxygen isotope variations on the Queen Elizabeth Island Ice Caps, Canada, *Journal of Glaciology*, 22(86), 25-41.

Koerner, R. M., (2005), Mass balance of glaciers in the Queen Elizabeth Islands, Nunavut, Canada, Ann. Glaciol., 42(1), 417–423, doi:10.3189/ 172756405781813122.

Lenaerts, J.T.M., J.H. van Angelen, M.R. van den Broeke, A.S. Gardner, B. Wouters, and E. van Meijgaard, (2013), Irreversible mass loss of Canadian Arctic Archipelago glaciers, *Geophysical Research Letters*, 40(5), 870-874, doi:10.1002/grl.50214.

Mair, D., D.O. Burgess, M. Sharp, J.A. Dowdeswell, T. J. Benham, S. Marshall and F. Cawkwell, (2009), Mass balance of the Prince of Wales Icefield, Ellesmere Island, Nunavut, Canada, *Journal of Geophysical Research*, 114F02011, doi:10.1029/2008JF001082.

Moholdt, G., T. Heid, T., Benham, J.A. Dowdeswell, (2012), Dynamic instability of marine-terminating glacier basins of Academy of Sciences Ice Cap, Russian High Arctic, *Annals of Glaciology*, 53(60), 193-201, doi: 10.3189/2012AoG60A117.

Mortimer, C. A., L. Copland, and D. R. Mueller, (2012), Volume and area changes of the Milne Ice Shelf, Ellesmere Island, Nunavut, Canada, since 1950, *Journal of Geophysical Research*, 117F04011, doi:10.1029/2011JF002074.

Müller, F., (1969), Was the Good Friday Glacier on Axel Heiberg Island surging?, *Canadian Journal of Earth Sciences*, 6(4), 891-894, doi: 10.1139/e69-091.

Narod, B. B., G.K.C. Clarke, and B.T. Prager, (1988), Airborne UHF sounding of glaciers and ice shelves, northern Ellesmere Island, Arctic Canada, *Canadian Journal of Earth Sciences*, 25(1), 95–105, doi: 10.1139/e88-010.

Ommanney, C.S.L., (1969), A study in glacier inventory: the ice masses of Axel Heiberg Island, Canadian Arctic Archipelago, *Axel Heiberg Island Research Reports*, McGill University, Montreal, Canada.

Paterson, W.S.B., (1994), *The Physics of Glaciers*, 3rd edition, Elsevier, Oxford.

Raymond, C.F., (1983), Deformation in the vicinity of ice divides, *Journal of Glaciology*, 29(103), 357-373.

Sharp, M., D. O. Burgess, J. G. Cogley, M. Ecclestone, C. Labine, and G. J. Wolken, (2011), Extreme melt on Canada's Arctic ice caps in the 21st century, *Geophysical Research Letters*, 38, L11501, doi:10.1029/2011GL047381.

Short, N. H. and A. L. Gray, (2004), Potential for RADARSAT-2 interferometry: glacier monitoring using speckle tracking, *Canadian Journal of Remote Sensing*, 30(3), 504-509, doi: 10.5589/m03-071.

Short, N. H. and A.L. Gray, (2005), Glacier dynamics in the Canadian High Arctic from RADARSAT-1 speckle tracking, *Canadian Journal of Remote Sensing*, 31(3), 225–239, doi: 10.5589/m05-010.

Van Wychen, W., L. Copland, L. Gray, D. O. Burgess, B. Danielson, M. Sharp, (2012), Spatial and temporal variation of ice motion and ice flux from Devon Ice Cap, Nunavut, Canada, *Journal of Glaciology*, 58(210), 657–664, doi: 10.3189/2012JoG11J164.

Williamson, S., M. Sharp, J. Dowdeswell, and T. Benham, (2008), Iceberg calving rates from northern Ellesmere Island ice caps, Canadian Arctic, 1999-2003, *Journal of Glaciology*, 54(186), 391-400.

Table 2-1: 2012 dynamic ice discharge from all tidewater calving glaciers in the Queen Elizabeth Islands.

Glacier	Lat	Long	Image dates (2012)	Centreline terminus thickness (m)	Terminus width (m)	Mean terminus velocity (m a^{-1})	Estimated terminus thickness change* (m)	Flux gate & data source	Mean ice discharge (Gt a^{-1})
Devon Ice Cap									
Belcher	75.67	-81.23	Apr09-May03	62	9 510	73.1	0	CS1	0.12 ± 0.01
East6	75.15	-79.75	Apr09-May03	110	2 850	24.0	-6.8	CS2	0.01 ± 0.01
East7	75.03	-80.26	Apr09-May03	169	4 950	26.7	0	CS1	0.02 ± 0.01
Eastern	75.83	-81.92	Jan31-Feb24	157	2 100	58.8	0	CS1	0.02 ± 0.01
Fitzroy	75.47	-80.32	Apr09-May03	140	4 170	83.6	0	CS1	0.07 ± 0.02
North1	75.82	-81.77	Apr09-May03	220	660	8.7	0	CS1	0.00 ± 0.00
North2	75.82	-81.67	Apr09-May03	185	480	10.9	0	CS1	0.00 ± 0.00
North Croker	74.88	-83.50	Apr09-May03	250	4 410	13.2	0	CS1	0.01 ± 0.01
South Croker[ST]	74.80	-83.17	Apr09-May03	75	3 300	61.6	0	CS1	0.01 ± 0.01
Southeast1ST	74.78	-80.07	Apr09-May03	112	12 840	9.7	0	CS1	0.02 ± 0.01
Southeast2*	75.01	-80.24	Apr09-May03	289	12 630	17.0	0	CS1	0.05 ± 0.02
Sverdrup	75.76	-83.22	Feb07-Mar02	312	2 430	16.1	0	CS1	0.01 ± 0.01
Unnamed5	75.64	-80.99	Apr09-May03	310	1 770	22.1	0	CS1	0.01 ± 0.01
									0.35 ± 0.14
Manson Icefield									
Mittie West Arm[ST]	76.94	-79.33	Apr09-May03	301	6 630	5.8	0	CS1	0.01 ± 0.01
Mittie East Arm[ST]	76.94	-79.11	Apr09-May03	219	7 480	5.5	0	CL1	0.01 ± 0.01
									0.02 ± 0.02
Sydkap Ice Cap									
SydkapST	76.62	-85.11	Jan12-Feb05	221	2 460	60.9	0	CS1	0.02 ± 0.01
									0.02 ± 0.01
Prince of Wales Icefield									
Ekblaw	78.52	-76.38	Apr09-May03	446	2 919	125.6	0	CL1	0.13 ± 0.02
Trinity	77.94	-78.16	Apr09-May03	236	6 817	691.0	-42.0	CL2	0.83 ± 0.17
Wykeham	77.88	-78.20	Apr09-May03	293	6 561	310.7	-30.8	CL2	0.45 ± 0.07
South1	77.36	-81.05	Apr09-May03	220	1 427	36.9	-9.2	CL2	0.01 ± 0.01
South2	77.29	-79.64	Apr09-May03	220	2 024	59.7	-7.2	CL2	0.02 ± 0.01
South Margin	77.71	-77.88	Apr09-May03	267	44 984	6.6	-9.2	CS2	0.05 ± 0.05
Stygge	78.81	-78.17	Apr09-May03	157	3 089	34.0	-2.9	CL2	0.01 ± 0.01
Cadogan	78.20	-76.52	Apr09-May03	453	9 097	30.3	-10.6	CL2	0.08 ± 0.03
Leffert	78.67	-74.65	Apr09-May03	179	6 620	67.5	0	CL1	0.05 ± 0.01
Unknown2	78.50	-75.31	Apr09-May03	165	1 980	49.6	0	CL1	0.01 ± 0.01
Unknown1	77.92	-77.42	Apr09-May03	191	2 240	10.0	0	CL1	0.01 ± 0.01
									1.65 ± 0.41
Agassiz Ice Cap									
Sawyer Bay[PST]	79.33	-77.80	Mar06-Apr09	282	6 349	12.7	-3.3	CL2	0.01 ± 0.01
Parrish[PST]	79.51	-77.08	Mar06-Apr09	257	3 500	20.4	0	CS1	0.02 ± 0.01
Cañon	79.67	-80.14	Mar06-Apr09	457	3 238	100.1	-3.9	CL2	0.12 ± 0.02
Eugenie	79.82	-74.56	Mar06-Apr09	306	3 770	14.6	-3.4	CL2	0.01 ± 0.01
John Richardson[PST]	80.07	-72.01	Mar06-Apr09	380	3 153	18.8	-14.7	CL2	0.02 ± 0.01
d'Iberville[PST]	80.59	-78.32	Jan12-Feb05	144	2 748	24.6	-2.4	CL2	0.01 ± 0.01
Antoinette	80.85	-76.65	Mar06-Apr09	223	4 450	12.6	0	CS1	0.01 ± 0.01
Tuborg[PST]	80.88	-76.61	Mar06-Apr09	146	2 897	63.0	-8.3	CL2	0.02 ± 0.01
									0.24 ± 0.09
Northern Ellesmere Icefields									
Otto[ST]	81.26	-85.20	Jan28-Feb21	155	4 140	218.1	-10.34	CS3	0.11 ± 0.03
Disraeli[PST]	82.74	-72.74	Jan27-Feb20	93	2 600	69.1	-26.7	CL4	0.01 ± 0.01
Milne[PST]	82.57	-80.85	Jan27-Feb20	152	4 280	54.5	0	CL4	0.03 ± 0.01
Yelverton Bay[PST]	81.86	-79.49	Jan27-Feb20	321	1 160	217.6	+8.3	CL3	0.06 ± 0.01
									0.21 ± 0.06
Müller and Steacie Ice Caps (Axel Heiberg Island)									
Iceberg[ST]	79.41	-92.66	Feb27-Mar22	174	5 000	9.4	0	CS1	0.01 ± 0.01
Good Friday Bay[ST]	78.55	-92.06	Feb27-Mar22	250	6 700	65.3	Unknown	CL5	0.09 ± 0.05
									0.11 ± 0.08
Queen Elizabeth Islands Total									2.59 ± 0.80

Ice thickness data sources ([1] = NASA 2012 (± 10 m at time of acquisition), [2] = Dowdeswell et al. 2004 (± 10 m at time of acquisition), [3] = NASA 2006 (± 10 m at time of acquisition), [4] = Narod 1981 (3 m per 100 m of ice thickness), [5] = Ommanney 1969 (40% of ice thickness). Fluxgate method (CS = CrossSection Method, CL = Centreline Method using a U-Shaped Valley). [ST] indicates confirmed surge-type glacier, [PST] indicates possible surge type glacier from Copland et al. [2003]. *Estimated terminus thickness change between the time of ice thickness acquisition and 2012 calculated by multiplying the average terminus elevation change calculated using ICESat data between 2003 and 2008 and the number of years elapsed between the year of acquisition of the ice thickness dataset and 2012.

Table 2-2: Error analysis determined from apparent motion over stationary regions (bedrock outcrops and ice divides).

Ice Mass	Number of points over bedrock	Mean error over bedrock (m a^{-1})	Standard deviation over bedrock (m a^{-1})	Number of points along ice divides	Mean error along ice divides (m a^{-1})	Standard deviation along ice divides (m a^{-1})
Prince of Wales Icefield	586821	5.9	4.5	111297	7.4	5.1
Agassiz Ice Cap	2335656	5.2	4.5	158771	6.0	2.9
Northern Ellesmere Icefield	4821405	6.4	7.1	69319	6.0	2.7
Müller & Steacie Ice Caps	2346456	6.4	6.6	131978	6.6	3.1
Sydkap Ice Cap	82387	9.8	6.5	39940	10.3	5.4
Manson Icefield	597211	4.4	3.7	26931	6.5	3.6
Devon Ice Cap	633306	5.7	5.0	74826	7.0	3.8
All Ice Caps	11417411	5.9	6.3	613042	6.8	3.9

Table 2-3: Pan-Arctic comparison of ice discharge estimates.

	Region	Period	Ice Discharge (Gt a^{-1})	% of Pan-Arctic Discharge (excluding Greenland)	Data Source
CAA	Queen Elizabeth Islands	2012	2.46	7.1	This Study
	Baffin & Bylot Islands	1999-2003	0.25	0.7	Gardner et al. [2011]
Alaska	All Glaciers	2006-2010	17.1	49.7	Burgess et al. [2013]
Russia	Academy of Sciences Ice Cap	2003-2009	1.4	4.1	Moholdt et al. [2012]
	Franz-Josef Land	1952-2001	4.3	12.5	Glazovsky and Macheret [2006]
	Novaya Zemlya	1952-2001	1.4	4.1	Glazovsky and Macheret [2006]
	Severnaya Zemlya	1952-2001	0.75	2.2	Glazovsky and Macheret [2006]
Svalbard	All Glaciers	2000-2006	6.75	19.6	Blaszczyk et al. [2009]
Pan-Arctic Glaciers and Ice Caps (excluding Greenland)			34.41	100	

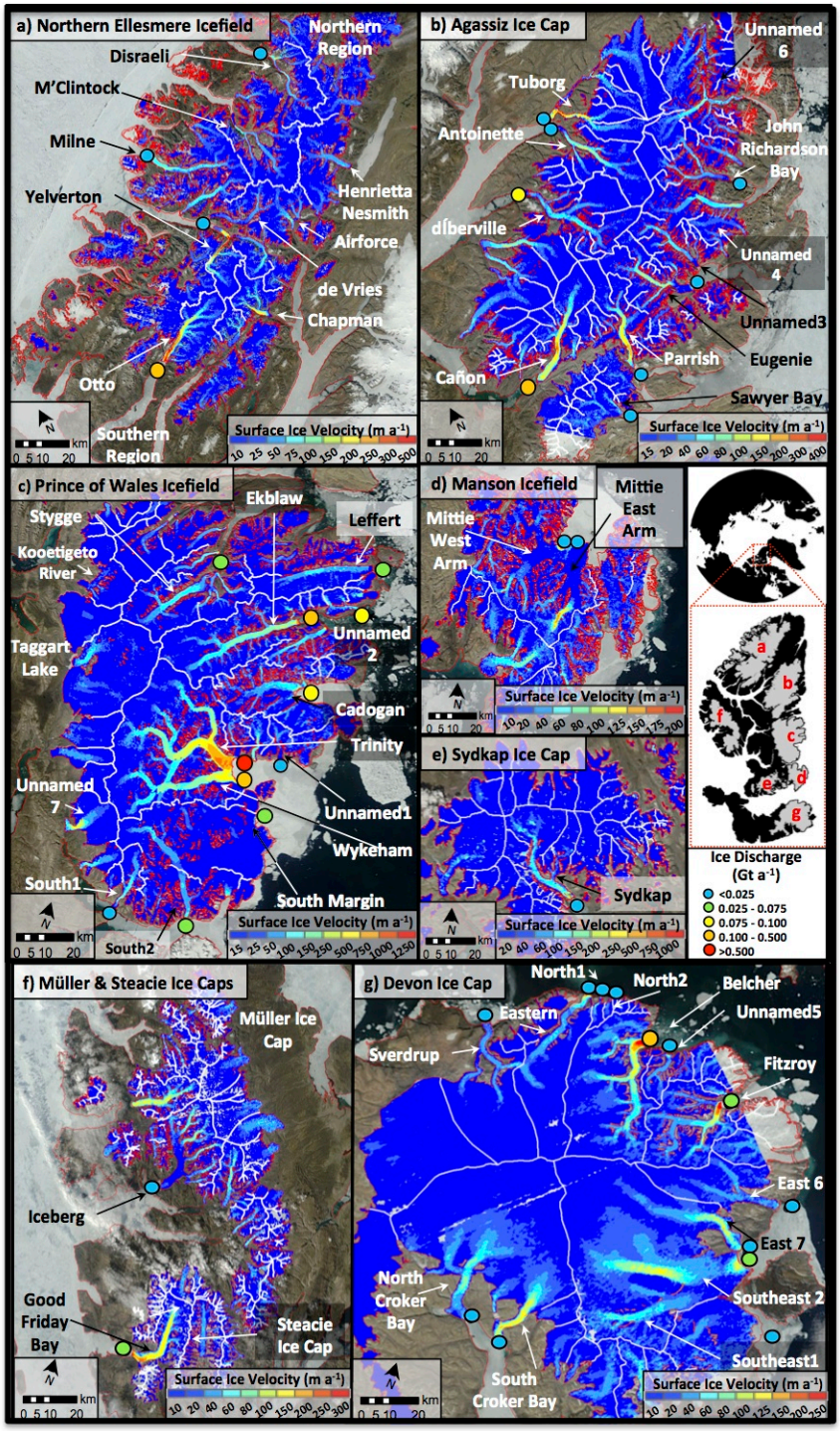

Figure 2-1: Surface velocities for: a) Northern Ellesmere Icefield; b) Agassiz Ice Cap; c) Prince of Wales Icefield; d) Manson Icefield; e) Sydkap Ice Cap; f) Müller and Steacie Ice Caps; g) Devon Ice Cap. Major ice divides used to determine errors denoted in white. Note difference in velocity scale between images, although ice discharge scale remains constant (Base Image: MODIS July 4th, 2011). Inset Map: Study Site.

CHAPTER THREE: Glacier Velocities and Dynamic Discharge from the Ice Masses of Baffin and Bylot Islands, Nunavut, Canada

Abstract:

Speckle tracking of ALOS PALSAR fine beam data from 2007-2011 is used to determine the surface motion of major ice masses on Baffin and Bylot Islands in the southern Canadian Arctic Archipelago. Glacier velocities are low overall, with peaks of ~100 m a^{-1} and means of ~20-60 m a^{-1} common along the main trunk of many outlet glaciers. Peak velocities on Penny and Bylot Island ice caps tend to occur near the mid-sections of their primary outlet glaciers, while the fastest velocities on all other glaciers usually occur near their termini due to relatively large accumulation areas draining through narrow outlets. Estimates of ice thickness at the fronts of tidewater terminating glaciers are combined with the velocity measurements to determine a regional dynamic discharge rate of between ~17 Mt a^{-1} and ~108 Mt a^{-1}, with a mid-point estimate of ~55 Mt a^{-1}, revising downward previous approximations. These velocities can be used as inputs for glacier flow models, and provide a baseline dataset against which future changes in ice dynamics can be detected.

3.1 Introduction

The southern Canadian Arctic Archipelago (CAA), consisting of Baffin and Bylot Islands (Figure 3-1), contain ~40,000 km^2 of glacier ice [Gardner et al. 2012]. Recent studies indicate that these ice masses are undergoing substantial change. Passive microwave records reveal that the average melt season on Barnes Ice Cap lengthened by ~33% between 1979-1987 and 2002-2010, and nearly doubled on Penny Ice Cap between 1979 and 2010 [Dupont et al. 2012; Zdanowicz et al. 2012]. Firn temperatures at 10 m depth near the summit of Penny Ice Cap have warmed by ~10°C between the mid-1990s and 2011, and recent surface melt rates are comparable to those experienced over 3000 years ago [Zdanowicz et al. 2012]. Geodetic methods indicate surface lowering of up to ~1 m a^{-1} on all ice masses on Baffin and Bylot Islands between 1963 and 2006, with greatest surface lowering concentrated on ice mass margins and low-lying outlet glaciers [Gardner et al. 2012]. From 2003-2011 the glaciers of the southern Canadian Arctic Archipelago lost ice at a rate of 23.8 ± 6.12 Gt a^{-1} and contributed 0.07 ± 0.02 mm a^{-1} to global sea level rise over this period (accounting for 16% of the total contribution from ice masses outside of the ice sheets) [Gardner et al. 2012]. There has been little change in regional precipitation and the main driver of accelerated ice loss has been an increase in summer air temperatures, with models projecting sustained mass loss within the region over the next century [Gardner et al. 2012; Lenaerts et al. 2013].

Despite the large area and volume of glacial ice contained within Baffin and Bylot Islands, no previous regional survey of glacier and ice cap motion has been undertaken. Only a single estimate of dynamic discharge has been previously reported (~0.25 Gt a^{-1}, equivalent to 250 Mt a^{-1}) based on the average ice flux per terminus width derived from sparse velocity data from the northern CAA [Gardner et al. 2011]. As a consequence, our knowledge of ice dynamics over a large portion of the Canadian Arctic is presently limited, and the current estimate of mass loss via dynamic discharge from Baffin and Bylot Islands is poorly constrained. Here we use speckle tracking of ALOS PALSAR fine beam (~9 m) RADAR imagery acquired between 2007-2011 to determine surface displacements and produce the first comprehensive velocity map for the major ice masses of the southern CAA. At the terminus of tidewater glaciers, surface ice velocities and estimated ice thicknesses (bounded by measurements from analogous glaciers by NASA's operation IceBridge) are used to calculate mass loss via dynamic discharge. Here dynamic

discharge is defined as mass loss via iceberg calving and subaqueous melt, following terminology consistent with other studies that utilize similar methods (e.g. Van Wychen et al. [2014]).

3.2 Study Site

The principal ice masses of the southern CAA are: Bylot Island Ice Cap (4783 km^2 in 2000), Penny Ice Cap (6478 km^2 in 2000), Barnes Ice Cap (5874 km^2 in 2000) and the coastal glaciers (21,835 km^2 in 2000) that fringe Baffin Bay (Figure 3-1). The Bylot Island Ice Cap occupies ~43% of Bylot Island, and is dissected by the Byam Martin Mountains which extend the entire 150 km length of Bylot Island in a northwest-southeast direction [Dowdeswell et al. 2007]. The distribution of glaciers reflects the island's topography, and consists of large outlet glaciers extending from the high elevation ice cap interior to the margins, separate remnant ice masses that have become detached from the ice cap proper, and isolated ice patches in low-lying areas [Dowdeswell et al. 2007]. There are two unnamed glaciers that terminate into the ocean located in the northeastern portion of the ice cap, and ten glaciers have been inferred as probable surge-type based on the identification of features which suggest previous surge activity (e.g. looped and deformed moraines, widespread crevassing, pronounced ice ramps, stagnant ice, potholes and over-steepened glacier termini) [Dowdeswell et al. 2007].

Penny Ice Cap is the southernmost large ice mass of the CAA and is a partial remnant of the Laurentide Ice Sheet [Zdanowicz et al. 2012]. Major glaciers radiate outward from the ice cap interior through constrained valleys toward the north, east and south. In the northwest the ice cap terminates in a broad, lobe-like region. The surface velocity structure of seven outlet glaciers has previously been determined utilizing optical feature tracking, with the finding that ice motion had generally slowed between the mid-1980s and mid-2000s due to a long-term negative mass balance [Heid and Kääb, 2012]. There are two tidewater terminating glaciers on Penny Ice Cap: Coronation Glacier located in the south-east, and an unnamed glacier located in the north-central region.

Barnes Ice Cap, also a remnant of the Laurentide Ice Sheet, is a dome shaped ice mass situated in the interior of Baffin Island on a broad plateau [Dupont et al. 2012; Sharp et al. 2014]. Maximum ice elevation rises to ~1100 m a.s.l. and the margins terminate at ~500 m a.s.l. [Dupont et al.

2012]. The majority of the ice cap terminates on land in a broad lobe-like structure, although small regions terminate in lakes located in the north and south. “Surge scars” have been used to infer past surging in the southwest of the ice cap, and measurements of basal ice temperature indicated ice at pressure melting point, providing a mechanism that would facilitate sliding [Holdsworth 1977].

There are a large number of smaller ice caps and glaciers that fringe the northern and eastern coastline of Baffin Island. Typically, these ice masses are characterized by a few outlet glaciers (some of which are tidewater terminating) that drain small ice caps through confined valleys. The larger coastal outlet glaciers have widths of ~1-3 km and in some cases extend ~30 km into ice cap interiors. Our velocity mapping covers ~93% of the glaciated area of Baffin and Bylot Islands. It notably excludes the Terra Nivea and Grinnell Ice Caps and the smaller coastal ice masses that fringe the far southern parts of Baffin Island, due to a lack of SAR imagery suitable for deriving glacier motion there.

3.3 Methods

3.3.1 Determination of Surface Motion

ALOS PALSAR data was obtained in level 0 CEOS format from the Alaska Satellite Facility’s Vertex Data Portal (https://vertex.daac.asf.alaska.edu/) from 2007-2011 (Table 3-1). ALOS PALSAR L-band data has proven effective for determining surface motion for temperate ice masses [e.g. Burgess et al. 2013] and imagery was acquired during winter months when changes to the glacier surface which affect coherence are minimized (e.g., snowfall, rainfall, melt). The Level 0 data was processed to Single Look Complex format using the GAMMA Modular SAR Processor, and surface motion was derived using a custom-written MATLAB^{TM} algorithm which estimates azimuth and slant range displacements between image pairs, and references these displacements to zero motion areas. If the conditions for interferometry are satisfied (Rosen et al. 2000) and the near surface conditions have not changed significantly between the times of data acquisition (a multiple of the 46 day ALOS repeat cycle) then the speckle pattern in the two images will be correlated (Gray et al. 2001). This approach is advantageous because if distinct image features (e.g. crevasses) exist in the image pair then the ‘speckle tracking’ algorithm will degrade to less accurate feature tracking, even if coherence between the two images is poor. This can then be described more generally as ‘offset’ tracking (Strozzi et al. 2002). However we find

that L-band imagery (e.g., ALOS) maintains coherence for longer time periods than C-band imagery (e.g., RADARSAT) and that the majority of our results were obtained with speckle tracking so we use this term for our description of the processing methodology.

To preserve bandwidth, and therefore image resolution, the complex SLC data were up-sampled by a factor of two in both range and azimuth, in the latter case taking account of the Doppler centroid frequency. After estimating a coarse image-to-image registration, image chips were selected from the master (earlier) image and a two-dimensional search was performed to identify the corresponding region in the second image. The resulting normalized two-dimensional cross-correlation function is up-sampled and the peak is used to give the best estimates of the range and azimuth shifts. This approach has previously been used to determine glacier displacement in the Canadian High Arctic [Short and Gray 2005; Van Wychen et al. 2012, 2014] and Yukon/Alaska [Waechter et al. in press]. Image chip size is variable, but in this case was ~400 m in both azimuth and ground range direction, with overlap of 50% between adjacent chips. Because the orbits are not repeated perfectly there can be a stereo component in the slant range direction due to the perpendicular baseline (Rosen et al. 2000), which leads to a topography dependent range displacement not associated with surface motion. The 1:250,000 Canadian Digital Elevation Dataset (CDED) was used to remove this topographic component of slant range displacement and even with a relatively large perpendicular baseline the accuracy of the CDED data is adequate to minimize any possible error. To remove systematic biases due to inaccuracies in satellite baseline estimates or squint effects between image acquisitions, displacements were calibrated using areas of zero motion (bedrock outcrops) to determine the local bias, which is then removed from the rest of the dataset. A further erroneous azimuth shift problem can arise, particularly with L-band SAR data, due to ionospheric disturbances [Gray et al. 2000]. In this case, care is taken to identify adjacent no-motion areas (e.g. bedrock on either side of an outlet glacier) to try to minimize any bias error in the azimuth shift not due to ice movement and remove this bias from the areas locally affected by streaking.

The MATLAB^{TM} speckle tracking code we utilize outputs a text file of geocoded point vectors of the strongest correlations between image chips in the master and slave images which we then import into ArcGIS for verification and filtering of erroneous matches. Mismatch errors occur when the speckle tracking algorithm finds a stronger correlation with an incorrect image chip

other than the "true" match. To identify and remove these errors from the velocity dataset, manual inspection and verification of the results was undertaken within ArcGIS 10.1 on all velocity results. Once mismatches were removed from the dataset the velocities were converted to a continuous raster surface (100 x 100 m pixels), using an inverse distance-weighting interpolation, which does not create pixel values beyond measured displacements. Rasters of surface ice velocity are mosaicked (using a minimum value in areas of overlap) into a single velocity dataset for each individual ice mass, and final raster datasets were clipped to the extent of the GLIMS Randolph Glacier Inventory (version 3.2, representing glacier extents in years ~1999-2001; available online: http://www.glims.org/RGI/). The use of an IDW interpolation method combined with the using minimum values in areas of overlap is consistent with previous methods of creating continuous rasters of glacier surface velocities in the Canadian High Arctic [Van Wychen et al. 2012; 2014]. This means that the surface velocities presented here are conservative and may slightly underestimate rates of ice motion and dynamic discharge.

3.3.2 Error Analysis

To provide an indication of the reliability of the speckle tracking results, velocities were extracted over known stationary regions (bedrock outcrops and ice divides). Mean displacement over 8,536,449 unique bedrock points yielded a mean value of 5.4 m a^{-1} and standard deviation of 4.9 m a^{-1}. Mean displacement over 32,518 unique ice divide locations (extracted from RGI v3.2) yielded a mean value of 5.1 m a^{-1} and standard deviation of 2.9 m a^{-1}. These error estimates are within ranges previously reported when using the same speckle tracking algorithm on RADARSAT-2 data in the Canadian High Arctic [Van Wychen et al. 2012, 2014].

In situ surveys of the motion of mass balance stakes on Penny Ice Cap between spring 2011 and 2012 provide validation for the remote sensing results and an assessment of how well velocities derived from winter ALOS data over a 46 day period represent annual motion. The stake positions were measured with a Trimble R7 dGPS unit, with the antenna inserted into the top of each mass balance stake for a period of 20-30 minutes during each visit. The dGPS data were post-processed with Natural Resources Canada's online Precise Point Positioning service (http://webapp.geod.nrcan.gc.ca/geod/tools-outils/ppp.php), and results are considered accurate within ±0.15 m horizontally. The mean absolute difference between 23 in situ measurements of surface ice displacement and those determined by speckle tracking was 7.9 m a^{-1} (Table 3-2).

60% (14 of 23) of the displacements derived from speckle tracking were within the error margins determined over stationary locations and ~90% (21 of 23) of the displacements derived from speckle tracking were within 15 m a^{-1}. The two locations with the greatest discrepancy (~21.5 m a^{-1}) between the two methods occurred on the lower sections of Coronation Glacier, where melt likely induces summer acceleration that is not captured in the winter-only speckle tracking measurements.

Each method of determining reliability of surface velocities has drawbacks: bedrock outcrops provide estimates of motion over non-moving regions which may not be representative of areas of motion, ice divides are poorly defined within the Canadian Arctic and as such may not provide exact locations of zero motion, and comparisons with in situ dGPS measurements and speckle tracking results are inexact due to the difference between monitoring periods (~1 year versus 46 days). Thus, in order to provide an estimate of confidence in our velocity results, we use the root sum of squares from all the separate sources of error (bedrock outcrops, ice divides and displacement stakes). This analysis yields ~±8.5 m a^{-1} as the uncertainty in the velocity dataset.

3.3.3 Determination of Dynamic Discharge

To quantify dynamic discharge from the study region, a visual assessment of Landsat 7/8 imagery and review of previous studies (e.g. Randolph Glacier Inventory; Gardner et al. 2011) was undertaken to identify which glaciers are tidewater terminating. This identified a total of 46 glaciers (denoted on Figures 3-2 to 3-4) that terminate in the ocean. Ice thickness information is needed to compute ice flux, but there is a sparse availability of ice thickness data on Baffin and Bylot Islands. We therefore adopted a scenario-based approach, where ice depths for flux gates at glacier termini are modeled based on the available measurements of analogous glaciers within the study region.

We use two different scenarios to distinguish between the morphology of large glaciers (outlet glaciers), which descend from ice mass interiors to the coastal margins, and the morphology of smaller glaciers (valley glaciers) that drain from relatively small accumulation areas to the ocean. For both scenarios, ice flux gates at the glacier termini are based on low, high, and midpoint measurements of ice depths on analogous glaciers within the study region. For the “outlet

glaciers" scenario, values were chosen based on airborne ice thickness measurements determined by NASA's Operation Icebridge (acquired May 5 and 12, 2011; ftp://data.cresis.ku.edu/data/rds/) along the lower (~15-20 km) terminus region of four large glaciers that descend from the interior of Bylot Island to the margins. This dataset provides a total of 4556 unique measurements with a mean ice thickness of ~276 m (minimum of 29.8 m and maximum of 413.9 m). Measured ice thicknesses less than 100 m are restricted to small isolated pockets along two glaciers, while measured ice thicknesses greater than 300 m tend to occur in higher elevation regions and are less likely to reflect the terminus glacier morphology. As such, we use the average of these values to establish a low thickness estimate of 100 m, a high estimate of 300 m, and a midpoint estimate of 200 m.

For the "valley glaciers" scenario, a low thickness estimate of 75 m was used based on 50 MHz ground penetrating radar measurements at the terminus of Fountain Glacier, Bylot Island, in 2007/2008 [Wainstein et al. 2014], while an upper limit of 150 m is based on the mean of 105 point ice thickness measurements determined by NASA's Operation Icebridge on April 12, 2013 on four valley glaciers (locations: 66.7°N, -65.2°W; 66.6°N, -65.1°W; 66.6°N, -65.1 °W; 66.5°N, -65.3°W) located in southern Penny Ice Cap. A midpoint estimate of 112.5 m is then taken as the average of these values.

To approximate the shape of the glacier cross-section at each flux gate, we use the methodology of Van Wychen et al. [2014], who assumed a "U" shaped morphology based on measurements of glaciers in the Canadian High Arctic [Gogineni, 2012] and modeling of valley form after periods of erosion [Harbor, 1992]. The "U" shaped morphology was modeled based upon:

$$T = ((10 - C)/D_1^2)) \times (D_2^2) + C \qquad (1)$$

Where T is the assumed ice thickness using a parabolic interpolation and the ice thickness scenarios based on the glacier centerline (C_{min} = 75 m/100 m, C_{mid} = 112.5 m/200 m, C_{max} = 150 m/300 m; first presented ice depth value represents the Valley Glacier Scenario and the second represents the Outlet Glacier Scenario for C_{min}, C_{mid} and C_{max}), D_1 is the distance from the glacier centreline to the margin, and D_2 is the distance from the centreline to the centre of the interpolated ice column. Ice column thicknesses are interpolated at 20 m intervals from the

centreline to the glacier margins, and the surface motion of each ice column is extracted from the raster of surface velocity at each of these locations (20 m intervals are used to maintain consistency and comparability with interpolated flux gates created in the northern CAA (e.g. Van Wychen et al. [2014])). Low (Q_{min}), medium (Q_{mid}) and high (Q_{max}) discharge estimates for each column are then calculated using the following equations:

$$Q_{min} = ((V - V_{error})*0.8) \times (T_{min}) \times (W) \quad (2)$$

$$Q_{mid} = (V) \times (T_{mid}) \times (W) \quad (3)$$

$$Q_{max} = (V + V_{error}) \times (T_{max}) \times (W) \quad (4)$$

Where V is the extracted surface ice velocity measurement derived from speckle tracking, V_{error} is the error associated with the speckle tracking dataset (8.5 m a^{-1}; previously discussed above) and W is the ice column width (20 m). For the Q_{min} ice flux estimate we assume a depth-averaged velocity of 80% of the measured surface velocity to account for internal deformation [Paterson, 1994] while for the Q_{mid} and Q_{max} estimates we assume that the motion at the glacier terminus is due to sliding alone and that the depth-averaged velocity is equal to the surface velocity.

Total Q_{min}, Q_{mid} and Q_{max} estimates for each cross section are calculated from the sum of individual ice columns and are converted to units of Mt a^{-1} (1 Mt = 0.001 Gt). This method of calculating iceberg discharge is consistent with previous methods in the Canadian High Arctic [Burgess et al. 2005; Van Wychen et al. 2012, 2014]. Other methods of estimating cross-sectional flux include using a “box-shaped” glacier geometry rather than a “U-shaped” glacier geometry [e.g. Williamson et al. 2008] or an ice-flux per unit of terminus width approach using estimated discharge rates from nearby areas and extrapolating them to other areas [e.g. Gardner et al. 2012]. Our method is superior to these as it uses a more realistic glacier geometry [Harbor 1992] and because it uses measured glacier velocities rather than velocities extrapolated from other regions that may not represent the ice dynamics of the region of interest.

3.4 Results and Discussion

3.4.1 Glacier Velocity Structure of Baffin and Bylot Islands

Surface velocities of the ice masses of Baffin and Bylot Island are generally low (Figures 3-2 to 3-4), with peak velocities of ~100 m a^{-1} and typical velocities of ~20-60 m a^{-1} along glacier centrelines. Surface motion of the interior of all ice caps is <20 m a^{-1}, suggestive of ice frozen to its bed and flowing by deformation only.

In the "Northern" part of the study region (Figure 3-2), velocities of ~40 m a^{-1} to 60 m a^{-1} are observed on four glaciers located in the south-central part of Bylot Island Ice Cap, and one in its north-central region (Figures 3-2a, 3-5a-d). Faster ice motion on these five land-terminating glaciers occurs near their middle sections (~750-1000 m a.s.l.), approximately coincident with the equilibrium line altitude (ELA ~800-900 m a.s.l. [Dowdeswell et al. 2007]). Ten glaciers on Bylot Island Ice Cap have previously been identified as possible surge-type (indicated in Figure 3-2) by Dowdeswell et al. [2007], and it is notable that three of the five faster flowing glaciers have been previously been identified as surge type. The remaining seven glaciers previously identified as possibly surge-type have surface flow speeds <20-30 m a^{-1}, which suggests that if they are surge-type they are currently in their quiescent phase. For the coastal glaciers of northern Baffin Island (Figure 3-2b), surface motion of 80-140 m a^{-1} occurs on several glaciers in locations where relatively large accumulation areas connect to narrow tributaries and outlet glaciers. These areas of higher surface velocity are likely due to large ice fluxes being funnelled through relatively narrow valleys, changes in basal conditions (transition from cold to warm bed), and increases in driving stress. Higher velocities on coastal glaciers are also likely driven by high accumulation rates due to their proximity to Baffin Bay. These patterns of ice motion are similar to those found in the northern CAA [Van Wychen et al. 2014].

The "Central" region of the study site includes the small glaciers and ice caps that fringe the central coastline of Baffin Island (Figures 3-3a, 3-4b) and Barnes Ice Cap (Figure 3-3b). The central coastal glaciers have velocity patterns similar to those described for the "northern" coastal glaciers and the mechanisms driving flow are likely the same, although peak velocities are generally lower (~50-80 m a^{-1}). Most of the margin of Barnes Ice Cap flows at speeds of <20 m a^{-1} and terminates in a broad lobe. Surface velocities >20 m a^{-1} are only found in small areas in the north-central and south-central parts of the ice cap, with maximum motion (~80 m a^{-1})

occurring in the north-central region at the front of a large lake-terminating glacier. This region of fast flow occurs across a ~5 km wide terminus, but only propagates into the ice cap interior by ~6 km (Figure 3-5e). In the south-central region, ice moves more slowly at a maximum rate of ~50 m a^{-1}, although the area of enhanced motion propagates further (~30 km) into the ice cap interior (Figure 3-5f). This area of faster ice flow coincides with a glacier previously identified as surge-type [Løken 1969; Holdsworth, 1973, 1977]. Løken [1969] proposed that this region likely surged in the past due to a surface morphology that suggested surface lowering at upper elevations and surface bulges at lower elevations, and an advanced ice front position in comparison to adjacent regions. Holdsworth [1977] identified three additional regions where surge activity was likely to have occurred on Barnes Ice Cap (identified in Figure 3-3b); our velocity results indicate that these glaciers are stagnant, suggesting that they're currently in quiescence if they are surge-type.

The highest observed motion for the southern CAA is found in the "Southern" region of Baffin Island and occurs on Penny Ice Cap (Figure 3-4a), where surface velocities of ~100-120 m a^{-1} are found on the main tributary of Coronation Glacier on the east side of the ice cap and on several unnamed outlet glaciers located in the southwest, north-central and northeastern portions of the ice cap. Slower motion of ~50–80 m a^{-1} occurs on several additional unnamed glaciers located in the western, northern and southern regions of the ice cap (Figure 3-5g-j). Similar to the smaller coastal glaciers, higher glacier velocities on Penny Ice Cap tend to occur in areas where large areas of accumulation connect with narrow outlets, and likely reflect local changes in basal conditions and driving stress. Unlike the glaciers in the northern CAA where higher velocities are maintained from the point of initiation to the terminus, the outlet glaciers on Penny Ice Cap tend to slow from these connection points to their calving margin. Unlike the glaciers of Barnes and Bylot Island Ice Caps, none of the glaciers on Penny Ice Cap have previously been identified as surge-type, and a visual analysis of historical Landsat imagery shows no evidence that would classify them as such (e.g., looped/distorted moraines, potholes, extensive crevassing, dramatic terminus advance/retreat). The surface velocities of the southeastern coastal glaciers (Figure 3-4c) are low, with only a few areas of motion above detection limits (30-60 m a^{-1}).

3.4.2 Dynamic Discharge

Our calculations indicate that total mass loss via dynamic discharge from the ice masses of the southern CAA lies between ~17 Mt a^{-1} and ~108 Mt a^{-1}, with a mid-point estimate of ~55 Mt a^{-1} (Table 3-3). The largest contributors to dynamic discharge are located on Penny Ice Cap with Coronation Glacier (ID 44) and Unnamed Glacier (ID 43) accounting for ~19% (Q_{mid}) and ~17% (Q_{mid}) of total dynamic discharge from the southern CAA. The next largest source of dynamic discharge is an Unnamed coastal glacier located on Northern Baffin Island (ID 20, responsible for ~13% of total southern CAA dynamic discharge) followed by the two tidewater terminating glaciers of Bylot Island Ice Cap (IDs 45 and 46). The total mass loss via dynamic discharge from all the glaciers on Baffin and Bylot Islands is only ~2% of that determined for the northern CAA, with each of the eight largest glaciers (e.g. Trinity, Wykeham, Belcher, Ekblaw, Otto, Good Friday Bay, Cadogan and Fitzroy Glaciers) in the Canadian high Arctic transferring more mass to the oceans than all glaciers in the southern CAA combined [Van Wychen et al. 2014]. This highlights the fact that iceberg discharge from the Canadian Arctic as a whole is dominated by a few glaciers in the northern CAA.

Gardner et al. [2011] provide the only previous estimate of dynamic discharge from Baffin and Bylot Islands, at ~250 Mt a^{-1}. Our estimate is considerably less than this, with Q_{min} ~94% less, Q_{mid} ~78% less and Q_{max} ~57% less. This discrepancy is likely because Gardner et al. [2011] overestimated ice flux for Baffin and Bylot Islands because they used previously published flux estimates from the Northern Canadian Arctic [e.g. Williamson et al. 2008; Burgess et al. 2005] to determine an average mass discharge per unit of terminus width and applied this value to the widths of all tidewater terminating glaciers on Baffin and Bylot Islands. There are two problems with this approach. First, the outlet glaciers in the Northern Canadian Arctic are generally faster flowing (typically ~150-250 m a^{-1} at their calving fronts [Van Wychen et al. 2014]) than those in the Southern Canadian Arctic (typically 20-60 m a^{-1} at their calving front), which would lead to an erroneously high discharge rate per terminus width when applied to the southern Canadian Arctic. Second, Gardner et al. [2011] in part based their average terminus width discharge rate on the flux rates provided by Williamson et al. [2008], who used a "box" shape to represent glacier geometry, rather than the more realistic "U" shape that we utilize here. Williamson et al. [2008] also derived glacier velocities using feature tracking of optical imagery, which provides velocity

results in areas with distinct surface features (e.g. crevasses) which are located in faster flow regions of the terminus. This means that the surface velocities used by Williamson et al. [2008] to calculate ice flux were likely biased to faster flowing regions, which would also lead to higher average rates of mass flux per terminus width. To assess these effects, we extract the glacier centerline velocity (i.e. areas of fast flow) of all glaciers in our study region and combine it with a box shaped glacier geometry for each ice thickness scenario, and find that using this approach increases the ice flux by ~276% for the Q_{min} scenario, ~207% for the Q_{mid} scenario and ~135% for the Q_{max} scenario. We therefore believe that our results are an improvement on previous ice flux estimates as they use more realistic glacier geometries and surface velocities across the calving front.

To determine the relative importance of iceberg calving as a regional ablation mechanism, our estimate of dynamic discharge can be compared with estimates of ice loss via surface melt and runoff derived from surface mass balance model driven by the output of the Regional Atmospheric Climate Model (RACMO2) and corrected for evolving glacier hypsometry [Lenaerts et al. 2013]. In 2011, Q_{mid} accounted for ~0.11% (0.054 Gt a^{-1}) of total ablation of 47.5 Gt a^{-1}. The average mass loss via surface melt and runoff between 2007 and 2011 was ~53.5 Gt a^{-1}, so dynamic discharge was even less important in these earlier years [Lenaerts, J. personal communication 2015]. The proportional importance of dynamic discharge compared to surface melt and runoff for Baffin and Bylot Islands is considerably smaller than in the northern CAA, where iceberg discharge accounted for ~3.1% of total ablation in 2012 [Van Wychen et al. 2014].

3.5 Conclusions

The surface velocity structure of the ice masses of Baffin and Bylot Islands is broadly similar to that of the ice masses located in the northern CAA, with slow-moving (<20 m a^{-1}) interior regions contrasting with areas of faster motion where tributaries and outlet glaciers discharge from the ice cap interior. The regions of speed-up likely arise due to ice from large accumulation areas being forced through relatively narrow valleys at lower altitudes, changes in basal conditions from a cold to a warm bed, and increases in driving stress as surface slopes steepen and ice thicknesses reach a maximum. However, in contrast to the northern CAA, where higher ice motion is typically maintained from the point of speed-up in the upper ablation area to the

glacier snout, glaciers of the southern CAA typically attain maximum velocities along their mid to upper ablation areas, and decelerate towards their termini.

Calculations based on the surface velocity and estimated ice thickness at the terminus of the 46 tidewater glaciers on Baffin and Bylot Islands indicates a regional dynamic discharge rate between ~17 Mt a^{-1} and ~108 Mt a^{-1}, with a mid-scenario estimate of ~55 Mt a^{-1}. This estimate of iceberg discharge is less than previously derived for the region by Gardner et al. [2011], and is only ~2% of that for the northern CAA. Van Wychen [2014] provided a comparison of iceberg discharge volumes for all reported Arctic glaciated regions (including the ice masses of Baffin and Bylot Island based on the discharge estimate of Gardner et al. [2011]), and showed that the southern CAA was responsible for 0.7% of total Arctic dynamic discharge. Using our revised Q_{mid} estimate of discharge, this number can be revised downwards, such that the ice masses of Baffin and Bylot Island are currently responsible for ~0.14% of total Arctic dynamic discharge. Comparison with outputs from regional climate models indicate that dynamic discharge in the southern CAA only accounts for a small proportion of total ice loss there (~0.11% in 2011 based on the Q_{mid} estimate of discharge), and further highlights the fact that currently observed mass loss in the Canadian Arctic is dominated by surface melt and runoff, rather than dynamic discharge (iceberg calving).

Future acquisitions of ice thickness datasets, updated regional digital elevation models and investigations of basal conditions in regions of faster ice motion would all be beneficial in order to advance the knowledge of the controls on glacier dynamics within the southern CAA. Continued velocity mapping will enable the temporal evolution of surface velocities to be determined and aid with the identification of surge-type glaciers and help refine the length and peak velocities of surges.

Acknowledgements

We thank NSERC, Canada Foundation for Innovation, Ontario Research Fund, ArcticNet, Ontario Graduate Scholarship, University of Ottawa, Polar Continental Shelf Program and the NSERC Canada Graduate Scholarship for funding. Support for D.O. Burgess was provided through the Climate Change Geoscience Program, Earth Sciences Sector (contribution number 20150077), Natural Resources Canada. ALOS PALSAR data was obtained through the Alaska

Satellite Facility. Parks Canada, Christian Zdanowicz and various field assistants are gratefully acknowledged for assistance with fieldwork on Penny Ice Cap.

3.6 References

Burgess, D. O., M. Sharp, D. Mair, J.A. Dowdeswell, and T.J. Benham, (2005), Flow dynamics and iceberg calving rates of Devon Ice Cap, Nunavut, Canada, *Journal of Glaciology*. 51(173), 219-230.

Burgess, E. W., R. R. Foster, and C. F. Larsen, (2013), Flow velocities of Alaskan glaciers, *Nature Communications*, 4(2146), 1–8, doi: 10.1038/ncomms3146.

Dowdeswell, E.K., J.A. Dowdeswell, and F. Cawkwell, (2007), On the glaciers of Bylot Island, Nunavut, Arctic Canada, *Arctic, Antarctic and Alpine Research*, 29(3), 402-4011. doi: 10.1657/1523-0430(05-123)[DOWDESWELL]2.0.CO;2

Dupont, F., Royer, A., Langlois, A., Gressent, A., Picard, G., Fily, M., Cliché, P., and M. Chum, (2012), Monitoring the melt season length of the Barnes Ice Cap over the 1979-2010 period using active and passive microwave remote sensing data, *Hydrological Processes*, 26, 2643-2652.

Gardner, A. S., M. Moholdt, B. Wouters, G.J. Wolken, D.O. Burgess, M. Sharp, J.G. Cogley, C. Braun and C. Labine, (2011), Sharply increased mass loss from glaciers and ice caps in the Canadian Arctic Archipelago, *Nature*, 473(7347), 357–360, doi: 10.1038/nature10089.

Gardner, A., G. Moholdt, A. Arendt, and B. Wouters, (2012), Accelerated contributions of Canada's Baffin and Bylot Island glaciers to sea level rise over the past half century, *The Cryosphere*. 6, 1103-1125.

Gogineni, P., (2012), Radar Depth Sounder Data Products, Lawrence, Kansas, USA. Digital media. http://data.cresis.ku.edu/

Gray, A.L., K.E. Mattar, and G. Sofko, (2000), Influence on ionospheric electron density fluctuations on satellite radar interferometry, *Geophysical Research Letters*, 27(10), 1451-1454. Doi: 10.1029/2000GL000016

Gray, A.L., N. Short, K.E. Mattar, and K.C. Jezek, (2001), Velocities and flux of the Filchner Ice Shelf and its tributaries determined from speckle tracking interferometry, *Canadian Journal of Remote Sensing*, 27(3), 193-206.

Harbor, J.M.. (1992), Numerical modelling of the development of U-shaped valleys by glacier erosion, *Geological Survey of America Bulletin*, 104(10), 1364-1375, doi: 10.1130/0016-7606(1992)104<1364:NMOTDO>2.3.CO;2.

Heid, T., and A. Kääb, (2012), Repeat optical satellite images reveal widespread and long term decrease in land terminating glacier speeds, *The Cryosphere*, 6, 467-478.

Holdsworth, G., (1973), Evidence of a surge on Barnes Ice Cap, Baffin Island, *Canadian Journal of Earth Science*, 10, 1565-1574.

Holdsworth, G., (1977), Surging activity on the Barnes Ice Cap, *Nature*, 269, 588-590.

Lenaerts, J. T. M., J. H. van Angelen, J.H., M. R. van den Broeke, A.S. Gardner, B. Wouters, and E. van Meijgaard, (2013), Irreversible mass loss of Canadian Arctic Archipelago glaciers, *Geophysical Research Letters*, 40, doi:10.1002/grl.50214

Løken, O. H., (1969), Evidence of surges on the Barnes Ice Cap, Baffin Island, *Canadian Journal of Earth Sciences*, 6, 899-901.

Paterson, W. S. B. (1994), *The Physics of Glaciers*, 3rd edition, Elsevier, Oxford.

Rosen, P., S. Hensley, I. Joughin, S. Madsen, E. Rodriguez, and R. Goldstein, (2000), Synthetic Aperture Radar Interferometry, *Proceedings of the IEEE: Transactions on Geoscience and Remote Sensing*, 88(3), 333-382. doi: 10.1109/5.838084

Sharp, M., D.O., Burgess, F., Cawkwell, L., Copland, J.A., Davis, E.K., Dowdeswell, J.A., Dowdeswell, A.S., Gardner, D., Mair, L., Wang, S.N., Williamson, G.J., Wolken, and F. Wyatt, (2014), Remote sensing of recent glacier changes in the Canadian Arctic**.** In: Kargel, J.S., Leonard, G.J., Bishop, M.P., Kääb, A. and Raup, B.H. (eds). *Global Land Ice Measurements from Space*, Ch. 9, pp. 205-228. Praxis-Springer. doi: 10.1007/978-3-540-79818-7_9.

Short, N. H. and A. L. Gray, (2005), Glacier dynamics in the Canadian High Arctic from RADARSAT-1 speckle tracking, *Canadian Journal of Remote Sensing*, 31(3), 225–239, doi: 10.5589/m05-010.

Strozzi, T., A. Luckman, T. Murray, U. Wegmuller, and C.L Werner, (2002), Glacier motion estimation using SAR offset-tracking, *Proceedings of the IEEE: Transactions on Geoscience and Remote Sensing*, 40(11), 2384-2391. doi: 10.1109/TGRS.2002.805079

Van Wychen, W., L. Copland, L. Gray, D. O. Burgess, B. Danielson, M. Sharp, (2012), Spatial and temporal variation of ice motion and ice flux from Devon Ice Cap, Nunavut, Canada, *Journal of Glaciology*, 58(210), 657–664, doi: 10.3189/2012JoG11J164.

Van Wychen, W., D. O. Burgess, L. Gray, L. Copland, M. Sharp, J. A. Dowdeswell, and T. J. Benham, (2014), Glacier velocities and dynamic ice discharge from the Queen Elizabeth Islands, Nunavut, Canada, *Geophysical Research Letters*, 41, doi: 10.1002/2013GL058558.

Waechter, A., L. Copland, and E. Herdes, (2015), Modern glacier velocities across the Icefield Ranges, St. Elias Mountains, and variability at selected glaciers from 1959 to 2012. Journal of Glaciology, 61(228), doi: 10.3189/2015JoG14J147.

Wainstein, P., B. Moorman, and K. Whitehead, (2014), Glacial conditions that contribute to the regeneration of Fountain Glacier proglacier icing, Bylot Island, Canada, *Hydrological*

Processes, 28, 2749-2760 doi:10.1002/2013GL058558.

Williamson, S., M. Sharp, J. Dowdeswell, and T. Benham, (2008), Iceberg calving rates from northern Ellesmere Island ice caps, Canadian Arctic, 1999-2003, *Journal of Glaciology*, 54(186), 391-400.

Zdanowicz, C., A. Smetny-Sowa, D. Fisher, N. Schaffer, L. Copland, J. Eley, and F. Dupont, (2012), Summer melt rates on Penny Ice Cap, Baffin Island: Past and recent trends and implications for regional climate, *Journal of Geophysical Research*, 117, F02006, doi:10.1029/2011JF002248.

Table 3-1: Summary of ALOS PALSAR imagery used in this study. All imagery was 9 m resolution, and all beam modes were fine beam single polarization, except for a single pair (22-10-2011 to 07-12-2011), which was fine beam double polarization.

Image Date 1 (dd-mm-yyyy)	Image Date 2 (dd-mm-yyyy)	Image Segments	Region
08-01-2011	23-02-2011	2	Barnes Ice Cap (West)
25-03-2007	10-05-2007	6	Barnes Ice Cap (East), Coastal Glaciers
19-12-2010	03-02-2011	2	Penny Ice Cap (West)
01-03-2010	04-16-2010	3	Penny Ice Cap (Central)
31-12-2010	15-02-2011	2	Penny Ice Cap (East)
12-01-2011	27-02-2011	2	Southeast Baffin Island
24-01-2011	11-03-2011	2	Southeast Baffin Island
08-01-2011	23-02-2011	4	Bylot Island Ice Cap (East)
30-01-2011	17-03-2011	3	Bylot Island Ice Cap (West)
06-01-2011	21-02-2011	1	Northwest Baffin Island
28-01-2011	15-03-2011	1	Northwest Baffin Island
29-12-2010	13-02-2011	2	Central Baffin Island Coastline
10-01-2011	25-02-2011	3	Central Baffin Island Coastline
22-10-2011	07-12-2011	3	Central Baffin Island Coastline

Table 3-2: Comparison of displacements derived from in situ (dGPS) and speckle-tracking measurements on a transect across Penny Ice Cap (location of dGPS stations are denoted on Figure 3-4a).

Lat (°N)	Long (°W)	dGPS ID	Displacement (m a^{-1})			
			dGPS (2011-2012)	Speckle-tracking (2011)	Difference	Difference (%)
67.28	-65.85	P000	1.6	1.8	0.3	+18.75
67.25	-65.88	P101	1.7	1.1	-0.6	-35.29%
67.23	-65.91	P102	9.0	9.2	0.3	+3.33
67.22	-65.96	P103	16.1	18.9	2.8	+17.39
67.21	-65.97	P104	20.8	17.9	-3.0	+14.42
67.20	-66.02	P105	34.8	47.9	13.1	+37.64
67.16	-66.13	P107	9.4	9.1	-0.4	-4.25
67.15	-66.16	P108	80.9	91.6	10.8	+13.34
67.13	-66.19	P109	102.5	103.4	0.9	+0.87
67.09	-66.23	P111	82.7	82.8	0.1	+0.12
67.07	-66.26	P112	80.1	84.0	3.9	+4.86
66.86	-66.26	P120	38.4	34.4	-4.0	+10.41
67.29	-65.85	P201	2.3	6.9	4.6	+200.00
67.34	-65.85	P202	1.6	1.4	-0.1	-6.25
67.39	-65.83	P203	1.6	8.0	6.4	+400.00
67.42	-65.75	P204	1.3	7.7	6.4	+492.30
67.43	-65.67	P205	2.8	6.7	3.9	+139.28
67.03	-65.26	CG01	91.4	105.2	13.8	+15.09
67.06	-65.16	CG02	58.3	37.0	-21.3	-36.53
67.13	-64.99	CG03	43.9	21.9	-22.0	-50.11
67.14	-65.02	CG04	27.2	23.3	3.9	+14.33
67.19	-64.87	CG05	44.1	30.9	-13.2	+29.93
67.19	-64.83	CG06	47.8	34.8	-13.1	+27.40
				Mean difference (absolute):	**7.9**	

Table 3-3: Estimated frontal ablation from the tidewater terminating glaciers of Baffin and Bylot Islands. "*" denote glaciers where the "Outlet" glacier scenario was used to estimate ice thickness.

Glacier ID	Lat (°N)	Long (°W)	Discharge (Mt a^{-1})		
			Q_{min}	Q_{mid}	Q_{max}
1	70.23	-70.63	0.3	0.9	1.7
2	70.25	-70.62	0.0	0.2	1.0
3	70.33	-70.60	0.0	0.1	0.7
4	66.60	-62.07	0.6	1.5	2.6
5	69.73	-69.81	0.0	0.2	0.5
6	69.92	-70.14	0.0	0.4	1.2
7	70.52	-71.68	0.0	0.5	1.2
8	70.45	-71.85	0.0	0.8	2.2
9	70.42	-71.98	0.5	1.2	2.0
10	70.54	-71.20	0.1	0.5	1.0
11	70.92	-72.33	0.0	0.2	0.7
12	71.05	-73.33	0.0	0.1	0.2
13	71.07	-73.26	0.0	0.1	0.4
14	71.11	-73.21	0.1	0.3	0.7
15	71.17	-73.16	0.0	0.1	0.4
16	72.01	-75.21	0.3	1.0	1.7
17	72.11	-74.87	0.0	0.2	0.8
18	71.74	-74.83	0.0	0.4	1.0
19	71.79	-75.69	0.0	0.1	0.3
20	71.87	-75.69	3.5	7.2	10.4
21	72.05	-75.99	0.0	0.1	0.2
22	72.09	-75.83	0.0	0.1	0.2
23	71.94	-75.62	1.7	3.7	5.6
24	71.73	-75.84	0.7	1.5	2.2
25	71.89	-76.25	0.1	0.3	0.7
26	72.00	-76.03	0.2	0.7	1.4
27	72.07	-75.92	0.1	0.3	0.6
28	72.61	-76.43	0.0	0.1	0.3
29	72.46	-76.07	0.0	0.2	0.6
30	72.14	-75.70	0.0	0.3	1.9
31	72.11	-75.90	0.0	0.2	0.4
32	72.07	-76.04	0.0	0.1	0.4
33	71.92	-76.31	0.2	0.6	1.2
34	71.85	-76.40	0.0	0.1	0.5
35	73.24	-81.13	0.0	0.2	0.5
36	73.23	-81.06	0.3	0.8	1.4
37	69.32	-69.17	0.0	0.5	1.3
38	69.58	-68.65	0.0	0.4	1.0
39	71.36	-73.96	0.0	0.3	0.6
40	71.44	-73.87	0.0	0.1	0.4
41	71.59	-74.53	0.1	0.4	0.8
42	71.59	-74.25	0.0	0.2	0.6
43*	67.58	-66.02	3.3	10.6	19.3
44*	67.19	-64.83	2.7	9.3	17.5
45*	73.68	-80.10	0.5	2.2	5.0
46*	73.64	-79.55	1.2	5.6	12.6
Total Discharge			**16.6**	**54.7**	**107.9**

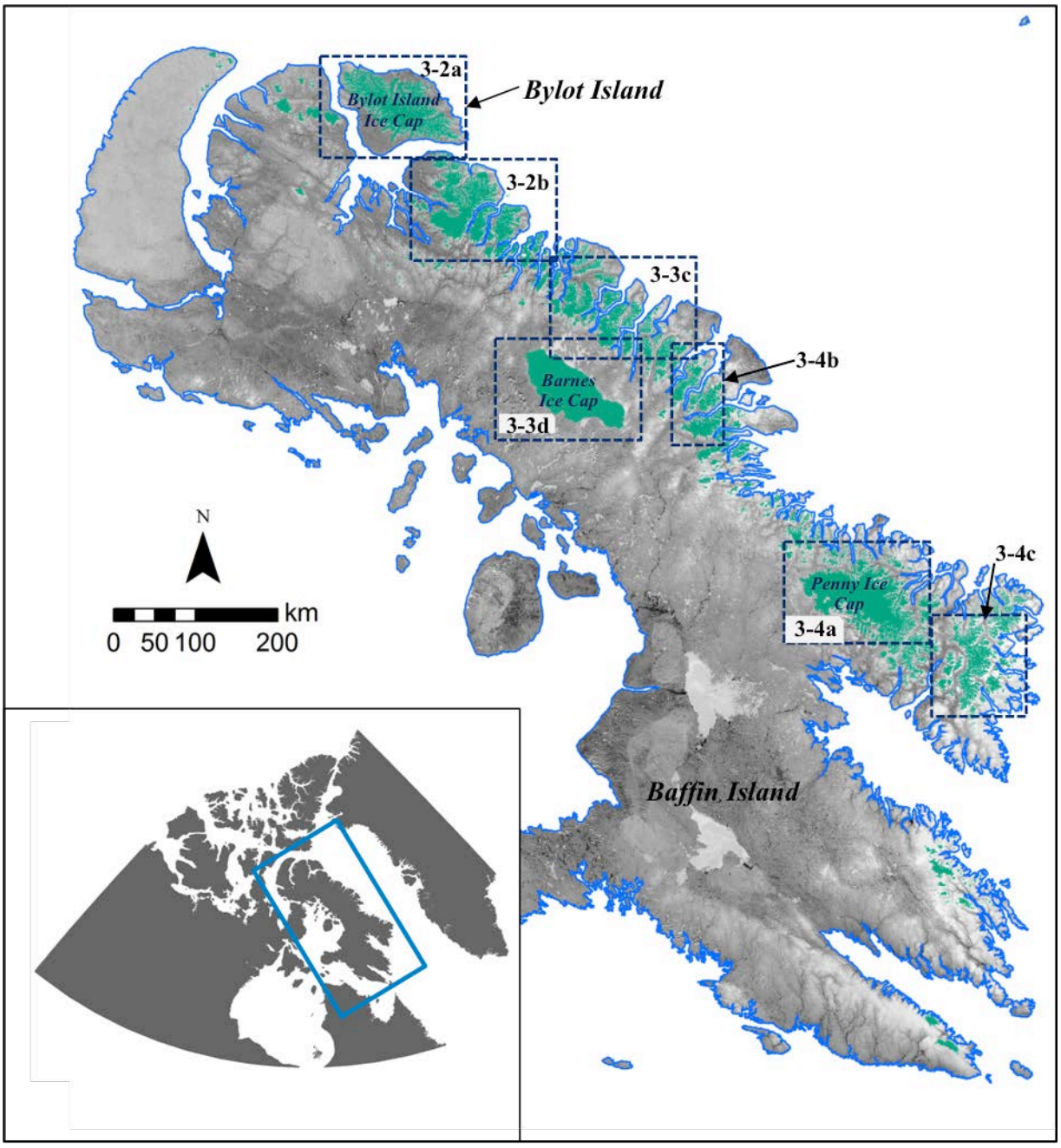

Figure 3-1: Location of the major ice masses of Baffin and Bylot Islands (shown in green). Base Image: MODIS Terra, July 2, 2011. Dashed boxes indicate the extents of Figures 3-2 to 3-4.

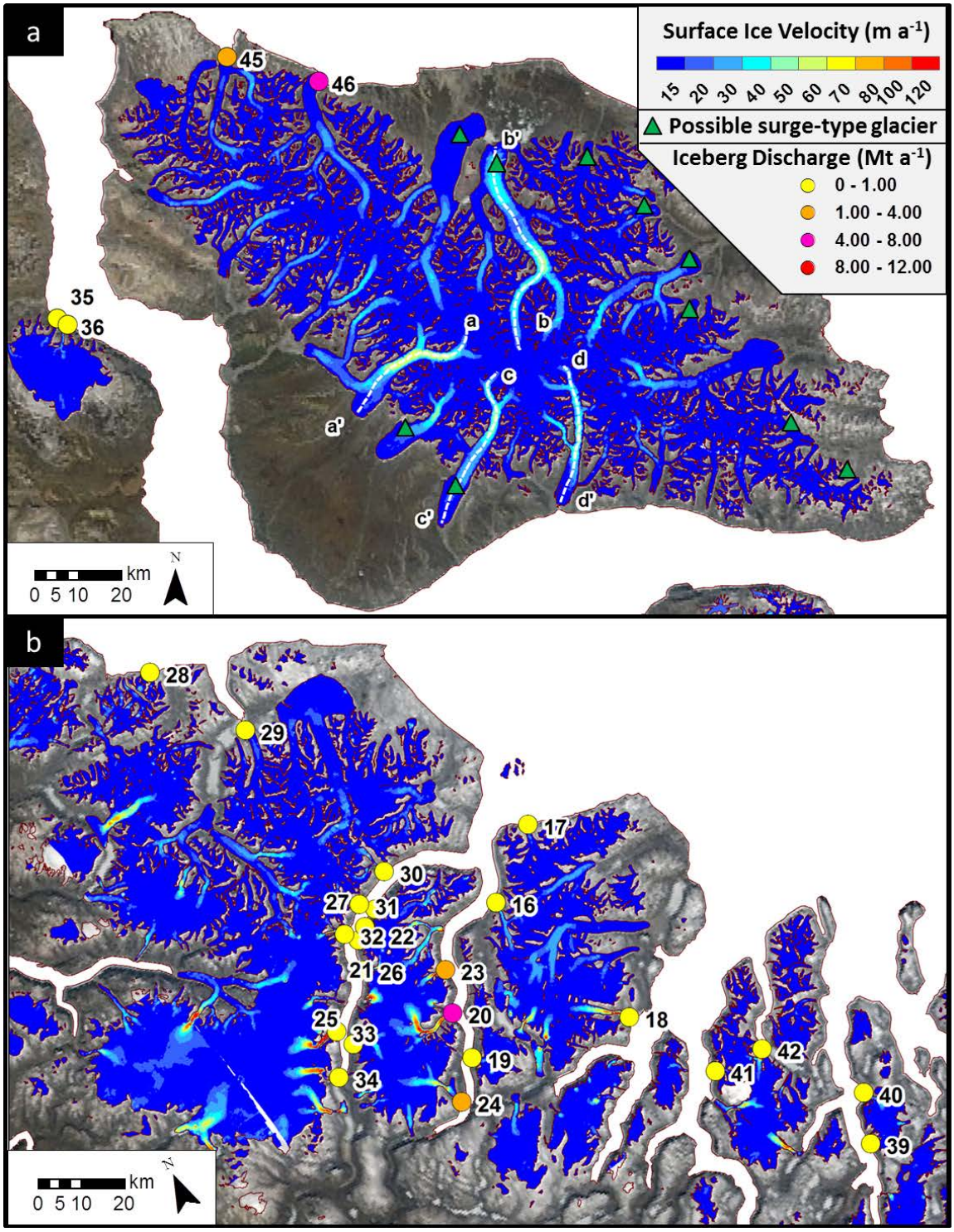

Figure 3-2: Surface velocity structure of a) Bylot Island Ice Cap and b) and the coastal glaciers of Northern Baffin Island. Standalone numbers denote glacier IDs presented in Table 3-3. White dashed lines and standalone letters indicate the location of extracted centerline velocities presented in Figure 3-5. Base Image: MODIS Terra, July 2, 2011.

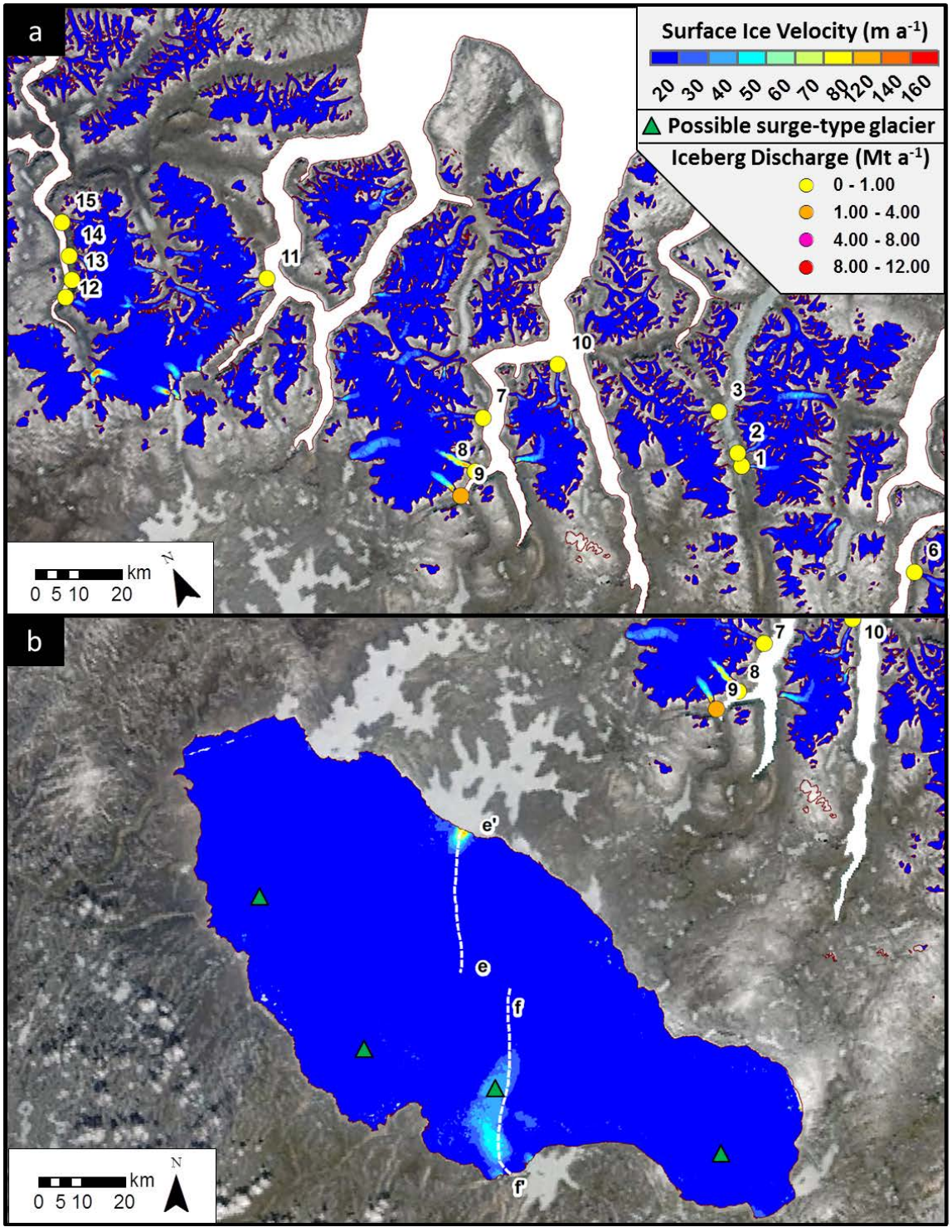

Figure 3-3: Surface velocity structure of a) the central coastal glaciers of Baffin Island and b) Barnes Ice Cap. Standalone numbers denote glacier IDs presented in Table 3-3. White dashed lines and standalone letters indicate the location of extracted centerline velocities presented in Figure 3-5. Base Image: MODIS Terra, July 2, 2011.

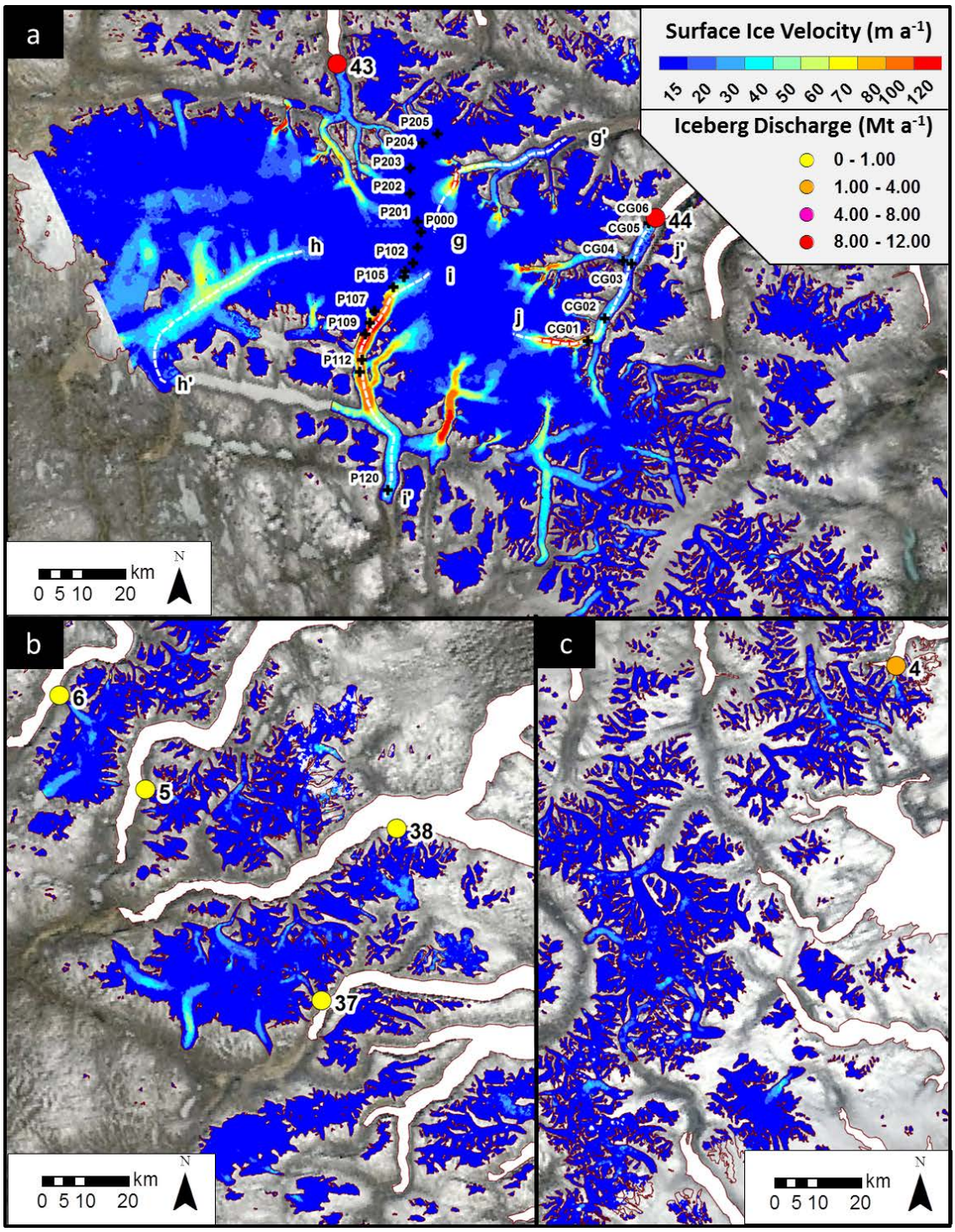

Figure 3-4: Surface velocity structure of (a) Penny Ice Cap, (b) central coastal glaciers and (c) southeastern coastal glaciers ("+" indicates locations of in situ dGPS observations and CG/P notations provide reference IDs referred to in Table 3-2). Standalone numbers denote glacier IDs presented in Table 3-3. White dashed lines and standalone letters indicate the location of extracted centerline velocities presented in Figure 3-5. Base Image: MODIS Terra, July 2, 2011.

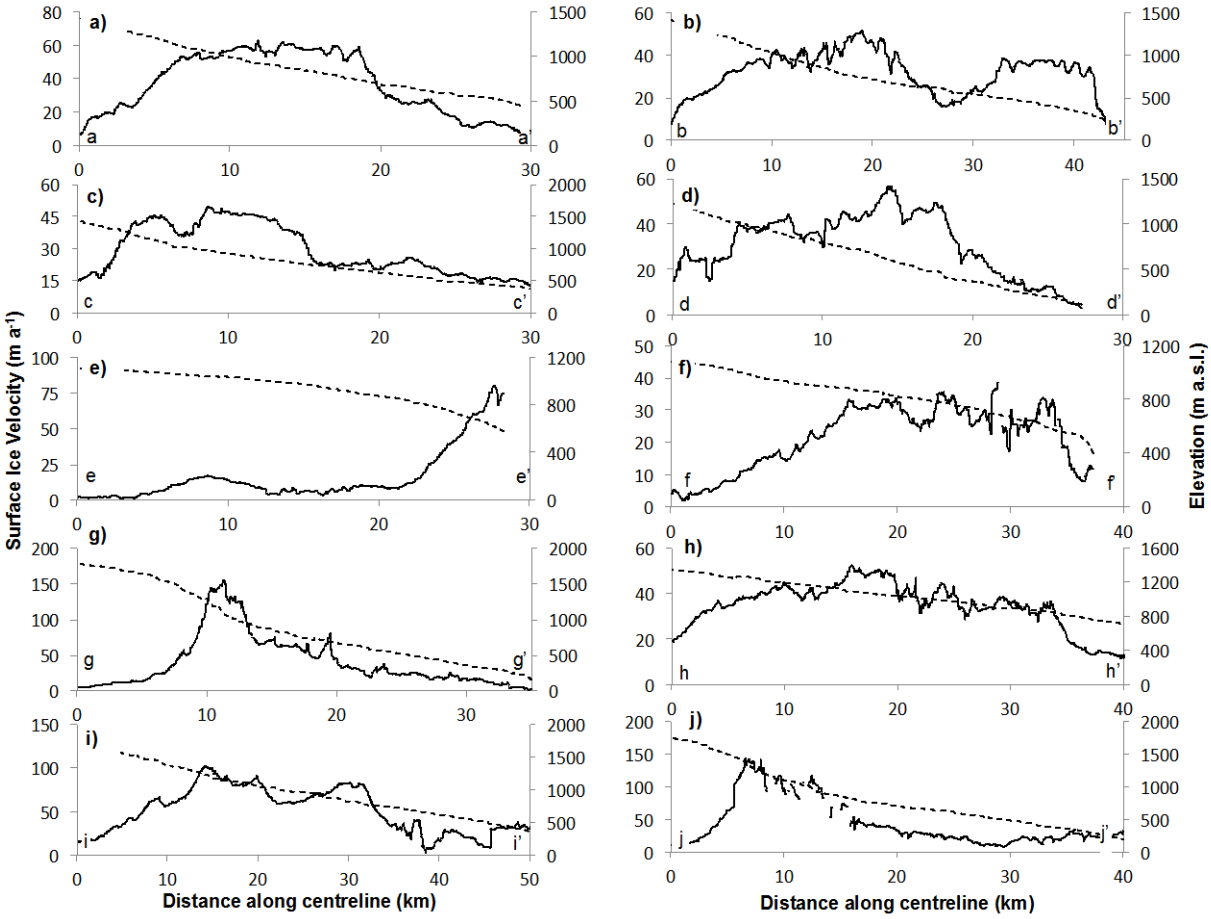

Figure 3-5: Solid lines denote centreline glacier velocities for select glaciers on Bylot Island Ice Cap (a-d), Barnes Ice Cap (e-f) and Penny Ice Cap (g-j). Exact locations of each centreline are presented in Figures 3-2 to 3-4. Dashed lines indicate the surface elevation profile of each glacier as extracted from the 1:250 000 Canadian Digital Elevation Dataset (CDED).

CHAPTER FOUR: Characterizing inter-annual variability of glacier dynamics and dynamic discharge (1999-2015) for the ice masses of Ellesmere and Axel Heiberg Islands, Nunavut, Canada

Abstract:

Landsat-7 and RADARSAT-1/2 satellite images are used to produce the most comprehensive record of glacier motion in the Canadian High Arctic to date, and to characterize spatial and temporal variability in ice flow over the past ~15 years. This allows an assessment of whether dynamically-driven glacier change can be attributed to "surging" or "pulsing", or whether other mechanisms are involved. RADAR velocity mapping allows annual regional dynamic discharge (iceberg calving) to be calculated for 2000 and the period 2011-2015 (yielding a mean regional discharge of 2.21 ± 0.68 Gt a^{-1}) and velocities derived from feature tracking of optical imagery allow for annual dynamic discharge to be calculated for select glaciers from 1999-2010. Since ~2011, several of the major tidewater-terminating glaciers within the region have decelerated and their dynamic discharge has decreased. Trinity and Wykeham Glaciers (Prince of Wales Icefield) represent a notable departure from this pattern as they have generally accelerated over the study period. The resulting increase in dynamic discharge from these glaciers entirely compensates (within error limits) for the decrease in discharge from the other tidewater glaciers across the study region. These two glaciers accounted for ~62% of total regional dynamic discharge in winter 2015 (compared to ~22% in 2000), demonstrating that total ice discharge from the Canadian High Arctic can be sensitive to variations in flow of just a few tidewater glaciers.

4.1 Background and Study Site

The area of the ice masses of Axel Heiberg and Ellesmere Islands (Figure 4-1 inset) was ~89,000 km^2 in ~2000, which is ~85% of the glacier area in the northern Canadian Arctic Archipelago [Sharp et al. 2014; Thomson et al. 2011]. Van Wychen et al. [2014] used winter 2012 RADARSAT-2 imagery to produce the first complete velocity maps and estimates of dynamic discharge from these ice masses (building on earlier regional measurements by Short and Gray [2005] and Williamson et al. [2008]). Hattersley-Smith [1969] and Mü1ler [1969] described dynamic variability (attributed to surging) within the region as early as the 1960s. Copland et al. [2003a] identified at least 51 surge-type glaciers on Devon, Axel Heiberg and Ellesmere Islands and provided the first comprehensive catalogue of the region's surge-type glaciers based on analysis of aerial photography (1959/1960) and Landsat-7 imagery (1999/2000). Together, these studies indicate that both glacier dynamics and iceberg discharge from the ice masses of Axel Heiberg and Ellesmere Islands vary both spatially and temporally.

There are several known mechanisms whereby glaciers in the Canadian Arctic can undergo dynamic changes on a seasonal basis. These include supraglacial hydrological forcing, whereby surface melt is transmitted to the bed, leading to enhanced glacier flow (e.g. Bingham et al. [2003]; Boon and Sharp [2003]; Copland et al [2003b]) and, for tidewater terminating glaciers, sea ice/mélange forcing, where reductions in sea ice/mélange strength reduce their buttressing effect on the glacier front, resulting in increased glacier velocities (e.g. Williamson et al. [2008]). Oceanic forcing, where increases in ocean temperature drive increased melt rates at glacier termini leading to thinning and acceleration, has been identified in nearby Greenland (e.g. Holland et al. [2008]; Murray et al. [2010]; Christoffersen et al. [2011]), and may also influence glacier dynamics within the Canadian Arctic. However the nature and causes of tidewater glacier velocity variability have not been well investigated in the Canadian Arctic, and most previously observed variations in the motion of tidewater glaciers have either been attributed to surging (e.g. Van Wychen et al. [2012]; Copland et al. [2003a]) or remain unexplained due to a lack of multi-year observations.

Surge-type glaciers undergo a cyclic behaviour, with periods of rapid acceleration and advance (active phase) followed by periods of slow flow where ice fluxes are less than balance fluxes

(quiescent phase) [Clarke 1987; Benn and Evans 2010]. Differences in the duration of the active and quiescent phases observed on surge-type glaciers in Alaska and Svalbard have led to the classification of surge-type glaciers as either "Alaskan-type" or "Svalbard-type" [Benn and Evans] and to speculation that there may be different mechanisms of surge initiation for the two types. The relatively short active (~1-4 years) and quiescent (~35-40 years) phases of "Alaskan-type" surge-type glaciers, combined with surge termination that is coincident with large outburst floods, suggest that build-up of water pressure in a linked-cavity subglacial drainage system plays an important role in the initiation of surges of these glaciers [Kamb et al. 1987; Murray et al. 2003]. The longer active (~7-15 years) and quiescent (~50-100 years) phases of "Svalbard-type" surge glaciers, combined with surge termination that occurs over a multi-year period [Dowdeswell et al. 1991; Murray et al. 1998], suggest that these surges are linked to changes in basal thermal conditions rather than subglacial water pressure [Murray et al. 2003]. The longer active phases reported on land-terminating glaciers in the Canadian Arctic (e.g., at least 10 years for Good Friday Bay Glacier) led Copland et al. [2003a] to surmise that surge-type behavior within the Canadian Arctic was likely similar to "Svalbard-type" surge glaciers.

A major limitation of earlier studies of variability in glacier motion within the Canadian Arctic is that dynamic change has largely been inferred rather than measured. In those cases where glacier velocities have been measured, measurements have been limited to short time periods (e.g. glacier velocities were only measured over 1-3 years). As a result, the spatial and temporal scales of variability in glacier dynamics have not been well constrained. This hinders identification of the mechanisms responsible for variability in ice flow within the region. Understanding the processes that are responsible for regulating ice flow is of paramount importance for explaining how and why mass loss via dynamic discharge varies over time, and for accurately projecting future contributions to sea level rise from the Canadian Arctic.

We produced surface velocity maps for all ice-covered terrain on Axel Heiberg and Ellesmere Islands from RADARSAT-1 fine beam data (8 m resolution; 2000, 2006-2007) and RADARSAT-2 fine and ultrafine beam data (8 m and 3 m resolution; 2009-2014) (Table 4-1). Feature tracking of Landsat-7 ETM+ (15 m resolution) imagery from 1999-2010 was also used to determine the motion of ~14-16 glaciers to extend the spatial and temporal record of ice

motion (Table 4-1). We use this ~15 year record of ice motion to quantify the timescale and magnitude of glacier dynamic fluctuations across the Canadian Arctic for the first time. This record is augmented with a record of glacier terminus positions to provide insight into the mechanisms that are driving the dynamic changes. Where available, we compare glacier bed, ice thickness and surface elevation profiles to understand topographic conditions in regions where velocity variability occurs and identify features (e.g. basal topographic features) that may be regulating ice motion. Additionally, the velocities (derived both from RADAR and optical imagery) are combined with measurements of the ice thickness of major outlet glaciers to estimate the regional dynamic discharge in 2000 and from 2011-2015 and, for select glaciers with available velocity data from 1999-2010. Here we define dynamic discharge (sometimes termed iceberg calving or frontal ablation in other studies) as the mass of ice passing through a fixed terminus flux gate and do not account for the effect on ice flux of terminus advance or retreat.

4.2 Methods and Data

4.2.1 Satellite Imagery

Radsarsat-1 imagery for the year 2000 was obtained from Alaska Satellite Facility's Vertex Data Portal (https://vertex.daac.asf.alaska.edu/) and for 2006 to 2008 from archives held by the Geological Survey of Canada. All RADARSAT-1 imagery was obtained in level 0 CEOS format, and processed to single look complex images with GAMMA Modular SAR Processor software. RADARSAT-2 data were obtained through Natural Resources Canada's RADARSAT-2 Government Data Allocation administered by the Canadian Space Agency. Nearly all RADARSAT-1 and -2 scenes were acquired from mid-fall to early spring (November-April), when the glacier surface remains relatively undisturbed between image acquisitions (e.g. snowfall is minimal and melting is rare). This increases the likelihood that the selected images will produce reliable velocity measurements.

Cloud-free and snow-free panchromatic (band 8) Landsat-7 Enhanced Thematic Mapper Plus (ETM+) images from 1999-2010 (used for feature tracking) and multi-spectral Landsat-8 Operational Land Imager (OLI) (used to derive terminus positions in 2013-2014) were obtained from the United States Geological Survey (USGS) data portal (http://earthexplorer.usgs.gov/).

Cloud-free and snow-free ASTER (Advanced Spaceborne Thermal Emission and Reflection Radiometer) L1B data (used to derive terminus positions and identify surface features indicative of surging from 2000-2012) were obtained from NASA's online data portal (http://reverb.echo.nasa.gov/). All Landsat-7/8 imagery was preprocessed with the USGS Level 1 product generation system that includes radiometric and geometric correction and transformation to the Universal Transverse Mercator projection. Due to the scan line corrector failure of Landsat-7, stripes occur across the non-central parts of imagery after May 31, 2003. Although estimates of surface velocities derived in the study are not affected by the data gaps [Haug et al. 2010], images that minimize data gaps were preferentially selected. Imagery was selected from the summer and early fall (~May to September) to minimize snow cover, and separated by ~365 days to minimize the effect of seasonal velocity fluctuations on estimates of annual mean displacement. An inventory of imagery used in this study is provided in Table 4-1.

4.2.2 Determination of Ice Motion

We determine ice motion using speckle tracking for RADAR imagery acquired during a single winter season and feature tracking for Landsat summer imagery acquired at ~1 year intervals. As a consequence, we refer to velocities derived from RADAR imagery as "winter velocities" (although the results are extrapolated to annual values) and to those derived from Landsat imagery as "annual velocities" in order to distinguish between the two. We expect a discrepancy between the two datasets, as the "annual velocities" are likely to include spring/summer speed-ups that increase total annual motion relative to that which would be derived by extrapolation of winter velocities.

4.2.1 Speckle Tracking of RADARSAT Data

Surface ice motion was determined using custom speckle-tracking code written in MATLAB^{TM} for both RADARSAT-1 and RADARSAT-2 datasets [Van Wychen et al. 2012; 2014; Short and Gray 2005]. This code utilizes a cross-correlation algorithm on image chips from co-registered 24-day or 48-day image pairs to determine the relative displacement of features between scenes. Due to poorer orbital knowledge of RADARSAT-1 relative to RADARSAT-2, an additional manual co-registration of the RADARSAT-1 image pairs was required. This involved identification of features common to both the master and slave images to determine the offset

between them. Overlapping image chips of ~450 m in azimuth direction and ~350 m in range were used to determine displacements. The 1:250,000 Canadian Digital Elevation Dataset, Level 1, was used to remove the topographic component in the slant range displacement. To remove systematic biases due to inaccuracies in satellite baseline estimates or squint effects between image acquisitions, displacements were calibrated using areas of zero motion (bedrock outcrops) to determine the local bias, which was then removed manually from the rest of the dataset. Final displacements were standardized to annual values and imported into ArcGIS™ 10.1 for verification. To identify and filter mismatches, manual checking of the dataset was undertaken using the following criteria [Van Wychen et al. 2012; 2014]:

1) due to lateral drag, surface velocities should be faster along glacier centerlines than at margins;
2) flow vectors should be constrained by topography and oriented with surface flow features (e.g., medial moraines);
3) flow vectors should depict relatively coherent flow units and should not deviate greatly from adjacent vectors.

Mismatches identified using the above criteria were manually removed from the dataset and the velocities were resampled to a 100 m resolution raster using inverse distance-weighting interpolation. Rasters derived from individual image pairs were mosaicked to produce a single raster dataset for each individual ice mass and clipped to the extent of version 3.2 of the GLIMS Randolph Glacier Inventory (RGI) for the Canadian High Arctic [Pfeffer et al. 2014]. In regions of raster overlap, the lowest velocity value was selected in order to provide a conservative estimate of surface motion, following the methodology of Short and Gray [2005] and Van Wychen et al. [2012, 2014].

4.2.2 Feature Tracking of Landsat-7 ETM+ Datasets

An automated, variable correlation block size MATLAB™ algorithm implemented in the frequency domain was developed to derive time series of glacier surface velocities from the Landsat-7 data. This method begins by automatically co-registering all imagery to a common base image (in this case, to imagery acquired in 2000) and then uses a cross-correlation

algorithm on co-registered intensity gradient images (similar to Haug et al. [2010]) to determine displacements between image pairs. After the images have been matched at the initial correlation block size and the resultant motion vectors have been calculated, a nearest neighbor filter is applied to the velocity field to identify incorrect matches (tolerance for mismatches is user defined). For each incorrect match, the block size is increased and the cross-correlation algorithm is automatically re-run. The process is repeated until an established maximum correlation block size is used. This approach is computationally efficient and effective for determining ice motion on glaciers with large spatial gradients in surface velocities (e.g. tributaries versus main glacier trunks). A comparison of the fixed-block and variable-block image cross correlation approach for deriving glacier motion is provided by Sharp et al. [2014]. Any remaining mismatches were manually removed from the dataset using the method described in section 2.2.1 and the final displacements were standardized to annual values.

4.2.3 Velocity Error Analysis

4.2.3.1 Speckle Tracking Error Analysis

Errors associated with the speckle tracking method and the random error associated with the cross-correlation technique between coherent complex image chips have been described in previous studies (e.g. Gray et al. [2001], Joughin [2002], Short and Gray [2004]). Speckle tracking applied to 24-day repeat imagery with good coherence (>~0.6) is able to produce velocity errors of 2-10 m a^{-1} in the Canadian Arctic [Short and Gray 2005]. In heavily-crevassed, faster-flowing regions, where the method reverts to feature tracking, errors of 10-20 m a^{-1} are more likely [Short and Gray 2005]. To determine error bounds for the velocity measurements of each ice mass for each year in this study, velocities were extracted from regions of known zero or near-zero motion. These regions consisted of bedrock outcrops within and adjacent to the ice masses, and ice divides as delineated in version 3.2 of the RGI. Non-zero velocity values derived over apparently stationary features ranged from 3.7 m a^{-1} (SD = 5.3 m a^{-1}) over Manson Icefield in 2014, to 21.1 m a^{-1} (SD = 7.2 m a^{-1}) over Manson Icefield in 2008 (Table 4-2). To provide an estimate of confidence in our speckle tracking results, we use the root sum of squares from all the separate sources of error (bedrock outcrops and ice divides) for each ice mass, which yields an uncertainty estimate of ± ~8.7 m a^{-1}.

4.2.3.2 Feature Tracking Error Analysis

For feature tracking displacements, the maximum error in the co-registration procedure was 0.75 of a pixel (11.25 m) in both the x and y image directions. There is an additional error associated with how the cross-correlation algorithm picks the sub-pixel location of the correlation peak, which is quantified as 0.5 pixels (7.5 m). Both of these errors are considered to be independent in the x and y directions. The resultant error in ice surface velocity derived from feature tracking of Landsat-7 data is then calculated to be ± 19 m a^{-1} by combining the co-registration and correlation peak errors.

4.3.4 Identification of Surge Features and Terminus Positions

ASTER (15 m resolution) and Landsat-8 OLI (30 m resolution) multispectral images were used to identify features indicative of surge activity such as looped moraines, extensive fresh crevassing, and digitate termini, as described by Copland et al. [2003a]. The lack of multi-temporal, high quality elevation data for the Canadian Arctic precludes the identification of glacier geometry changes associated with surges (e.g. reservoir area thinning and receiving area thickening) for most of the region's glaciers, although terminus advance coincident with increases in glacier motion can be used as a proxy for such changes, albeit an imperfect one. Thus, for the larger tidewater terminating glaciers that experienced significant changes in surface velocity between the beginning and end of the study period, we also used ASTER and Landsat-8 panchromatic data (15 m resolution) to quantify the annual pattern of terminus advance, stagnation or retreat. Positional error in this imagery is assumed to be roughly the size of the image pixel. Monitoring of the terminus positions aids in the determination of whether dynamic changes observed over the period 2000-2014 were associated with changes in the glacier geometry, the patterns of which can be used to infer whether the dynamic changes can be explained in terms of surging, or whether other mechanisms are required.

4.3.5 Determination of Dynamic Discharge

We define dynamic discharge as the mass passing through a terminus flux gate per unit time. However, our analysis does not account for changes in discharge due to terminus retreat or advance. To compute dynamic discharge, we determine the amount of mass transferred through a cross-section near the grounding line of each tidewater glacier within the study region (all flux

gates are fixed in space and are located within 1-5 km of the 2014 glacier calving front). To define flux gates, ice thicknesses were derived from airborne-radar measurements made with the Multichannel Coherent RADAR Depth Sounder (MCoRDS) sensor during the NASA Airborne Topographic Mapping (ATM) mission in the spring of 2006 and NASA Operation Icebridge campaigns in 2012 and 2014. Error in the ice depth measurements recorded by the MCoRDS sensor is ~±10 m and provides the value used for the ice thickness error (H_{error}) in equations (1) and (2) below [Gogineni, 2012; Van Wychen et al. 2014].

For glaciers where ice thickness measurements were acquired perpendicular to glacier flow (23 of 49 glaciers), a cross-sectional fluxgate was created whereby the terminus width was divided into evenly spaced columns. In limited instances where ice thickness data were missing from parts of the cross section (3 of 23 glaciers), we used a linear interpolation to fill in missing data. Interpolated ice column widths of 20 m were used to be consistent with the measurements provided by MCoRDS. For each column, the measured surface velocities were converted to a depth-averaged value (80% of surface velocity [Paterson 1994] for the lower estimate (Q_{min}), and 100% of surface velocity (which assumes all flow is by basal slip) for the upper estimate (Q_{max})). Minimum and maximum estimates of discharge were then made for each column width (W) using:

$$Q_{min} = (0.8 * (V - V_{error})) * (H - H_{error}) * (W) \quad (1)$$

$$Q_{max} = (V + V_{error}) * (H + H_{error}) * (W) \quad (2)$$

where V is surface velocity, V_{error} is the error associated with each velocity dataset (Table 4-2 provides uncertainty estimates for the RADAR velocity dataset while an uncertainty of ±19 m a^{-1} is used for velocities derived from Landsat ETM+ imagery), and H is the ice thickness. Both Q_{min} and Q_{max} are then summed across the entire flux gate, and the reported dynamic discharge is the average of the two, with Q_{min} and Q_{max} providing the lower and upper error margins, respectively.

For glaciers where only centerline ice depth measurements are available (26 of 49 glaciers), we used the following parabolic function to create a "U" shaped fluxgate:

$$H_{interpolated} = ((10\text{-}C/ D_1^2) \text{ x } (D_2^2) + C \quad (3)$$

Where $H_{interpolated}$ is the interpolated ice thickness measured from the centerline depth to the glacier marginal ice depth of 10 m, C is the measured centerline depth, D_1 is the distance from the centerline to the glacier margin, and D_2 is the distance from the centerline to the center of the interpolated ice column. Ice column thickness was interpolated at 20 m intervals from the centerline to the margins of each glacier.

This method provides approximations of glacier morphology that are consistent with known depth distributions of tidewater glaciers within the Canadian High Arctic [e.g. Gogineni, 2012], and is consistent with methods used previously to interpolate fluxgates in the study region [Van Wychen et al. 2014]. Van Wychen et al. [2014] compared glacier depths derived using the parabolic interpolation function with those obtained where the actual bedrock form was measured. They found that the modeled geometry tended to underestimate the true cross-sectional area by ~12%.

The RADAR derived flux estimates do not include summer speed-up events (e.g. enhanced motion associated with supraglacial drainage or sea ice buttressing) and are likely to provide conservative estimates of total annual discharge. Flux derived from feature tracking velocities more accurately represents annual mass loss via calving, however is restricted to ~10-15 glaciers within the region with distinct surface features to track which provide reliable velocities across the entire terminus flux gate.

4.3.5.1 Longitudinal Bed Elevation Profiles

To investigate the influence of glacier bed topography on dynamics we use longitudinal bed elevation profiles collected over the Canadian Arctic in 2000 [Dowdeswell et al. 2004]. These profiles were collected roughly along glacier centerlines using an airborne 100 MHz ice-penetrating RADAR system (details on sensor characteristics and data processing are provided by [Dowdeswell et al. 2004]). Error associated with the measurements is ~ ±10 m based on the comparison of coincident elevations derived from crossing flight paths.

4.4 Results

4.4.1 General Ice Dynamics of Ellesmere and Axel Heiberg Islands

The velocity structure of the Ellesmere and Axel Heiberg island ice caps measured in this study (Figure 4-1) is consistent with the pattern of ice motion described previously for ice caps in the Canadian High Arctic [e.g. Van Wychen et al. 2014; Short and Gray 2005; Williamson et al. 2008], although the temporal coverage is greatly improved. In general, velocities are low (<20 m a^{-1}) in interior regions of ice caps, suggesting that ice in these regions is frozen to the bed and flowing by internal deformation alone. Velocities tend to increase along the main trunk of outlet glaciers as they descend towards glacier termini. These down-glacier velocity increases may be linked to a transition from cold to warm basal conditions as ice is channeled into relatively deep and narrow troughs in the ablation area, or to changes in bedrock topography (sills and steps), the presence/absence of subglacial sediments, or changes in subglacial sediment type [Burgess et al. 2005; Copland et al. 2003a]. Surface velocities measured in this study rarely exceed 75 m a^{-1} for land terminating glaciers and 400 m a^{-1} for the terminal regions of tidewater glaciers (notable exceptions are the Otto, Mittie (pre-2004), and Trinity and Wykeham Glaciers). There is a tendency for higher flow rates in glaciers draining the eastern edge of the archipelago that is likely driven primarily by locally high rates of accumulation. These are associated with the proximity of Baffin Bay, the region's major moisture source, and regional climate patterns that result in relatively high accumulation rates on the seaward margins of ice masses and lower accumulation rates on their more continental margins [Koerner 1979; 2005].

4.4.2 Comparison of "Winter" (Speckle Tracking) and "Annual" (Feature Tracking) Velocities

To determine how well velocity maps derived from speckle tracking of winter RADARSAT imagery capture annual glacier motion we differenced them from the annual Landsat-7 feature tracking results for all years with spatial and temporal overlap. Based on a total of 970,803 overlapping points, the winter velocities were ~13.6% (SD = 40%) lower than the annual velocities, which can be explained by enhanced glacier motion during the summer months when: a) surface melt may penetrate to the glacier bed and enhance basal sliding and/or b) absence of sea ice/mélange may reduce back pressure on the terminus, facilitating more rapid flow across the grounding line of tidewater terminating glaciers. To assess whether these differences varied at the terminus we extracted a cross-sectional velocity profile within 5 km of the calving front for

seven glaciers with coincident velocity data derived both from RADAR and optical data (Figure 4-2). Within the lowermost terminus region, the difference between winter and annual velocities becomes larger, with winter speckle tracking velocities typically ~15-25% lower than annual feature tracking results. This suggests that dynamic discharges calculated from speckle tracking velocities are a conservative estimate of annual mass flux.

4.4.3 Areas of Velocity Change

The annual surface velocity mosaics were differenced from each other to identify regions where significant (>~20 m a^{-1}) velocity changes have occurred during the last ~10-15 years. Overall, the majority of glaciers (101 of 117, ~86%) showed no significant velocity changes over the period 1999-2015 (Figure 4-1). The remaining 16 glaciers exhibited long term velocity changes in excess of the error associated with the individual datasets and the greater than expected seasonal differences between velocities derived from winter only data and velocities derived from nearly annually separated imagery. For these glaciers, the glacier centerline velocity structure was plotted separately for glaciers that either slowed down (Figure 4-3), displayed temporally variable velocities (Figure 4-4), or sped up (Figure 4-5). The following discussion focuses on these three sets of glaciers.

4.4.3.1 Glaciers with Velocity Decrease

Eight of 117 glaciers (~7%) exhibited a significant multi-year reduction in velocity during the observation period (Figure 4-3, Table 4-3). These glaciers are distributed throughout the study region and show no distinct spatial pattern, although they are predominantly large and tidewater-terminating (Middle Glacier is the only land terminating glacier in this group). The combined speckle tracking and feature tracking velocities reveal that deceleration of many of the glaciers occurred over a five to seven year period, and for the glaciers that showed the most dramatic velocity decreases (Antoinette, Eugenie, Iceberg, Mittie) the glacier became essentially stagnant (velocities < 20 m a^{-1}). The glaciers that slowed down less dramatically (Tuborg, Ekblaw, Good Friday Bay, Middle) did so over a 5-10 year period, but they are not currently stagnant in their lower regions, which may mean that they are still decelerating.

4.4.3.2 Glaciers with Variable Velocity Change

Six of 117 glaciers (~5%) exhibited bi-directional velocity changes (speed-up followed by slow down, or vice versa) during the observation period (Figure 4-4, Table 4-3). Dobbin, Parrish and Sydkap glaciers (Figure 4-4a, c, d) were nearly stagnant in their terminal regions in the early 2000s, but their velocities all increased to peak between ~2004-2006, and then declined gradually to values similar to those observed in the early 2000s by 2013-2015. Velocities in the lowermost ~10 km of Cañon Glacier were ~110-130 m a^{-1} in 1999-2000, decreased to ~80-100 m a^{-1} from 2001-2007, and then increased again to ~140-150 m a^{-1} by 2009-2011 (Figure 4-4b). Notably, in the winter of 2012, Cañon Glacier's surface velocity decreased to ~90-100 m a^{-1} in its lowermost region (and in some locations it had the lowest velocities observed during the entire study period), before returning to speeds of ~140-150 m a^{-1} in 2013 and ~170-180 m a^{-1} in winter 2015.

Chapman Glacier (Figure 4-4e) had velocities of ~5-50 m a^{-1} in the lowermost 20 km of its main trunk in winter 2000, but by 2011 these had increased to ~200 m a^{-1}. In each subsequent winter from 2011 to 2015 the velocities in the region ~5-20 km upglacier from the glacier terminus decreased, while those in the lowermost ~1-5 km of the glacier increased (the lowermost ~1km region of Chapman Glacier was nearly stagnant over the entire observation period, and may indicate that this region is frozen to its bed). Otto Glacier (Figure 4-4f) sped up from ~200-400 m a^{-1} in 2000 in its lower ~10 km, to reach peak velocities of ~600-700 m a^{-1} in the winters of 2007 and 2008 in the lowermost 5 km of the glacier. Velocities in this area then declined to ~250-300 m a^{-1} by the winters of 2009 and 2010, and by 2013-2015 this part of the glacier was stagnant.

4.4.3.3 Glaciers with Velocity Increase

Surface velocities of Wykeham Glacier generally increased over the observation period (Figure 4-5a), albeit with some year-to-year variability. Velocities were ~250 m a^{-1} over the lowermost 5 km of the glacier from 1999-2000, increased to ~350 m a^{-1} in the same region by 2004-2005, and then decreased to a minimum of just under ~200 m a^{-1} in 2007-2008. Surface velocity then increased consistently from 2009-2014, reaching up to ~450 m a^{-1} ~5 km upglacier from the

calving front in winter 2015 (although the highest near terminus velocities were observed in 2004-2005).

Trinity Glacier also accelerated over most of the observation period (Figure 4-5b, Table 4-3). Velocities were ~300-550 m a^{-1} in the lowermost ~30 km of the main glacier from 1999-2002. They increased to ~600-900 m a^{-1} in the summers from 2005-2008, and to ~800-1250 m a^{-1} in the winters from 2011-2015. The speed-up has not been unidirectional, however, as velocities in 2007-2008 were slightly lower than in 2006-2007, and velocities in winter 2013 were lower than those in the winters of 2012 and 2014. Overall, the mean speed of Trinity Glacier has more than doubled over the past decade, and it is currently the fastest flowing glacier in the study region.

4.4.4 Bed Elevations and Velocity Variability

For glaciers for which bed elevation information is available, the onset location of inter-annual variability typically occurs immediately downglacier of the location where the bed elevation initially drops below sea level (Figure 4-3 a-c, e; Figure 4-4 a-c, e; Figure 4-5). Upglacier of these locations, glacier velocities exhibit little to no inter-annual variability. Dobbin Glacier (Figure 4-4a) provides one of the clearest examples of this, as the lowermost ~15 km of the glacier that is grounded below sea level exhibited speed-up and slow-down over the observation period, while there was negligible velocity variability in the 5 km section upglacier from the location where bed elevations rise above sea level. This pattern of velocity variability, being mainly restricted to areas where the glacier is grounded below sea level, is also evident on Trinity, Parrish, Wykeham, Antoinette, Tuborg, Eugenie and Ekblaw Glaciers.

4.4.5 Patterns of Dynamic Change

Characterizing the spatio-temporal pattern of velocity change provides an opportunity to determine whether faster flow initiated upglacier and propagated toward the terminus or vice versa, and can provide insights into the causes of dynamic change. We therefore present maps of the annual surface velocities and inter-annual velocity differences for Dobbin (Figure 4-6a-b), Parrish (Figure 4-7a-b) and Trinity Glaciers (Figure 4-8a-b). These glaciers have the most continuous velocity records along their entire lengths for computation of interannual velocity

changes. The point where the bed of each glacier descends below sea level is also indicated on Figure 4-6, along with sill locations.

For Dobbin Glacier (Figure 4-6a-b), glacier speed-up originated in the lowermost terminus region between 2003/2004 and 2004/2005. Between 2004-2005 and 2005-2006 velocities near the terminus changed little, although the region of higher velocities expanded into the region ~4-8 km from the terminus. The slowdown between 2005-2006 and 2006-2007 originated in the lowermost terminus region and spread upglacier. For Parrish Glacier (Figure 4-7a), the speed-up event also began in the lowermost terminus region (within ~7 km of the calving front) in the summers from 2004-2005 to 2006-2007 (Figure 4-6c). Velocity differencing (Figure 4-7b) indicates that the subsequent slowdown also initiated in this area. The patterns of velocity change on both Dobbin and Parrish Glaciers indicate that dynamic variability in both of these glaciers originates, and has the greatest variability, in areas which are grounded below sea level and downglacier of bedrock sills. There is less pronounced dynamic variability in areas where the bed is grounded below sea level, but upglacier of the sills. However, the speed-up along this portion of the glacier lags behind that of the lowermost terminus region, which is likely due to longitudinal coupling and ice being "pulled" from this region as the terminus accelerates.

For Trinity Glacier (Figure 4-8a-b), we see no evidence of significant velocity variability upglacier of the point where the bed descends below sea level. Rather, it is evident that the lowermost terminus region (~10 km from the calving front) underwent significant speed-up from 2006-2011, and that this speed-up initiated in this part of the glacier. It is also evident that elevated flow speeds have extended progressively further upglacier over time and that larger areas of the glacier were flowing faster in the latter years of the study period. Unlike Parrish and Dobbin Glaciers, Trinity Glacier does not have a sill (Figure 4-8c) located in the regions where it is grounded below sea level, which may explain why large regions of it were able to accelerate progressively through the observation period.

4.4.6 Velocity Fluctuations and Terminus Positions

To understand the causes of the observed changes in motion of the 16 glaciers that underwent significant variations over the study period, it is useful to look at the temporal changes in the

terminus position of these glaciers (Table 4-3). Among the glaciers that advanced, Good Friday Bay and Middle glaciers advanced by ~2 km and ~1 km, respectively. Parrish Glacier advanced by ~2 km between 2000 and 2012, with the maximum advance occurring between 2000 and 2009, coincident with a period of faster flow that originated in its terminus region which likely led to longitudinal extension which may explain the terminus advance observed at this time. Between 2012 and 2014 the terminus of Parrish Glacier retreated by ~300 m after velocities across the lower terminus reached stagnation. This retreat was likely caused by an overextension of the terminus region coupled with lower ice velocities which could not replace mass being lost by iceberg calving and surface and/or oceanic melt.

Frontal retreat was the most common terminus behavior within the study region over the observation period, with retreat of ~1-4 km occurring on glaciers which transitioned from high velocities early in the study period to near stagnation in their lowermost terminus regions in later years (e.g. Antoinette, Eugenie, Iceberg, Mittie, Parrish, Otto glaciers; Table 4-3). Significant, although generally less, terminus retreat (~0.5-2 km), also occurred on glaciers where near-terminus velocity decreased, but not to the point of terminus stagnation (e.g. Ekblaw and Sydkap glaciers) and on those where velocity fluctuated during the observation period (e.g. Cañon Glacier). The retreat of these termini may also be linked to overextension due to the advance of the terminus during previous periods of faster flow, with retreat beginning once velocities decrease and flow can no longer replace mass being lost at the glacier front.

Trinity and Wykeham glaciers are the only glaciers that underwent a significant and near-continuous acceleration throughout the study period that was accompanied by terminus retreat (of up to 4 km for Trinity Glacier; Table 4-3). This pattern of terminus behavior may be linked to increasing longitudinal extension as the lowermost terminus of the glacier accelerates faster than portions of the trunk located upglacier, leading to thinning of the main glacier trunk and possibly floatation. The pattern of dynamic change for Trinity Glacier shows that the speed-up originated in the lowermost terminus the glacier, which is consistent with this interpretation. Chapman Glacier is the only glacier that underwent significant change in dynamics coupled with no appreciable change in terminus position; a pattern similar to the 1990s surge of Bakaninbreen, Svalbard [Murray et al. 1998].

4.5 Discussion

On the basis of the observations presented above, we identify three primary types of velocity variability (Table 4-3). Distribution of the glaciers undergoing these types of velocity variability is presented in Figure 4-9.

4.5.1 Surge-Type Flow Variability

We attribute the velocity variability of Mittie, Good Friday Bay, Middle, Iceberg, Otto and Chapman Glaciers to surging, primarily because each of these glaciers underwent velocity changes of one or two orders of magnitude above background levels. Otto and Good Friday Bay Glaciers both experienced periods of fast flow in the 1960s [Hattersley-Smith 1969; Müller 1969; Copland et al. 2003a], which suggests a cyclical velocity fluctuation for them. Rapid flow was evident over the entire ~35 km trunk of Iceberg Glacier in 2000. It appears that the subsequent slow-down began and occurred most rapidly in the lowermost terminus region and then spread upglacier until ~2010, at which point the entire glacier trunk was nearly stagnant. Terminus retreat was coincident with the slowdown, a pattern similar to that observed after surges of Otto and Mittie Glaciers. We classify the behavior of Mittie and Middle Glaciers as surge-type because terminus advance coincided with the speed-up of the main trunk of each glacier and because the velocity patterns indicate that enhanced surface velocities occurred over nearly their entire lengths. Chapman Glacier is classified as surge-type because the peak surface velocities migrated downstream from ~20-30 km upglacier from the terminus in 2000, to the region 10-20 km upglacier from the terminus in 2011. This pattern suggests that the Chapman Glacier surged between 2000 and 2011 and that the surge originated upglacier and propagated downglacier but appears to have ceased before activating faster flow in the lowermost terminus region.

Given the 5-10 year active phases and ~30-35 year quiescent phases observed for Otto and Good Friday Bay glaciers (the only glaciers within the study region for which we have evidence of two active phases to constrain the length of the surge cycle), the surges of these glaciers may be thermally controlled, as has been suggested for surge-type glaciers in Svalbard. More study is

required to determine the details of these patterns and how common they are throughout the Canadian Arctic and how they compare to surges observed in Svalbard.

4.5.2 Pulse-Type Flow Variability

Many of the glaciers within the study region have experienced significant velocity variability, but there is insufficient evidence to definitively classify them as "surge-type". We therefore identify these glaciers as "pulse-type", and apply this designation to Antoinette, Tuborg, Eugenie, Dobbin, Cañon, Parrish, Ekblaw and Sydkap glaciers (Table 4-3). Most of these glaciers exhibited either a multi-year slow down or a multi-year speed-up followed by slow-down during the observation period. The relationship between terminus position and velocity structure is similar to that of the glaciers identified as surge-type (i.e., terminus advance as surface ice velocity increases in the terminus region and terminus retreat as the termini slow to stagnation). However, the major distinction between the glaciers identified as "pulse-type" and "surge-type", is that nearly all of the velocity variability of pulse-type glaciers initiates in and propagates upglacier from the lowermost sections of the glacier near the terminus. Another distinction is that the velocity variability is largely restricted to regions where the bed lies below sea level.

Comparison of the longitudinal velocity profiles with bed elevation profiles indicates that velocity variability of pulse-type glaciers is confined to sections of the bed grounded below sea-level and is not transmitted upglacier of the point at which the bed rises above sea level. In essence, the longitudinal velocity gradient in the terminus region behaves like a flap attached to a hinge point located where the bed crosses sea level. The fact that elevated surface velocities are not transmitted upglacier of this point is in contrast to the velocity variability of surge-type glaciers, where the entire length of the main glacier trunk is activated during a surge. This suggests that bed elevation may be an important control on the variability of ice motion for "pulse-type" glaciers in the Canadian High Arctic in that it limits how far velocity variations can propagate upglacier and affect ice motion in the interior of ice masses.

Our repeated velocity mapping captured the acceleration and deceleration phases of "pulse" events on Parrish and Dobbin glaciers. Both glaciers have nearly co-incident (within ~150 m

horizontally) ice thickness profiles acquired both before (in 2000) and after (in 2014) the pulse event occurred, allowing investigation of how the glacier geometry in the lower ablation area changed due to the velocity perturbation (Figure 4-8). To verify the accuracy of these ice thickness measurements, we compared ice elevation changes derived for Dobbin Glacier from ICESat (± 0.1 m) [Gardner et al. 2011] with those collected within a 150 m radius of the ice thickness flight lines. The average rate of surface elevation change derived from ICESat was ~-1.4 m a^{-1} from 2003-2009, which if extrapolated to the 2000-2015 period would equate to ~21 m of thinning. Our ice thickness profiles reveal ice thinning of ~17 m in the same region between 2000 and 2014, which is similar to the thinning rate determined from the ICESat data and within the quoted (± 10 m) error margins of the ice thickness profiles.

Both Dobbin (Figure 4-6c) and Parrish (Figure 4-7c) Glaciers are grounded below sea level for the majority of their ~20 km lengths, but both have a sill that rises above sea level upglacier of their calving front (~4.5-5 km upglacier for Dobbin Glacier and ~8-12 km upglacier for Parrish Glacier). Dobbin (Figure 4-6d) and Parrish (Figure 4-7d) glaciers also have a common pattern of thinning in the region between where the bed first goes below sea level and the sill, with a localized region of thickening coincident with the sill. Downglacier of the sill, both glaciers have an area of thinning that extends roughly half the distance to the calving front and transitions to an area of thickening in the lowermost region of the terminus, particularly for Parrish Glacier. These patterns suggest that the speed-up of these glaciers has transferred mass from upglacier locations to regions above the sill and to the lowermost 3 km of the glacier. Although our data are limited, it is possible that as ice thickens at these locations it also steepens, which results in increased flow rates until the flux increases enough that it results in a "pulse" of discharge that is transferred to the terminus region.

Copland et al. [2003a] previously identified Tuborg, Sydkap and Dobbin Bay glaciers as "likely or possibly surge-type", while all of the other glaciers identified here as "pulse type" have not previously been classified. Copland et al. [2003a] based their classification on the identification of features that suggested past surge activity (e.g., looped moraines, extensive crevassing, shear margins, folding, digitate termini and terminus retreat), but it is possible that these features could be created from a "pulse-type" event rather than by surging. Conversely, it is possible that what

we identify here as “pulse-type” events represents a form of surging that is restricted to the lowermost terminus region of tidewater glaciers.

The definition that we use here to describe “pulse-type” glaciers relates to the spatial expression of temporal dynamic changes (i.e., velocity variability that is restricted to regions of the bed grounded below sea level). This definition differs from previously published literature related to “pulsing” glaciers (e.g. Mayo [1978]; Raymond [1987]; Glazovskiy [1991]; Turrin et al. [2014]), which defines pulse-type glaciers as those that undergo “*multi-year, periodic, pulselike increases of speed that are not large enough to produce the large ice displacements usually associated with glacier surges and therefore appear to be intermediate between surge-type glaciers and normal glaciers*” [Raymond 1987]. The definition used here is meant to provide a distinction between solely “surge-type” glaciers and glaciers with a dynamic mechanism that appears to be distinct from surging, meaning that the glaciers identified here as “pulse-type” may not be exactly comparable to those presented in other literature. Table 4-4 summarizes the main characteristics used in this study to distinguish between glaciers defined as “pulse-type” and “surge-type” in the Canadian High Arctic.

4.5.3 Consistent Acceleration

Trinity and Wykeham glaciers, which drain southeast Prince of Wales Icefield, are the only glaciers that sped-up fairly consistently throughout the study period. These speed-ups occurred simultaneously with retreat of both termini (~3-4 km for Trinity Glacier and ~1 km for Wykeham Glacier). This pattern of velocity increase, in conjunction with terminus retreat, is at odds with the behavior of all other glaciers measured in our study region. For other glaciers where we have evidence of speed-up, both pulse-type and surge-type, terminus advance occurred at the same time. We therefore interpret the dynamic changes on Trinity and Wykeham glaciers as involving a mechanism that is different from that which caused the velocity fluctuations of all other glaciers in this study.

To investigate this further, we compared surface elevations of Trinity and Wykeham glaciers in 2008 (using a digital elevation model (DEM) derived from SPOT imagery (± ~6 m)) and 2014 (using NASA ATM data obtained during Operation IceBridge (± ~10 cm)) to examine patterns of thickness change over these glaciers (Figure 4-8d). Our results indicate surface lowering of

~2-5 m a^{-1} in the lowermost ~15 km section of Trinity Glacier. This thinning is similar to the rate of ~3.5 m a^{-1} determined from a comparison of repeat ICESat surface elevation profiles acquired between 2003 and 2009 [Gardner et al. 2011]. In comparison, surface elevation changes of two glaciers located within ~8 km and ~15 km of the Trinity/Wykeham calving front (also derived from the 2008 SPOT DEM and the 2014 NASA ATM data) averaged ~-0.61 m a^{-1}, while mass balance measurements and modeling suggest that surface ablation via melting in this area is < 2 m a^{-1} [Mair et al. 2009; Marshall et al. 2007]. This implies that at least half of the observed thinning rate of the terminus of Trinity Glacier is attributable to changes in dynamics.

This combination of terminus acceleration, thinning, and terminus retreat is similar to that described for tidewater-terminating Helheim Glacier, Greenland, which retreated by ~8 km between 2000 and 2005, while its surface speed increased from ~6-8 km a^{-1} to ~8-11 km a^{-1} in the lowermost ~15 km of the glacier [Howat et al. 2005; Joughin et al. 2008]. The retreat of Helheim Glacier has been attributed to thinning of the glacier front (either by oceanic or atmospheric forcing, or some combination of the two) that removed longitudinal resistive stresses and initiated faster flow [Joughin et al. 2012]. The terminus retreat and acceleration on Trinity and Wykeham Glaciers is also analogous to the retreat pattern of Columbia Glacier, Alaska, which has been attributed to the "retreat phase" of a tidewater glacier cycle [Meier and Post 1987; Pfeffer 2007]. The retreat phase of the tidewater glacier cycle initiates due to accelerated ice flow in the lowermost terminus region, which acts to thin upstream ice and reduce effective pressure at the glacier bed, which in turn allows flow to accelerate and the ice to thin further so that acceleration propagates upglacier from the terminus [Meier and Post 1987; Pfeffer 2007]. It is possible that the prolonged retreat of both Trinity and Wykeham Glaciers (~8 km for Trinity Glacier and ~4 km for Wykeham Glacier since the 1960s [Sharp et al. 2014] has reduced the resistive stresses at their combined front, allowing them to accelerate and thin in recent years. If Trinity Glacier is undergoing a retreat driven by acceleration and thinning leading to glacier flotation then the fact that its bed lies below sea level for ~45 km upglacier from its current calving front, together with the lack of a prominent sill, may make it prone to significant further retreat before re-stabilization occurs.

4.5.4 Dynamic Discharge

Given the wide variability in the velocity behavior of individual glaciers described above, an important question is whether the total dynamic discharge has changed significantly over time. To evaluate this, Table 4-5 presents the dynamic discharge derived from RADAR velocities for all tidewater glaciers of Axel Heiberg and Ellesmere Islands with available data from 2000 and 2007-2015 and Table 4-6 presents the dynamic discharge derived from feature tracking velocities from 1999-2010 for 17 glaciers located on Axel Heiberg and Ellesmere Islands. The mean annual discharge calculated for 2000 and from 2011 to 2015 when RADAR imagery was available for the majority of the region's outlet glaciers, was 2.21 ± 0.68 Gt a^{-1}. However, the majority of glaciers have been losing less mass via dynamic discharge in recent years due to the dominance of glacier slow down across the study region. Notable exceptions are the rapid increase in dynamic discharge from Trinity and Wykeham glaciers, which has increased from a combined total of 0.55 ± 0.12 Gt a^{-1} in 2000 to 1.43 ± 0.23 Gt a^{-1} in 2015. These glaciers alone currently account for ~62% of the total regional mass loss via dynamic discharge, and their recent discharge increases approximately offset the reduction in dynamic discharge from the rest of the region's marine terminating glaciers. Our results indicate that ~10 glaciers at a time account for ~70% of the total dynamic discharge in a given year (similar to Van Wychen et al. [2014] for glacier discharges of the QEI as a whole in 2012), although which glaciers account for this discharge varies over time. This variability in glacier dynamic discharge necessitates the continued monitoring of all major tidewater glaciers within the study region to identify the primary sources of iceberg discharge each year.

4.6 Conclusions

Speckle tracking of pairs of RADARSAT-1/2 imagery and feature tracking of Landsat-7 optical image scenes has allowed detection and quantification of dynamic change of all major glaciers on Axel Heiberg and Ellesmere Islands over the period 1999-2015. When combined with a record of terminus positions and surface features indicative of surging, our analysis updates the inventory of surge-type glaciers originally completed by Copland et al. [2003a]. Based on our observations we identify Otto, Chapman, Good Friday Bay, Iceberg, Middle and Mittie Glaciers as surge-type. Our analysis also expands on the inventory of Copland et al. [2003a] by

identifying new “pulse-type” and “consistent acceleration” classifications to better describe observed velocity variability within the Canadian high Arctic.

Pulse-type glaciers share some characteristics with surge-type glaciers, such as periods of speed-up and slowdown, and terminus advance coincident with acceleration, but the key difference is that all of their velocity variability appears to be restricted to their lowermost terminus region that is grounded below sea level. We observe very little year to year variability in ice motion on pulse-type glaciers upglacier of the point where the glacier bed rises above sea level, suggesting that velocity variability is limited by how far it can be transmitted upglacier. Comparison of bed elevation and ice thickness profiles for Dobbin and Parrish Glaciers from before and after a pulse event suggests that increased basal friction over sills leads to compressive ice flow and localized ice thickening upstream of the sill which may be important for causing localized steepening in the vicinity of the sill and initiating accelerated motion in the lowermost terminus regions of pulse-type glaciers. More investigation is required to better understand the drivers of dynamic change for these glaciers and what role the glacier bed properties and geometry may play in regulating ice motion.

The marked speed-up of Trinity and Wykeham Glaciers, which has been accompanied by prolonged terminus thinning and retreat, suggests that the velocity variability on these glaciers is not due to surging or pulsing, but rather driven by variations in the stability of the main trunks of both glaciers. As a consequence, we classify these glaciers as displaying “consistent acceleration”. The pattern of terminus retreat and acceleration for these two glaciers is similar to that displayed by both Helheim Glacier (Greenland) and Columbia Glacier (Alaska), which has been attributed to reductions in resistive stresses at the glacier front that allow the glacier to accelerate and thin, and we may be witnessing the beginning of the retreat phase of a tidewater glacier cycle.

By combining velocities with ice thickness measurements we provide the most comprehensive record of temporal variability in dynamic ice discharge from Axel Heiberg and Ellesmere Islands to date. Mean dynamic discharge is 2.21 ± 0.68 Gt a^{-1}, with a low of 1.80 ± 0.66 Gt a^{-1} in 2013 and high of 2.51 ± 0.84 Gt a^{-1} in 2000. Ten glaciers account for ~70% of total ice discharge in

any given year, but exactly which glaciers are responsible varies over time due to the high level of velocity variability observed. Total dynamic discharge from surge-type and pulse-type glaciers has generally decreased over time due to many large tidewater glaciers transitioning into periods of slower flow. However, the reduction in total regional dynamic discharge from these glaciers has been offset by the increase in discharge due to the acceleration of the Trinity and Wykeham glaciers in recent years, which together accounted for ~60% of all dynamic discharge from 2011-2014. Due to the widespread speed-up and evidence of dynamically induced thinning of the Trinity Glacier there is a great need to better understand the drivers of the recent acceleration of this glacier.

Acknowledgements

We thank NSERC (Discovery Grants and Northern Research supplements to L. Copland and M. Sharp), Canada Foundation for Innovation, Ontario Research Fund, ArcticNet, Ontario Graduate Scholarship and Polar Continental Shelf Program for funding. Support to D. Burgess is provided through the Climate Change Geosciences Program, Earth Sciences Sector, Natural Resources Canada (Contribution #20150295). RADARSAT imagery is made available from the Alaska Satellite Facility, archives at Natural Resources Canada and the RADARSAT-2 Natural Resources Canada data allocation. We thank Julian Dowdeswell and Toby Benham for providing ice thickness and bed elevation profiles utilized by this study and acknowledge support from U.K NERC for grants GR3/12469 and NE/K004999 to J. Dowdeswell.

4.7 References

Benn, D.I. and D.J.A. Evans, (2010), Glaciers and Glaciation (2nd Edition), 802 pp, Arnold, London, U.K.

Bingham, R., P. Nienow, and M. Sharp, (2003), Intra-annual and intra-seasonal flow dynamics of a High Arctic polythermal valley glacier**.** *Annals of Glaciology, 37, 181-188.*

Boon, S., and M. Sharp, (2003), The role of hydrologically-driven ice fracture in drainage system evolution on an Arctic glacier. *Geophysical Research Letters,* 30. doi:10.1029/2003GL018034.

Burgess, D. O., M. Sharp, D.W.F. Mair, J.A. Dowdeswell, and T.J. Benham, (2005), Flow dynamics and iceberg calving rates of Devon Ice Cap, Nunavut, Canada. *Journal of Glaciology,* 51, 173, 219- 230.

Christoffersen, P., R. Mugford, K.J. Heywood, I. Joughin, J.A. Dowdeswell, J.P.M. Syvitski, A. Luckman, A. and T.J. Benham, (2011), Warming of waters in an East Greenland fjord prior to glacier retreat: mechanisms and connection to large-scale atmospheric forcing. *The Cryosphere,* 5: 701-714. doi: 10.5194/tc-5-701-2011.

Clarke, G.K.C., (1987), Fast glacier flow: Ice streams, surging, and tidewater glaciers. *Journal of Geophysical Research,* 92(B9): 8835-8841.

Copland, L., M. Sharp, and J.A. Dowdeswell, (2003a), The distribution and flow characteristics of surge-type glaciers in the Canadian High Arctic. *Annals of Glaciology,* 36, 73-81.

Copland, L., M. Sharp, and P. Nienow, (2003b), Links between short-term velocity variations and the subglacial hydrology of a polythermal glacier. *Journal of Glaciology,* 49, 407-414.

Dowdeswell, J.A., G. S. Hamilton, and J. O. Hagen, (1991), The duration of the active phase on surge-type glaciers: contrasts between Svalbard and other regions. *Journal of Glaciology,* 37, 127: 388-400.

Dowdeswell, J. A., T. J. Benham, M. R. Gorman, D. O. Burgess, and M. Sharp, (2004), Form and flow of the Devon Island ice cap, Canadian Arctic, *Journal of Geophysical Research,* 109, F02002, doi:10.1029/2003JF000095.

Gardner, A. S., M. Moholdt, B. Wouters, G.J. Wolken, D.O. Burgess, M. Sharp, J.G. Cogley, C. Braun and C. Labine, (2011), Sharply increased mass loss from glaciers and ice caps in the Canadian Arctic Archipelago. *Nature.* 473(7347), 357–360, doi: 10.1038/nature10089.

Gogineni, P., (2012), Radar Depth Sounder Data Products, Lawrence, Kansas, USA. Digital media. http://data.cresis.ku.edu/

Gray, A.L., N. Short, K.E., Mattar, and K.C. Jezek, (2001), Velocities and flux of the Filchner Ice Shelf and its tributaries determined from speckle tracking interferometry. *Canadian Journal of Remote Sensing*, 27(3), 193-206.

Glazovskiy, A.F., (1991), The Problem with Surge-type Glaciers. In: *Variations of Snow and Ice in the past and at present on a Global and Regional Scale*. (ed Kotlyakov, V.M.) An International Hydrological Program Publication.

Hattersley-Smith , G., (1969). Recent Observations on the surging of Otto Glacier, Ellesmere Island. Canadian Journal of Earth Sciences, 6(4), 883–889.

Haug, T., A. Kääb, and P. Skvarca, (2010), Monitoring ice shelf velocities from repeat MODIS and Landsat data – a method study on the Larsen C ice shelf, Antarctic Peninsula, and 10 other ice shelves around Antarctica. *The Cryosphere*, 4: 161-178. doi: 10.5194/tc-4-161-2010.

Holland, D. M., R. H. Thomas, B. de Young, M. H. Ribergaard and B. Lyberth, (2008), Acceleration of Jakobshavn Isbrae triggered by warm subsurface ocean waters. *Nature Geoscience,* 1: 659-664. doi: 10.1038/ngeo316

Howat, I.M., I., Joughin, S. Tulaczyk and S. Gogineni, (2005), Rapid retreat and acceleration of Helheim Glacier, east Greenland, *Geophysical Research Letters*, 32, doi: 10.1029/2005GL024737.

Joughin, I., (2002), Ice-sheet velocity mapping: a combined interferometric and speckle tracking approach. *Annals of Glaciology*, 34: 195–201.

Joughin, I., I. Howat, R. B. Alley, G. Ekstrom, M. Fahnestock, T. Moon, M. Nettles, M. Truffer, and V. C. Tsai, (2008), Ice-front variation and tidewater behavior on Helheim and Kangerdlugssuaq Glaciers, Greenland. *Journal of Geophysical Research,* 113, F01004, doi: 10.1029/2007JF000837.

Joughin, I., R.B. Alley and D.M. Holland, (2012), Ice-sheet response to oceanic forcing, *Science*, 338(6111), 1172-1176. doi: 10.1126/science.1226481.

Kamb, B., (1987), Glacier surge mechanism based on linked cavity configuration of the basal water conduit system. *Journal of Geophysical Research*, 92(B9): 9083-9100. doi: 10.1029.JB092iB09p09083.

Koerner, R. M., (1979), Accumulation, ablation, and oxygen isotope variations on the Queen Elizabeth Island Ice Caps, Canada. *Journal of Glaciology*, 22(86), 25-41.

Koerner, R.M., (2005), Mass balance of glaciers in the Queen Elizabeth Islands, Nunavut, Canada. *Annals of Glaciology*, 42, 417–423. doi: 10.3189/172756405781813122

Mair, D., D.O. Burgess, M. Sharp, J.A. Dowdeswell, T. J. Benham, S. Marshall and F.

Cawkwell, (2009), Mass balance of the Prince of Wales Icefield, Ellesmere Island, Nunavut, Canada. *Journal of Geophysical Research,* 114, F02011. doi: 10.1029/2008JF001082

Marshall, S., M. Sharp, D.O. Burgess, and F. Anslow, (2007), Surface temperature lapse rate variability on the Prince of Wales Icefield, Ellesmere Island, Canada: implications for regional-scale downscaling of temperature. *International Journal of Climatology*, 27: 385-398.

Mayo, L.R., (1978), Identification of unstable glaciers intermediate between normal and surging glaciers, *Mater. Glyatsiol. Issled,* 133: 133-135.

Meier, M.F. and A. Post, (1987), Fast tidewater glacier, *Journal of Geophysical Research.,* 92(B9), 9051-9058. doi: 10.1029/Jb092iB09p09051.

Müller, F., (1969), Was the Good Friday Glacier on Axel Heiberg Island surging? *Canadian Journal of Earth Sciences*, 6(4), 891–894, doi: 10.1139/e69-091.

Murray, T., J.A. Dowdeswell, D.J. Drewry, D.J. and I. Frearson, (1998), Geometric evolution and ice dynamics during a surge of Bakaninbreen, Svalbard. *Journal of Glaciology,* 44, 147: 263-272.

Murray, T., T. Strozzi, A. Luckman, H. Jiskoot and P. Christakos, (2003), Is there a single surge mechanism? Contrasts in dynamics between glacier surges in Svalbard and other regions. *Journal of Geophysical Research,* 108 (B52237): 1-15. doi: 10.1029/2002JB001906.

Murray, T., K. Scharrer, T. D. James, S. R. Dye, E. Hanna, A. D. Booth, N. Selmes, A. Luckmand, A. L. C. Hughes, S. Cook and P. Huybrechts, (2010), Ocean regulation hypothesis for glacier dynamics in southeast Greenland and implications for ice sheet mass changes. *Journal of Geophysical Research,* 115(F03026): 1-15. doi: 10.1029/2009Jf001522.

Paterson, W. S. B., (1994), *The Physics of Glaciers*, 3rd edition, Elsevier, Oxford.

Pfeffer, W. T., (2007), A simple mechanism for irreversible tidewater glacier retreat, *Journal of Geophysical Research,* 112, F03S25, doi: 10.1029/2006JF000590.

Pfeffer, W.T., A.A., Arendt, A. Bliss, T., Bolch,J.G., Cogley, A.S., Gardner, J.O., Hagen, R., Hock, G., Kaser, C., Kienholz, E.S., Miles, G., Moholdt, N., Moelg, F., Paul, V., Radic, P., Rastner, B., Raup, J., Rich, M.J., Sharp, and the Randolph Consortium, (2014), The Randolph Glacier Inventory: a globally complete inventory of glaciers. *Journal of Glaciology,* 60, 537-552. doi:10.3189/2014JoG13J176.

Raymond, C.F., (1987), How do glaciers surge? A Review, Journal of Geophysical Research, 92 (B9): 9121-9134.

Sharp, M., D.O. Burgess, F. Cawkwell, L. Copland, J.A. Davis, E.K. Dowdeswell, J. A. Dowdeswell, A. S. Gardner, D. Mair, L. Wang, S.N. Williamson, G. J. Wolken, and F. Wyatt, (2014), Remote sensing of recent glacier changes in the Canadian Arctic. In: Kargel, J.S., Leonard, G.J., Bishop, M.P., Kääb, A. and Raup, B.H. (eds). *Global Land Ice Measurements from Space,* Ch. 9, pp. 205-228. Praxis-Springer. doi: 10.1007/978-3-540-79818-7_9.

Short, N. H. and A. L. Gray, (2004), Potential for RADARSAT-2 interferometry: glacier monitoring using speckle tracking. *Canadian Journal of Remote Sensing*, 30(3), 504-509.

Short, N. H. and A.L. Gray, (2005), Glacier dynamics in the Canadian High Arctic from RADARSAT-1 speckle tracking. *Canadian Journal of Remote Sensing*, 31(3), 225–239.

Thomson, L.I., G.R. Osinski, and C.S.L. Ommanney, (2011), Glacier change on Axel Heiberg Island, Nunavut, Canada, *Journal of Glaciology*, 57 (206), 1079-1086. doi: 10.3189/002214311798843287.

Turrin, J.B., R.R. Forster, J.M. Sauber, D.K. Hall, R.L. Braun, (2014), Effects of bedrock lithology and subglacial till on the motion of Ruth Glacier, Alaska, deduced from five pulses from 1973 to 2012, *Journal of Glaciology*, 60 (222). doi: 10.3189/2014JoG13J182.

Van Wychen, W., L. Copland, L. Gray, D. O. Burgess, B. Danielson, M. Sharp, (2012), Spatial and temporal variation of ice motion and ice flux from Devon Ice Cap, Nunavut, Canada. *Journal of Glaciology*, 58(210), 657–664. doi: 10.3189/2012JoG11J164.

Van Wychen, W., D. O. Burgess, L. Gray, L. Copland, M. Sharp, J. A. Dowdeswell, and T. J. Benham, (2014), Glacier velocities and dynamic ice discharge from the Queen Elizabeth Islands, Nunavut, Canada, *Geophysical Research Letters,* 41. doi: 10.1002/2013GL058558.

Williamson, S., M. Sharp, J. Dowdeswell, and T. Benham, (2008), Iceberg calving rates from northern Ellesmere Island ice caps, Canadian Arctic, 1999-2003. *Journal of Glaciology*, 54(186), 391-400. doi: 10.3189/002214308785837048.

Table 4-1: Summary of remote sensing imagery used in this study. SAR image pairs from 2000-2008 were RADARSAT-1 Fine Beam (9m resolution); from 2009-2011 RADARSAT-2 Fine Beam (9 m resolution); from 2011-2014 RADARSAT-2 Wide Fine Beam (9 m resolution).

	RADARSAT Imagery (Speckle Tracking: DD/MM/YY Image Segments)														
	Image 1	**Image 2**		**Image 1**	**Image 2**		**Image 1**	**Image 2**		**Image 1**	**Image 2**		**Image 1**	**Image 2**	
Northern Ellesmere	20/10/00	13/11/00	1	16/12/00	09/1/01	4	25/2/07	21/3/07	1	13/1/11	06/2/11	4	16/1/14	09/2/14	2
	30/10/00	23/11/00	3	19/12/00	12/1/01	1	18/3/08	11/4/08	1	26/1/11	19/2/11	5	17/1/14	10/2/14	3
	03/11/00	21/12/00	1	19/12/00	12/1/01	1	13/4/09	07/5/09	1	27/1/11	20/2/11	4	11/1/15	40/2/15	3
	12/11/00	30/12/00	3	21/12/00	14/1/01	1	20/2/10	16/3/10	1	30/1/11	23/2/11	5	01/3/15	25/3/15	3
	21/11/00	15/12/00	2	23/12/00	16/1/01	1	07/1/11	31/1/11	2	01/2/11	25/2/11	4			
	12/12/00	05/1/01	2	02/3/06	26/3/06	1	10/1/11	03/2/11	4	27/1/12	20/2/12	2			
	13/12/00	06/1/01	2	09/3/06	02/4/06	1	11/1/11	04/2/11	5	28/1/12	21/2/12	3			
Prince of Wales	14/10/00	07/11/00	1	18/12/00	11/1/01	2	28/2/07	24/3/07	1	26/1/11	19/2/11	3	07/12/13	31/12/13	2
	17/10/00	10/11/00	4	28/12/00	21/1/01	1	18/3/08	11/4/08	1	22/2/11	18/3/11	5	08/12/13	01/01/14	2
	21/11/00	08/1/01	1	29/12/00	22/1/01	2	01/4/08	25/4/08	1	25/2/11	21/3/11	5	3/12/14	27/12/14	2
	28/11/00	15/1/01	1	23/2/06	19/3/06	1	19/2/09	15/3/09	1	09/4/12	03/5/12	2	26/12/14	19/1/15	2
	01/12/00	25/12/00	2	05/3/06	22/4/06	1	01/3/09	25/3/09	1	05/1/13	29/1/13	2			
	08/12/00	01/1/01	1	18/2/07	14/3/07	1	25/2/10	21/3/10	2	06/1/13	30/1/13	1			
Agassiz	04/12/00	28/12/00	1	09/12/00	02/1/01	1	03/3/07	27/3/07	1	11/3/10	04/4/10	1	06/1/13	30/1/13	2
	08/11/00	02/12/00	1	16/12/00	09/1/01	3	06/3/07	30/3/07	1	01/1/11	25/1/11	3	24/1/14	17/2/14	2
	09/11/00	03/12/00	1	29/12/00	22/1/01	2	28/4/08	22/5/08	1	05/1/11	29/1/11	3	25/1/14	18/2/14	1
	27/12/00	20/1/01	1	23/12/00	16/1/01	1	05/3/09	29/3/09	1	08/1/11	01/2/11	5	3/12/14	27/12/14	2
	30/12/00	23/1/01	3	23/2/06	19/3/06	1	31/3/09	24/4/09	2	12/1/12	05/2/12	1			
	28/12/00	21/1/01	3	11/3/06	04/4/06	1	23/2/10	18/3/10	1	09/4/12	03/5/12	2			
Müller & Steacie	17/12/00	10/1/01	5	01/3/07	25/3/07	1	29/4/08	23/5/08	1	01/2/11	25/2/11	3	04/1/13	28/1/13	2
	20/12/00	13/1/01	1	02/3/07	26/3/07	1	17/2/09	13/3/09	1	18/2/11	14/3/11	3	23/1/14	18/2/14	2
	06/03/06	30/3/06	5	05/3/07	29/3/07	1	05/3/09	29/3/09	1	27/2/12	22/3/12	3	18/1/15	11/2/15	2
Manson	14/10/00	07/11/00	1	04/3/07	28/3/07	1	09/4/12	03/5/12	1	07/12/14	31/12/1	1	12/2/15	08/3/15	1
	18/12/00	11/01/01	1	15/3/08	08/4/08	1	05/1/13	29/1/13	1						
Sydkap	27/2/12	22/3/12	1	30/1/13	23/2/13	1	08/12/14	01/12/14	1	3/12/14	27/12/1	1			
	Landsat-7 Imagery (Feature Tracking: DD/MM/YY Path-Row)														
Northern	02/7/99 57-1	18/6/00 57-1		14/6/01 56-1	17/6/02 56-1		25/7/05 58-1	05/7/06 57-1		22/7/07 59-1	10/7/08 58-1		25/6/09 59-1	28/6/10 59-1	
	08/6/00 57-1	14/6/01 56-1		13/6/04 57-1	25/7/05 58-1		05/7/06 57-1	22/7/07 59-1		10/7/08 58-1	25/6/09 59-1				
Prince of Wales	09/7/99 42-4	27/6/00 40-4		22/7/03 42-4	17/7/04 39-4		07/6/05 42-4	10/6/06 42-4		24/7/07 41-4	01/7/08 42-4		17/6/08 40-4	11/6/09 41-4	
	27/6/00 40-4	12/6/01 42-4		04/6/04 40-4	23/6/05 42-4		09/7/05 42-4	28/7/06 42-4		24/7/07 41-4	10/7/08 41-4		11/6/09 41-4	30/6/10 41-4	
	12/6/01 42-4	15/6/02 42-4		04/6/04 40-4	09/6/05 42-4		28/7/06 42-4	27/7/07 42-4		01/7/08 41-4	13/7/09 41-4		13/7/09 41-4	60/6/10 41-4	
	15/6/02 42-4	22/7/03 40-4													
Agassiz	03/7/99 48-2	28/6/00 47-2		17/6/01 45-3	02/7/02 49-2		16/7/03 46-2	11/7/04 45-3		02/7/06 48-2	12/7/07 48-2		27/6/08 46-2	16/7/09 46-2	
	08/7/99 51-1	24/6/00 51-1		11/6/01 51-1	19/6/02 54-1		21/6/04 49-2	28/7/05 47-2		08/7/06 46-3	27/7/07 46-2		16/7/09 46-2	03/7/10 46-2	

	10/7/99 49-2	28/6/00 47-2	15/6/01 47-2	11/6/02 46-2	19/7/04 53-1	15/7/05 52-1	25/7/07 48-2	04/7/08 47-5	16/7/09 46-2	26/7/10 47-2
	03/7/99 48-2	28/6/00 47-2	02/7/02 49-2	18/7/03 44-3	11/7/04 45-3	05/7/05 46-2	12/7/07 53-1	28/6/08 53-1	14/7/09 48-2	01/7/10 48-2
	05/7/99 46-2	28/6/00 47-2	01/8/02 51-1	26/7/03 52-1	28/7/05 47-2	06/7/06 48-2	11/7/07 46-2	27/6/08 46-2	10/7/09 52-1	14/8/10 52-1
	28/6/00 47-2	15/6/01 47-2	02/7/02 49-2	16/7/03 46-2	20/6/05 53-1	02/7/06 52-1	04/7/08 47-2	14/7/09 48-2		
	24/6/00 51-1	11/6/01 51-1	18/7/03 44-3	21/6/04 49-2	05/7/05 46-2	08/7/06 46-2	28/6/08 53-1	10/7/09 52-1		
	28/6/00 48-2	15/6/01 47-2	26/7/03 52-1	19/7/04 53-1	06/7/06 48-2	25/7/07 48-2	27/6/08 46-2	14/6/09 46-2		
Müller & Steacie	23/7/99 60-2	18/6/00 57-2	26/6/01 60-2	06/6/02 59-2	02/6/05 55-3	07/7/06 55-3	10/7/07 55-3	12/7/08 55-3	13/7/09 57-2	30/6/10 57-2
	18/6/00 57-2	26/6/01 60-2	15/6/04 55-3	02/6/05 55-3	07/7/06 55-3	10/7/07 55-3	12/7/08 55-3	15/7/09 55-3		
Sydkap	02/7/99 41-5	18/6/00 41-5	23/5/02 41-6	26/5/03 41-6	04/6/04 42-5	07/6/05 42-5	10/6/06 42-5	29/6/07 42-5	01/7/08 42-5	18/6/09 42-5
	09/6/00 42-5	12/6/01 42-5	26/5/03 41-6	04/6/04 42-5	07/6/05 42-5	10/6/06 42-5	29/6/07 42-5	01/7/08 42-5	18/6/09 42-5	07/7/10 42-5
	12/6/01 42-5	13/6/02 44-5								
Manson	13/7/99 38-5	29/6/00 38-5	19/7/02 40-5	11/8/03 36-6	10/7/04 39-5	04/7/05 38-5	30/6/06 38-5	03/7/07 38-5	21/7/08 38-5	22/7/09 40-5
	11/6/00 40-5	14/6/01 40-5	11/8/03 36-6	17/7/04 39-5	04/7/05 39-5	30/6/06 38-5	03/7/07 38-5	05/7/08 38-5	29/6/09 39-5	23/6/10 40-5
	14/6/01 40-5	10/6/02 39-5								
ASTER/Landsat-8 (Terminus Position: DD/MM/YY) (Path, Row provided for Landsat Imagery)										
Northern	25/6/00	28/9/03	01/6/04	03/7/06	22/7/07	26/7/09	15/8/10	03/7/11	30/6/12	24/8/14 46-248
	15/6/02	01/6/04								
Prince of Wales	18/4/01	27/4/03	24/7/04	12/4/08	13/6/10	02/7/12	01/8/12	06/8/13	22/8/14	7/9/14 39-4
	02/7/02	03/7/03	23/5/07	14/6/09						
Agassiz	29/7/00	03/7/02	19/7/04	20/6/05	11/7/07	26/6/09	27/7/10	09/6/11	06/8/12	13/6/13
	18/8/01	04/8/03	20/6/05	30/6/06	07/8/07	25/7/09	21/6/10	01/7/11	31/7/13	25/8/14 45-3
	19/7/01	27/6/04	14/8/05	09/7/06	13/5/08	24/7/10				
Müller & Steacie	22/7/00	19/8/01	01/7/02	24/7/04	12/8/05	23/4/07	13/8/10	23/9/11	20/9/12	18/8/14 88-242
	29/7/00	25/5/02	11/7/03	29/7/05	09/7/06	19/9/10	05/7/10	15/9/12	12/8/14 51-4	24/8/14 52-3
	20/7/01	16/7/02	27/6/03							
Manson	27/6/00	12/7/03	26/7/04	29/6/06	30/7/09	17/8/12	30/7/13	22/8/14 36-6		
Sydkap	18/4/01	10/5/02	17/8/06	17/8/07	16/8/14 40-6					

Table 4-2: Error analysis determined from apparent motion over stationary regions (Bedrock (BR) and Ice Divides (ID)). Estimates of ice divides are not possible in 2006-2010 due to surface velocity mosaics that are restricted to the lower regions of ice masses. Superscripts indicate the standard deviation of the dataset. Units in m a^{-1}.

Ice Mass	2000		2006	2007	2008	2009	2010	2011		2012		2013		2014		2015	
	BR	ID	BR	BR	BR	BR	BR	BR	ID	BR	ID	BR	ID	BR	ID	BR	ID
Manson	$16.4^{8.5}$	$16.0^{5.3}$		$11.1^{7.4}$	$21.1^{7.2}$	$9.0^{5.3}$				$4.4^{3.7}$	$6.5^{3.6}$	$4.9^{6.6}$	$6.6^{4.7}$	$3.7^{5.3}$	$6.0^{3.7}$	$6.6^{5.1}$	$7.7^{3.6}$
Sydkap										$9.8^{6.5}$	$10.3^{5.4}$	$8.6^{8.2}$	$9.5^{6.1}$	$6.1^{3.5}$	$7.0^{3.7}$	$7.3^{8.6}$	$7.6^{4.0}$
Prince of Wales	$12.0^{9.9}$	$15.4^{8.9}$	$12.3^{13.0}$	$9.3^{9.3}$	$12.1^{10.2}$	$11.1^{5.6}$	$12.1^{6.8}$	$6.9^{6.5}$	$9.2^{5.9}$	$5.9^{4.5}$	$7.7^{5.5}$	$6.2^{4.1}$	$7.8^{5.6}$	$5.0^{4.5}$	$8.5^{5.9}$	$8.0^{6.7}$	$7.0^{5.8}$
Agassiz	$11.0^{8.1}$	$11.2^{5.4}$	$7.3^{7.6}$	$6.1^{7.3}$	$7.7^{6.3}$	$4.7^{4.2}$	$6.1^{9.4}$	$6.2^{3.4}$	$7.8^{4.3}$	$5.2^{4.5}$	$6.1^{2.9}$	$5.9^{4.0}$	$6.0^{3.2}$	$5.7^{4.0}$	$4.7^{2.8}$	$6.7^{9.2}$	$7.6^{4.1}$
Northern Ellesmere	$9.4^{9.0}$	$9.8^{6.3}$	$6.3^{6.4}$	$7.9^{11.8}$	$4.5^{6.8}$	$15.5^{16.1}$	$6.7^{4.2}$	$7.1^{5.0}$	$8.9^{5.2}$	$6.4^{7.1}$	$6.1^{2.6}$	$6.6^{7.4}$	$5.3^{3.7}$	$5.9^{7.9}$	$6.1^{3.4}$	$10.0^{6.2}$	$9.3^{4.4}$
Müller & Steacie	$11.6^{6.6}$	$12.3^{7.5}$	$4.6^{5.0}$	$5.2^{4.7}$	$15.8^{6.2}$	$4.4^{4.4}$	$4.1^{3.4}$	$6.2^{3.7}$	$8.2^{3.4}$	$6.4^{6.6}$	$6.5^{3.2}$	$6.4^{4.1}$	$7.8^{4.3}$	$6.5^{3.5}$	$6.8^{3.8}$	$9.6^{6.6}$	$10.5^{5.7}$

Table 4-3: Dynamic change, terminus response and identification of surface features indicative of surging for the 16 glaciers that underwent significant velocity variation over the 1999-2015 period. "*" indicates glaciers that have previously been identified as surge-type by Copland et al. [2003a].

Glacier	Ice Mass	Type	Dynamic Change	Terminus Position	Surge features
Antoinette	Agassiz	Pulse	***Slow down*** (~100 m a^{-1} in 2000; stagnant in 2015)	***Retreat*** (~1.1 km: 2002-2014)	
Tuborg*	Agassiz	Pulse	***Slow down*** (~180 m a^{-1} in 2000; slowing to ~90 m a^{-1} in 2015)	***Retreat*** (~2.25 km: 2002-2014)	Digitate terminus
Eugenie	Agassiz	Pulse	***Slow down*** (~300-400 m a^{-1} 2000; stagnant 2012-2015)	***Retreat*** (~1.2 km: 2002-2014)	Longitudinal crevassing
Iceberg*	Müller	Surge	***Slow down*** (~75-100 m a^{-1} in 2000; stagnant in 2015)	**Retreat** (~1.5-2.5 km: 2000-2004)	Looped moraines
Mittie*	Manson	Surge	***Slow down*** (~750 m a^{-1} in 2000; Stagnant by 2015)	***Retreat*** (~4 km: 2002-2014)	Heavy terminus crevassing
Ekblaw	Prince of Wales	Pulse	***Slow down*** (~500 m a^{-1} in 2000; ~100 m a^{-1} in 2015)	***Retreat*** (~0.5 km: 2000-2014)	
Good Friday Bay*	Steacie	Surge	***Slow down*** (~200-300 m a^{-1} in 2006; ~150-200 m a^{-1} in 2015)	***Advance*** (~2 km: 2000-2014)	Extensive crevassing, looped moraines (2014)
Middle*	Müller	Surge	***Slow down*** (~165 m a^{-1} in 2000; slowing to ~75 m a^{-1} in 2015)	***Advance*** (~1 km: 2000-2014)	Looped moraines
Dobbin	Prince of Wales	Pulse	***Variable*** (~160-180 m a^{-1} in 2000; ~100-120 m a^{-1} in 2015)	***Retreat*** (0.8 km: 2000-2014)	
Canõn*	Agassiz	Pulse	***Variable*** (~100-125 m a^{-1} 2000-2008; ~150-175 m a^{-1} in 2015)	***Retreat*** (~2 km: 2002-2014)	
Parrish*	Agassiz	Pulse	***Variable*** (~80 m a^{-1} in 2000; ~200-250 m a^{-1} in 2011; slowing 2012-2015)	***Variable*** (~Advance ~2km: ~2000-2012; Retreat 300 m 2012-2014)	
Sydkap	Sydkap	Pulse	***Variable*** (~100 m a^{-1} in 2000; ~400 m a^{-1} in 2006; ~100 m a^{-1} in 2015)	***Retreat*** (1.2 km: 2007-2014)	
Chapman*	Northern Ellesmere	Surge	***Variable*** (~40-80 m a^{-1} in 2000; ~150-200 m a^{-1} by 2011)	***Stable*** (2002-2014)	Looped and distorted moraines
Otto*	Northern Ellesmere	Surge	***Variable*** (~800 m a^{-1} in lower terminus in 2000; stagnant in 2015)	***Retreat*** (~1.2 km: 2002-2014)	
Wykeham	Prince of Wales	Pulse	***Speed-up*** (~200-300 m a^{-1} in 2000; increasing to 500 m a^{-1} by 2015)	***Retreat*** (~1 km: 2000-2014)	
Trinity	Prince of Wales	Accelerating	***Speed-up*** (~500-750 m a^{-1} in 2000; 750-1250 m a^{-1} in 2015)	***Retreat*** (~3-4 km: 2000-2014)	

Table 4-4: Characteristics used to distinguish between glaciers identified as "pulse-type" vs. "surge-type" in the Canadian High Arctic

	Pulse-type glacier	**Surge-type glacier**
Spatial dynamic change	Dynamic change is restricted to regions of the glacier bed grounded below sea level, with no evidence of dynamic change propagating upglacier of these locations.	Dynamic change appears to occur over the entire trunk of the glacier, with elevated velocities beginning upglacier and propagating downglacier over time.
Temporal dynamic change	No previous or minimal evidence of cyclical dynamic behaviour.	Evidence of past dynamic variability occurring in cyclic intervals, eg, looped moraines, degraded flow strips, heavily crevassed/rough surface topography.
Bed morphology	Evidence that sills may play a role in regulating ice motion in the lowermost terminus region.	No evidence that sills play a significant role in regulating ice motion in the lowermost terminus region.

Table 4-5: Temporal variability in dynamic discharge for individual glaciers and ice masses of the Canadian High Arctic. Ice thickness data sources: [1] = 2014 NASA Operation IceBridge, [2] = 2012 NASA Operation IceBridge, [3] = 2006 NASA Operation IceBridge. Fluxgate method: CS = Cross Section, CS_{int} = Cross Section with interpolated ice thickness values to fill in partial missing data, CL = Centreline Method. Superscript notation presents (±) uncertainty for each estimate.

Glacier	Lat	Long	Dynamic Discharge (Gt a^{-1})										
			2000	2006	2007	2008	2009	2010	2011	2012	2013	2014	2015
Mittie East(CS[3]) & West (CL[3]) Arms	76.85	-79.33	$0.90^{.25}$		$0.09^{.05}$	$0.07^{.07}$	$0.03^{.03}$			$0.02^{.02}$	$0.02^{.02}$	$0.02^{.02}$	$0.02^{.02}$
Dynamic discharge			**$0.90^{.25}$**		**$0.09^{.09}$**	**$0.07^{.07}$**	**$0.03^{.03}$**			**$0.02^{.02}$**	**$0.02^{.02}$**	**$0.02^{.02}$**	**$0.02^{.02}$**
Sydkap (CS3)	76.62	-85.11								$0.02^{.01}$	$0.02^{.01}$	$0.03^{.01}$	$0.04^{.01}$
Dynamic discharge										**$0.02^{.01}$**	**$0.02^{.01}$**	**$0.03^{.01}$**	**$0.04^{.01}$**
Cadogan (CS[1])	78.23	-76.94	$0.09^{.03}$	$0.14^{.03}$	$0.13^{.03}$	$0.10^{.03}$		$0.08^{.02}$	$0.08^{.02}$	$0.06^{.02}$	$0.05^{.02}$	$0.06^{.02}$	$0.06^{.02}$
Wyville Thomson (CS[1])	78.42	-75.50	$0.01^{.01}$							$0.01^{.01}$	$0.01^{.01}$	$0.01^{.01}$	$0.01^{.01}$
Cadogan South2 (CS[1])	78.39	-75.29	$0.01^{.01}$								$0.01^{.01}$	$0.01^{.01}$	$0.01^{.01}$
Cadogan South3 (CS[1])	78.38	-75.22									$0.00^{.01}$	$0.00^{.01}$	$0.00^{.01}$
Ekblaw (CS[1])	78.51	-76.71	$0.14^{.03}$	$0.20^{.03}$	$0.20^{.03}$	$0.17^{.03}$	$0.15^{.03}$	$0.15^{.03}$	$0.12^{.03}$	$0.11^{.02}$	$0.08^{.02}$	$0.07^{.02}$	$0.08^{.02}$
Tanquary (CL[1])	78.46	-76.08	$0.03^{.02}$				$0.05^{.02}$		$0.07^{.02}$	$0.05^{.02}$	$0.04^{.01}$	$0.04^{.01}$	$0.05^{.01}$
Leffert (CS_{int}[1])	78.69	-74.92	$0.02^{.01}$							$0.00^{.00}$	$0.01^{.00}$	$0.01^{.00}$	$0.01^{.00}$
Palisade (CL[1])	77.39	-80.99	$0.02^{.01}$							$0.00^{.00}$	$0.00^{.00}$	$0.00^{.00}$	$0.00^{.00}$
South 2 (CL[1])	77.33	-79.62	$0.01^{.01}$						$0.01^{.04}$	$0.02^{.04}$	$0.02^{.04}$	$0.02^{.04}$	$0.02^{.01}$
South 3 (CL[1])	77.31	-80.30	$0.01^{.01}$							$0.00^{.00}$	$0.00^{.00}$	$0.00^{.00}$	$0.00^{.00}$
South 4 (CS[1])	77.33	-79.05							$0.00^{.00}$	$0.00^{.00}$	$0.00^{.00}$	$0.00^{.00}$	$0.00^{.00}$
South 5 (CS[1])	77.38	-78.90	$0.00^{.00}$						$0.00^{.00}$	$0.00^{.00}$	$0.00^{.00}$	$0.00^{.00}$	$0.00^{.00}$
South 6 (CS[1])	77.37	-78.93	$0.00^{.00}$						$0.00^{.00}$	$0.00^{.00}$	$0.00^{.00}$	$0.00^{.00}$	$0.00^{.00}$
South 7(CS[1])	77.41	-78.76	$0.02^{.01}$						$0.03^{.01}$	$0.02^{.01}$	$0.02^{.01}$	$0.02^{.01}$	$0.02^{.01}$
Stygge (CS[1])	78.77	-78.24	$0.01^{.01}$						$0.01^{.01}$	$0.01^{.01}$	$0.01^{.01}$	$0.01^{.01}$	$0.01^{.01}$
Sands (CL[1])	78.95	-78.06							$0.00^{.00}$	$0.01^{.01}$	$0.01^{.01}$	$0.01^{.01}$	$0.01^{.01}$
Trinity (CS[1])	77.97	-78.57	$0.38^{.08}$	$0.75^{.12}$	$0.84^{.14}$	$0.66^{.11}$	$0.92^{.15}$	$0.94^{.15}$	$1.05^{.17}$	$0.90^{.14}$	$0.71^{.12}$	$0.95^{.15}$	$1.02^{.16}$
Wykeham (CS[1])	77.89	-78.61	$0.17^{.04}$	$0.25^{.05}$	$0.29^{.05}$	$0.18^{.04}$	$0.25^{.05}$	$0.25^{.05}$	$0.32^{.05}$	$0.31^{.05}$	$0.30^{.05}$	$0.37^{.06}$	$0.41^{.07}$
Talbot (CS_{in-t}[1])	78.00	-78.24	$0.02^{.01}$	$0.01^{.01}$	$0.01^{.01}$	$0.01^{.01}$	$0.01^{.01}$	$0.01^{.01}$	$0.01^{.01}$	$0.00^{.01}$	$0.00^{.01}$	$0.00^{.01}$	$0.00^{.01}$
Unnamed1 (CL[1])	77.98	-77.36	$0.02^{.01}$					$0.01^{.01}$	$0.01^{.01}$	$0.00^{.00}$	$0.01^{.01}$	$0.00^{.00}$	$0.00^{.00}$
Unnamed1 South (CS_{int}[1])	77.90	-77.92	$0.04^{.01}$				$0.03^{.01}$	$0.04^{.01}$	$0.03^{.01}$	$0.03^{.01}$	$0.02^{.01}$	$0.03^{.01}$	$0.02^{.01}$
MacMillian (CL[1])	78.52	-75.31	$0.01^{.01}$							$0.01^{.01}$	$0.01^{.01}$	$0.01^{.01}$	$0.01^{.01}$
South Margin (CS[1])	77.71	-77.88	$0.06^{.05}$	$0.02^{.01}$	$0.02^{.01}$	$0.02^{.02}$	$0.03.^{02}$	$0.01^{.01}$	$0.07^{.05}$	$0.06^{.06}$	$0.06^{.06}$	$0.08^{.06}$	$0.06^{.06}$
Dynamic discharge			**$0.92^{.36}$**	**$1.19^{.25}$**	**$1.49^{.27}$**	**$1.14^{.51}$**	**$1.44^{.29}$**	**$1.49^{.29}$**	**$1.99^{.38}$**	**$1.60^{.42}$**	**$1.37^{.42}$**	**$1.70^{.45}$**	**$1.80^{.44}$**
Antoinette (CS[2])	80.81	-76.30	$0.04^{.01}$	$0.01^{.01}$	$0.01^{.01}$		$0.01^{.01}$	$0.01^{.01}$	$0.01^{.01}$	$0.00^{.00}$	$0.00^{.00}$	$0.00^{.00}$	$0.01.^{01}$
Cañon (CL[1])	79.68	-79.64	$0.04^{.01}$	$0.03^{.01}$	$0.03^{.01}$	$0.03^{.01}$	$0.04^{.01}$			$0.04^{.01}$	$0.06^{.01}$	$0.06^{.01}$	$0.07^{.02}$
d'Iberville (CL[1])	80.56	-77.92	$0.01^{.01}$	$0.01^{.01}$			$0.01^{.01}$	$0.01^{.01}$	$0.01^{.01}$	$0.01^{.01}$	$0.01^{.01}$	$0.01^{.01}$	$0.01^{.01}$
Eugenie (CL[1])	79.82	-74.93	$0.11^{.02}$						$0.00^{.01}$	$0.00^{.01}$	$0.00^{.01}$	$0.00^{.01}$	$0.00^{.01}$
John Richardson (CL[1])	80.23	-72.41	$0.01^{.01}$						$0.00^{.01}$	$0.00^{.01}$	$0.00^{.01}$	$0.00^{.01}$	$0.00^{.01}$
Parrish (CL[1])	79.57	-77.18	$0.02^{.01}$						$0.05^{.01}$	$0.01^{.01}$	$0.01^{.01}$	$0.01^{.01}$	$0.01^{.01}$
Sawyer Bay (CS[2])	79.36	-78.05	$0.01^{.01}$	$0.01^{.01}$		$0.01^{.01}$				$0.01^{.01}$	$0.01^{.01}$	$0.01^{.01}$	$0.01^{.01}$
Tuborg (CL[1])	80.89	-76.14	$0.03^{.01}$	$0.03^{.01}$	$0.03^{.01}$		$0.03^{.01}$	$0.03^{.01}$	$0.04^{.01}$	$0.02^{.01}$	$0.03^{.01}$	$0.03^{.01}$	$0.03^{.01}$
Dobbin (CL[1])	79.89	-74.34	$0.02^{.01}$						$0.00^{.01}$	$0.00^{.01}$	$0.00^{.01}$	$0.00^{.01}$	$0.00^{.01}$
Unnamed4 (CL[1])	80.07	-72.39	$0.01^{.01}$						$0.02^{.01}$	$0.01^{.01}$	$0.01^{.01}$	$0.01^{.01}$	$0.01^{.01}$
Dynamic discharge			**$0.30^{.11}$**	**$0.09^{.05}$**	**$0.07^{.03}$**	**$0.04^{.02}$**	**$0.09^{.04}$**	**$0.05^{.03}$**	**$0.13^{.08}$**	**$0.10^{.09}$**	**$0.13^{.09}$**	**$0.13^{.09}$**	**$0.15^{.11}$**
Iceberg (CL[1])	79.43	-92.37	$0.03^{.01}$	$0.00^{.00}$	$0.00^{.00}$	$0.01^{.01}$	$0.00^{.00}$	$0.01^{.01}$	$0.01^{.01}$	$0.00^{.00}$	$0.00^{.00}$	$0.00^{.00}$	$0.00^{.00}$
Good Friday Bay (CL[1])	78.55	-91.76			$0.08^{.01}$		$0.07^{.01}$			$0.06^{.01}$	$0.05^{.01}$	$0.05^{.01}$	$0.05^{.01}$
Dynamic discharge			**$0.03^{.01}$**	**$0.00^{.00}$**	**$0.08^{.01}$**	**$0.01^{.01}$**	**$0.07^{.01}$**	**$0.01^{.01}$**	**$0.01^{.01}$**	**$0.06^{.01}$**	**$0.05^{.01}$**	**$0.05^{.01}$**	**$0.05^{.01}$**
Disraeli (CL[1])	82.67	-72.50	$0.01^{.01}$						$0.01^{.01}$	$0.02^{.01}$	$0.01^{.01}$	$0.02^{.01}$	$0.01.^{01}$
Disraeli North (CL[1])	82.84	-70.79	$0.01^{.01}$						$0.01^{.01}$	$0.02^{.01}$	$0.01^{.01}$	$0.01^{.01}$	$0.01^{.01}$
DeVries (CL[1])	82.01	-79.60							$0.01^{.01}$	$0.01^{.01}$	$0.01^{.01}$	$0.01^{.01}$	$0.01^{.01}$
M'Clintock (CL[1])	82.43	-76.15							$0.01^{.01}$	$0.01^{.01}$	$0.01^{.01}$	$0.01^{.01}$	$0.01^{.01}$
Marine (CS[2])	82.24	-81.72	$0.01^{.01}$						$0.01^{.01}$	$0.01^{.01}$	$0.01^{.01}$	$0.01^{.01}$	$0.01^{.01}$
Marine North (CS[2])	82.42	-82.54	$0.02^{.01}$						$0.01^{.01}$	$0.00^{.01}$	$0.01^{.01}$	$0.01^{.01}$	$0.02^{.01}$
Milne (CL[1])	82.44	-80.22	$0.07^{.02}$						$0.06^{.01}$	$0.06^{.01}$	$0.05^{.01}$	$0.05^{.01}$	$0.06^{.02}$
Otto (CL[1])	81.30	-84.70	$0.11^{.02}$	$0.15^{.03}$	$0.17^{.03}$	$0.15^{.03}$	$0.09^{.02}$	$0.07^{.01}$	$0.11^{.02}$	$0.09^{.02}$	$0.01^{.01}$	$0.00^{.01}$	$0.01^{.01}$
Vanier (CL[1])	82.14	-80.75	$0.01^{.01}$						$0.01^{.01}$	$0.01^{.01}$	$0.01^{.01}$	$0.01^{.01}$	$0.01^{.01}$
Yelverton (CL[1])	81.84	-79.43	$0.12^{.02}$						$0.06^{.01}$	$0.07^{.01}$	$0.08^{.02}$	$0.08^{.02}$	$0.08^{.02}$
Dynamic discharge			**$0.36^{.11}$**	**$0.15^{.03}$**	**$0.17^{.03}$**	**$0.15^{.03}$**	**$0.09^{.02}$**	**$0.07^{.01}$**	**$0.30^{.11}$**	**$0.30^{.11}$**	**$0.21^{.11}$**	**$0.21^{.11}$**	**$0.23^{.12}$**
Dynamic discharge			**$2.51^{.84}$**	**$1.43^{.33}$**	**$1.90^{.43}$**	**$1.41^{.64}$**	**$1.72^{.39}$**	**$1.62^{.34}$**	**$2.43^{.58}$**	**$2.08^{.64}$**	**$1.80^{.66}$**	**$2.14^{.69}$**	**$2.29^{.71}$**

Table 4-6: Temporal variability in dynamic discharge for individual glaciers and ice masses of the Canadian High Arctic. Ice thickness data sources: 1 = 2014 NASA Operation IceBridge, 2 = 2012 NASA Operation IceBridge, 3 = 2006 NASA Operation IceBridge. Fluxgate method: CS = Cross Section, CL = Centreline Method. Superscript notation presents (±) uncertainty for each estimate.

Glacier	Lat	Long	Dynamic Discharge (Gt a^{-1})										
			1999-2000	2000-2001	2001-2002	2002-2003	2003-2004	2004-2005	2005-2006	2006-2007	2007-2008	2008-2009	2009-2010
Manson Icefield													
Mittie East (CS^{2})	76.85	-79.33	$1.03^{.13}$	$0.83^{.13}$	$0.66^{.11}$	$0.75^{.12}$	$0.60^{.10}$	$0.67^{.11}$	$0.51^{.09}$	$0.18^{.04}$			
Sydkap Ice Cap													
Sydkap (CS^{3})	76.62	-85.11	$0.04^{.01}$	$0.03^{.01}$	$0.04^{.03}$	$0.04^{.01}$	$0.03^{.01}$	$0.05^{.01}$	$0.05^{.01}$		$0.04^{.01}$	$0.04^{.01}$	$0.04^{.01}$
Prince of Wales Icefield													
Cadogan (CS^{1})	78.23	-76.94	$0.09^{.03}$	$0.06^{.02}$	$0.07^{.03}$	$0.09^{.03}$	$0.10^{.03}$	$0.11^{.03}$	$0.12^{.03}$	$0.11^{.03}$	$0.09^{.03}$	$0.07^{.02}$	$0.8^{.03}$
Ekblaw (CS^{1})	78.81	-76.71	$0.13^{.03}$	$0.12^{.03}$	$0.15^{.03}$	$0.05^{.01}$	$0.11^{.02}$	$0.16^{.03}$	$0.12^{.02}$				
Trinity (CS^{1})	77.97	-78.57	$0.47^{.09}$	$0.35^{.07}$	$0.43^{.08}$								
Wykeham (CS^{1})	77.89	78.61	$0.11^{.03}$	$0.12^{.03}$	$0.12^{.03}$	$0.16^{.03}$	$0.14^{.03}$	$0.19^{.04}$	$0.11^{.02}$				
Agassiz Ice Cap													
Antoinette (CS^{2})	80.81	-76.30	$0.06^{.02}$	$0.05^{.01}$	$0.04^{.01}$	$0.05^{.01}$	$0.03^{.01}$	$0.04^{.01}$	$0.03^{.01}$	$0.02^{.01}$	$0.01^{.01}$	$0.01^{.01}$	$0.01^{.01}$
Cañon (CL^{1})	79.68	-79.64	$0.05^{.01}$	$0.04^{.01}$	$0.04^{.01}$	$0.04^{.01}$	$0.04^{.01}$	$0.04^{.01}$	$0.04^{.01}$	$0.04^{.01}$	$0.04^{.01}$	$0.05^{.02}$	$0.05^{.01}$
d'Iberville (CL^{1})	80.56	-77.92	$0.01^{.01}$	$0.01^{.01}$	$0.01^{.01}$	$0.01^{.01}$	$0.01^{.01}$	$0.01^{.01}$	$0.01^{.01}$	$0.01^{.01}$	$0.01^{.01}$		$0.01^{.01}$
Eugenie (CL^{1})	79.82	-74.93	$0.12^{.03}$	$0.12^{.03}$	$0.11^{.03}$	$0.13^{.03}$	$0.12^{.03}$	$0.14^{.03}$	$0.14^{.03}$	$0.12^{.03}$	$0.07^{.02}$	$0.04^{.01}$	$0.01^{.01}$
John Richardson (CL^{1})	80.23	-72.41											
Parrish (CL^{1})	79.57	-77.18	$0.01^{.01}$	$0.02^{.01}$	$0.02^{.01}$	$0.03^{.01}$	$0.05^{.01}$	$0.05^{.01}$	$0.06^{.01}$		$0.11^{.02}$	$0.11^{.02}$	$0.09^{.02}$
Tuborg (CL^{1})	80.89	-76.14	$0.05^{.01}$	$0.05^{.01}$	$0.05^{.01}$	$0.06^{.01}$	$0.06^{.01}$	$0.06^{.01}$	$0.04^{.01}$	$0.05^{.01}$	$0.05^{.01}$	$0.05^{.01}$	$0.05^{.01}$
Dobbin (CL^{1})	79.89	-74.34	$0.02^{.01}$	$0.01^{.01}$	$0.02^{.01}$	$0.03^{.01}$	$0.04^{.01}$	$0.08^{.01}$		$0.07^{.01}$	$0.04^{.01}$	$0.02^{.01}$	$0.01^{.01}$
Unnamed4 (CL^{1})	80.07	-72.39	$0.01^{.01}$	$0.02^{.01}$	$0.01^{.01}$	$0.01^{.02}$	$0.02^{.01}$	$0.01^{.01}$	$0.01^{.01}$	$0.01^{.01}$	$0.01^{.01}$	$0.01^{.01}$	$0.01^{.01}$
Müller Ice Cap													
Iceberg (CL^{1})	79.43	-92.37	$0.06^{.01}$	$0.03^{.01}$	$0.02^{.01}$			$0.01^{.01}$	$0.01^{.01}$	$0.01^{.01}$	$0.00^{.01}$	$0.01^{.01}$	$0.00^{.01}$
Northern Ellesmere Icefield													
Otto (CL^{1})	81.30	-84.70	$0.11^{.02}$	$0.11^{.02}$	$0.11^{.02}$			$0.08^{.01}$					

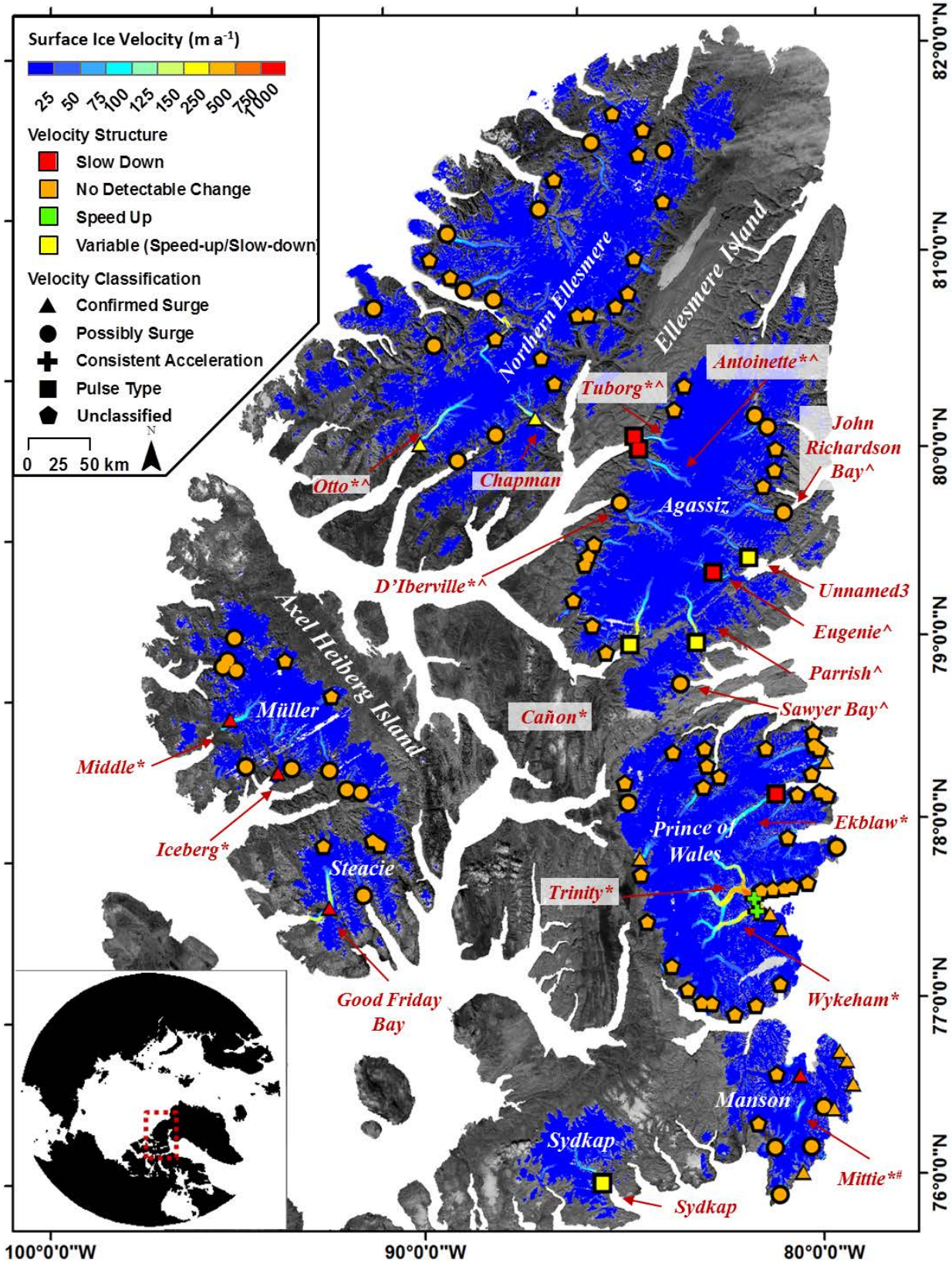

Figure 4-1: Distribution of dynamic changes and velocity classification for major glaciers measured in this study. "*" indicates glaciers with previous velocity maps derived by Short and Gray [2005], "^" derived by Williamson et al. [2008] and "#" derived by Copland et al [2003a].

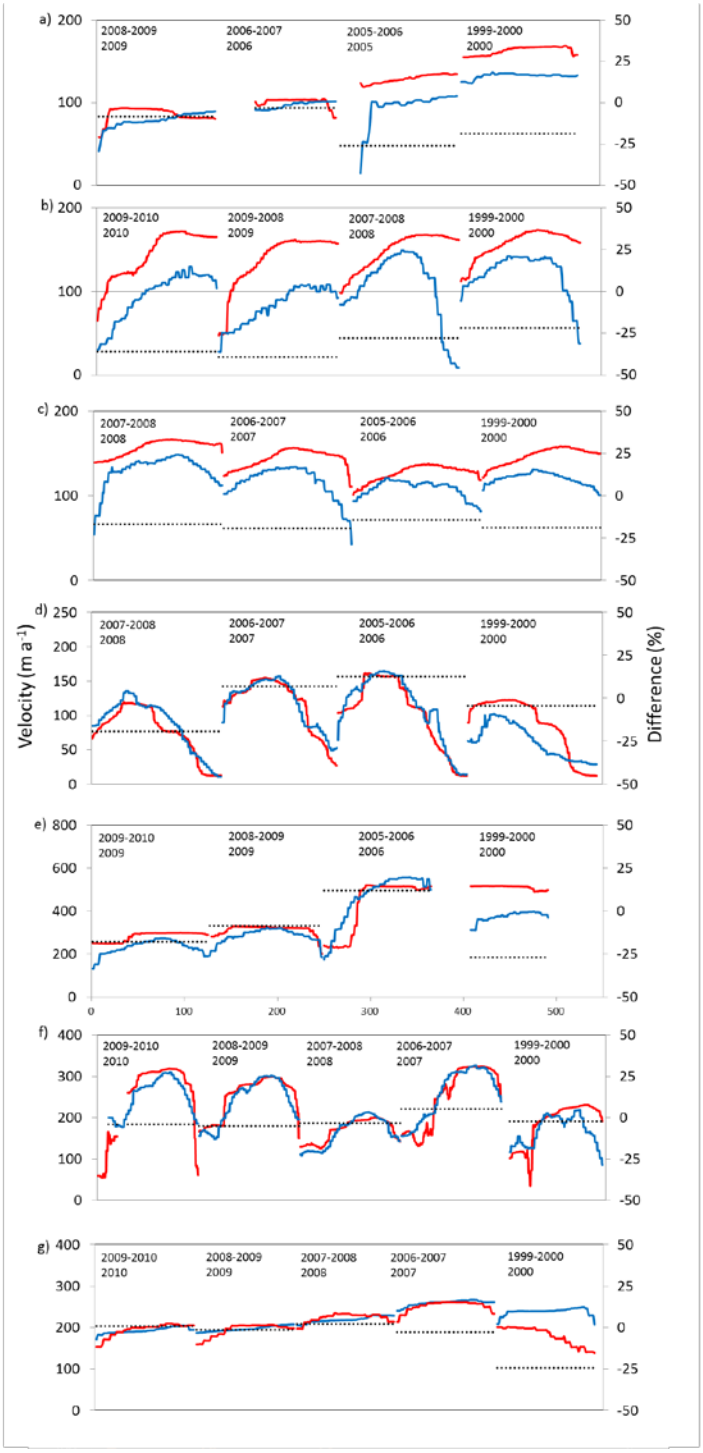

Figure 4-2: Comparison of near terminus glacier velocities derived from feature tracking of summer Landsat-7 imagery ("Annual" velocities: Red line) and glacier velocities derived from speckle tracking of winter Radarsat imagery ("Winter" velocities": blue line), black dashed lines indicate the average difference across the flux gate for a) Antoinette Glacier, b) Tuborg Glacier, c) Canon Glacier, d) Cadogan Glacier, e) Otto Glacier, f) Wykeham Glacier, g) Ekblaw Glacier.

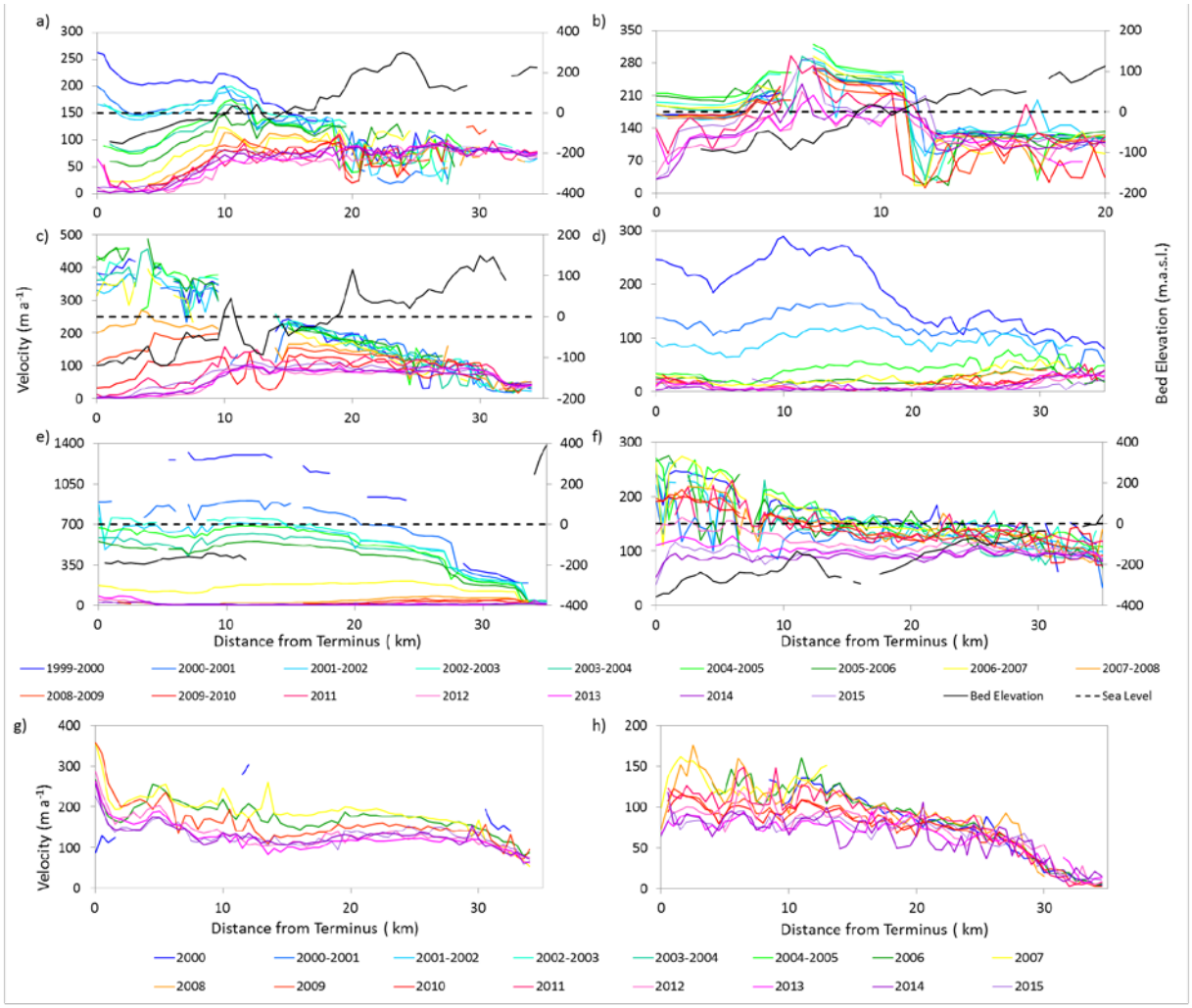

Figure 4-3: Temporal evolution (slow down) of centerline glacier surface velocities for a) Antoinette Glacier, b) Tuborg Glacier, c) Eugenie Glacier, d) Iceberg Glacier, e) Mittie Glacier, f) Ekblaw Glacier, g) Good Friday Bay Glacier, h) Middle Glacier. Where available, solid black line indicates glacier bed elevation, dashed black line indicates sea level (both plotted on secondary axis). Note: Velocity profiles that span more than one year represent displacements derived from feature tracking (i.e., "annual velocities") and profiles plotted for a single year represent displacements derived from speckle tracking (i.e., "winter velocities").

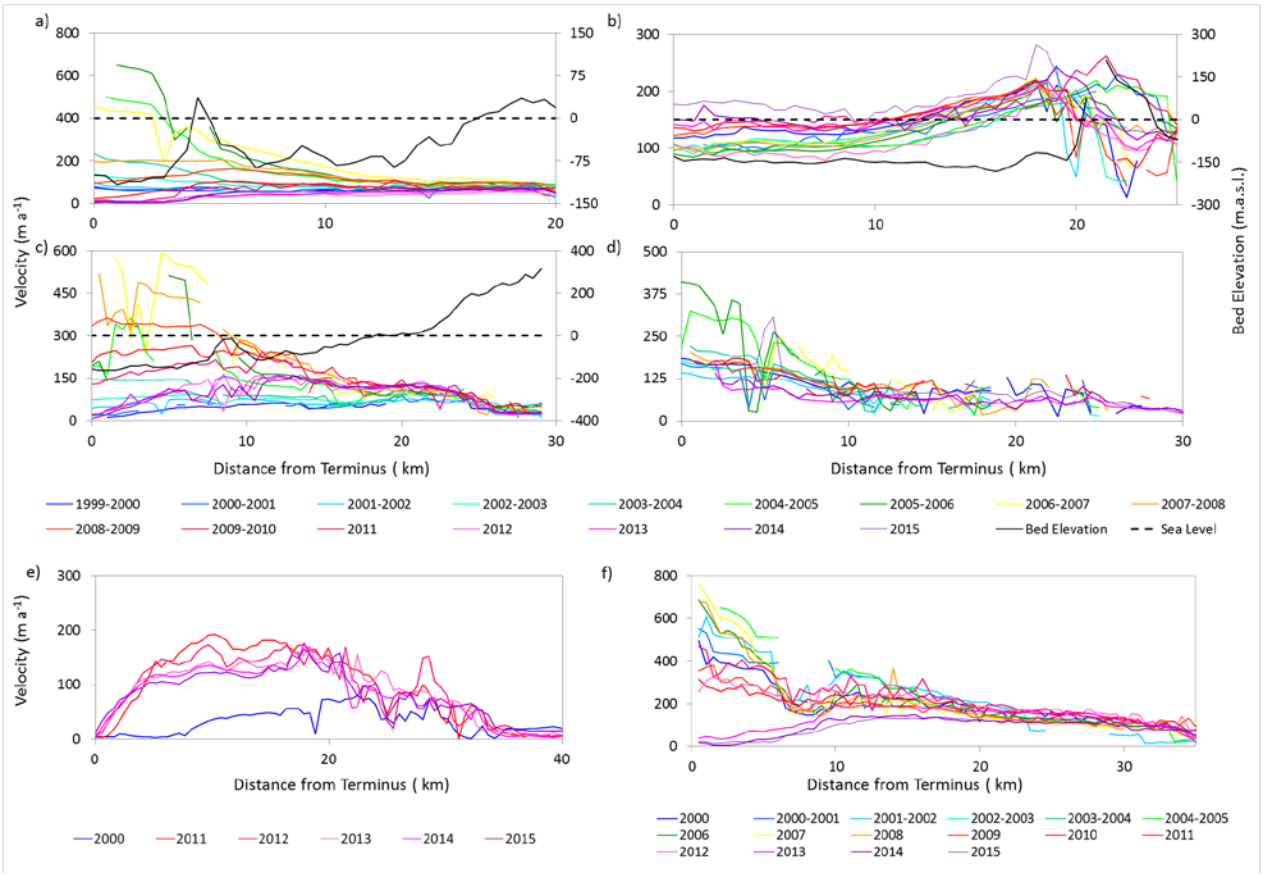

Figure 4-4: Temporal evolution of centerline glacier surface velocities for a) Dobbin Glacier, b) Cañon Glacier, c) Parrish Glacier, d) Sydkap Glacier, e) Chapman Glacier, f) Otto Glacier. Where available, solid black line indicates glacier bed elevation, dashed black line indicates sea level (both plotted on secondary axis). Note: Velocity profiles that span more than one year represent displacements derived from feature tracking (i.e., "annual velocities") and profiles plotted for a single year represent displacements derived from speckle tracking (i.e., "winter velocities").

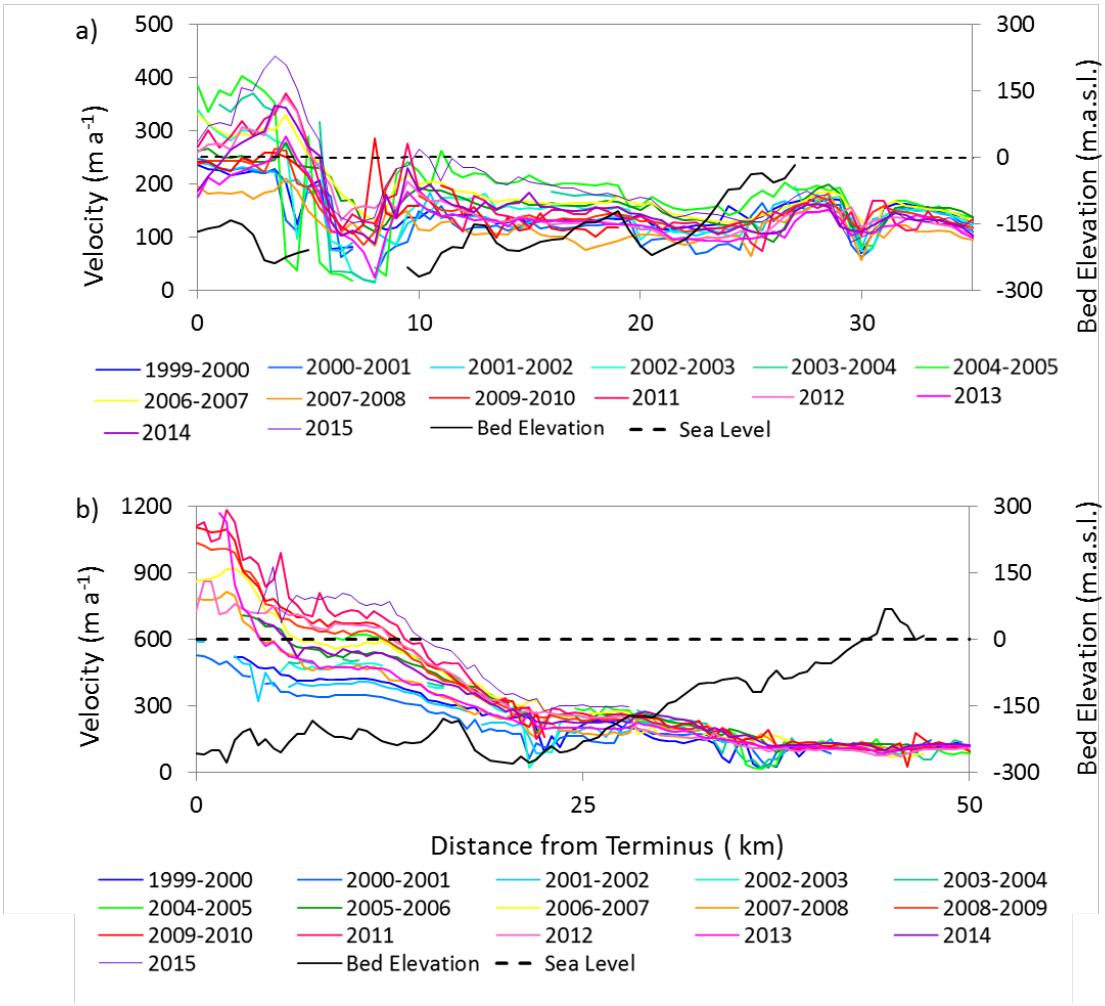

Figure 4-5: Temporal evolution (speed-up) of centerline glacier surface velocities for a) Wykeham Glacier, b) Trinity Glacier, both of Prince of Wales Icefield. Solid black line indicates glacier bed elevation, dashed black line indicates sea level (both plotted on secondary axis). Note: Velocity profiles that span more than one year represent displacements derived from feature tracking (i.e., "annual velocities") and profiles plotted for a single year represent displacements derived from speckle tracking (i.e., "winter velocities").

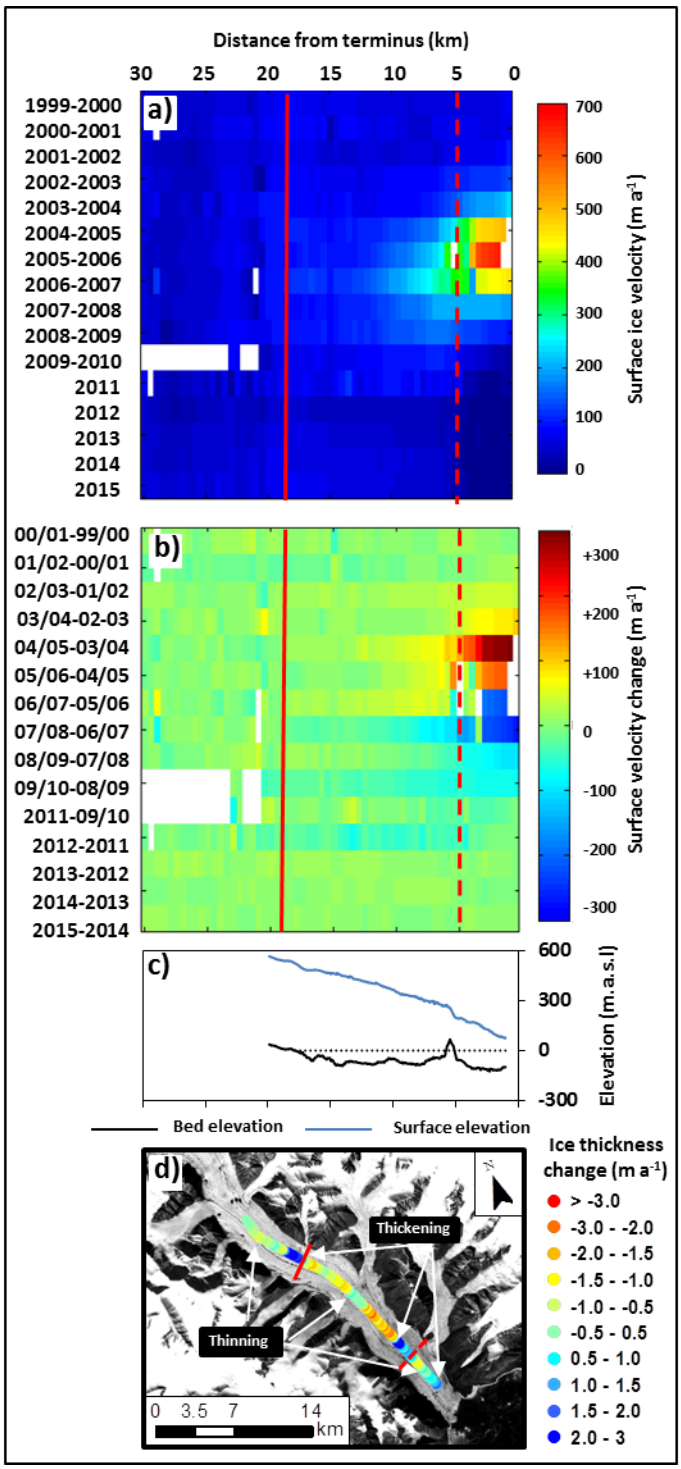

Figure 4-6: a) Patterns of annual surface ice velocity extracted every 500 m along the centreline of Dobbin Glacier, b) patterns of surface ice velocity difference along the centreline of Dobbin Glacier c) surface elevation and bed profile of Dobbin Glacier (black dashed line indicates sea level), d) change in centreline ice thickness profiles between 2000 (derived by Dowdeswell et al. [2004]) and 2014 (derived by NASA Operation IceBridge MCoRDS sensor) for Dobbin Glacier, background image: ASTER scene acquired June 11, 2012 (for Figures 4-6a,b,d: solid red lines indicate the location where the bed descends below sea level, dashed red line indicates sill location).

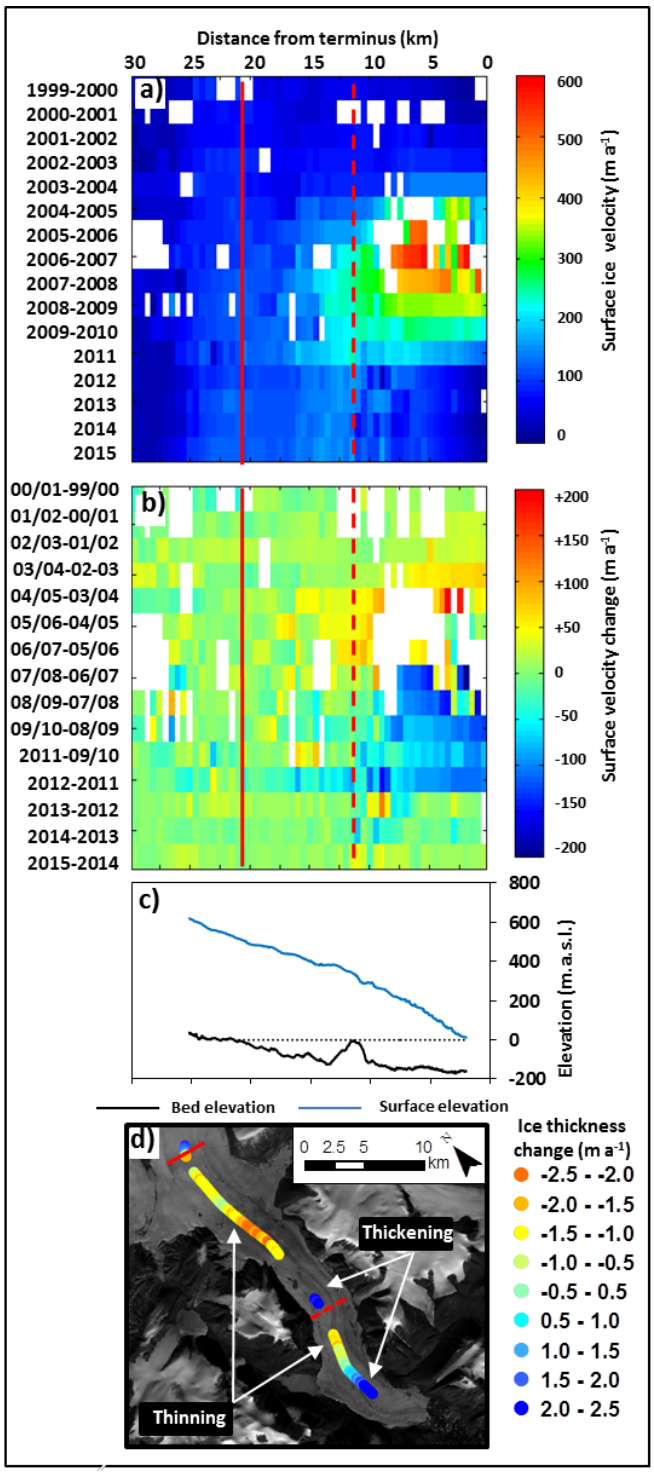

Figure 4-7: a) Patterns of annual surface ice velocity extracted every 500 m along the centreline of Parrish Glacier, b) patterns of surface ice velocity difference along the centreline of Parrish Glacier c) surface elevation and bed profile of Parrish Glacier (black dashed line indicates sea level), d)) change in centreline ice thickness profiles between 2000 (derived by Dowdeswell et al. [2004]) and 2014 (derived by NASA Operation IceBridge MCoRDS sensor) for Parrish Glacier, background image: ASTER scene acquired August 4, 2013 (for Figures 4-7a,b,d: solid red lines indicate the location where the bed descends below sea level, dashed red line indicates sill location).

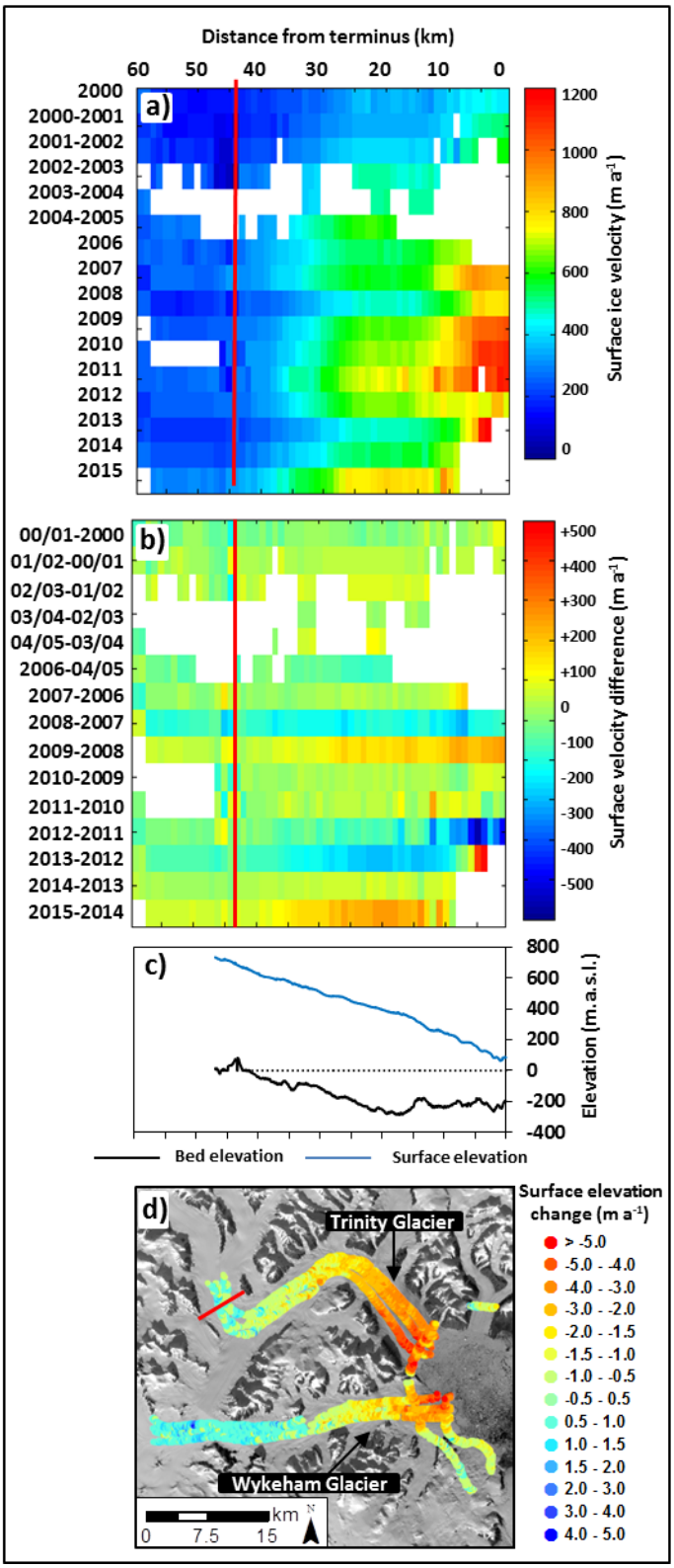

Figure 4-8: a) Patterns of annual surface ice velocity extracted every 500 m along the centreline of Trinity Glacier, b) patterns of surface ice velocity difference along the centreline of Trinity Glacier c) surface elevation and bed profile of Trinity Glacier (black dashed line indicates sea level), d) surface elevation change from 2008 (SPOT DEM) and 2014 NASA Operation IceBridge ATM data for Trinity Glacier, background image: Landsat-8 scene acquired Sept 7, 2014 (for Figures 4-8a, b, d: solid red lines indicate the location where the bed descends below sea level).

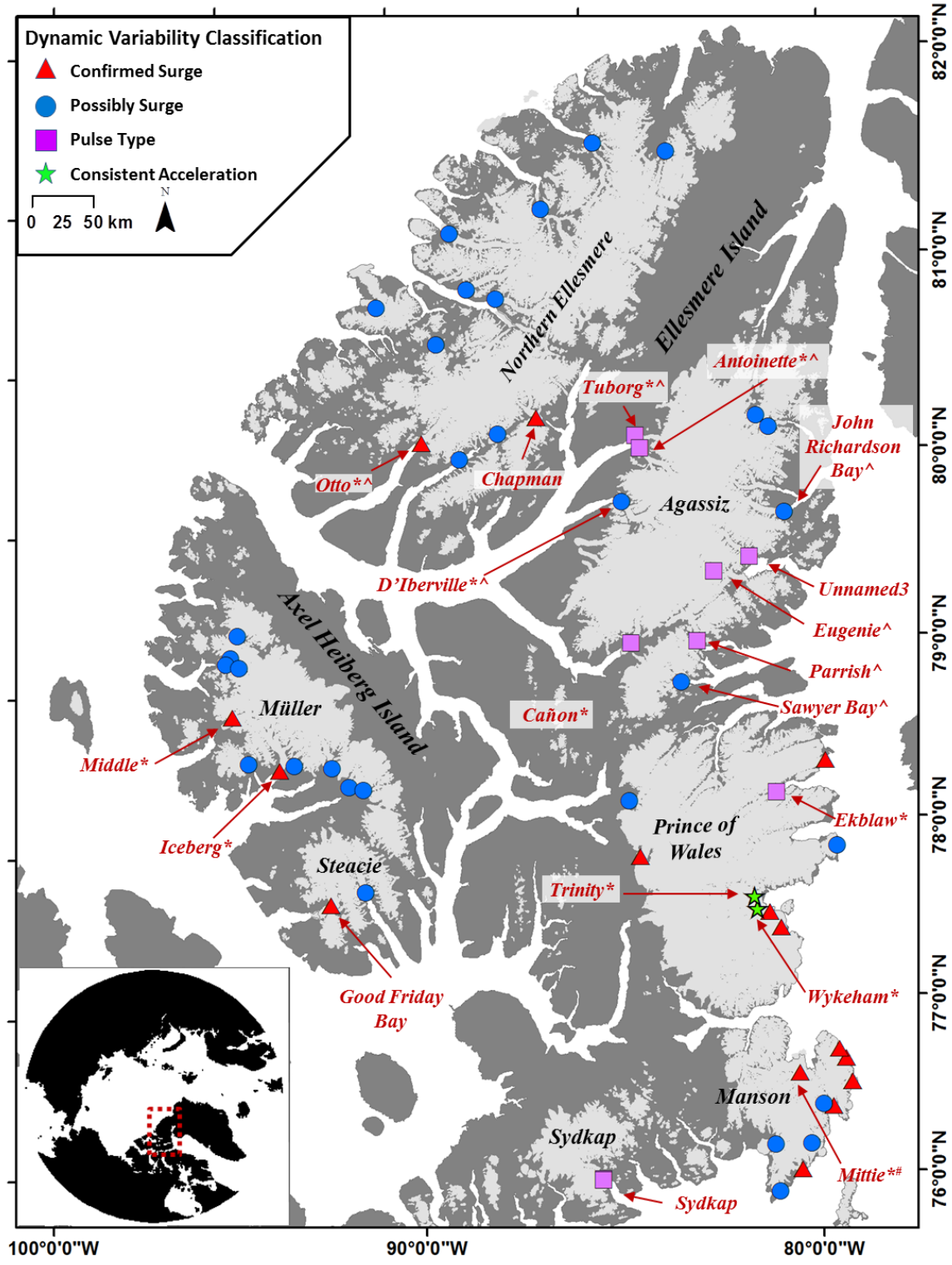

Figure 4-9: Distribution of glaciers identified as "surge", "pulse" and "consistent acceleration" across the QEI.

CHAPTER FIVE: Variability in Ice Motion and Dynamic Discharge from Devon Ice Cap, Nunavut, Canada

Abstract

Feature tracking of Landsat-7 ETM+ imagery acquired from 1999-2010 and speckle tracking of 24-day separated RADARSAT-2 imagery acquired from 2009-2015 reveal that motion of the major tidewater glaciers of Devon Ice Cap is more variable than previously described. The flow of several outlet glaciers (East-5, East-6, East-7, Fitzroy, North and South Croker Bay Glaciers) slowed over the observation period, while the termini of the Belcher, Southeast-1 and Southeast-2 Glaciers sped-up in the most recent years of observation. The North Croker Bay Glacier showed the greatest variability in motion, slowing by ~40 m a^{-1} between 2000/2001 and 2001/2002, speeding-up by ~50 m a^{-1} between 2003/2004 and 2004/2005 and slowing again by 40-80 m a^{-1} between 2010 and 2011 to its lowest speeds of the entire observation period. Comparisons between areas of dynamic variability and glacier bed elevations indicate that regions of velocity variability are largely restricted to regions where the glacier bed is grounded below sea level. A combination of the derived velocities and measurements of ice thickness at the front of tidewater glaciers yields a mean annual dynamic discharge of ~0.37 ± 0.15 Gt a^{-1} for Devon Ice Cap for 2009 and 2011-2015. Updated and expanded flow regime maps for the ice cap originally produced by Burgess et al. [2005] indicate that the North Croker Bay Glacier appears to have become more resistant to flow in recent years, while basal sliding appears to have become a larger component of ice motion in the terminus regions of the Southeast-1 and Southeast-2 glaciers.

5.1 Introduction

The glaciers, icefields and ice caps of the Canadian High Arctic have become an increasingly important region of mass loss in recent years as a result of higher summer air temperatures that have increased surface melt and run-off rates [Gardner et al. 2011, 2012; Sharp et al. 2011]. Climate projections, using moderate warming scenarios, indicate that increased mass losses from this region over the next century (due to enhanced meltwater production) will not be compensated for by increases in snowfall, leading to continued regional mass loss [Lenaerts et al. 2013]. Although the amount of mass loss via dynamic discharge (iceberg calving) for Devon Ice Cap has been previously determined (e.g. Burgess et al. [2005]; Van Wychen et al. [2012; 2014]), the current mass loss via dynamic discharge, and its past variability, have not been well constrained. This limits our ability to project how mass losses via dynamic discharge from the Canadian Arctic may evolve in the future. To investigate these issues, we use a ~15 year record of surface ice motion to quantify the temporal variability in dynamics of the major tidewater terminating glaciers of Devon Ice Cap. When combined with the findings of Chapter 4 [Van Wychen et al. *submitted*], these results provide a comprehensive record of velocity variability and dynamic discharge for the ice masses of the Queen Elizabeth Islands (Devon, Ellesmere, Axel Heiberg Islands) from 1999 to 2015.

This analysis builds upon the work of Van Wychen et al. [2012], which investigated the change in surface velocities of Devon Ice Cap between single snapshots in the ~mid-1990s and 2009. Although Van Wychen et al. [2012] were able to identify regions of change between the two periods, the lack of a continuous record of annual velocities precluded characterization of the extent and magnitude of velocity variability during the intervening period. Here, by utilizing a larger velocity dataset and bed profiles collected along the centerlines of tidewater glaciers, we provide a more complete assessment of the dynamics of Devon Ice Cap and of the nature and magnitude of spatial and temporal variations in the velocity of its major outlet glaciers. New velocity mapping from RADARSAT-2 imagery allows expansion and updating of the flow regime mapping originally completed by Burgess et al. [2005] for Devon Ice Cap. Finally, we compute new values of annual dynamic discharge (sometimes termed iceberg discharge or frontal ablation in other studies) from the ice cap for the period 1999-2015. Here we define

dynamic discharge as mass passing through a fixed flux gate near the terminus of a marine terminating outlet glacier.

5.2 Study Site

Devon Ice Cap occupies the eastern portion of Devon Island (Figure 5-1; inset) and has an area of ~14 400 km^2 and a volume of ~4400 km^3 [Burgess and Sharp 2004; Dowdeswell et al. 2004]. Mass balance studies on Devon Ice Cap began in ~1960 [Koerner 2005, Sharp et al 2011], and indicate that very negative mass balances have become increasingly common since 2005 [Sharp et al. 2011]. This has occurred in conjunction with an increase in summer air temperatures, particularly since the late 1980s [Gardner and Sharp 2007].

Despite the long-term record of mass balance observations, there have been few studies of the dynamics of Devon Ice Cap. Burgess et al. [2005] provided the first regional assessment of surface velocities and an estimate of iceberg discharge (~0.52 Gt a^{-1}) from the ice cap using interferometric measurements of ERS 1/2 data acquired in the mid-1990s and speckle tracking of RADARSAT-1 data acquired in 2000. Shepherd et al. [2007] applied interferometry to the same ERS-1/2 datasets to derive ice motion and dynamic discharge for the ice cap. Both studies found slow ice motion (<10 m a^{-1}) in the ice cap interior (indicative of ice frozen to its bed) and faster ice flow restricted to outlet glaciers. Burgess et al. [2005] further classified the flow of Devon Ice Cap into four distinct regimes, based on the relationship between the ratio of surface velocity to ice thickness and driving stress. This classification was then used to identify regions where basal sliding was inferred to be an increasingly important component of overall ice motion. Wyatt and Sharp [2015] used Landsat-7 ETM+ imagery to map the supraglacial drainage network on the ice cap and determined surface velocities of its major outlet glaciers. They found that inter-annual velocity variability was greatest near meltwater sink points (e.g. moulins) located in regions characterized by flow regimes that Burgess et al. [2005] had suggested were associated with flow by basal sliding. They took this to be indicative of local hydrological forcing of basal sliding.

Van Wychen et al. [2012] built on the work of Burgess et al. [2005] by utilizing speckle tracking of RADARSAT-2 fine beam imagery acquired in winter 2009 to determine the surface velocity structure of the entire ice cap. The velocity patterns were broadly similar in both imaging periods (i.e., mid-1990s and 2009), and the computed dynamic discharge was identical within error

margins. However, differencing the velocity maps produced by the two studies revealed some areas of dynamic change, the biggest of which was that the lowermost ~10 km of East-5 glacier was flowing ~100 m a^{-1} faster in 2009 than in the mid-1990s. Surface velocities of Southeast-2 glacier had also increased by ~50 m a^{-1} along its lower 20 km, indicative of the down-glacier propagation of a surge front (previously described by Burgess and Sharp [2008]).

5.3 Methods

This study utilizes feature tracking of summer (May-September) Landsat-7 ETM+ scenes acquired from 1999-2010 (Table 5-1) and speckle tracking of winter/spring (January-April) RADARSAT-2 scenes acquired from 2009-2015 (Table 5-2) to determine the velocity history of the major outlet glaciers of Devon Ice Cap. Speckle tracking of the RADAR scenes allows ice motion to be determined over the entire ice cap, but only provides a "winter" snapshot of velocities, as the method only works well when there is little change in the glacier surface properties between image acquisitions (e.g. minimal melt). Feature tracking of optical imagery provides a better record of "annual" ice displacements as summer images are typically used, and includes enhanced flow associated with events such as the seasonal input of supraglacial meltwater to the glacier bed. However, feature tracking is restricted to regions where there are distinctive surface features to track (e.g., crevasses), thus restricting the results to the faster flowing regions of outlet glaciers.

5.3.1 Feature Tracking of Landsat-7 Imagery

An automated, variable block size correlation algorithm (developed within MATLAB^{TM}) was implemented in the frequency domain to derive glacier surface displacements from Landsat-7 ETM+ imagery. This method is similar to that of Haug et al. [2010] in that it applies a cross-correlation algorithm to accurately co-registered intensity gradient images. However, after matching has been completed using the initial correlation block window size and motion vectors have been determined, a nearest neighbor filter is applied to the velocity field to automatically identify mismatches. For each identified mismatch, the algorithm automatically increases the block size and the cross-correlation algorithm is re-run. This process continues until the algorithm either no longer identifies mismatches or a maximum, user-defined block window size is used. This approach is computationally efficient for determining motion on glaciers with large

spatial gradients in surface motion (e.g. glaciers with flow speeds ranging from 10s to 100s of m a^{-1}) and/or for glaciers that exhibit large temporal variations in motion (e.g. surge-type glaciers).

5.3.2 Speckle Tracking of RADARSAT-2 Imagery

We apply a custom-written MATLAB^{TM} speckle tracking script to RADARSAT-2 imagery to determine the velocity structure of Devon Ice Cap, as has been applied in previous studies of glacier motion in the Canadian Arctic (Short and Gray [2004; 2005], Van Wychen et al. [2012; 2014; *in press*]). For the method to perform well, the surface ice structure must remain relatively undisturbed between image acquisitions (e.g. little snowfall, rainfall or melt). As a consequence, we utilize imagery acquired in the winter to early spring (December to ~ late-April), when these changes are minimal. Our method of deriving displacements uses a normalized cross-correlation algorithm to determine the relative motion between two accurately co-registered pairs of RADARSAT-2 images. Displacements are determined in both the azimuth and range directions of the image, using chip sizes of ~400 m in range and azimuth. The 1:250 000 Canadian Digital Elevation Dataset (CDED) with 100 m grid spacing is used to remove the topographic component of the slant range displacement and allow the conversion from the slant range to ground range displacement. We assume that ice motion is parallel to the surface. Displacements are calibrated using areas of known velocity (e.g. bedrock outcrops) and final velocities are standardized to annual values.

5.3.3 Removal of Erroneous Displacements and Creation of Velocity Rasters

Although the feature tracking and speckle tracking methods provide good results over most areas of interest, mismatches or blunders still occur. Mismatches arise when the cross-correlation algorithms find a stronger correlation with an incorrect image chip than with the true image chip. As a consequence, velocity results were imported in to ESRI ArcGIS 10.1 for manual verification and filtering. To identify erroneous points, the following criteria were used (following Van Wychen et al [2012; 2014]): 1) motion should be faster along the glacier centerline than at the margins due to lateral friction; 2) flow vectors should be oriented parallel to surface flow features (e.g. lateral moraines) and topography (e.g. valley walls) and; 3) motion should be consistent in both magnitude and orientation over short distances. Any displacements that did not conform to these criteria were removed from the dataset and all velocity points were manually inspected. An inverse distance weighting (IDW) interpolation method (which provides

a conservative approach to interpolation as the interpolated values cannot exceed those determined by the cross-correlation technique) was used to create a continuous raster surface from the filtered displacements. Feature tracking displacements were posted to a 50 m grid spacing, while speckle-tracking displacements were posted to a 100 m grid spacing.

5.3.4 Ice Displacement Error Analysis

For feature tracking, the maximum error during the co-registration of image pairs was 0.75 of a pixel (11.25 m for Landsat-7 ETM+ imagery) in both the x- and y-directions of the image. Error also arises due to the way in which the cross-correlation algorithm selects the sub-pixel location of the maximum correlation peak, which is a maximum of 0.50 of a pixel (7.5 m for Landsat-7 ETM+ imagery). Together, these errors combine to provide an overall error of ± 19 m. This level of error is consistent with the uncertainty bounds for feature tracking of Landsat-7 ETM+ imagery provided by other studies (e.g. Haug et al. [2010]; Waechter et al. [2015]).

To assess the error associated with our speckle tracking datasets we extracted velocities from areas where horizontal velocity is near zero (e.g. bedrock outcrops and ice divides) and computed the root sum of squares from all separate sources of error in all years. This provides an uncertainty of ±5.97 m a^{-1} for the speckle tracking dataset, which is similar to the error quoted by previous studies using the same methodology (e.g. Van Wychen et al. [2012]; [2014]; Waechter et al. [2015])

5.3.5 Glacier Bed Profiles

Bed elevation profiles for Fitzroy, East-5, East-6, East-7, Sverdrup and Eastern glaciers were obtained from airborne RADAR (100 MHz) measurements collected over Devon Ice Cap in 2000 [Dowdeswell et al. 2004]. These elevation profiles were collected approximately along the centrelines of the major outlet glaciers of the ice cap and have an error of ~±10 m (details on error analysis and data processing are available in Dowdeswell et al. [2004]). For Belcher, North Croker Bay, South Croker Bay, Southeast-1 and Southeast-2 Glaciers we used the updated 2012 Operation IceBridge dataset to derive the glacier bed elevation profiles, which also have an uncertainty of ~±10 m [Gogineni, 2012].

5.3.6 Flow Regime Mapping

Burgess et al. [2005] used the relationship between the driving stress (τ_d) and the ratio of the surface velocity to the ice thickness (v/h) to classify the motion of Devon Ice Cap into four distinct "flow regimes". When ice flow occurs due to ice deformation alone, (v/h) represents the mean shear strain rate through the ice column, but when basal motion contributes to ice flow the ratio of (τ_d) to (v/h) provides a measure of the effective viscosity of the glacier system (with units of Pascal seconds) [Burgess et al. 2005]. A full review of the classification and interpretation of these flow regimes is available in Burgess et al. [2005], but briefly:

- Flow regime 1 (FR1: $v/h < 0.075$ a^{-1}, high positive correlation with τ_d) represents ice that is frozen to its bed and motion is solely by internal deformation;
- Flow regime 2 (FR2: $v/h > 0.075$ a^{-1} and < 0.28 a^{-1})) represents regions where the basal ice temperature is at or approaching the pressure melting point and basal motion (or enhanced deformation of basal ice) begins to contribute to overall motion;
- Flow regime 3 (FR3: $v/h > 0.28$ a^{-1}, $\tau_d > 0.075$ MPa) is characterized by a further reduction in the viscosity of the ice and a greater contribution of basal motion to overall surface velocity;
- Flow regime 4 (FR4; $v/h > 0.28$ a^{-1}, $\tau_d < 0.075$ MPa) represents areas of low basal friction, which indicates high basal motion and may suggest that deformation of subglacial sediments is playing a role in overall ice motion.

Here we update and expand the flow regime mapping for Devon Ice Cap using data from 2015, with τ_d derived from:

$$\tau_d = \rho_i g h \sin \alpha \quad (1)$$

where ρ_i is the density of ice (910 kg m^{-3}) and g is the acceleration due to gravity (9.81 m s^{-2}). The influence of local variations in surface topography was removed by averaging the surface slope of over distances of ~10 times the ice thickness. We mapped flow regimes for all years with velocity data that cover the entire surface of Devon Ice Cap (2009, 2011-2015). A final flow regime map (Figure 5-6) was created by mosaicking all individual rasters together and selecting the majority class (mode) value for all overlapping points. A low pass (3 x 3) filter was used to smooth the data and eliminate small features which are likely related to artifacts in the input datasets.

5.3.7 Calculation of Dynamic Discharge

To calculate the dynamic discharge from the ice cap, we combined our surface ice velocities (derived both from feature tracking of Landsat-7 ETM+ imagery and speckle tracking of RADARSAT-2 data) with measured and interpolated ice thicknesses to determine the mass passing through defined flux gates at the fronts of the tidewater terminating glaciers of Devon Ice Cap. These flux gates are located within ~1-5 km of the calving front and are fixed in time and space (locations of flux gates are denoted on Figure 5-1). These estimates of dynamic discharge do not account for mass changes due to terminus advance or retreat.

For 10 of the 11 major outlet glaciers of Devon Ice Cap, ice thickness measurements were acquired perpendicular to ice flow as part of NASA's Operation IceBridge airborne campaign in spring 2012. These measurements were collected using the Multichannel Coherent RADAR Depth Sounder (MCoRDS). Here we use the MCoRDS post-processed L2 dataset, which includes measurements of time, latitude, longitude, elevation, glacier surface elevation, glacier bed elevation and ice thickness [Gogineni 2012]. All data were downloaded from the National Snow and Ice Data Center (https://nsidc.org/data/icebridge/). The ice thickness measurements have an uncertainty of ~±10 m [Gogineni 2012] and are used to create flux gates where the entire cross sectional morphology of the glacier is known.

To create a flux gate for East-5 glacier (the only glacier lacking flow-perpendicular ice thickness measurements from the IceBridge campaign), we extracted ice thicknesses every 20 m across a profile located ~1 km from the calving front that was derived from an interpolated raster of ice thicknesses measured on Devon Ice Cap in 2000 [Dowdeswell et al. 2004]. Uncertainty in this dataset is ~±10 m, although the ~9-15 year gap between the acquisition of this dataset and the imagery used in this study means that those measurements likely overestimate current ice thicknesses (ICESat altimetry measurements indicate surface thinning of ~2.47 m a^{-1} between 2004 and 2009 on East-5 Glacier [Gardner et al. 2011]).

To calculate maximum and minimum estimates of the mass passing through each segment of a flux gate, we use the following equations:

$$Q_{min} = (0.8 * (V - V_{error})) * (H - H_{error}) * (W) \quad (2)$$

$$Q_{max} = (V + V_{error}) * (H + H_{error}) * (W) \quad (3)$$

Where, for each segment width (W, ~20 m), V is the velocity extracted from the surface ice motion datasets, V_{error} is the error associated with the velocity mapping, H is ice thickness, and H_{error} is the ice thickness error (~±10 m). For Q_{min}, we use 80% of the surface velocity to characterize the depth-averaged velocity [Paterson 1994], while for Q_{max} we assume that all motion occurs due to basal sliding and that the depth-averaged velocity is equivalent to the surface motion. To derive minimum and maximum estimates of the ice flux from each glacier, Q_{min} and Q_{max} are summed (separately) across the entire width of the flux gate. The dynamic discharges reported here are the averages of the estimates of the total Q_{min} and Q_{max}; the values of Q_{min} and Q_{max} then provide the lower and upper uncertainty bounds.

5.4 Results

5.4.1 Ice Dynamics

Glacier velocities on Devon Ice Cap are typically low (Figure 5-1), with the interior regions of the ice cap moving at <20 m a^{-1}, suggestive of ice frozen to its bed. Surface velocities >20 m a^{-1} occur on outlet glaciers, with the highest velocities on tidewater glaciers. The ice motion described here conforms to previous measurements derived for the ice cap (e.g. Van Wychen et al. [2012; 2014]; Burgess et al. [2005]; Shepherd et al. [2007]), with topography providing the dominant control on overall ice dynamics. Higher flow rates occur mainly in the eastern sector of the ice cap, where accumulation rates are higher (Koerner, 1979) and motion is dominated by flow through confined bedrock valleys. Slower sheet flow dominates the flat, plateau-like topography of the western sector [Dowdeswell et al. 2004]. The highest ice velocities observed (~300 m a^{-1}) occur at the termini of Belcher and Fitzroy glaciers, while velocities of ~60-150 m a^{-1} are typically found at the fronts of all other tidewater outlet glaciers.

5.4.2 Areas of Dynamic Change

In assessing temporal variations in ice motion, it is important to distinguish between variations due to differences in measurement period and variations due to changes in ice dynamics. In particular, it is likely that our velocities derived from feature tracking of annually-separated optical images include some enhanced motion in the summer [Wyatt and Sharp 2015; Danielson

and Sharp 2013; Cress and Wyness 1961], which does not contribute to velocities derived from speckle tracking of winter RADARSAT-2 imagery. To quantify this effect, we compare 495,363 points located on six major outlet glaciers (Belcher, Sverdrup, North Croker Bay, South Croker Bay, Southeast-1 and Southeast-2) for which surface displacements were derived using both methods. We find that velocities derived from speckle-tracking were, on average, ~11% lower than those derived using feature tracking. This difference increases in a downglacier direction, as the average difference in velocity across the flux gate locations on the six largest tidewater-terminating glaciers (Belcher, Sverdrup, North Croker, South Croker, Easter and Fitzroy; Figure 5-1) was ~19% (Figure 5-2).

In order to integrate the two datasets to produce a time series of glacier velocity change for the entire period of study, we only consider velocity changes between years to be significant if they are greater than the combined ~11-19% seasonal variability and error associated with each method. When assessing the significance of velocity changes detected by comparison of velocity fields derived using the same method, only the error associated with that method needs to be taken into account. Note that the resulting estimates of annual mass loss via dynamic discharge should be considered conservative because they do not take into account the effects of changes in glacier terminus position.

5.4.2.1 Variability in Annual Motion 1999-2010

Surface velocity fields of 8 major outlet glaciers were derived by feature tracking applied to Landsat-7 ETM+ image pairs acquired annually between 1999-2010 (Figures 5-3, 5-4). Results indicate that Belcher Glacier (Figure 5-3a, i) and Fitzroy Glacier (Figure 5-3b, j) have similar velocity characteristics, with velocities beginning to rise ~5-7 km from their fronts and attaining maximum values of ~260-300 m a^{-1} at their termini. Neither glacier displays any velocity variability in excess of the error margins for feature tracking during the period 1999-2010. Maximum velocities of both Southeast-1 and Southeast-2 glaciers occurred in the upper regions of the main trunks of both glaciers (~25-45 km from their shared terminus) in 1999-2000, with velocities in these regions beginning to decrease after 2000-2001. Velocities in the shared terminus region of the two glaciers were close to zero over the 1999-2010 period (Figure 5-3c, d, k, l).

Longitudinal velocity profiles of North Croker Bay Glacier (Figure 5-4c, k) varied considerably. The lowest velocities (~50-100 m a^{-1}) were measured in 2002-2003 in the lower 15 km of the glacier, but increased abruptly to 100-140 m a^{-1} in 2003-2004 and reached maximum values of 150-200 m a^{-1} in 2005-2006. Velocities in this region then decreased in each subsequent year to 2009-2010. The greatest velocity variation occurred in the lower 5 km section of the glacier, where velocities increased from ~50 m a^{-1} in 2001-2002 to ~180-200 m a^{-1} by 2005-2006 (Figure 5-4c). The nearby South Croker Bay Glacier displayed much less inter-annual variability (Figure 5-4d), with peak velocities along the lowermost ~20 km section of the glacier ranging between ~120-180 m a^{-1} in nearly all years from 1999-2010. Anomalously high velocities of ~240 m a^{-1} occurred in the lowermost terminus region in 2005-2006. However, the temporal pattern of velocity fluctuations over the observation period was broadly similar between the two glaciers, with lower velocities in 2001-2002 and 2002-2003, maximum velocities in 2005-2006, and deceleration of the glacier in later years of observation.

5.4.2.2 Variability in Winter Motion 2009-2015

Speckle tracking of RADARSAT-2 imagery generated surface velocity fields for nearly all the major outlet glaciers of Devon Ice Cap for the winters of 2009 to 2015 (Figures 5-3e-h, 5-4e-h, 5-5a-c). From 2009 to 2014 the speckle tracking-derived velocity structure of Belcher Glacier (Figure 5-3e, i) was similar to the pattern derived from the feature tracking results (Figure 5-3a), with velocities increasing in the lower ~10 km of the glacier and reaching maximum values of ~250-300 m a^{-1} in the lowermost terminus region. The inter-annual velocity variability in this period was generally within error margins, but motion in winter 2015 was distinctly faster than observed in all other years by either speckle tracking or feature tracking, particularly in the lowermost 3 km of the glacier (Figure 5-3i).

The speckle tracking velocity structure of Fitzroy Glacier (Figure 5-3f) is also very similar to that described from the feature tracking results (Figure 5-3b). The 2015 velocities are significantly lower than those determined for all other years, especially in the section of the glacier located between ~2 and 5 km from the calving front (Figure 5-3n). The magnitude of this slowdown is greater than the ~10-20% variability associated with seasonality, and builds on a multi-year slowdown over the speckle tracking measurement period. Speckle tracking derived velocity fields of Southeast-1 (Figure 5-3g) and Southeast-2 glaciers (Figure 5-3f) reveal

continued deceleration of the upper sections of both glaciers (~25-45 km from the terminus). However, velocities have increased to >100 m a^{-1} in the lowermost ~2-5 km of both glaciers (roughly doubling between 2009 and 2015, and significantly higher than the values determined for that region between 1999 and 2010).

Velocities of Sverdrup Glacier (Figure 5-4e) were generally low (20-40 m a^{-1}) along its entire ~25 km length from 2009 to 2015, with variability largely within error limits (Figure 5-4m). Eastern Glacier (Figure 5-4j) has surface velocities of ~40-60 m a^{-1} along most of its ~30 km length, but these increase to ~100 m a^{-1} near the calving front. The glacier slowed slightly in the section ~3-10 km from the calving front from 2009 to 2015 but appeared to increase in the downstream section 1-3 km from the terminus over the same period. Speckle tracking velocities reveal that North Croker Bay Glacier decelerated (by ~50-70 m a^{-1}) between 2010 and 2011 (Figure 5-4o), with low values persisting along its entire length from 2011 to 2015 (Figure 5-4g, k), similar to the situation during the period of slow flow from 2001-2004. South Croker Bay Glacier's velocity field (Figure 5-4h) was generally similar to that determined by feature tracking, with the notable exception of winters 2011-2013, when velocities along the section 1-15 km from the terminus were ~50% lower than in all other years.

East-5 Glacier (Figure 5-5a, d) had surface velocities of ~100-175 m a^{-1} in its lowermost 10 km in 2009. These decreased to ~50 m a^{-1} in winter 2011 and approached zero from 2013-2015. East-6 Glacier (Figure 5-5b, e) has a similar velocity structure to Sverdrup Glacier, in that velocities were typically low (~10-35 m a^{-1}) along the entire lower section of the glacier. This glacier slowed by ~20 m a^{-1} between 2010 and 2011 (Figure 5-5b, e), and velocities in 2015 were the lowest in the entire observation period. Finally, velocities of East-7 Glacier (Figure 5-5c, f) peaked in winter 2009 over the entire lower ~15 km of the glacier and thereafter decreased significantly (beyond error limits) in each subsequent year until winter 2015, when the lowest recorded velocities were observed along the entire length of the glacier.

5.4.3 Bed Morphology and Areas of Dynamic Variability

It is notable that areas of the greatest velocity variability typically occur in areas where the bed elevation descends below sea level (Figure 5-3q-t, 5-4q-t, 5-5i-k). This relationship is clearest for Belcher Glacier (Figure 5-3a, e, i, m), North Croker Bay Glacier (Figure 5-4c, g, k, o), East-5

Glacier (Figure 5-5a, d, g) and East-7 Glacier (Figure 5-5c, f, i). Upglacier of the location where the bed descends below sea level, ice velocities typically display much less variability between years. These findings suggest that the bed morphology, and possibly a transition from bedrock to marine sediments at the glacier bed (Dowdeswell et al. [2004]), play significant roles in regulating on the flow of Devon Ice Cap. On Belcher Glacier, for example, the region where velocity increased from 2009-2015 was grounded below sea level, while the region of velocity decrease was located where the bed rises above sea level. The point at which the bed descends below sea level thus seems to divide the glacier into regions with different dynamic behaviours.

Bed elevation profiles also suggest that bedrock bumps located upglacier of the point where the bed descends below sea level may influence the surface motion of some outlet glaciers of Devon Ice Cap. Such bedrock bumps are apparent in the bed profiles of both Fitzroy (Figure 5-3n) and East-7 (Figure 5-5i) glaciers in locations where they slowed down most dramatically between 2009-2015 (Figure 5-3f, Figure 5-5c). The flow of East-7 Glacier over the bedrock bump is consistently slower than in regions located both upglacier and downglacier from it (Figure 5-5f).

5.4.4 Updated Flow Regime Mapping

Our flow regime mapping (Figure 5-6) indicates that FR1 is the most extensive flow region on Devon Ice cap, and that it covers most of its upper interior plateau regions. FR2 is found primarily along the upper portions of the main trunks of outlet glaciers, while FR3 occurs in the lower sections of some, but not all, major outlet glaciers (Belcher, Fitzroy, South Croker Bay, East-7) and in a small area located ~30 km from the terminus of Southeast-2 Glacier. FR4 is found in the lowermost terminus regions of Belcher, South Croker, Fitzroy, East-7 and Southeast-2 glaciers. There are some differences between the flow regime map produced in this study and the previous map of Burgess et al. [2005]. Areas of difference include the two major tributary arms of Belcher Glacier (which change from FR3 to FR2), the Cunningham Glaciers (which change from FR3/4 to FR2), the main trunk of the North Croker Bay Glacier (which changed from FR3/4 to FR2) and the shared terminus region of the Southeast-1 and Southeast-2 Glaciers (which changed from FR1 to FR2).

5.5 Discussion

5.5.1 Spatial and Temporal Evolution of the Flow of Devon Ice Cap

Chapter 4 characterized the observed variability in the dynamics of the ice masses of Axel Heiberg and Ellesmere Islands as either "surging", "pulsing" or "consistent acceleration". In order for the variability to be attributed to "surging", the glacier had to undergo multi-year periods of velocity variability, with evidence that fast flow initiated in upper regions and propagated downglacier over time, and that velocity variability occurred over the entire length of the glacier (though not necessarily simultaneously). For multi-year periods of velocity variability to be characterized as "pulsing", there had to be evidence that the variability in ice motion was initiated at, or near, the calving front, that it was restricted largely to areas of the glacier that are grounded below sea level, and that it did not propagate upglacier beyond the point where the bed rises above sea level. Several "pulse-type" glaciers also had prominent bedrock bumps or sills located near their termini, and the greatest variability in ice motion occurred downglacier of these points. For a glacier to be identified as undergoing "consistent acceleration" there had to be evidence of a nearly continuous increase in glacier velocities over the observation period, accompanied by significant terminus thinning and retreat. Here, we use the classification scheme of Chapter 4 to characterize the spatio-temporal evolution of the flow of Devon Ice Cap.

5.5.1.1 Velocity Variability Attributed to Surging

We attribute the velocity variability of Southeast-1, Southeast-2, Eastern, East-5, East-7, and Cunningham West Glaciers to surging. The velocity variability of the Southeast-1 and Southeast-2 glaciers has previously been attributed to surging [Burgess and Sharp 2008; Van Wychen et al. 2012] and the results derived here support this interpretation. Faster ice motion began in the upper regions of both glaciers and spread downglacier over the observation period, which is consistent with classic surge theory [Sharp 1988] and the classification scheme of Chapter 4. Thickening of the shared terminus region of the Southeast-1 and Southeast-2 Glaciers has been reported in previous studies [Burgess and Sharp; Gardner et al. 2011] and has been attributed to faster moving ice from the upper regions of the Southeast basin running into slower moving ice located in the lower sections of the glaciers. The longer-term velocity record presented here (Figure 5-3k, l) provides further support for this interpretation. The propagation of a surge front also explains why the flow regime in the shared terminus section of the southeast basin has

changed from FR1 to FR2 (Figure 5-6). As the surge travelled through the glacier as a kinematic wave, it activated faster velocities in the form of basal motion in the lowermost terminus region.

The pattern of velocity change along Eastern Glacier from 2009-2015 (Figure 5-4f) is similar (albeit less dramatic) to that described for the Southeast Glaciers, with velocities decreasing in the upper regions of the main glacier trunk and increasing in the lowermost terminus region. This suggests that a surge may also have propagated along the length of Eastern Glacier throughout the period of observation.

Van Wychen et al. [2012] reported that the surface velocities of East-5 Glacier were significantly higher in 2009 than in the mid-1990s, indicating that the glacier had accelerated at some point between the mid-1990s and 2009. The velocity record presented here (Figure 5-5a, d) indicates that the glacier has undergone a multi-annual slowdown since 2009 and that, by 2015, it had become nearly stagnant along most of its length (returning to velocities similar to those in the mid-1990s). Unfortunately, we are unable to definitively confirm whether East-5 Glacier is surge-type as we do not have velocity measurements from the period between the mid-1990s and 2009 that would enable determination of whether higher rates of flow initiated in the upper region of the glacier and spread downglacier over time. However, the fact that the glacier has slowed to stagnation in recent years, together with the lack of a prominent sill in its lowermost regions (common for pulse-type glaciers), suggests that the velocity variability is more likely due to surging than pulsing. We also attribute the velocity variability of East-7 Glacier to surging because its pattern of dynamic change is similar to that reported for East-5 Glacier, although it has not yet reached stagnation (Figure 5-5c, f).

Copland et al. [2003] inferred that the Cunningham Glaciers were possibly surge-type, based on their extensive folding of surface moraines between 1959 and 1999 and the ~2 km retreat of the eastern margin of the western-most glacier. The surface velocities presented here, when compared with those reported by Burgess et al. [2005] (20-60 m a^{-1} in the mid-1990s) and Van Wychen et al [2012] (nearly stagnant in 2009), indicate that these glaciers decelerated by ~20-30 m a^{-1} between 1999 and 2009-2015. This suggests that these glaciers were surging in the mid-1990s but are quiescent at present. The flow regime mapping indicates that these glaciers have transitioned from FR3/4 to FR2, which is consistent with the termination of a surge.

5.5.1.2 Velocity Variability Attributed to Pulsing

We attribute the velocity variability of Fitzroy Glacier (which had not previously been identified as a region of dynamic change) to "pulsing". The repeated velocity mapping indicates that the largest variation in ice motion occurs downglacier of a prominent sill in the bed profile (located ~1.5 km from the 2014 calving front), and that in 2015 the greatest slowdown (compared to all other years of observation) occurs at the sill location. These findings indicate that the sill plays an important role in regulating the flow of the glacier, which is a characteristic shared with other glaciers on Axel Heiberg and Ellesmere Islands that have been identified as pulse-type glaciers [Chapter 4; Van Wychen et al. *submitted*]. Velocities determined for regions upglacier from the point where the bed descends below sea level are largely constant over time (except where prominent basal topographic features are large enough to influence ice motion, e.g. Fitzroy and East-7 Glaciers), consistent with the classification criteria for pulse-type glaciers proposed in Chapter 4). The ~15 year velocity record presented here also provides no indication that velocity variability of Fitzroy Glacier began in the upper reaches of the glacier and propagated towards the terminus, as would be expected on a surge-type glacier.

5.5.1.3 Other Forms of Velocity Variability

The velocity variability observed on the Belcher, North Croker Bay and South Croker Bay Glaciers appears to differ from that associated with surging and pulsing. Other mechanisms are therefore needed to explain their dynamics.

After a period of limited velocity variability from 1999-2009, Belcher Glacier has undergone a multi-annual acceleration over its lower ~15 km, reaching a peak in 2015, and a multi-annual deceleration in the region 20-40 km upglacier from the terminus. These variations suggest that the glacier is currently undergoing a change in its dynamics. The highest level of velocity variability on Belcher Glacier occurs downglacier of a sill located below sea level ~2-3 km from the calving front, which is a common characteristic of "pulse-type" glaciers (Chapter 4; Van Wychen et al. [*submitted*]). However, it is also evident that velocities at this sill location never approached stagnation during the ~15 year observation period (as has been observed on other glaciers identified as "pulse-type", e.g. Fitzroy Glacier (section 5.1.2); Parrish and Dobbin Glaciers (Chapter 4; Van Wychen et al. [*submitted*]). The progressive speed-up of Belcher

Glacier between 2009 and 2015 (Figure 5-3e) is more reminiscent of the "consistent acceleration" observed on the Trinity and Wykeham Glaciers of Prince of Wales Icefield, which was likely driven by terminus thinning that facilitated faster ice flow [Chapter 4; Van Wychen et al. *submitted*].

This study classified the northern arm of the Belcher Glacier as FR2 while Burgess et al. [2005] classified it as FR3, which might suggest a change in dynamics in this area. However, this study does classify some portions of the northern arm of Belcher Glacier as FR3 in some years. The discrepancy in derived flow regimes between the results presented here and Burgess et al. [2005] likely does not represent a real change in dynamics but rather that the flow regime at this location is sensitive to small changes in inputs (e.g., due to uncertainty in input data) as it lies at the threshold between FR2 and FR3 flow regimes.

The surface velocity fields of the North Croker Bay and South Croker Bay Glaciers defy easy classification as "surge-type" or "pulse-type". Both glaciers have undergone multi-year periods of slowdown and speedup associated with "pulse" and "surge" mechanisms, but the ~15 year velocity record presented here indicates that at no time did either of these glaciers slow to complete stagnation (which would indicate a surge-type glacier slowing into a quiescent phase). Additionally, the surface velocities of both glaciers oscillated between periods of faster and slower flow over unequal temporal intervals (e.g. 3 years of relatively slow flow, followed by 9 years of faster flow, followed by 5 years of slow flow for North Croker Bay Glacier (Figure 5-4k)). These patterns of velocity variation are inconsistent with the pattern observed on surge-type glaciers within the CAA, which typically undergo relatively long periods of slow (quiescent) flow (e.g. 30-40 years) and shorter periods of faster (surge) flow (e.g. 5-7 years) [Chapter 4; Van Wychen et al. *submitted*]; Copland et al. 2003]. For these reasons, the North Croker Bay and South Croker Bay glaciers do not fit the classification of a "surge-type" glacier. However, we are also unable to classify these glaciers as "pulse-type" as: (i) velocity variability appears to occur simultaneously over the entire main trunk of both glaciers; (ii) it does not appear to originate at or near the calving front; and (iii) the velocity slowdown occurs upglacier of the point where the bed rises above sea level.

Thus, some other mechanism appears to be causing the variability in motion of the Croker Bay glaciers, however more in situ data (e.g. ocean and air temperatures) are required to determine whether or not a regional control is regulating their flow. Whatever mechanism is driving their velocity variability, it has been enough to cause the main trunk of the North Croker Bay Glacier to transition from FR3/4 to FR2 in recent years, a change which suggests that the main trunk of the glacier has become more viscous over that time period.

5.5.3 Dynamic Discharge

Given the large degree of variability in ice motion discussed above, it is informative to determine how dynamic discharge has changed over time. Table 5-3 presents the dynamic discharge calculated for 1999-2010 using feature tracking of Landsat-7 ETM+ imagery, while Table 5-4 presents the dynamic discharge for 2009-2015 derived from speckle tracking of RADARSAT-2 data. The dynamic discharge of Devon Ice Cap is dominated by the flux from a few key glaciers, with Belcher, Fitzroy, Southeast-1 and Southeast-2 glaciers accounting for ~66% of the total dynamic discharge over the observation period. Belcher Glacier is the single largest contributor, accounting for between ~22% of the total dynamic discharge in winter 2009 and ~42% in winter 2015, or an average of ~32% over the study period. Conversely, multi-year slow-downs of Eastern, North Croker Bay, East-5 and East-7 glaciers have resulted in decreased dynamic discharge (beyond error margins) from these glaciers in recent years. The decrease in dynamic discharge from East-5 and North Croker Bay glaciers has been the most significant, with each glacier accounting for ~12% of total dynamic discharge in winter 2009, but only ~2% in winter 2015.

For Devon Ice Cap as a whole, the average dynamic discharge over the period for which speckle tracking data are available (2009, 2011-2015) was ~0.37 ± 0.15 Gt a^{-1} (Table 5-4) which is within the error margins of previous estimates of dynamic discharge from the ice cap [Burgess et al. 2005; Van Wychen et al. 2012; 2014]. It is notable that the total dynamic discharge from the ice cap was relatively constant between years, despite the large variability in the motion of individual glaciers. This suggests that as some glaciers diminish in their importance, others increase to replace them, which seems to be a common characteristic of ice caps in the Canadian High Arctic [Chapter 4; Van Wychen et al. 2014; *submitted*].

5.6 Conclusions

Feature tracking using Landsat-7 ETM+ imagery and speckle tracking using RADARSAT-2 imagery were used to generate the longest record of velocity variations on Devon Ice Cap to date. The results provide insight into the timescales of variability in glacier dynamics in the Canadian Arctic. The dynamics of Devon Ice Cap are more variable than previously recognized, with significant variations in the motion of the North Croker Bay, South Croker Bay, East-6 and East-7 glaciers that were not revealed by earlier studies (e.g. Van Wychen et al. [2012]). Velocity mapping indicates that significant dynamic changes can occur on both relatively short (e.g. 1-3 years: North Croker Bay Glacier) and long (e.g. 10-15 years: Southeast-1, Southeast-2 glaciers) timescales on Devon Ice Cap. These likely reflect changes driven by different dynamic processes. In addition we update and expand the mapping of ice cap flow regimes originally identified by Burgess et al. [2005], and find that basal sliding has become a component of the motion of the shared terminus region of the Southeast-1 and Southeast-2 Glaciers, while the trunk of the North Croker Bay Glacier appears to have become more resistant to basal flow over time.

From application of the "surge" and "pulse" classification scheme proposed in Chapter 4 [Van Wychen et al. *submitted*], "surging" is able to explain the velocity variability of Southeast-1, Southeast-2, East-5, East-7 and Eastern Glaciers, while "pulsing" can explain the velocity variability of Fitzroy Glacier. However, the velocity variability observed on the Belcher, North Croker Bay and South Croker Bay glaciers does not fit well within this classification scheme and suggests that mechanisms distinct from "surging" and "pulsing" control the dynamics of these glaciers. The recent speedup of Belcher Glacier is reminiscent of the consistent acceleration reported for Trinity and Wykeham Glaciers on Ellesmere Island, but more study is required to determine whether the recent speedup will be a prolonged event. The synchronous velocity responses of the North Croker Bay and South Croker Bay glaciers suggest that a common external forcing mechanism (e.g. oceanic or atmospheric) may be influencing their flow, but more in situ data are needed to identify what this forcing may be.

Average dynamic discharge from Devon ice cap over the period 2009 and 2011-2015 was ~0.37 ± 0.15 Gt a^{-1}, with approximately two thirds of all discharge coming from 4 glaciers (Belcher, Fitzroy, Southeast-1 and Southeast-2). These findings are consistent with previous studies (e.g.

Burgess et al. [2005]; Van Wychen et al. [2012; 2012]), and do not suggest any long-term change in mean discharge from the ice cap since the mid-1990s.

Acknowledgements

We acknowledge NSERC (Discovery Grants and Northern Research Supplements to LC and MS), the Canada Foundation for Innovation, Ontario Research Fund, Alberta Innovates Technology Futures, ArcticNet, Transport Canada, Ontario Graduate Scholarship and the Polar Continental Shelf Project (Natural Resources Canada) for support of this work. DB is supported by the Climate Change Geosciences Program, Earth Sciences Sector, Natural Resources Canada. RADARSAT imagery was made available from the Alaska Satellite Facility, the archives of Natural Resources Canada, and the RADARSAT-2 Natural Resources Canada data allocation. We thank NASA's Operation IceBridge (especially John Sonntag) for supporting the collection of ice thickness datasets for Devon Ice Cap.

5.7 References:

Burgess D.O. and M. J. Sharp, (2004), Recent changes in areal extent of the Devon ice cap, Nunavut, Canada. *Arctic, Antarctic and Alpine Research*, 36(2): 261–271

Burgess, D. O., M. Sharp, D.W.F. Mair, J.A. Dowdeswell, and T.J. Benham, (2005), Flow dynamics and iceberg calving rates of Devon Ice Cap, Nunavut, Canada. *Journal of Glaciology. Glaciol*, 51, 173, 219-230.

Burgess D. O. and M. Sharp, (2008), Recent changes in thickness of the Devon Island ice cap, Canada. *Journal of Geophysical Research*., 113(B7), B07204. doi: 10.1029/2007JB005238

Cress, P. and R., Wyness, (1961), The Devon Island expedition, observations of glacial movements. *Arctic*, 14(4), 257–259.

Copland, L., M. Sharp, and J. Dowdeswell, (2003), The distribution and flow characteristics of surge-type glaciers in the Canadian High Arctic. *Annals of Glaciology.* 36, 73-81.

Clason, C., D.W.F. Mair, D.O., Burgess, & P.W. Nienow, (2012), 'Modelling the delivery of supraglacial meltwater to the ice/bed interface: application to southwest Devon Ice Cap, Nunavut, Canada'. *Journal of Glaciology, 58(208):* 361-374. doi: 10.3189/2012JoG11j129

Danielson, B., and M. Sharp, (2013), Development and application of a time-lapse photograph analysis method to investigate the link between tidewater glacier flow variations and supraglacial drainage events. *Journal of Glaciology*, 59: 287-302.

Dowdeswell, J.A., T.J., Benham, M.R., Gorman, D., Burgess, and M. Sharp, (2004), Form and flow of the Devon Island ice cap, Canadian Arctic. *Journal of Geophysical Research,* 109(F2), F02002 doi: 10.1029/2003JF000095

Haug, T., A. Kääb, and P. Skvarca, (2010), Monitoring ice shelf velocities from repeat MODIS and Landsat data – a method study on the Larsen C ice shelf, Antarctic Peninsula, and 10 other ice shelves around Antarctica. *The Cryosphere*, 4: 161-178.

Koerner, R.M., (2005), Mass balance of glaciers in the Queen Elizabeth Islands, Nunavut, Canada. *Annals of Glaciology*, 42: 417–423 doi: 10.3189/172756405781813122

Gardner, A.S. and M. Sharp, (2007), Influence of the Arctic circumpolar vortex on the mass balance of Canadian high Arctic Glaciers. *Journal of Climate*, 20: 4586-4598.

Gardner, A. S., M. Moholdt, B. Wouters, G.J. Wolken, D.O. Burgess, M. Sharp, J.G. Cogley, C. Braun and C. Labine, (2011), Sharply increased mass loss from glaciers and ice caps in the Canadian Arctic Archipelago. *Nature.* 473(7347): 357–360. doi: 10.1038/nature10089.

Gardner, A., G. Moholdt, A. Arendt, and B. Wouters, (2012), Accelerated contributions of Canada's Baffin and Bylot Island glaciers to sea level rise over the past half century. *The Cryosphere*. 6: 1103-1125.

Gogineni, P., (2012), Radar Depth Sounder Data Products, Lawrence, Kansas, USA. Digital media. http://data.cresis.ku.edu/

Lenaerts, J. T. M., J. H. van Angelen, J.H., M. R. van den Broeke, ,A.S. Gardner, B. Wouters, and E. van Meijgaard, (2013), Irreversible mass loss of Canadian Arctic Archipelago glaciers. *Geophysical Research Letters*, 40. doi:10.1002/grl.50214

Sharp, M., D.O. Burgess, J.G. Cogley, M. Ecclestone, C. Labine, and G. Wolken, (2011), Extreme melt on Canada's Arctic ice caps in the 21st century. *Geophysical Research Letters*, 38(L11501). doi: 10.1029/ 2011GL047381

Sharp, M., (1988), Surging glaciers: behavior and mechanisms. *Progress in Physical Geography*, 12: 349-370.

Sharp, M., D. O. Burgess, F. Cawkwell, L. Copland, J.A. Davis, E.K. Dowdeswell, J.A. Dowdeswell, A. Gardner, D. Mair, L. Wang, S. Williamson, G.J. Wolken, and F. Wyatt, (2014), Remote sensing of recent glacier changes in the Canadian Arctic**.** In: Kargel, J.S., Leonard, G.J., Bishop, M.P., Kääb, A. and Raup, B.H. (eds). *Global Land Ice Measurements from Space*, Ch. 9, pp. 205-228. Praxis-Springer. doi: 10.1007/978-3-540-79818-7_9.

Shepherd, A., Z. Du, T.J. Benham, J.A. Dowdeswell, and E.M. Morris, (2007), Mass balance of Devon Ice Cap, Canadian Arctic. *Annals of Glaciology*, 46: 249–254. doi:10.3189/172756407782871279

Short, N. H. and A. L. Gray, (2004), Potential for RADARSAT-2 interferometry: glacier monitoring using speckle tracking. *Canadian Journal of Remote Sensing.* 30(3): 504-509.

Short, N. H. and A.L. Gray, (2005), Glacier dynamics in the Canadian High Arctic from RADARSAT-1 speckle tracking. *Canandian Journal of Remote Sensing*. 31(3): 225–239.

Waechter, A., L. Copland, and E. Herdes, (2015), Modern glacier velocities across the Icefield Ranges, St. Elias Mountains, and variability at selected glaciers from 1959 to 2012. Journal of Glaciology, 61(228), doi: 10.3189/2015JoG14J147

Van Wychen, W., L. Copland, L. Gray, D. O. Burgess, B. Danielson, M. Sharp, (2012), Spatial and temporal variation of ice motion and ice flux from Devon Ice Cap, Nunavut, Canada. *Journal of Glaciology*, 58(210): 657–664. doi: 10.3189/2012JoG11J164.

Van Wychen, W., D. O. Burgess, L. Gray, L. Copland, M. Sharp, J. A. Dowdeswell, and T. J. Benham, (2014), Glacier velocities and dynamic ice discharge from the Queen Elizabeth Islands, Nunavut, Canada. *Geophysical Research Letters*, 41.

doi:10.1002/2013GL058558.

Van Wychen, W., L. Copland, D. Burgess, L. Gray, L. and N. Schaffer, [*In press*]. Glacier velocities and dynamic discharge from the ice masses of Baffin and Bylot Islands, Nunavut, Canada. *Canadian Journal of Earth Sciences.* doi: 10.1139/cjes-2015-0087

Van Wychen, W., J. Davis, D.O. Burgess, L. Copland, L. Gray, M. Sharp, C. Mortimer, (*submitted Aug 26, 2015*) Characterizing inter-annual variability of glacier dynamics (1999-2015) and dynamic discharg*e* (2000, 2011-2015) for the ice masses of Ellesmere and Axel Heiberg Islands, Nunavut, Canada. *Journal of Geophysical Research - Earth Surface*, (manuscript number: 2015JF003708).

Williamson, S., M. Sharp, J. Dowdeswell, and T. Benham, (2008), Iceberg calving rates from northern Ellesmere Island ice caps, Canadian Arctic, 1999-2003. *Journal of Glaciology*, 54(186): 391-400. doi: 10.3189/002214308785837048.

Wyatt, F. and M. Sharp, (2015), Linking surface hydrology to flow regimes and patterns of velocity variability of the Devon Ice Cap, Nunavut, *Journal of Glaciology*, 61: 387-399.

Table 5-1: Summary of Landsat-7 image pairs used to derive velocity maps via the feature tracking method. BL = Belcher Glacier, SV = Sverdrup Glacier, ES = Eastern Glacier, FZ = Fitzroy Glacier, NC = North Croker Bay Glacier, SC = South Croker Bay Glacier, SE1 = Southeast 1 Glacier, SE2 = Southeast 2 Glacier; Glacier locations are denoted on Figure 5-1.

Image Date 1	Path	Row	Image Date 2	Path	Row	Glaciers
13/07/1999	38	6	24/07/2000	37	6	BL, SV, ES, FZ
06/07/1999	37	7	24/07/2000	37	7	NC, SC
05/10/1999	34	7	03/09/2000	36	7	SE1, SE2
25/08/2000	37	6	28/08/2001	37	6	BL, SV, ES, FZ
24/07/2000	37	7	20/07/2001	37	6	NC, SC
03/09/2000	36	7	21/08/2001	36	6	SE1, SE2
28/08/2001	37	6	07/09/2002	38	6	BL, SV, ES, FZ
28/08/2001	37	7	31/08/2002	37	7	NC, SC
21/08/2001	36	7	09/09/2002	36	7	SE1, SE2
07/09/2002	38	6	25/08/2003	38	6	BL, SV, ES, FZ
31/08/2002	37	7	19/09/2003	37	7	NC, SC
09/09/2002	36	7	20/08/2003	35	7	SE1, SE2
25/08/2003	38	6	12/09/2004	38	6	BL, SV, ES, FZ
25/08/2003	38	7	10/07/2004	38	7	NC, SC
25/08/2003	38	6	12/09/2004	38	6	SE1, SE2
12/09/2004	38	6	14/08/2005	38	6	BL, SV, ES, FZ
01/06/2004	37	7	06/06/2005	35	7	NC, SC
31/08/2004	34	7	09/08/2005	35	7	SE1, SE2
14/08/2005	38	6	26/08/2006	37	6	BL, SV, ES, FZ
31/07/2005	36	7	09/07/2006	37	7	NC, SC
09/08/2005	35	7	06/09/2006	35	7	SE1, SE2
26/08/2006	37	6	29/08/2007	37	6	BL, SV, ES, FZ
09/07/2006	37	7	05/07/2007	36	7	NC, SC
06/09/2006	34	7	31/08/2007	35	7	SE1, SE2
29/08/2007	37	6	31/08/2008	37	6	BL, SV, ES, FZ
14/09/2007	37	7	24/08/2008	36	7	NC, SC
31/08/2007	35	7	26/08/2008	34	7	SE1, SE2
31/08/2008	37	6	25/08/2009	38	6	BL, SV, ES, FZ
24/08/2008	36	7	02/08/2009	37	7	NC, SC
26/08/2008	34	7	27/08/2009	36	7	SE1, SE2
25/08/2009	38	6	06/09/2010	37	6	BL, SV, ES, FZ
02/08/2009	37	7	30/08/2010	37	7	NC, SC
27/08/2009	36	7	30/08/2010	36	7	SE1, SE2

Table 5-2: Summary of Radarsat-2 image pairs used to derive velocity maps of Devon Ice Cap via the speckle tracking method. BL = Belcher Glacier, SV = Sverdrup Glacier, ES = Eastern Glacier, FZ = Fitzroy Glacier, NC = North Croker Bay Glacier, SC = South Croker Bay Glacier, SE1 = Southeast 1 Glacier, SE2 = Southeast 2 Glacier, SE3 = Southeast 3 Glacier, E5 = East 5 Glacier, E6 = East 6 Glacier, E7 = East 7 Glacier; Glacier locations are denoted on Figure 5-1.

RADARSAT-2 Speckle Tracking Imagery				
Image Date 1	Image Date 2	Beam Mode	Segments	Glaciers
01/03/2009	25/03/2009	Fine (9m)	3	SV, NC, SC
02/03/2009	26/03/2009	Fine (9m)	3	BL
05/03/2009	29/03/2009	Fine (9m)	3	FZ, E5, E6, E7, SE1, SE2, SE3
07/02/2010	03/03/2010	Ultrafine (3m)	1	BL
17/02/2010	13/03/2010	Ultrafine (3m)	1	SE1, SE2, E7
20/02/2010	16/03/2010	Ultrafine (3m)	1	SV
21/02/2010	17/03/2010	Ultrafine (3m)	1	NC, SC
16/02/2011	12/03/2011	Fine (9m)	2	FZ, E5, E6, E7, SE1, SE2
11/03/2011	04/04/2001	Fine (9m)	3	BL, ES
03/04/2001	27/04/2011	Fine (9m)	3	NC, SC, SV
07/02/2012	02/03/2012	Wide Ultrafine (3m)	1	SV
09/04/2012	03/05/2012	Wide Fine (9m)	1	BL, NC, SC, SE1, SE2, SE3, E5, E6, E7, FZ
31/12/2012	24/01/2013	Wide Fine (9m)	1	SV
05/01/2013	29/01/2013	Wide Fine (9m)	1	BL, NC, SC, SE1, SE2, SE3, E5, E6, E7, FZ
02/12/2014	26/12/2012	Wide Fine (9m)	1	SV
07/12/2014	31/12/2014	Wide Fine (9m)	1	BL, NC, SC, SE1, SE2, SE3, E5, E6, E7, FZ
26/12/2015	01/01/2015	Wide Fine (9m)	1	SV
07/02/2015	03/03/2015	Wide Fine (9m)	1	BL, NC, SC, SE1, SE2, SE3, E5, E6, E7, FZ

Table 5-3: Dynamic discharge for major glaciers of Devon Ice Cap calculated from surface velocities derived from Landsat 7 ETM+ imagery (1999-2010). Flux gate locations are denoted on Figure 5-1. Note: flux could only be calculated from the Southern Arms (SA) of Belcher and Fitzroy Glaciers. Uncertainty (±) value for each estimate is presented as superscript. Overall mean discharge for Devon Ice Cap is not presented due to missing data from prominent glaciers over this time period.

Glacier	Dynamic discharge (Gt a^{-1})												
	1999 2000	2000 2001	2001 2002	2002 2003	2003 2004	2004 2005	2005 2006	2006 2007	2007 2008	2008 2009	2009 2010	Mean	SD
Belcher (SA)	$0.08^{.02}$	$0.09^{.02}$	$0.09^{.02}$	$0.10^{.02}$	$0.09^{.02}$	$0.11^{.02}$	$0.09^{.02}$	$0.11^{.02}$	$0.10^{.02}$	$0.10^{.02}$	$0.10^{.02}$	$0.10^{.02}$	0.01
Sverdrup	$0.01^{.01}$	$0.01^{.01}$	$0.01^{.01}$	$0.01^{.01}$	$0.03^{.01}$	$0.02^{.01}$	$0.01^{.01}$	$0.01^{.01}$	$0.01^{.01}$	$0.01^{.01}$	$0.00^{.01}$	$0.01^{.01}$	0.01
N. Croker Bay	$0.04^{.01}$	$0.04^{.01}$	$0.03^{.01}$	$0.02^{.01}$	$0.03^{.01}$	$0.05^{.02}$	$0.06^{.02}$	$0.08^{.02}$	$0.06^{.02}$	$0.06^{.02}$	$0.06^{.02}$	$0.05^{.02}$	0.02
S. Croker Bay	$0.04^{.01}$	$0.04^{.01}$	$0.03^{.01}$	$0.04^{.01}$	$0.04^{.01}$	$0.04^{.01}$	$0.05^{.01}$	$0.05^{.01}$	$0.04^{.01}$	$0.04^{.01}$	$0.04^{.01}$	$0.04^{.01}$	0.01
Eastern	$0.03^{.01}$	$0.02^{.01}$	$0.02^{.01}$	$0.03^{.01}$	$0.02^{.01}$	$0.03^{.01}$	$0.03^{.01}$	$0.02.^{01}$	$0.02^{.01}$	$0.03^{.01}$	$0.02^{.01}$	$0.03^{.01}$	0.01
Fitzroy (SA)	$0.07^{.02}$	$0.08^{.02}$	$0.07^{.02}$	$0.07^{.02}$	$0.08^{.02}$	$0.09^{.02}$	$0.11^{.02}$	$0.08^{.02}$	$0.08^{.02}$	$0.11^{.02}$	$0.08^{.02}$	$0.08^{.02}$	0.01

Table 5-4: Dynamic discharge for Devon Ice Cap calculated from Radarsat-2 derived surface ice velocities. Location of flux gates are denoted on Figure 5-1. Flux from Belcher and Fitzroy glaciers are calculated separately for the Northern Arm (NA) and Southern Arm (SA) of each glacier. Uncertainty (±) value for each estimate is presented as superscript.

Glacier	Dynamic discharge (Gt a^{-1})								
	2009	2010	2011	2012	2013	2014	2015	Mean	SD
Belcher (NA)	$0.01^{.01}$	$0.01^{.01}$	$0.01^{.01}$	$0.01^{.01}$	$0.00^{.01}$	$0.00^{.01}$	$0.00^{.01}$	$0.01^{.01}$	0.01
Belcher (SA)	$0.09^{.02}$	$0.10^{.02}$	$0.09^{.02}$	$0.10^{.02}$	$0.12^{.02}$	$0.11^{.02}$	$0.14^{.03}$	$0.10^{.02}$	0.02
Sverdrup	$0.01^{.00}$	$0.01^{.01}$	$0.01^{.01}$	$0.01^{.01}$	$0.01^{.01}$	$0.01^{.01}$	$0.00^{.01}$	$0.01^{.01}$	0.00
N. Croker Bay	$0.05^{.01}$	$0.05^{.01}$	$0.02^{.01}$	$0.01^{.01}$	$0.01^{.01}$	$0.01^{.01}$	$0.01^{.01}$	$0.03^{.01}$	0.02
S. Croker Bay	$0.06^{.01}$	$0.05^{.01}$	$0.04^{.01}$	$0.04^{.01}$	$0.05^{.01}$	$0.06^{.01}$	$0.06^{.01}$	$0.05^{.01}$	0.01
Eastern	$0.02^{.01}$		$0.02^{.01}$	$0.02^{.01}$	$0.01^{.01}$	$0.02^{.01}$	$0.01^{.01}$	$0.02^{.01}$	0.01
Fitzroy (NA)	$0.00^{.01}$		$0.01^{.01}$	$0.00^{.01}$	$0.00^{.01}$	$0.00^{.01}$	$0.00^{.01}$	$0.00^{.01}$	0.00
Fitzroy (SA)	$0.07^{.01}$		$0.08^{.02}$	$0.07^{.01}$	$0.07^{.01}$	$0.07^{.01}$	$0.07^{.01}$	$0.07^{.01}$	0.00
East 5	$0.03^{.01}$		$0.02^{.01}$		$0.00^{.01}$	$0.00^{.01}$	$0.00^{.01}$	$0.01^{.01}$	0.01
East 6	$0.00^{.01}$		$0.00^{.01}$	$0.00^{.01}$	$0.00^{.01}$	$0.00^{.01}$	$0.00^{.01}$	$0.00^{.01}$	0.00
East 7	$0.04^{.01}$	$0.03^{.01}$	$0.03^{.01}$	$0.02^{.01}$	$0.03^{.02}$	$0.02^{.01}$	$0.02^{.01}$	$0.03^{.01}$	0.01
Southeast 1/2	$0.03^{.02}$	$0.03^{.02}$	$0.04^{.03}$	$0.04^{.02}$	$0.03^{.02}$	$0.05^{.02}$	$0.05^{.02}$	$0.04^{.02}$	0.01
Southeast 3	$0.01^{.01}$		$0.01^{.01}$	$0.02^{.01}$	$0.01^{.01}$	$0.01^{.01}$	$0.01^{.01}$	$0.01^{.01}$	0.00
Devon Ice Cap	$\mathbf{0.42^{.14}}$		$\mathbf{0.38^{.17}}$	$\mathbf{0.34^{.14}}$	$\mathbf{0.34^{.16}}$	$\mathbf{0.36^{.15}}$	$\mathbf{0.38^{.16}}$	$\mathbf{0.37^{.15}}$	**0.03**

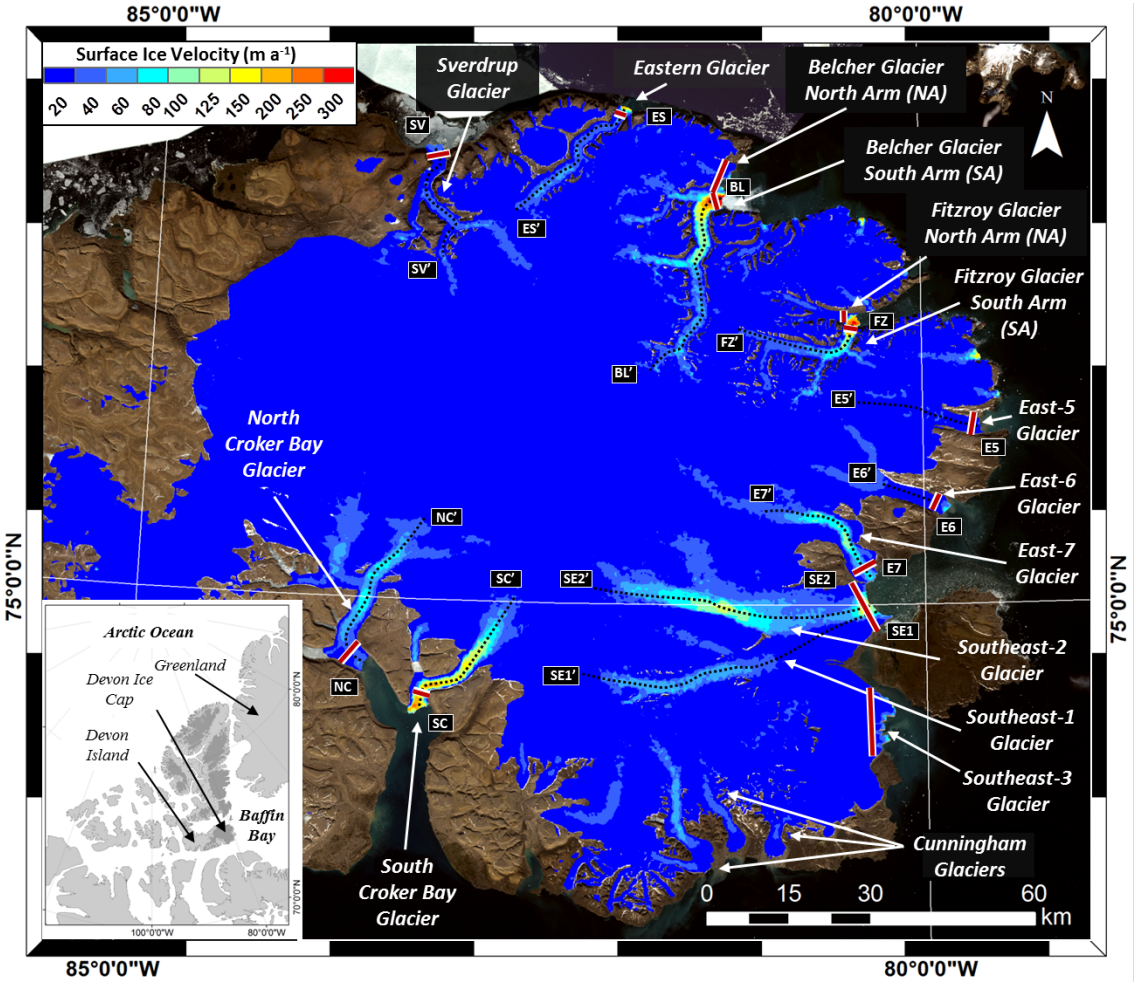

Figure 5-1: Devon Ice Cap velocity structure derived from speckle tracking of Radarsat-2 Wide Fine imagery acquired in winter 2015. Red on white lines indicate locations of flux gates used to determine dynamic discharge estimates in Figure 5-2; black dashed lines indicate locations of centerline velocities shown in Figures 5-3, 5-4 and 5-5; Dark grey areas on inset map indicate glaciated terrain in the Canadian High Arctic.

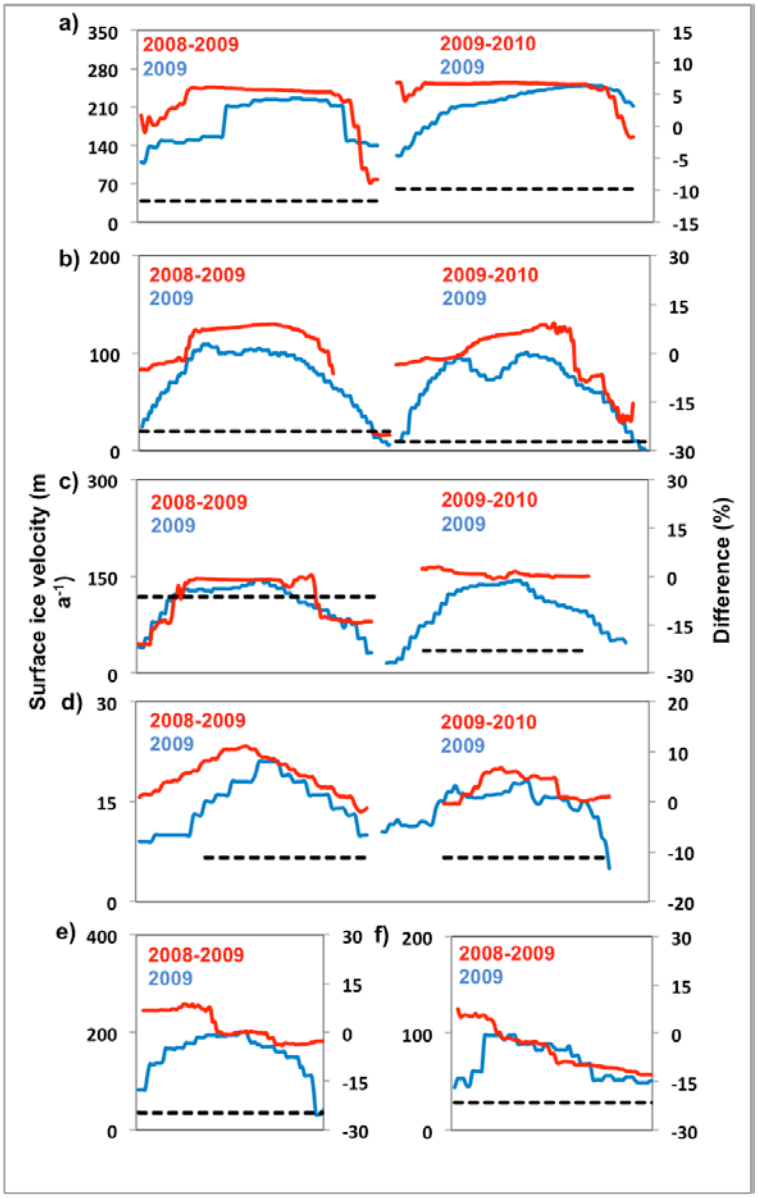

Figure 5-2: Comparison of near terminus velocities at flux gates (see Figure 5-1 for location) derived from feature tracking (red line) and speckle tracking (blue line) for: a) Belcher Glacier, b) North Croker Bay Glacier, c) South Croker Bay Glacier, d) Sverdrup Glacier, e) Fitzroy Glacier, f) Eastern Glacier. Dashed lines indicate mean percent difference between feature tracking and speckle tracking velocities across each terminus flux gate.

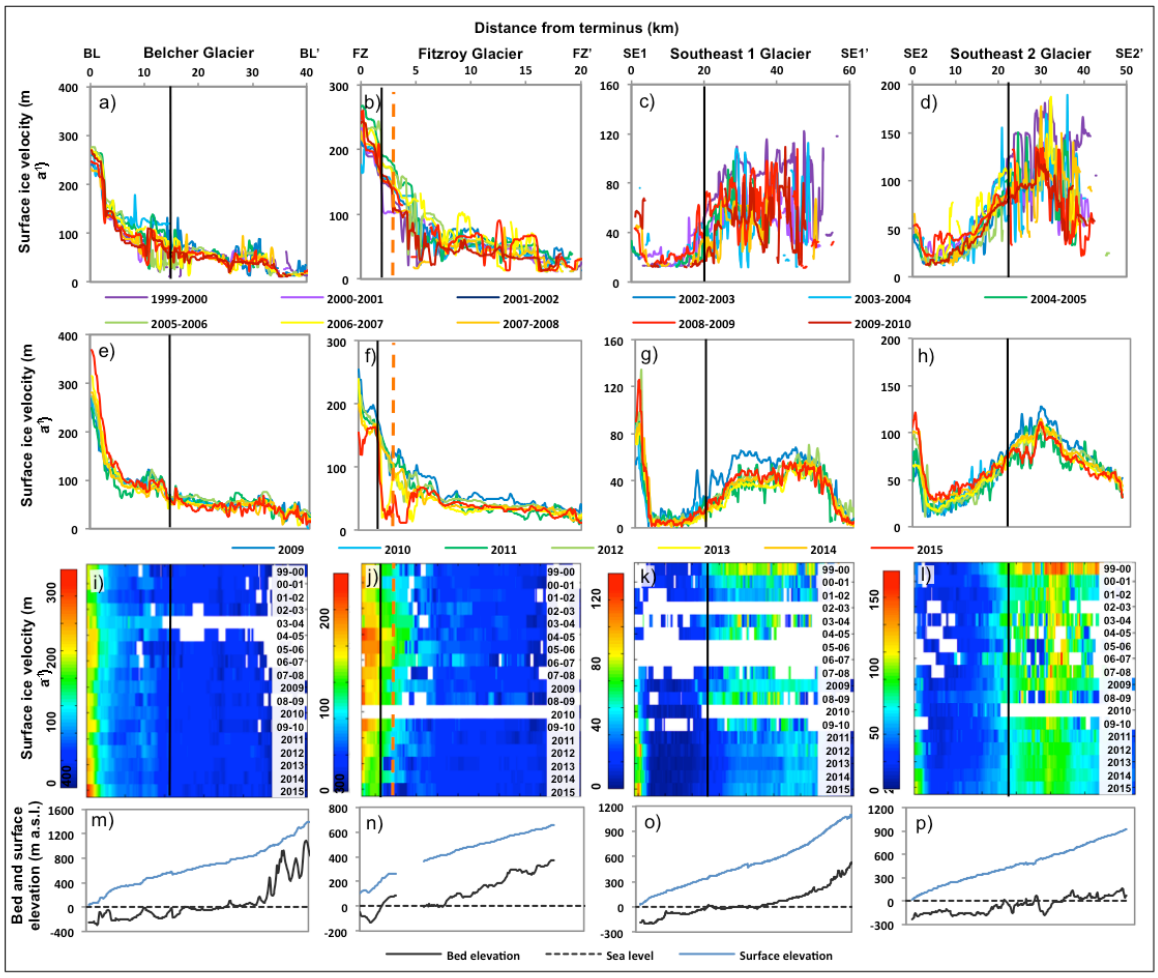

Figure 5-3: For the centrelines of Belcher (location denoted as BL-BL' on Figure 5-1), Fitzroy (location denoted as FZ-FZ' on Figure 5-1), Southeast-1 (location denoted as SE1-SE1' on Figure 5-1) and Southeast-2 (location denoted as SE2-SE2' on Figure 5-1) glaciers, respectively: (a-d) Surface velocities from 1999-2010 derived from feature tracking; (e-h) Surface velocities from 2009-2015 derived from speckle tracking; (i-l) Surface velocities from 1999-2015 derived from both feature tracking and speckle tracking; (m-p) Bed and surface elevation profiles. Solid black lines denote the location where the glacier bed descends below sea level, red dashed lines indicate basal topographic features that influence ice motion for glaciers described in text.

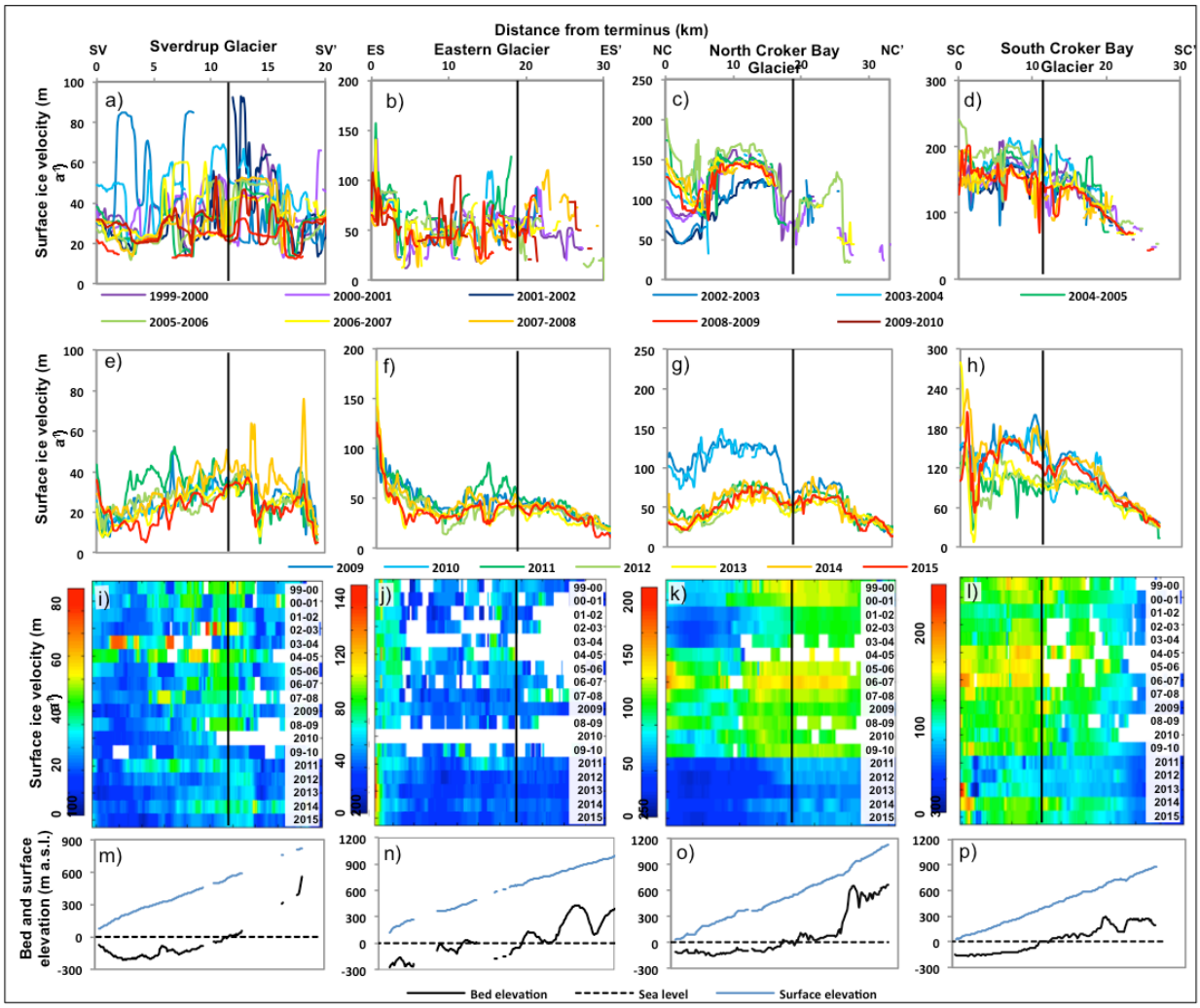

Figure 5-4: For the centrelines of Sverdrup (location denoted as SV-SV' on Figure 5-1), Eastern (location denoted as ES-ES' on Figure 5-1), North Croker Bay (location denoted as NCB-NCB' on Figure 5-1) and South Croker Bay (location denoted as SCB-SCB' on Figure 5-1) glaciers, respectively: (a-d) Surface velocities from 1999-2010 derived from feature tracking; (e-h) Surface velocities from 2009-2015 derived from speckle tracking; (i-l) Surface velocities from 1999-2015 derived from both feature tracking and speckle tracking; (m-p) Bed and surface elevation profiles. Solid black lines indication where the glacier bed descends below sea level.

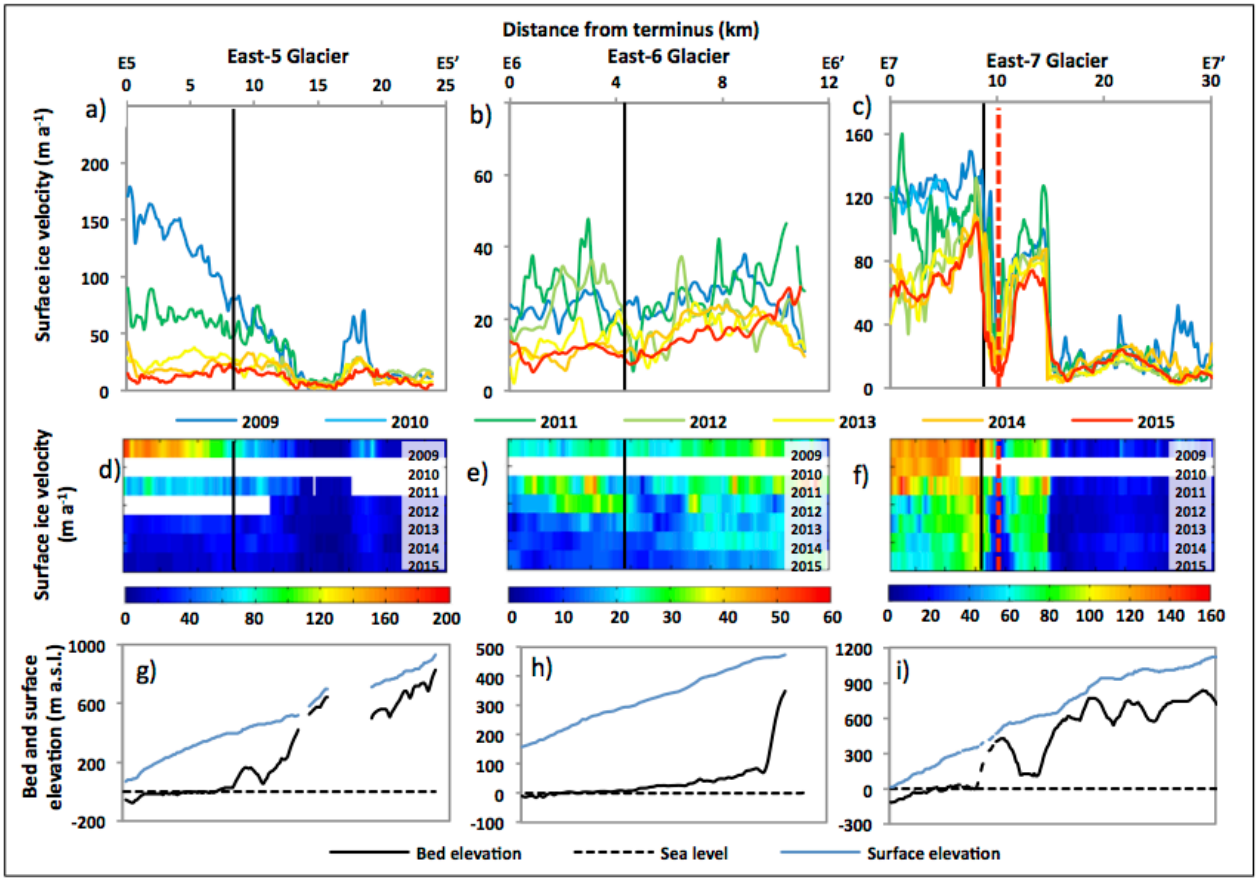

Figure 5-5: For the centrelines of East-5 (location denoted as E5-E5' on Figure 5-1), East-6 (location denoted as E6-E6' on Figure 5-1) and East-7 (location denoted as E7-E7' on Figure 5-1) glaciers, respectively: (a-c) Surface velocities from 2009-2015 derived from speckle tracking; (d-f) Surface velocities from 1999-2015 derived from both feature tracking and speckle tracking; (g-i) Bed and surface elevation profiles. Solid black lines indicate the location where the glacier bed descends below sea level, red dashed lines indicate basal topographic features that influence ice motion for glaciers described in text.

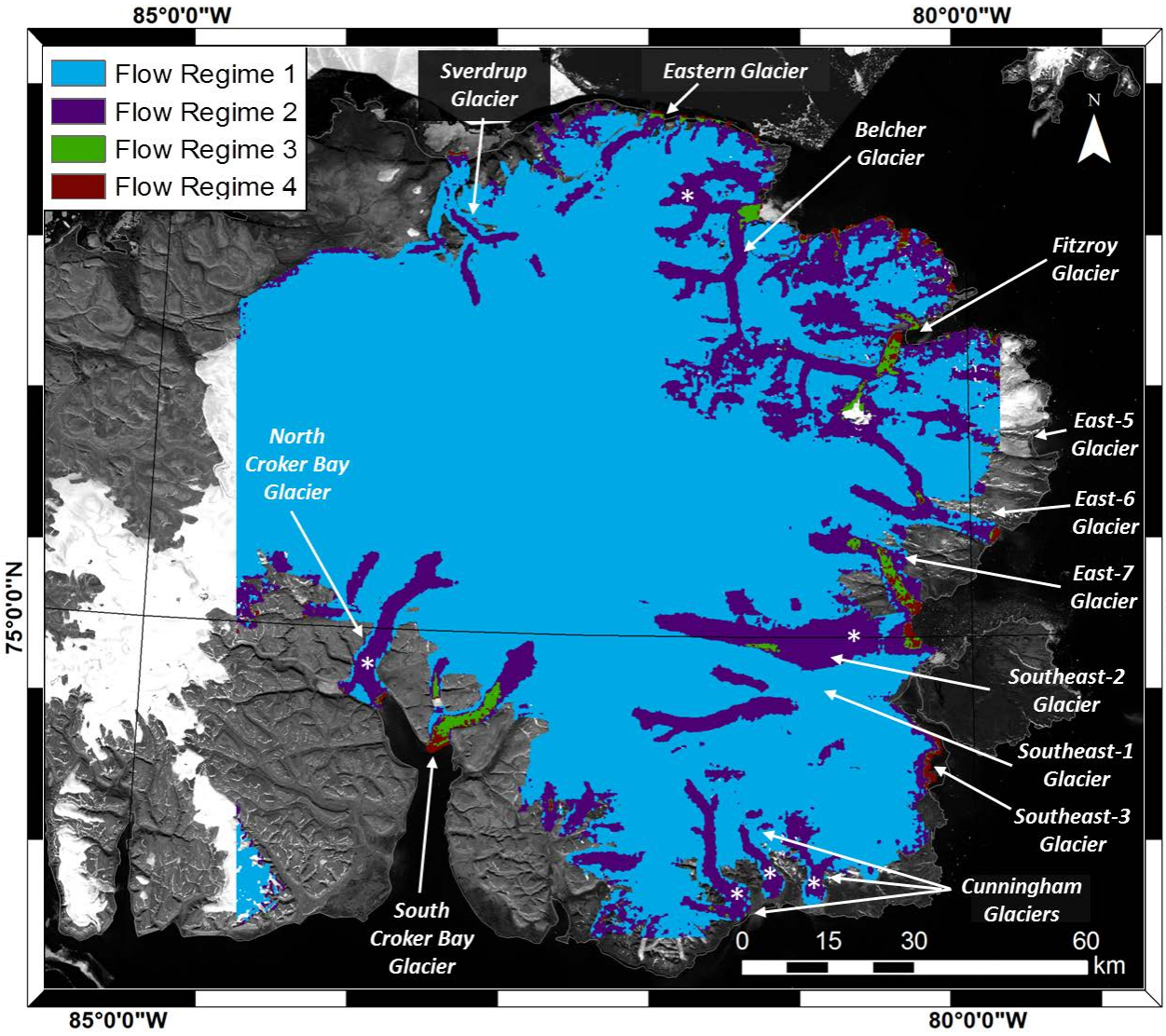

Figure 5-6: Flow regime map of Devon Ice Cap, "*" indicates areas classified as flow regimes different from those derived by Burgess et al. [2005].

CHAPTER SIX: Conclusions

6.1 Summary and Conclusions

Speckle tracking of synthetic aperture RADAR (SAR) satellite data (RADARSAT-1, RADARSAT-2, ALOS PALSAR) and feature tracking of Landsat 7 ETM+ imagery has been used to determine the most comprehensive record of glacier dynamics in the Canadian Arctic to date. Within the region ice surface motion is typically low, with interior regions flowing at rates of ~< 10 m a^{-1}, indicative of motion by internal deformation alone. Motion is faster (typically ~30-200 m a^{-1}) on tidewater outlet glaciers where basal sliding likely dominates. The Trinity and Wykeham Glacier complex of Prince of Wales Icefield is currently the fastest moving ice mass, with maximum surface velocities of up to ~1200 m a^{-1} in recent years. Generally, ice motion is slower for the ice masses located in the southern Canadian Arctic (Baffin and Bylot Islands) than in the northern Canadian Arctic (Queen Elizabeth Islands (QEI): Devon, Ellesmere and Axel Heiberg Islands).

The long term record of surface velocities provided here reveals a large degree of spatial and temporal variability in ice motion in the Canadian Arctic over the last ~15 years, with the majority of the large tidewater glaciers of the QEI undergoing multi-year (3-7 year) slowdowns. The most dramatic example of this was observed on the Mittie Glacier of Manson Icefield, which had surface velocities of ~1200-1400 m a^{-1} along its entire length in 2000, but was stagnant (<20 m a^{-1}) by 2007-2008. The record of surface velocities also reveals that a lesser number of glaciers in the QEI have undergone a speed-up followed by a slow down over the ~15 year observation period. By characterizing these spatial and temporal variations in ice motion, most of the observed velocity variability can be attributed to “surge” and “pulse” mechanisms. To distinguish between these mechanisms, glaciers are classified as being “surge-type” when there is evidence that nearly their entire length is influenced by faster motion, and that these higher velocities originate in the upper regions of a glacier and propagate downglacier. In contrast, glaciers are classified as “pulse-type” when the observed variations in motion initiate in, and are restricted to, the lowermost terminus region that is grounded below sea level. For “pulse-type” glaciers there is also evidence that sills located in this region grounded below sea level regulate ice motion, with the greatest amount of dynamic variability occurring downglacier of these

features. The distinction between “surge-type” and “pulse-type” glaciers indicates that there are differing processes that cause variability in glacier dynamics within the Canadian Arctic. This thesis represents the first time that “pulse-type” glaciers have been identified for the Canadian Arctic, and is also the first time that “pulse” behaviour has been distinguished from glacier surging.

The Trinity and Wykeham Glaciers are the only glaciers in the Canadian Arctic that underwent constant acceleration throughout the 1999-2015 period. The speed-up of these glaciers has occurred coincident with widespread thinning (~2-5 m a^{-1}) of their main glacier trunks between 2008-2014. The observed pattern of surface velocity increase, combined with prolonged retreat of their shared terminus, is analogous to the rapid terminus retreat and acceleration of Helheim Glacier (Greenland) from 2002 to 2005 [Howat et al. 2007] and Columbia Glacier (Alaska) which initiated in 1982 and continues to present [Pfeffer 2007; McNabb et al. 2015]; these changes were driven by terminus thinning due to atmospheric and oceanic warming which reduced effective pressure at the glacier bed and facilitated faster ice motion. Consequently, the Trinity and Wykeham Glaciers are identified in this study as having undergone “consistent acceleration” given that thinning appears to have resulted in floatation of the terminus and associated faster ice motion and terminus break up. The bed morphology of these two glaciers may make them prone to continued acceleration and retreat before re-stabilization can occur, as their beds remain below sea level for ~45 km upglacier from their 2014 calving front.

At the termini of tidewater glaciers, surface velocities were combined with measured and modelled ice thicknesses in order to calculate mass loss via dynamic (iceberg) discharge. The dynamic discharge for the ice masses of Baffin and Bylot Islands lies between ~17 and ~108 Mt a^{-1}, with a midpoint estimate of ~55 Mt a^{-1} (revising previous estimates downward by ~50%; Gardner et al. [2012]). In comparison, mean dynamic discharge from the QEI between 2011-2015 was ~2.47 ± 0.88 Gt a^{-1}. A comparison of iceberg discharge with rates of mass loss via climatic mass balance (surface melt and runoff) indicates that dynamic discharge accounts for ~3.1% of total ablation for the Northern Canadian Arctic Archipelago and ~0.11% of total ablation for the Southern Canadian Arctic Archipelago. This reveals that mass loss in the Canadian Arctic is currently dominated by surface melt and runoff. The data presented here

indicates that only a few glaciers are responsible for the majority of mass loss via iceberg discharge, with 8 glaciers accounting for ~75% of total dynamic discharge, and the Trinity and Wykeham Glaciers alone accounting for ~50% of dynamic discharge (and up to ~62% in recent years). The majority of glaciers in the Canadian Arctic that have experienced velocity variability over the observation period have slowed in recent years and their resultant iceberg discharge has diminished. The reduction in dynamic discharge from these glaciers has been offset by the speed-up and resultant increase in dynamic discharge from the Trinity and Wykeham Glaciers. This highlights that total dynamic discharge from the Canadian Arctic can be sensitive to the variations in dynamics of just a few glaciers.

6.2 Key Contributions

This thesis has provided several key contributions, which together represent a significant advance in knowledge in the field of Canadian glaciology. First, the surface velocity maps created by this research provide a regionally comprehensive record of ice velocities for the entire glaciated region of the Canadian Arctic for the first time. Rates and patterns of surface motion reported by this thesis are largely in agreement with the findings of previous local studies (e.g. Burgess et al. [2005]; Shepherd et al. [2007]; Short and Gray [2004], [2005]; Williamson et al. [2008]; Van Wychen et al. [2012]). However, this study builds upon the earlier research by providing a much more expansive record (both spatial and temporal) of glacier dynamics within the region. For example, this thesis provides a record of surface ice motion for many locations where previously no record existed (i.e., Sydkap, Penny, Barnes and Bylot Island Ice Caps; interior regions of Prince of Wales and Manson Icefields; interior regions of Agassiz, Müller, Steacie and Northern Ellesmere Ice Caps). Additionally, this research provides a much longer and more continuous record of ice motion for ice masses where previous measurements did exist (i.e., Devon Ice Cap)2.54

Second, this thesis, for the first time, quantified regional rates of mass loss via dynamic discharge for the entire Canadian Arctic. Previous estimates of dynamic discharge have been sparse and have largely detailed iceberg discharge from a few (~8-10) large tidewater outlet glaciers located on Ellesmere and Axel Heiberg Islands (e.g. Short and Gray [2005]; Williamson et al. [2008]) or at most, from a single ice mass (e.g. Devon Ice Cap: Burgess et al. [2005];

Shepherd et al. [2007]; Van Wychen et al. [2012]). As a consequence, a regional estimate of mass loss via dynamic discharge for the CAA (e.g., Gardner et al. [2011]) could only be determined by using previously published estimates of mass flux per terminus width from a few select tidewater glaciers, then multiplying this value by the width of all tidewater glaciers terminating within the region. There are major drawbacks to using this approach, such as the fact that it does not account for temporal variability in ice motion that has been demonstrated in this study, and that it assumes that mass flux from a few large tidewater glaciers is representative of all glaciers within the region. This research has quantified dynamic discharge for all tidewater glaciers within the Canadian Arctic using measured glacier velocities, thus reducing the uncertainty surrounding total mass balance within the Canadian Arctic (e.g. Gardner et al. [2011]; Lenaerts et al. [2012]). The ice masses of the Canadian High Arctic account for ~7% of reported Arctic dynamic discharge outside of Greenland.

Third, the long-term record of surface velocities compiled by this study provides more insight into the spatial and temporal evolution of glacier motion within the Canadian Arctic. Copland et al. [2003b] used optical imagery to identify surface features indicative of variations in glacier flow speeds (e.g. terminus advance, looped moraines, fresh and extensive crevassing) to create the first catalogue of "surge-type" glaciers for the Canadian Arctic. By utilizing the long-term record of ice motion complied by this thesis, this "surge" inventory has been updated and expanded by adding "pulse-type" and "consistent acceleration" designations to the classification scheme in order to better characterize the velocity variability observed within the Canadian Arctic. Finally, the widespread consistent acceleration of the Trinity and Wykeham Glaciers driven by terminus thinning is identified as a potential mechanism of rapid dynamic mass loss for the Canadian Arctic and builds on previous research which has identified rapid acceleration and retreat of glaciers in other Arctic regions (e.g. Holland et al. 2008; Howat et al. [2005], [2007]; Joughin et al. [2008], [2012]; Meier and Post [1987]; Murray et al. [2010]; Pfeffer [2007])

6.3 Future Research Directions

This thesis has shown the utility of using SAR speckle tracking to provide regional scale velocity mapping and establishes a methodological framework for an annual, semi-operational glacier

dynamics monitoring program within the Canadian Arctic. Future research should continue to utilize speckle tracking of RADARSAT-2 fine beam (or similar) imagery to build upon the record of glacier dynamics and iceberg discharge initiated by this study. From a methodological standpoint, focus should be placed on modifying the speckle tracking algorithm to utilize datasets from new SAR sensors as they become available (e.g. Sentinel 1A/1B; ALOS PALSAR-2; RADARSAT Constellation). As data from new and planned sensors becomes more freely available, the opportunity exists whereby glacier velocities across the Canadian High Arctic can be determined with little to no data acquisitions costs, allowing for the expanded monitoring of Canada's glaciers.

From a glaciological standpoint, recently acquired ice thickness datasets collected by NASA's Operation IceBridge (especially those available for 3D tomography processing) will provide a much more detailed record of glacier bed topography and ice thicknesses in the near future. Future research should focus on exploiting these new datasets in order to better define flux gates and reduce uncertainty surrounding dynamic discharge estimates. This dataset can also be used to further investigate the relationship between bed topography and areas of dynamic variability in the Canadian Arctic. Furthermore, more research is necessary to better understand the differing processes that drive "surge-type" and "pulse-type" glaciers within the Canadian Arctic. Future research should also focus on better understanding of the external forcing that is driving the recent speed-up of the Trinity and Wykeham Glaciers.

A limitation of this study is a lack of climate datasets with long temporal resolution that could have been utilized to better understand glacier dynamics within the region. As a consequence, future work should concentrate on obtaining high quality climate data across the Canadian Arctic for this purpose. These datasets could provide significant insights into the fundamental drivers of glacier dynamics (e.g. mass balance, surface melt), whether there are connections between the climate and mass balance on surge-type glaciers, and be used to understand how glaciers within the Canadian Arctic are likely to respond in a warming climate. Insights gleaned from a better understanding of links between regional glacier dynamics and regional climatology may be applicable to other locations in the Arctic (e.g., Svalbard, Greenland) and aid in understanding how glacier dynamics will evolve in the future.

6.4 Thesis References

Alley, R.B., P.U. Clark, P. Huybrechts, I. Joughin, (2005), Ice-sheet and sea-level changes, *Science*, 310(5747): 456-460. doi: 10.1126/sciences.1114613.

Arendt, A., T. Bolch, J.G. Cogley, A. Gardner, J.O. Hagen, R. Hock, G. Kaser, W.T. Pfeffer, G. Moholdt, F. Paul, V. Radić, L. Andreassen, S. Bajracharya, N. Barrand, M. Beedle, E. Berthier, R. Bhambri, A. Bliss, I. Brown, E.Burgess, D. Burgess, F. Cawkwell, T. Chinn, L. Copland, B. Davies, H. De Angelis, E. Dolgova, K. Filbert, R. Forester, A. Fountain, H. Frey, B. Giffen, N. Glasser, S. Gurney, W. Hagg, D. Hall, U.K. Haritashya, G. Hartmann, C. Helm, S. Herreid, I. Howat, G. Kapustin, T. Khromova, C. Kienholz, M. Koenig, J. Kohler, D. Kriegel, S. Kutuzov, I. Lavrenti ev, R. LeBris, J. Lund, W. Manley, C. Mayer, E. Miles, X. Li, B. Menounos, A. Mercer, N. Moelg,P. Mool, G. Nosenko, A. Negrete, C. Nuth, R. Pettersson, A. Racoviteanu, R. Ranzi, P. Rastner, F. Rau, B. Raup, J. Rich, H. Rott, C. Schneider, Y. Seliverstov, M. Sharp, O. Sigurðsson, C. Stokes, R. Wheate, S. Winsvold, G. Wolken, F. Wyatt, N. Zheltyhina. (2012), Randolph Glacier Inventory [v3.0]: A Dataset of Global Glacier Outlines. Global Land Ice Measurements from Space, Boulder Colorado, USA. Digital Media.

Benn, D.I. and D.J.A. Evans, (2010), Glaciers and Glaciation (2nd Edition), 802 pp, Arnold, London, U.K.

Bingham, R., P. Nienow, and M. Sharp, (2003), Intra-annual and intra-seasonal flow dynamics of a High Arctic polythermal valley glacier**.** *Annals of Glaciology, 37, 181-188.*

Blaszczyk, M., J.A. Jania, and J.O. Hagen, (2009), Tidewater glaciers of Svalbard: Recent changes and estimates of calving fluxes, *Polish Polar Research*, 30(2), 85-142.

Boon, S., and M. Sharp, (2003), The role of hydrologically-driven ice fracture in drainage system evolution on an Arctic glacier. *Geophysical Research Letters*, 30, doi:10.1029/2003GL018034.

Braithwaite, R.J., (2005), Mass balance characteristics of arctic glaciers, *Annals of Glaciology*, 42(1), 225-229.

Burgess, E.W., R. R. Foster, and C. F. Larsen, (2013a), Flow velocities of Alaskan glaciers, *Nature Communications*, 4(2146), 1-8, doi: 10.1038/ncomms3146.

Burgess, E. W., C. F. Larsen, and R. R. Forster, (2013b), Summer melt regulates winter glacier flow speeds throughout Alaska, *Geophysical Research Letters*, 40, 6160–6164, doi:10.1002/2013GL058228.

Burgess D. and M. Sharp, (2004), Recent changes in areal extent of the Devon ice cap, Nunavut, Canada. *Arctic, Antarctic and Alpine Research*, 36(2), 261–271

Burgess, D., M. Sharp, D. Mair, J.A. Dowdeswell, and T.J. Benham, (2005), Flow dynamics and iceberg calving rates of Devon Ice Cap, Nunavut, Canada, *Journal of Glaciology*, 51, 173: 219-230.

Burgess D. and M. Sharp, (2008), Recent changes in thickness of the Devon Island ice cap, Canada, *Journal of Geophysical Research*, 113(B7), B07204. doi: 10.1029/2007JB005238

Clason, C., D.W.F. Mair, D.O., Burgess, and P.W. Nienow, (2012), Modelling the delivery of supraglacial meltwater to the ice/bed interface: application to southwest Devon Ice Cap, Nunavut, Canada. *Journal of Glaciology*. 58, 361-374. doi: 10.3189/2012JoG11j129

Copland, L., M. Sharp, and P. Nienow, (2003a), Links between short-term velocity variations and the subglacial hydrology of a polythermal glacier. *Journal of Glaciology*. 49, 407-414.

Copland, L., M. Sharp, and J.A. Dowdeswell, (2003b), The distribution and flow characteristics of surge-type glaciers in the Canadian High Arctic. *Annals of Glaciology*. 36, 73-81.

Cress, P. and R. Wyness, (1961), The Devon Island expedition, observations of glacial movements. *Arctic*, 14(4), 257–259.

Danielson, B., and M. Sharp, (2013), Development and application of a time-lapse photograph analysis method to investigate the link between tidewater glacier flow variations and supraglacial drainage events. *Journal of Glaciology*. 59, 287-302.

Danielson, B.D. (2014), Velocity variability of Devon Ice Cap tidewater glaciers. Ph.D. Thesis, University of Alberta.

Danielson, B., and M. Sharp, (2013), Development and application of a time-lapse photograph analysis method to investigate the link between tidewater glacier flow variations and supraglacial drainage events. *Journal of Glaciology*. 59, 287-302.

Dowdeswell, E.K., Dowdeswell, J.A., and F. Cawkwell, (2007), On the glaciers of Bylot Island, Nunavut, Arctic Canada, *Arctic, Antarctic and Alpine Research*, 29(3), 402-4011. doi: 10.1657/1523-0430(05-123)[DOWDESWELL]2.0.CO;2

Dowdeswell, J.A., T.J., Benham, M.R., Gorman, D., Burgess, and M. Sharp, (2004), Form and flow of the Devon Island ice cap, Canadian Arctic. *Journal of Geophysical Research*, 109(F2), F02002 doi: 10.1029/2003JF000095

Dowdeswell, J.A., T.J. Benham, T. Strozzi, and J.O. Hagen, (2008), Iceberg calving flux and mass balance of the Austfonna ice cap on Nordaustlandet, Svalbard, *Journal of Geophysical Research*, 113, F03022, doi:10.1029/2007JF000905.

Dupont, F., A. Royer, A. Langlois, A. Gressent, G. Picard, M. Fily, P. Cliché, and M. Chum, (2012), Monitoring the melt season length of the Barnes Ice Cap over the 1979-2010

period using active and passive microwave remote sensing data, *Hydrological Processes*, 26, 2643-2652.

Gardner, A.S. and M. Sharp, (2007), Influence of the Arctic circumpolar vortex on the mass balance of Canadian high Arctic Glaciers, *Journal of Climate,* 20: 4586-4598.

Gardner, A. S., M. Moholdt, B. Wouters, G.J. Wolken, D.O. Burgess, M. Sharp, J.G. Cogley, C. Braun and C. Labine, (2011), Sharply increased mass loss from glaciers and ice caps in the Canadian Arctic Archipelago, *Nature,* 473(7347): 357–360. doi: 10.1038/nature10089.

Gardner, A., G. Moholdt, A. Arendt, and B. Wouters, (2012), Accelerated contributions of Canada's Baffin and Bylot Island glaciers to sea level rise over the past half century, *The Cryosphere,* 6: 1103-1125.

Glazovskiy, A.F., (1991), The Problem with Surge-type Glaciers. In: *Variations of Snow and Ice in the past and at present on a Global and Regional Scale*. (ed Kotlyakov, V.M.) An International Hydrological Program Publication.

Glazovsky, A. and Y. Macheret, (2006), Eurasian Arctic.in, Glaciation in north and central Eurasian in present time [in Russian with English Translation], editied by V.M., Kotlyakov, 97-114 and 438-445, Nauka, Moscow.

Gogineni, P. (2012), Radar Depth Sounder Data Products, Lawrence, Kansas, USA. Digital media. http://data.cresis.ku.edu/

Gray, A.L., K.E. Mattar, and G. Sofko, (2000), Influence on ionospheric electron density fluctuations on satellite radar interferometry, *Geophysical Research Letters*. 27(10), 1451-1454. doi: 10.1029/2000GL000016

Gray, A.L., N. Short, K.E. Mattar, and K. C. Jezek, (2001), Velocities and flux of the Filchner Ice Shelf and its tributaries determined from speckle tracking interferometry, *Canadian Journal of Remote Sensing*, 27(3), 193-206.

Harbor, J.M. (1992), Numerical modelling of the development of U-shaped valleys by glacier erosion, *Geological Society of America Bulletin*, 104(10), 1364-1375, doi:10.1130/0016-7606(1992)104<1364:NMOTDO>2.3.CO;2.

Hattersley-Smith, G. (1969), Recent Observations on the surging of Otto Glacier, Ellesmere Island, *Canadian Journal of Earth Sciences,* 6(4): 883–889.

Haug, T., A. Kääb, and P. Skvarca (2010), Monitoring ice shelf velocities from repeat MODIS and Landsat data – a method study on the Larsen C ice shelf, Antarctic Peninsula, and 10 other ice shelves around Antarctica, *The Cryosphere,* 4: 161-178.

Heid, T., and A. Kääb, (2012), Repeat optical satellite images reveal widespread and long term

decrease in land terminating glacier speeds, *The Cryosphere,* 6: 467-478.

Herdes, E., L. Copland, B. Danielson, and M. Sharp, (2012), Relationships between iceberg plumes and sea-ice conditions on northeast Devon Ice Cap, Nunavut, Canada, *Annals of Glaciology*, 53(60), 1-9, doi: 10.3189/2012AoG60A163.

Holdsworth, G., (1973), Evidence of a surge on Barnes Ice Cap, Baffin Island, *Canadian Journal of Earth Sciences,* 10: 1565-1574.

Holdsworth, G. (1977), Surging activity on the Barnes Ice Cap, *Nature*, 269: 588-590.

Holland, D. M., R. H. Thomas, B. de Young, M. H. Ribergaard and B. Lyberth (2008), Acceleration of Jakobshavn Isbrae triggered by warm subsurface ocean waters, *Nature Geoscience*, 1: 659-664. doi: 10.1038/ngeo316

Howat, I.M., I., Joughin, S. Tulaczyk and S. Gogineni (2005), Rapid retreat and acceleration of Helheim Glacier, east Greenland, *Geophysical Research Letters*, 32, doi: 10.1029/2005GL024737.

Howat, I. M., I. Joughin, T. A. Scambos, (2007), Rapid retreat and acceleration of Helheim Glacier, east Greenland. Geophysical Research Letters, 32, L22502, doi:10.1029/2005gl024737.

Joughin, I. (2002), Ice-sheet velocity mapping: a combined interferometric and speckle tracking approach, *Annals of Glaciology*, 34: 195–201.

Joughin, I., I. Howat, R. B. Alley, G. Ekstrom, M. Fahnestock, T. Moon, M. Nettles, M. Truffer, and V. C. Tsai (2008), Ice-front variation and tidewater behavior on Helheim and Kangerdlugssuaq Glaciers, Greenland, *Journal of Geophysical Research*, 113: F01004, doi:10.1029/2007JF000837.

Joughin, I., R.B. Alley and D.M. Holland (2012), Ice-sheet response to oceanic forcing, *Science*, 338(6111): 1172-1176. doi: 10.1126/science.1226481.

Kamb, B., (1987), Glacier surge mechanism based on linked cavity configuration of the basal water conduit system, *Journal of Geophysical Research*, 92(B9): 9083-9100. Doi:10.1029.JB092iB09p09083.

Koerner, R. M. (1979), Accumulation, ablation, and oxygen isotope variations on the Queen Elizabeth Island Ice Caps, Canada, *Journal of Glaciology*, 22(86): 25-41.

Koerner, R.M. (2005), Mass balance of glaciers in the Queen Elizabeth Islands, Nunavut, Canada. *Annals of Glaciology*, 42: 417–423. doi: 10.3189/172756405781813122

Lenaerts, J. T. M., J. H. van Angelen, M. R. van den Broeke, A.S. Gardner, B. Wouters, and E. van Meijgaard, (2013), Irreversible mass loss of Canadian Arctic Archipelago glaciers,

Geophysical Research Letters, 40. doi:10.1002/grl.50214

Løken, O. H., (1969), Evidence of surges on the Barnes Ice Cap, Baffin Island, *Canadian Journal of Earth Sciences*, 6: 899-901.

Mair, D., D.O. Burgess, M. Sharp, J. A. Dowdeswell, T. J. Benham, S. Marshall and F. Cawkwell, (2009), Mass balance of the Prince of Wales Icefield, Ellesmere Island, Nunavut, Canada, *Journal of Geophysical Research*, 114, F02011. doi:10.1029/2008JF001082

Marshall, S., M. Sharp, D. O. Burgess, and F. Anslow, (2007), Surface temperature lapse rate variability on the Prince of Wales Icefield, Ellesmere Island, Canada: implications for regional-scale downscaling of temperature, *International Journal of Climatology*, 27: 385-398.

Mayo, L.R., (1978), Identification of unstable glaciers intermediate between normal and surging glaciers, *Mater. Glyatsiol. Issled*, 133: 133-135.

McNabb, R. W., R. Hock, and M. Huss (2015), Variations in Alaska tidewater glacier frontal ablation, 1985–2013, *Journal of Geophysical Research, Earth Surface*, 120: 120–136. doi:10.1002/2014JF003276.

Meier, M.F. and A. Post, (1987), Fast tidewater glacier, *Journal of Geophysical Research*, 92(B9): 9051-9058. doi:10.1029/Jb092iB09p09051.

Moholdt, G., T. Heid, T., Benham, J.A. Dowdeswell, (2012), Dynamic instability of marine-terminating glacier basins of Academy of Sciences Ice Cap, Russian High Arctic, *Annals of Glaciology*, 53(60): 193-201. doi: 10.3189/2012AoG60A117.

Mortimer, C. A., L. Copland, and D. R. Mueller, (2012), Volume and area changes of the Milne Ice Shelf, Ellesmere Island, Nunavut, Canada, since 1950, *Journal of Geophysical Research*, 117F04011. doi:10.1029/2011JF002074.

Müller, F., (1969), Was the Good Friday Glacier on Axel Heiberg Island surging?, *Canadian Journal of Earth Sciences*, 6(4): 891–894. doi:10.1139/e69-091.

Müller, F., and A. Iken, (1973), Velocity fluctuations and water regime of Arctic valley glaciers. *International Association of Scientific Hydrology Publication*. (95): 165–182.

Murray, T., J.A. Dowdeswell, D.J. Drewry, D.J. and I. Frearson, (1998), Geometric evolution and ice dynamics during a surge of Bakaninbreen, Svalbard. *Journal of Glaciology*, 44, 147: 263-272.

Murray, T., T. Strozzi, A. Luckman, H. Jiskoot and P. Christakos, (2003), Is there a single surge mechanism? Contrasts in dynamics between glacier surges in Svalbard and other regions, *Journal of Geophysical Research*, 108 (B52237): 1-15. doi: 10.1029/2002JB001906.

Murray, T., K. Scharrer, T. D. James, S. R. Dye, E. Hanna, A. D. Booth, N. Selmes, A. Luckman, A. L. C. Hughes, S. Cook and P. Huybrechts, (2010), Ocean regulation hypothesis for glacier dynamics in southeast Greenland and implications for ice sheet mass changes, *Journal of Geophysical Research*, 115(F03026): 1-15. doi: 10.1029/2009Jf001522.

Narod, B. B., G.K.C. Clarke, and B.T. Prager, (1988), Airborne UHF sounding of glaciers and ice shelves, northern Ellesmere Island, Arctic Canada, *Canadian Journal of Earth Sciences*, 25(1): 95–105. doi: 10.1139/e88-010.

Ommanney, C.S.L., (1969), A study in glacier inventory: the ice masses of Axel Heiberg Island, Canadian Arctic Archipelago, *Axel Heiberg Island Research Reports*, McGill University, Montreal, Canada.

Paterson, W.S.B., (1994), *The physics of glaciers*, third edition, Elsevier, Oxford.

Pfeffer, W. T., (2007), A simple mechanism for irreversible tidewater glacier retreat, *Journal of Geophysical Research*. 112, F03S25. doi:10.1029/2006JF000590.

Pfeffer, W.T., A.A. Arendt, A. Bliss, T., Bolch, J.G. Cogley, A.S. Gardner, J.O. Hagen, R. Hock, G. Kaser, C. Kienholz, E.S. Miles, G. Moholdt, N. Moelg, F. Paul, V. Radic, P. Rastner, B. Raup, J. Rich, M.J. Sharp, and the Randolph Consortium. The Randolph Glacier Inventory: a globally complete inventory of glaciers, *Journal of Glaciology*, 60: 537-552. doi:10.3189/2014JoG13J176.

Raymond, C.F. (1983), Deformation in the vicinity of ice divides, *Journal of Glaciology*, 29(103): 357-373.

Raymond, C.F., (1987), How do glaciers surge? A Review, Journal of Geophysical Research, 92 (B9): 9121-9134.

Rosen, P., S. Hensley, I. Joughin, S. Madsen, E. Rodriguez, and R. Goldstein, (2000), Synthetic Aperture Radar Interferometry, *Proceedings of the IEEE Transactions on Geoscience and Remote Sensing*, 88(3): 333-382. doi: 10.1109/5.838084

Sharp, M., D.O. Burgess, J.G. Cogley, M. Ecclestone, C. Labine, and G. Wolken, (2011), Extreme melt on Canada's Arctic ice caps in the 21st century, *Geophysical Research Letters*, 38(L11501) doi: 10.1029/ 2011GL047381

Sharp, M., D.O Burgess, F. Cawkwell, L. Copland, J.A. Davis, E.K. Dowdeswell, J.A. Dowdeswell, A. Gardner, D. Mair, L. Wang, S. Williamson, G.J. Wolken, and F. Wyatt, (2014), Remote sensing of recent glacier changes in the Canadian Arctic. In: Kargel, J.S., Leonard, G.J., Bishop, M.P., Kääb, A. and Raup, B.H. (eds). *Global Land Ice Measurements from Space,* Ch. 9, pp. 205-228. Praxis-Springer. doi: 10.1007/978-3-540-

79818-7_9.

Shepherd, A., Z. Du, T.J. Benham, J.A. Dowdeswell, and E.M. Morris, (2007), Mass balance of Devon Ice Cap, Canadian Arctic, *Annals of Glaciology*, 46, 249–254 doi:10.3189/172756407782871279

Short, N. H. and A. L. Gray, (2004), Potential for RADARSAT-2 interferometry: glacier monitoring using speckle tracking, *Canadian Journal of Remote Sensing*. 30(3): 504-509.

Short, N. H. and A.L. Gray, (2005), Glacier dynamics in the Canadian High Arctic from RADARSAT-1 speckle tracking, *Canadian Journal of Remote Sensing*, 31(3): 225–239.

Strozzi, T., A. Luckman, T. Murray, U. Wegmuller, and C. L. Werner, (2002), Glacier motion estimation using SAR offset-tracking, *Proceedings of the IEEE Transactions on Geoscience and Remote Sensing*, 40(11): 2384-2391. doi: 10.1109/TGRS.2002.805079

Thomson, L.I., G.R. Osinski, and C.S.L. Ommanney, (2011), Glacier change on Axel Heiberg Island, Nunavut, Canada, *Journal of Glaciology*, 57(206): 1079-1086, doi: 10.3189/002214311798843287.

Turrin, J.B., R.R. Forster, J.M. Sauber, D.K. Hall, R.L. Braun, (2014), Effects of bedrock lithology and subglacial till on the motion of Ruth Glacier, Alaska, deduced from five pulses from 1973 to 2012, *Journal of Glaciology*, 60 (222). doi: 10.3189/2014JoG13J182.

Van Wychen, W., L. Copland, L. Gray, D. O. Burgess, B. Danielson, M. Sharp, (2012), Spatial and temporal variation of ice motion and ice flux from Devon Ice Cap, Nunavut, Canada. *Journal of Glaciology*, 58(210): 657–664. doi: 10.3189/2012JoG11J164.

Van Wychen, W., D. O. Burgess, L. Gray, L. Copland, M. Sharp, J. A. Dowdeswell, and T. J. Benham, (2014), Glacier velocities and dynamic ice discharge from the Queen Elizabeth Islands, Nunavut, Canada, *Geophysical Research Letters*, 41, doi:10.1002/2013GL058558.

Van Wychen, W., L. Copland, D.O. Burgess, L. Gray and N. Schaffer, (in press), Glacier velocities and dynamic discharge from the ice masses of Baffin and Bylot Islands, Nunavut, Canada. *Canadian Journal of Earth Sciences.* doi: 0.1139/cjes-2015-0087 (Accepted July 20th, 2015).

Van Wychen, W., J. Davis, D.O. Burgess, L. Copland, L. Gray, M. Sharp, C. Mortimer, (*submitted Aug 26, 2015*) Characterizing inter-annual variability of glacier dynamics (1999-2015) and dynamic discharge (2000, 2011-2015) for the ice masses of Ellesmere and Axel Heiberg Islands, Nunavut, Canada, submitted to Journal of Geophysical Research - Earth Surface, (manuscript number: 2015JF003708).

Waechter, A., L. Copland, and E. Herdes, (2015), Modern glacier velocities across the Icefield

Ranges, St. Elias Mountains, and variability at selected glaciers from 1959 to 2012. Journal of Glaciology, 61(228), doi: 10.3189/2015JoG14J147

Wainstein, P., B. Moorman, and K. Whitehead, (2014), Glacial conditions that contribute to the regeneration of Fountain Glacier proglacier icing, Bylot Island, Canada, *Hydrological Processes*, 28: 2749-2760. doi:10.1002/2013GL058558.

Williamson, S., M. Sharp, J. Dowdeswell, and T. Benham, (2008), Iceberg calving rates from northern Ellesmere Island ice caps, Canadian Arctic, 1999-2003. *Journal of Glaciology*, 54(186): 391-400. doi: 10.3189/002214308785837048.

Wyatt, F. and M. Sharp, (2015), Linking surface hydrology to flow regimes and patterns of velocity variability of the Devon Ice Cap, Nunavut, *Journal of Glaciology*, 61: 387-399.

Zdanowicz, C., A. Smetny-Sowa, D. Fisher, N. Schaffer, L. Copland, J. Eley, and F. Dupont, (2012), Summer melt rates on Penny Ice Cap, Baffin Island: Past and recent trends and implications for regional climate, *Journal of Geophysical Research*, 117, F02006, doi:10.1029/2011JF002248.